Studies on Pyrolysis Kinetics of Commodity Plastics

Thesis

Submitted in partial fulfillment of the requirements for the degree of

DOCTOR OF PHILOSOPHY

By

Biswanath Saha

Under the Supervision of

Dr. A. K. Ghoshal

Associate Professor

Indian Institute of Technology Guwahati

Department of Chemical Engineering

Indian Institute of Technology Guwahati

Guwahati – 781039, Assam, India

2007

Dedication

I dedicate this work to my parents & grandparents who have always supported me in everything I did.

Acknowledgement

I wish to express my sincere gratitude to my supervisor, **Dr. Aloke Kumar Ghoshal**, Head of Department, Department of Chemical Engineering, Indian Institute of Technology Guwahati**,** for his valuable guidance and assistance during my research endeavor at Indian Institute of Technology, Guwahati. I thank him for his patience and understanding. It has been a great privilege to work under him.

I must also thank my doctoral committee members, **Prof. Arun Chattopadhyay,** Department of Chemistry**, Dr. Prabirkumar Saha** and **Dr. Sasidhar Gumma,** Department of Chemical Engineering**,** for their valuable suggestions and varied contributions towards my research work.

I also wish to extend my deep sense of appreciation to my former mentor Prof. Sujay Basu, Jadavpur University, whose guidance has been instrumental in pursuance of this doctoral work.

I must also thank the faculty members of the Department of Chemical Engineering for their kind cooperation during my stay here and in particular, Dr. Ramagopal Uppaluri for his help and constant encouragement.

I would also like to thank Mr. Prasun Bhattacharjee and Mr. Balen Chandra Mahanta for their assistance during my experimental work. I would also like to thank Mr. Bipul Kumar Bora, Mr. Bhagya Boro, and Mr. Pankaj Sekhar Baruah for their assistance in various forms.

I must thank the Department of Chemistry, Centre of Nanotechnology and the Central Instruments Facility of IIT Guwahati for allowing me to utilize their experimental resources that have been vital in my research work.

I express my sincere thanks to Mr. Sanjay Kumar Chattopadhyay, Chief Manager (Project), CIPET Guwahati for his kind help in providing me with Virgin Plastic samples.

I thank IOCL Noonmati, Guwahati for providing the FCC catalyst samples.

The contribution of my friends Mrs. Haimanti Paul, Mr. Saurangshu Pandey and Mr. Rajiv Ganguly in providing access to valuable resources requires a special mention.

I am also grateful to my friends Mr. Barun Nandi, Mr. Mehabub Rahaman, Mr. Pradip Chowdhury, Ms. Ujwala Hujuri, and Mr. Arnab Karmakar for their help and support.

Acknowledgement

I wish to extend my special thanks to my friends **Mr. Debasish Ghosh, Mr. Subham Paul and Ms. Sumedha Sharma** for doing millions little things to help me out over the years.

I must thank my co-worker **Mr. A. K. Maity, Mr. P. Karthik Reddy,** and **Mr. Aie Cheng King Chowlu** for their suggestions and co operation during the experimental works.

Finally, I am deeply indebted to my parents, brother, sister, their family members, and my friend Mr. Animesh Pal and his bother late Tapas Pal for their moral support, patience, and constant encouragement. Without their support, it would have been impossible to see the completion of this work.

Abstract

Noncatalytic and catalytic decomposition behaviour of commodity plastics such as waste and virgin polyethylene terephthalate (PET), waste low density polyethylene (LDPE), waste polyethylene (PE) and pure polypropylene (PP) are carried out using thermogravimetric analyzer (TGA). Catalyst used in this study are commercially available ZSM-5, fresh and spent FCC catalysts, laboratory synthesized sol-gel and hydrothermal mesoporous catalysts Al-MCM-41 of different aluminium contents and high external surface area containing nanocrystalline n-HZSM-5. Polymer samples are characterized by differential scanning calorimetry (DSC). Catalysts are characterized by X-ray diffraction (XRD) analysis, Scanning Electron Microscopy (SEM) and surface area analysis using BET analyzer. Gaseous products of decomposition experiments were analyzed by gas chromatography (GC). Experimental data on decomposition studies suggest that thermal decomposition behaviors of plastic samples are similar, showing the constant pattern TG curves at different heating rates and a single peak in derivative thermogravimetric (DTG) curves. Higher heating rate finishes the decomposition phenomenon faster. During catalytic decomposition, catalysts are selective to the plastics and significantly reduce decomposition temperature. Catalytic decomposition shows single as well as multi-peaks in the DTG curves for different plastics, indicating possible existence of multi-step reactions taking place in presence of catalysts. Catalytic effect in terms of reduction in T_m on waste LDPE follows the sequence ZSM-5>Al-41-P(15)>Al-41-P(30)>Al-41-P(60)>Al-41-P(100)>Fresh FCC>Spent FCC and on PP follows the sequence n-HZSM-5>Al-41-P(15)≈Al-41-P(30)>Al-41-P(60)>Fresh FCC>Al-41-P(100)>Spent FCC>ZSM-5. Product analysis indicates that microporous ZSM-5 and high external surface area containing n-HZSM-5 produce high amount of light hydrocarbons

whereas mesoporous Al-MCM-41 produce high amount of heavier hydrocarbons, which is also supported by the literature findings. The optimum catalysts percentage obtained for decomposition of waste LDPE over ZSM-5, PP over Al-MCM-41, and waste LDPE over n-HZSM-5 are around 20, 18.5 and 50 wt % respectively. Reusability study suggests that Al-MCM-41 is still very active even after its use for seven times.

Kinetics analysis of both noncatalytic and catalytic decomposition is carried out using model fitting and model-free (isoconversional) methods. Model fitting methods provide the information on the optimum kinetics triplet (activation energy, pre-exponential factor, and reaction order) and model-free (isoconversional) method provides the information on the variation of activation energy with conversion. Suitability of different model fitting methods along with development/improvement is reported in the present work. Several model-fitting methods such as nth-order model, ASTM E698, Freeman-Carroll, Friedman, and Chang techniques, which are applicable for single heating rate TGA curve, are employed. nth-order model, which is suggested first time in this work, shows better results compared to others. Standard deviation minimization technique (SDMT) is developed and shown to be a promising model-fitting technique as it takes care of both single and multi heating rate TGA curves. Sensisitivity analysis is also performed to reduce the multi parameter optimization problem into a single parameter optimization problem. Reaction order is found to be the most sensitive one and activation energy to be the least sensitive one. Evaluation of the optimized kinetics triplet by the above methods are associated with draw backs such as the selection of appropriate model and initial guess of kinetics parameters, which may lead to uncertainty in the estimated kinetics triplet. Finally hybrid genetic algorithm is successfully employed, to avoid uncertainty as

above, to estimate the globally optimum kinetics triplet. Akaike's Information Criteria (AIC) is also applied to choose the appropriate reaction model. Vyazovkin nonlinear model-free (isoconversional) analysis is carried out with several approximation and direct numerical integration of the temperature integral. It is applied to both noncatalytic and catalytic decomposition showing different trends for different cases in the variation of activation energy with conversion. This trend also helps getting first hand information on the possible reaction steps involved during pyrolysis e.g. model-free analysis indicates the possible existence of four different reaction mechanisms in the different steps during catalytic decomposition of LDPE over ZSM-5 catalyst. The nonlinear Vyazovkin model-free analysis approach also narrows down the range of guess values of activation energy for optimization using traditional model-fitting methods. The estimated optimized kinetics triplet obtained by the model-free coupled with local optimization method (LOA) successfully predicted the experimental TGA data. The present work demonstrated that model-free coupled with local optimization method (LOA) is as good as HGA for estimating the kinetics triplet.

Key words:

thermal pyrolysis; catalytic pyrolysis; low density polyethylene; polyethylene terephatalate; polyethylene; polypropylene; ZSM-5; n-HZSM-5; Al-MCM-41; FFC; model-fitting method; model-free (isoconversional) method; kinetics triplet; activation energy; reaction model; hybrid genetic algorithm; product analysis

Summary

The Ph. D thesis consists of investigation in the following four major topics:

- Experimental studies on non-catalytic pyrolysis of commodity plastics such as waste and virgin poly (ethylene terephthalate) (PET), waste low density polyethylene (LDPE), waste polyethylene (PE), and polypropylene (PP).
- Catalytic pyrolysis of waste LDPE and PP over commercially available catalysts (ZSM-5 and FCC), laboratory synthesized mesoporous catalysts Al-MCM-41 with different aluminum content, and high external surface area catalyst nanocrystalline n-HZSM-5.
- Catalyst reusability, optimum catalyst concentration and analysis of the gaseous products from both non-catalytic and catalytic decomposition experiments.
- Evaluation of reliable globally optimized overall kinetics triplets for both the non-catalytic and catalytic pyrolysis. Model fitting methods, model free method, hybrid genetic algorithm (HGA) and model-free coupled local optimization algorithm (LOA) methods are applied for finding the overall kinetics triplets.

The thesis is divided into following chapters:

Chapter 1: Introduction and literature Review

Chapter 2: Kinetics analysis

Chapter 3: Experimental

Chapter 4: Results and discussion

Chapter 5: Conclusions

Brief descriptions on each of the chapters are presented below.

Summary

Chapter 1: Introduction and literature Review

This chapter discusses the usage of plastics and advantages and disadvantages of different existing methods such as land filling, incineration, and recycling for treatment of solid wastes generated from the plastics use. It elaborates the background of the research work. Importance and objectives of the present work are highlighted in this chapter. The chapter subsequently presents detailed literature review that include thermal and catalytic pyrolytic decomposition of waste plastics, thermal and catalytic dehydrochlorination (DHC), co-processing of waste plastics, thermal and catalytic pyrolysis/decomposition kinetics analysis of polymers, thermal and catalytic decomposition mechanism, sensitivity analysis and hybrid genetic algorithm.

Chapter 2: Kinetics Analysis

This chapter gives a complete description of the detailed development of various model-fitting and model-free kinetics analysis techniques for both thermal and catalytic pyrolysis of plastic samples. To start with, it elaborates the existing model fitting techniques such as nth-order model, ASTM E698, Freeman-Carroll, Friedman, and Chang techniques for estimation of kinetics triplet from the non-isothermal experimental decomposition data. It discusses the model-free methods for isothermal and non-isothermal conditions. Evaluation of the temperature integral obtained from the single step kinetic model by using direct numerical integration and by using several approximation techniques of Coats Redfern, Gorbachev, Agrawal and Sivasubramanian and Cai et al. is described. This chapter further reports the development of first order, second order and second order cross sensitivity matrices and their computation methods

and development of single and multi-parameter objective functions for estimation of kinetics triplet using the experimental TGA data. Applying sensitivity analysis the three-parameter optimization is reduced to a simple but reliable single parameter optimization. Akaike's Information Criteria (AIC) is also applied to choose the appropriate reaction model. Model-free coupled with local optimization algorithm (LOA) is employed to estimate kinetics parameters. Finally, the hybrid genetic algorithm (HGA) (GA coupled with LOA) is employed to estimate the globally optimum kinetics triplet. Simulation procedures for prediction of the TGA data both for thermal and catalytic decompositions of plastics used are also discussed in this chapter.

Chapter 3: Experimental

This chapter mainly discusses the procedures of synthesis of sol-gel and hydrothermal mesoporous catalysts Al-MCM-41 of different aluminium contents and high external surface area containing nanocrystalline n-HZSM-5 catalysts in laboratory; characterization of the polymers waste and virgin PET, waste LDPE, waste PE, and PP; characterization of the commercially available catalysts (ZSM-5 and fresh and spent FCC) and laboratory synthesized catalysts used for the present work; thermal and catalytic polymer decomposition experiments using thermogravimetric analyzer (TGA); and product distribution using gas chromatographic (GC) analysis. This chapter also discusses the experiments on reusability study of the catalysts used. Polymer samples are characterized by differential scanning calorimetry (DSC). Catalysts are characterized by X-ray diffraction (XRD) analysis, Scanning Electron Microscopy (SEM) and surface area analysis using BET analyzer.

Chapter 4: Results and discussion

This chapter presents the results and discussion of the research work under the following major topics.

- Characterization of catalysts and polymers
- Noncatalytic and catalytic pyrolytic decomposition of plastic samples
- Evaluation of optimum catalyst percentage for catalytic decomposition
- Reusability of catalyst
- Analyses of the products in the gaseous substance coming out of all the thermal and catalytic pyrolysis experiments through gas chromatography
- Kinetics analyses of these experimental results using model-fitting and model-free (isoconversional) techniques and simulation of the kinetics model for prediction of the experimental data

Chapter 5: Conclusion

This chapter reports the inferences drawn from the research work. Major inferences are presented below.

- Thermal (noncatalytic) decomposition behaviors of plastic samples are similar, showing the constant pattern TG curves at different heating rates and a single peak in derivative thermogravimetric (DTG) curves. Higher heating rate completes the decomposition phenomenon faster.
- During catalytic decomposition, catalysts are selective to the plastics and significantly reduce decomposition temperature. Catalytic decomposition shows single as well as multi-peaks in the DTG curves for different plastics, indicating possible existence of

multi-step reactions taking place in presence of catalysts. Catalytic effect in terms of reduction in T_m on waste LDPE follows the sequence ZSM-5>Al-41-P(15)>Al-41-P(30)>Al-41-P(60)>Al-41-P(100)>Fresh FCC>Spent FCC and on PP follows the sequence n-HZSM-5>Al-41-P(15)≈Al-41-P(30)>Al-41-P(60)>Fresh FCC>Al-41-P(100)>Spent FCC>ZSM-5.

- Product analysis indicates that microporous ZSM-5 and high external surface area containing n-HZSM-5 produce high amount of light hydrocarbons whereas mesoporous Al-MCM-41 produce high amount of heavier hydrocarbons, which is also supported by the literature findings.
- The optimum catalysts percentage obtained for decomposition of waste LDPE over ZSM-5, PP over Al-MCM-41, and waste LDPE over n-HZSM-5 are around 20, 18.5 and 50 wt % respectively.
- Reusability study suggests that Al-MCM-41 is still very active even after its use for seven times.
- n^{th} order model, which is suggested first time in this work, shows better results compared to ASTM E698, Freeman-Carroll, Friedman, and Chang techniques. All the techniques are based on single heating rate TGA curve. Standard deviation minimization technique (SDMT) is developed and shown to be a promising model-fitting technique as it takes care of both single and multi heating rate TGA curves. According to the sensisitivity analysis, reaction order is found to be the most sensitive one and activation energy to be the least sensitive one. Hybrid genetic algorithm is successfully employed to estimate the globally optimum kinetics triplet. Akaike's Information Criteria (AIC) is also applied to choose the appropriate reaction model.

Summary

- Vyazovkin nonlinear model-free (isoconversional) analysis showed different trends for different cases in the variation of activation energy with conversion. This trend also helps getting first hand information on the possible reaction steps involved during pyrolysis e.g. model-free analysis indicates the possible existence of four different reaction mechanisms in the different steps during catalytic decomposition of LDPE over ZSM-5 catalyst. The nonlinear Vyazovkin model-free analysis approach also narrows down the range of guess values of activation energy for optimization using traditional model-fitting methods. The estimated optimized kinetics triplet obtained by the model-free coupled with local optimization method (LOA) successfully predicted the experimental TGA data.
- The present work demonstrated that model-free analysis coupled with local optimization method (LOA) is as good as HGA for estimating the kinetics triplet.

List of Tables

Table 1.1. Plastic waste generation (Figures in thousands tones) in India

Table 1.2. Demand scenario for key commodity plastics (Figures in thousand tonnes) in India

Table 1.3. Indian PET market (tonnes) - current and projected

Table 1.4. Product yield from fluidized bed pyrolysis

Table 1.5. Composition of liquid fraction cracking of waste plastic

Table 1.6. Gas composition from the fluidised bed pyrolysis of LDPE in relation to pyrolysis temperature

Table 1.7. Aromatic compounds in the oils from the fluidised bed pyrolysis of LDPE waste in relation to temperature of pyrolysis (ppm)

Table 2.1. Various kinetics model functions and their integral forms

Table 2.2. Ranges of kinetics parameters used for sensitivity analysis

Table 3.1. Nonisothermal experimental conditions for TGA studies

Table 3.2. Isothermal experimental conditions for TGA studies

Table 3.3. The composition of Al-MCM-41 catalysts containing different amounts of aluminum

Table 3.4. TGA experimental conditions of catalytic decomposition of LDPE and PP over various commercial and synthesized catalysts for 20 wt% catalysts

Table 3.5. Experimental conditions for TGA studies using different percentages of catalysts

Table 3.6. Experimental conditions for TGA studies using optimum catalysts percentages

Table 3.7. Experimental conditions for reusability test

Table 4.1. Characteristics of samples (LDPE, PET, and PP)

Table 4.2. Textural properties of ZSM-5, FCC and n-HZSM-5

Table 4.3. Chemical composition and textural properties of Al-MCM-41 (present work and literature data)

Table 4.4. Effect of catalysts on PE decomposition temperatures

List of Tables

Table.4.5. Kinetics parameters derived from experiments for waste PET

Table 4.6. Kinetic parameters using different non-isothermal model fitting techniques

Table 4.7. Akaike's criterion analysis for isothermal curve fitting

Table 4.8. Present work and literature reported kinetic parameters

Table 4.9. Average values of kinetic parameters for waste LDPE

Table 4.10. Average values of kinetic parameters for waste PET

Table 4.11. Average values of kinetic parameters for waste PP

Table 4.12. Present work and literature reported kinetics parameters (N_2 atmosphere)

Table 4.13. Optimum kinetics triplet for PP decomposition with and without of Al-MCM-41 (sol-gel) using HGA

Table 4.14. The equation for calculation AIC_c results

Table 4.15. Activation energy and the effect of different catalysts on PP decomposition temperatures

Table 4.16. Start and end temperatures of different steps of ZSM-5 catalyzed waste LDPE sample

Table 4.17. Optimum kinetics triplet for LDPE decomposition in absence of ZSM-5

Table 4.18. Optimum kinetics triplet for LDPE decomposition in presence of ZSM-5 using HGA

Table 4.19. Optimum kinetics triplet for LDPE decomposition in presence of ZSM-5 using Model-free method coupled with direct search method

List of Figures

Figure 1.1. Waste management scenario in European Union

Figure 4.1. DSC analysis of waste PET sample

Figure 4.2. DSC analysis of virgin PET sample

Figure 4.3. DSC analysis of colorless waste LDPE sample

Figure 4.4. DSC analysis of color waste PE sample

Figure 4.5. DSC analysis of PP sample

Figure 4.6. Variation of conversion (α) with temperature during non-isothermal pyrolysis of waste LDPE sample at multiple heating rates

Figure 4.7. Variation of conversion (α) with temperature during thermal pyrolysis of waste PE samples

Figure 4.8. Variation of conversion (α) with temperature during non-isothermal pyrolysis of PP sample at multiple heating rates

Figure 4.9. Variation of conversion (α) with temperature during nonisothermal pyrolysis of virgin and waste PET sample

Figure 4.10. Variation of conversion (α) with temperature during pyrolysis of Pepsi bottles

Figure 4.11. Variation of rate of decomposition (dα/dT) with average temperature during non-isothermal pyrolysis of waste LDPE sample at multiple heating rates

Figure 4.12. Variation of rate of decomposition (dα/dT) with average temperature during non-isothermal pyrolysis of waste PE sample at multiple heating rates

Figure 4.13. Variation of rate of decomposition (dα/dT) with average temperature during non-isothermal pyrolysis of PP sample at multiple heating rates

Figure 4.14. Variation of rate of reaction (dα/dT) with temperature during nonisothermal pyrolysis of virgin and waste PET sample

Figure 4.15. Variation of rate of reaction (dα/dT) with temperature during pyrolysis of Pepsi bottles

Figure 4.16. Variation of conversion (α) with time during isothermal pyrolysis of waste and virgin PET sample

List of Figures

Figure 4.17. Variation of conversion (α) with time during isothermal pyrolysis of waste PE samples

Figure 4.18. XRD pattern of ZSM-5 zeolite catalyst

Figure 4.19. SEM micrograph of ZSM-5 zelolite catalyst

Figure 4.20. Nitrogen adsorption isotherm at 77 K of ZSM-5 catalysts

Figure 4.21. BJH (Desorption) pore size distribution of ZSM-5 catalyst

Figure 4.22. XRD pattern of fresh FCC catalysts

Figure 4.23. XRD pattern of spent FCC catalysts

Figure 4.24. EDX of fresh FCC catalysts

Figure 4.25. EDX of spent FCC catalysts

Figure 4.26. SEM of fresh FCC

Figure 4.27. SEM of spent FCC

Figure 4.28. Nitrogen adsorption isotherm at 77K of FCC catalysts

Figure 4.29. XRD pattern of Al-MCM-41 (hyd) catalysts

Figure 4.30. XRD pattern of Al-MCM-41 (sol-gel) catalysts

Figure 4.31. Nitrogen adsorption isotherm at 77 K of Al-MCM-41 (hyd) catalysts

Figure 4.32. Nitrogen adsorption isotherm at 77K of Al-MCM-41 (sol-gel) catalysts

Figure 4.33. BJH (Desorption) pore size distribution of Al-MCM-41 catalyst

Figure 4.34. XRD pattern of n-HZSM-5 catalysts

Figure 4.35. Nitrogen adsorption isotherm at 77K of n-HZSM-5 catalysts

Figure 4.36. SEM micrographs of n-HZSM-5

Figure 4.37. SEM micrograph of n-HZSM-5

Figure 4.38. Experimental TG curves for the catalytic pyrolysis of waste LDPE with different catalysts at 20wt %

Figure 4.39. Experimental DTG curves for the catalytic pyrolysis of waste LDPE with different catalysts at 20wt %

Figure 4.40. Experimental TG curves for the catalytic pyrolysis of PP with different catalysts at 20wt %

Figure 4.41. Experimental DTG curves for the catalytic pyrolysis of PP with different catalysts at 20wt %

List of Figures

Figure.4.42. Experimental TG curves for the catalytic pyrolysis of waste LDPE with different catalyst (ZSM-5) percentage

Figure. 4.43. Experimental DTG curves for the catalytic pyrolysis of waste LDPE with different catalyst (ZSM-5) percentage

Figure 4.44. Effect of catalyst (ZSM-5) on the maximum decomposition temperature

Figure 4.45. Variation of conversion (α) with temperature during catalytic nonisothermal pyrolysis of waste LDPE sample

Figure 4.46. Variation of rate of decomposition (dα/dT) with temperature during catalytic nonisothermal pyrolysis of waste LDPE sample

Figure 4.47. Experimental DTG curves for the catalytic pyrolysis of waste PP with different catalyst [Al-MCM-41(sol-gel) and Al-MCM-41(hyd)] percentage

Figure 4.48. Experimental TG curves for the catalytic pyrolysis of waste PP with different catalyst (Al-MCM-41(sol-gel)) percentage

Figure 4.49. Experimental DTG curves for the catalytic pyrolysis of waste PP with different catalyst (Al-MCM-41(sol-gel)) percentage

Figure 4.50. Effect of catalysts (Al-MCM-41) on reduction in maximum decomposition Temperature (ΔT_m)

Figure 4.51. Variation of conversion (α) with temperature during catalytic nonisothermal pyrolysis (18.5 wt % catalyst) of PP sample

Figure 4.52. Variation of rate of decomposition (dα/dT) with temperature during catalytic nonisothermal pyrolysis (18.5 wt % catalyst) of PP sample

Figure 4.53. Experimental TG curves for the different cycles of catalytic pyrolysis of PP with 17% catalyst (Al-MCM-41(sol-gel)

Figure 4.54. XRD pattern of Al-MCM-41(sol-gel) catalyst after seventh cycle (using Step Size=0.01º and Step time 0.5s)

Figure.4.55. Experimental TG curves for the catalytic pyrolysis of PP with different catalyst (n-HZSM-5) percentage

Figure 4.56. Experimental DTG curves for the catalytic pyrolysis of PP with different catalyst (n-HZSM-5) percentage

List of Figures

Figure 4.57. Effect of catalysts (n-HZSM-5) on reduction in maximum decomposition Temperature (ΔT_m)

Figure 4.58. Variation of conversion (α) with temperature during catalytic nonisothermal pyrolysis (50 wt % n-HZSM-5 catalyst) of PP sample

Figure 4.59. Variation of rate of decomposition (dα/dT) with temperature during catalytic nonisothermal pyrolysis (50 wt % n-HZSM-5 catalyst) of PP sample

Figure 4.60. GC chromatogram for pure propane

Figure 4.61. GC chromatogram for n-hexane

Figure 4.62. GC chromatogram for heptanes

Figure 4.63. GC chromatogram for benzene

Figure 4.64. GC chromatogram for pure toluene

Figure 4.65. GC chromatogram for indene

Figure 4.66. GC chromatogram for naphthalene (0.005% naphthalene, 99.99% toluene)

Figure 4.67. GC chromatogram for biphenyl (2% Biphenyl, 49% acetonitrile, and 49% tetrahydrofuran)

Figure 4.68. GC chromatogram for fluorene (0.5% fluorene, methanol 99.5%)

Figure 4.69. GC chromatogram for the thermal decomposition of waste PET

Figure 4.70. GC chromatogram for the thermal decomposition of waste LDPE sample

Figure 4.71. GC plot for the thermal decomposition of LDPE

Figure 4.72. GC plot for the thermal decomposition of LDPE

Figure 4.73. GC chromatogram for the thermal decomposition of PP sample

Figure 4.74. GC plot for the thermal decomposition of PP sample

Figure 4.75. GC plot for the thermal decomposition of PP sample

Figure 4.76. GC plot for the catalytic decomposition of waste LDPE over fresh FCC catalysts

Figure 4.77. GC plot for the catalytic decomposition of PP over fresh FCC catalysts

Figure 4.78. GC plot for the catalytic decomposition of waste LDPE over ZSM-5 catalysts

List of Figures

Figure 4.79. GC plot for the catalytic decomposition of waste LDPE over ZSM-5 catalysts [66]

Figure 4.80. GC plot for the catalytic decomposition of PP over ZSM-5 catalysts

Figure 4.81. GC plot for the catalytic decomposition of waste LDPE over Al-MCM-41 catalysts

Figure 4.82. GC plot for the catalytic decomposition of waste LDPE over Al-MCM-41 catalysts [66]

Figure 4.83. GC plot for the catalytic decomposition of PP over Al-MCM-41 catalysts

Figure 4.84. GC plot for the catalytic decomposition of waste LDPE over n-HZSM-5 catalysts

Figure 4.85. GC plot for the catalytic decomposition of waste LDPE over n-HZSM-5 catalysts [66]

Figure 4.86. GC plot for the catalytic decomposition of PP over n-HZSM-5 catalysts

Figure 4.87. Dependency of exact and optimal $\ln(k_0/\beta)$ upon optimal E obtained from SDMT technique

Figure 4.88. Percentage deviation of the simulation results for nonisothermal

Figure 4.89. Simulations and the experimental data for nonisothermal decomposition (waste PET) using SDMT (multiple heating rates) for first order model

Figure 4.90. Simulations and the experimental data for nonisothermal decomposition (waste PE) using SDMT (multiple heating rates) for first order model (with standard deviation 0.02314, 0.03063, 0.002266 and 0.030359 respectively)

Figure 4.91. Isothermal (685K) prediction from various model fitting kinetics analysis techniques at a heating rate of 10K min^{-1}

Figure 4.92. Isothermal (711K) prediction from SDMT (multiple heating rates)

Figure 4.93. Dependency of First order sensitivity coefficient on temperature for $\tilde{K}_0$

Figure 4.94. Dependency of First order sensitivity coefficient on temperature for E

Figure 4.95. Dependency of First order sensitivity coefficient on temperature for n

Figure 4.96. Dependency of First order sensitivity coefficient on temperature for β

Figure 4.97. Dependency of second order sensitivity coefficient on temperature for $\tilde{K}_0$

List of Figures

Figure 4.98. Dependency of second order sensitivity coefficient on temperature for E

Figure 4.99. Dependency of second order sensitivity coefficient on temperature for n

Figure 4.100. Dependency of second order sensitivity coefficient on temperature for β

Figure 4.101. Dependency of cross second order sensitivity coefficient on temperature for $\tilde{K}_0$ E

Figure 4.102. Dependency of cross second order sensitivity coefficient on temperature for $\tilde{K}_0$ n

Figure 4.103. Dependency of cross second order sensitivity coefficient on temperature for $\tilde{K}_0$ β

Figure 4.104. Dependency of cross second order sensitivity coefficient on temperature for En

Figure 4.105. Dependency of cross second order sensitivity coefficient on temperature for Eβ

Figure 4.106. Dependency of cross second order sensitivity coefficient on temperature for nβ

Figure 4.107. Comparison between simulated (using HGA predicted kinetics triplet) and experimental mass loss during non-isothermal pyrolysis of LDPE at five different heating rates for nucletion and growth (n=2/3) model (Experimental data and Simulated data)

Figure 4.108. Comparison between simulated (using HGA predicted kinetics triplet) and experimental mass loss during non-isothermal pyrolysis of PET at four different heating rates for nucletion and growth (n=2/3) model (Experimental data and Simulated data)

Figure 4.109. Comparison between simulated (using HGA predicted kinetics triplet) and experimental mass loss during non-isothermal pyrolysis of PP at five different heating rates for nucletion and growth (n=2/3) model (Experimental data and Simulated data)

Figure 4.110. Comparison of (mass loss Vs temperature) curves of different models having very less AIC_c scores with experimental values for LDPE and at 10Kmin^{-1}

List of Figures

Figure 4.111. Comparison between simulated (using HGA predicted kinetics triplet) and experimental mass loss during catalytic decomposition of PP over Al-MCM-41 (sol-gel) catalyst at five different heating rates for n^{th} order reaction model (Exp, Experimental data and Cal, Calculated data)

Figure 4.112. Comparison between simulated (using HGA predicted kinetics triplet) and experimental mass loss during catalytic decomposition of PP over Al-MCM-41 (sol-gel) catalyst at five different heating rates for Nucleation and Growth model (n=2/3) (Exp, Experimental data and Cal, Calculated data)

Figure 4.113. Comparison between simulated (using HGA predicted kinetics triplet) and experimental mass loss during catalytic decomposition of PP over n-HZSM-5 catalyst at five different heating rates for Nucleation and Growth model (n=2/3) (exp, experimental data and simu, simulated data)

Figure 4.114. Dependency of activation energy on conversion of nonisothermal decomposition of waste PET samples using model free isoconversion technique and Agrawal and Sivasubramanian approximation method to evaluate the temperature integral

Figure 4.115. Comparison of direct integration method and approximation relations used in model free kinetics analysis.

Figure 4.116. Dependency of activation energy on conversion using model free iso-conversion technique for nonisothermal (Agrawal and Sivasubramanian approximation [187]) and isothermal decomposition of waste PET samples

Figure 4.117. Percentage deviation from experimental data for isothermal (685K) prediction at different heating rates using Agrawal and Sivasubramanian approximation [187] (The ARD values are 11.59, 1.51, 11.80 and 9.24 respectively for heating rates 5, 10, 15 and 25°C min^{-1})

Figure 4.118. Dependency of activation energy on conversion of nonisothermal decomposition of waste PE sample using model free isoconversion

technique using direct numerical integration and approximation of Cai et al. [186] to evaluate the temperature integral

Figure 4.119. Percentage deviation from direct numerical integration (The %ARD values are 0.04225, 0.01145, 0.00377 and 0.00104 respectively for Coats and Redfern, Gorbachev, Agrawal &Subramanian [187] and New approximation (Cai et al. [186]))

Figure 4.120. Comparison of the dependency of activation energy on conversion using model free isoconversion technique under nonisothermal (direct numerical integration) and isothermal for decomposition of waste PE and PET [174] samples

Figure 4.121. Comparison between present work and the literature reported data (Lyon [157], Peterson et al. [38], and Gao et al. [134]) for variation of E_α with α

Figure 4.122. Prediction at different heating rates using direct integration for isothermal data (708K) (The %ARD values are 21.133, 5.4928, 18.674and 12.229 respectively for heating rates 10, 15, 20 and 25°C min^{-1})

Figure 4.123. Dependency of activation energy on conversion of catalytic and noncatalytic nonisothermal decomposition of waste LDPE sample (present work and literature reported data)

Figure 4.124. Dependency of activation energy on conversion of catalytic and noncatalytic nonisothermal decomposition of PP sample (present work and literature reported data)

Figure 4.125. Dependency of activation energy on conversion of catalytic nonisothermal decomposition of waste LDPE sample

Figure 4.126. Variation of rate of decomposition ($d\alpha/dT$) with temperature during catalytic nonisothermal pyrolysis of waste LDPE sample at 10$Kmin^{-1}$ heating rate

Figure 4.127. Comparison between simulated (using HGA predicted kinetics triplet) and experimental mass loss during noncatalytic and catalytic decomposition of

waste LDPE at heating rate of 10 K min^{-1} (Standard Deviation: 0.031 and 0.009 for noncatalytic and catalytic decompositions respectively)

Figure 4.128. Comparison between simulated (using Model-free coupled with direct search method) and experimental mass loss during noncatalytic and catalytic decomposition of waste LDPE at heating rate of 10 K min^{-1} (Standard Deviation: 0.034 and 0.007 for noncatalytic and catalytic decompositions respectively)

List of Symbols

α	the conversion of the reaction, $\alpha = (W_0 - W)/(W_0 - W_\infty)$
W_0	the initial weight of the sample, (mg)
W	the sample weight at any temperature T, (mg)
W_∞	the final sample weight, (mg)
t	time (minutes)
T	the temperature (K)
T_{w0}	the temperature at which $\alpha=0$, (K)
T_d	the temperature at which decomposition starts, (K)
T_m	the temperature at which the maximum weight loss rate occurs, (K)
$T_{W\infty}$	the temperature at the end of the pyrolysis step, (K)
$\frac{d\alpha}{dt}$	the rate of reaction (min^{-1}),
$f(\alpha)$	the reaction model
n	order of the chemical reaction
k_0	the pre-exponential factor (K^{-1})
E	the activation energy (kJ mol^{-1})
R	the universal gas constant (kJ mol^{-1} K^{-1}).
β	the heating rate (K min^{-1})
$\frac{d\alpha}{dT}$	the rate of conversion or reaction (K^{-1})
T_{avg}	average temperature (K), $(T_{i+1}+T_i)/2$
$g_m(\alpha)$	the integral form of reaction model, m
E_α	activation energy, at a particular conversion, α
$Ei(u)$	$\int_u^\infty \frac{\exp(-u)}{u} du$, exponenial integral
u	the ratio of $\frac{E_\alpha}{RT}$
$\tilde{K}_0$	logarithm of the ratio of $\frac{k_0}{\beta}$
$\Omega(E_\alpha)$	a minimization function of E_α for model-free analysis technique

List of Symbols

$\Delta(E, K_0, n)$	a minimization function of kinetics triplet for model-fitting analysis technique
Δ (E)	a minimization function of E for SDMT technique
$I(E_\alpha, T_{\alpha i})$	temperature integral of Arrhenius equation
AIC	score of Akaike's Information Criteria
AIC_c	the corrected score of Akaike's Information Criteria
SS	sum of square of vertical distance of the points from the centre
$\sigma^2(p_i)$	variance of parameters p_i (i.e. $\tilde{K}_0$, E, n and β)
$S^{\langle 1 \rangle}_{\alpha p_i}$	first order sensitivity co-efficient of parameter p_i
$S^{\langle 2 \rangle}_{p_i}$	second order sensitivity co-efficient
$S^{\langle 2 \rangle}_{p_i p_j}$	second order cross sensitivity co-efficient with respect to other parameter p_j, where i≠j
$M_{Exp,i,l,0}$	the initial weight
$M_{Exp,i,l,\infty}$	the final weight

Subscripts

i	data point counter
j	data point counter
l	heating rate
m	the reaction model
o	initial data point
∞	end data point
Exp	Experimental data
Cal	Calculated data

Table of Contents

Abstract i

Summary iv

List of Tables x

List of Figures xii

List of Symbols xxi

Chapter 1. Introduction and literature review 1

1.1. Introduction 1

1.1.1. Land filling 3

1.1.2. Incineration 4

1.1.3. Mechanical material recycling 5

1.2. Importance of the work 7

1.3. Objectives of the work 9

1.4. Literature review 10

1.4.1. Thermal decomposition of waste plastic 10

1.4.1.1. Thermal pyrolysis reactors and products 10

1.4.1.2. Thermal dehydrochlorination (DHC) 13

1.4.1.3. Thermal decomposition mechanism of polymers 14

1.4.1.4. Co-processing of waste plastic 19

1.4.2. Catalytic decomposition of waste plastics 20

1.4.2.1. Catalytic dehydrochlorination (DHC) 24

1.4.2.2. Catalytic pyrolysis mechanism of polymers 25

1.4.3. Pyrolysis kinetics analysis 32

1.4.3.1. Mechanistic model for kinetics analysis 33

1.4.3.2. Thermogravimetric kinetics analysis 35

1.4.3.2.1. Model-fitting method of analysis for noncatalytic decomposition 35

Table of Contents

1.4.3.2.2. Model-free (isoconversional) method of analysis for noncatalytic decomposition 40

1.4.3.2.3. Model-fitting method of analysis for catalytic decomposition 42

1.4.3.2.4. Model-free (isoconversional) method of analysis for catalytic decomposition 42

1.4.3.3. Optimization techniques for the kinetics analysis of TGA data 44

Table 1.1.-1.7. 48

Figure 1.1. 53

Chapter 2. Kinetics analysis 54

2.1. Single step kinetics model 54

2.1.1. Model-fitting methods of kinetics analysis using TGA experimental data 55

2.1.1.1. Model-fitting method for isothermal experiments Akaike's Information Criteria (AIC) 56

2.1.1.2. Model-fitting methods for nonisothermal experiments using single heating rate 57

2.1.1.2.1. n^{th} Order Model technique 57

2.1.1.2.2. Friedman technique 58

2.1.1.2.3. Freeman-Carroll technique 58

2.1.1.2.4. Chang technique 59

2.1.2. ASTM E698 technique 59

2.2. Model-free isoconversional method 60

Table of Contents

2.2.1. Model-free isoconversional method for isothermal condition 60

2.2.2. Vyazovkin model-free kinetics technique for non-isothermal condition 61

2.2.2.1. Direct integration of temperature integral 63

2.2.2.2. Approximations for integration of the temperature integral 64

2.3. Development of objective function (multi-parameter) for optimization of kinetics triplet using single and multi-heating rate(s) 65

2.4. Sensitivity analysis of pyrolysis kinetics 66

2.4.1. Computation of first order sensitivity matrix 67

2.4.2. Computation of second order and second order cross sensitivity matrix 68

2.5. Development of single-parameter objective function 69

2.5.1. Standard deviation minimization technique (SDMT) for non-isothermal condition using multi-heating rates 70

2.6. Simulation of TGA data 71

2.6.1. Nonisothermal data prediction 71

2.6.2. Prediction of isothermal kinetics from nonisothermal data 72

2.6.3. ASTM E698 prediction 73

2.7. Multi-steps and multi-heating rates model-fitting method for nonisothermal experiments 74

2.7.1. Multi-parameter optimization 74

2.7.1.1. Model-free coupled multi-parameters optimizations 75

2.7.1.2. Hybrid genetic algorithm (HGA) for three-parameter optimization 76

Table of Contents

2.7.1.2.1. The structure of a hybrid genetic algorithm 76

2.7.1.2.2. Structure of HGA used for the present work 77

Table 2.1.-2.2. 78

Chapter 3. Experimental 80

3.1. Polymer materials for noncatalytic pyrolysis 80

3. 2. Characterization of polymers 80

3.2.1. Differential scanning calorimetry (DSC) analysis 81

3.3. Experimental procedure and instrument for thermal pyrolysis 81

3.3.1. Nonisothermal thermogravimetry experiments for polymer 81

3.3.2. Isothermal thermogravimetry experiments 82

3.4. Experimental procedure and instrument for catalytic pyrolysis of polymers 83

3.4.1. Polymer materials for catalytic pyrolysis 83

3.4.2. Catalysts 83

3.4.3. Catalysts synthesis 83

3.4.3.1. Synthesis of sol-gel Al-MCM-41 83

3.4.3.2. Synthesis of hydrothermal Al-MCM-41 84

3.4.3.3. Synthesis of n-HZSM-5 84

3.4.3.4. Calcination 85

3.4.4. Catalysts characterization 85

3.4.4.1. X-ray diffraction method 85

3.4.4.2. Scanning Electron Microscopy (SEM) 86

3.4.4.3. BET analysis 86

3.4.5. Catalytic decomposition 86

3.4. 5.1. Experimental procedure and equipment 86

Table of Contents

3. 4.5.2. Reusability of Al-MCM-41 (sol-gel) 87

3.5. Products analysis 87

Table 3.1.-3.7. 89

Chapter 4. Results and discussion 96

4.1 Characterization of the polymers used 96

4.1.1. DSC analysis 97

4.2. Thermal pyrolysis of plastics 97

4.2.1. Nonisothermal decomposition 97

4.2.2. Isothermal decomposition 99

4.3. Characterization of catalysts 100

4.3.1. Characterization of ZSM-5 catalyst 100

4.3.2. Characterization of Fresh FCC and spent FCC catalysts 101

4.3.3. Characterization of Al-MCM-41 catalysts 102

4.3.4. Characterization of n-HZSM-5 catalysts 103

4.4. Comparison of Catalytic activities of different catalysts determined by TG analysis 104

4.4.1. Catalytic activities of different catalysts on waste LDPE 104

4.4.2. Catalytic activities of different catalysts on pure PP 106

4.5. Individual Catalyst activity on plastics 107

4.5.1. Catalytic activity of ZSM-5 for waste LDPE decomposition 108

4.5.1.1 Catalytic nonisothermal decomposition at several heating rates 110

4.5.2. Catalytic activity of sol-gel and hydrothermal Al-MCM-41 for PP decomposition 111

4.5.2.1. Determination of optimum catalyst (sol-gel Al-MCM-41) concentration 112

4.5.2.2. Catalytic nonisothermal decomposition at several heating rates 114

Table of Contents

4.5.2.3. Reusability study of sol-gel Al-MCM-41 catalyst 114

4.5.3 Catalytic activity of n-HZSM-5 for PP decomposition 114

4.5.3.1 Catalytic nonisothermal decomposition at several heating rates 116

4.6. Product analysis using Gas chromatograph (GC) 117

4.6.1. GC analysis of standard samples 117

4.6.2. GC analysis of thermal decomposition products 118

4.6.2.1. GC analysis of products from waste PET sample 118

4.6.2.2 GC analysis of products from waste LDPE sample 118

4.6.2.3 GC analysis of products from PP sample 119

4.6.3. GC analysis of catalytic decomposition products 120

4.6.3.1. GC analysis of catalytic decomposition of waste LDPE and PP samples over fresh FCC catalysts 120

4.6.3.2. GC analysis of catalytic decomposition of waste LDPE and PP samples over ZSM-5 catalysts 121

4.6.3.3. GC analysis of catalytic decomposition of waste LDPE and PP samples over Al-MCM-41 catalysts 122

4.6.3.4. GC analysis of catalytic decomposition of waste LDPE and PP samples over n-HZSM-5 catalysts 123

4.7. Kinetics analysis of pyrolysis of plastics 124

4.7.1. Model-fitting methods for nonisothermal experiments using single and multiple heating rate(s) 124

4.7.1.1. n^{th} order model and ASTM E698 techniques 124

4.7.1.2. Freeman-Carroll, Friedman, and Chang techniques 126

Table of Contents

4.7.1.3. Standard deviation minimization technique (SDMT) for non-isothermal condition using single and multi-heating rate(s) 127

4.7.2. Model-fitting methods for isothermal experiments 128

4.7.3. Numerical simulation 129

4.7.3.1. Nonisothermal data prediction 129

4.7.3.2. Isothermal data prediction 129

4.7.4. Sensitivity analysis 130

4.7.4.1. First order sensitivity analysis 130

4.7.4.2. Second order sensitivity analysis 131

4.7.4.3. Second order cross sensitivity analysis 131

4.7.5. Hybrid genetic algorithm (HGA) to find the best model and the globally optimized overall kinetics parameters for thermal decomposition of plastics 132

4.7.5.1. Prediction of experimental TGA data 133

4.7.5.2. Hybrid genetic algorithm (HGA) for pyrolysis kinetics of Al-MCM-41 and n-HZSM-5 catalyzed decomposition of PP 135

4.7.6. Model-free analysis 137

4.7.6.1. Model-free analysis for waste PET sample 137

4.7.6.2. Model-free analysis for waste PE sample 139

4.7.6.3. Model-free analysis for waste LDPE sample 143

4.7.6.4. Model-free analysis for PP sample 143

4.7.6.5. Model-free analysis for waste LDPE over ZSM-5 144

Table of Contents

4.7.6.6. Model-free analysis for waste PP over Al-MCM-41and n-HZSM-5 144

4.7.7. Hybrid genetic algorithm (HGA) and model free coupled direct search methods for pyrolysis kinetics of ZSM-5 catalyzed decomposition of waste LDPE 147

4.7.7.1 Prediction of experimental TGA data 148

Table 4.1.- 4.19. 150

Figure 4.1.- 4.128. 167

Chapter 5. Conclusion 280

Scope of Future Work 284

Literature cited 285

Appendix I 303

Appendix II 311

Chapter 1

1. Introduction and literature review

Waste generation rate is a result of socio-economic development of a country. The waste usually includes food waste, newsprint, corrugated cardboard, mixed cardboard, polyethylene (PE), polypropylene (PP), polystyrene (PS), polyvinyl chloride (PVC), polyethylene terephthalate (PET) and tyres. Thermal and/or catalytic pyrolysis of waste plastics is drawing more and more interest on the perspective of solid waste management since they are alternative source of energy and/or chemical raw materials.

This chapter discusses the use of plastics as well as advantages and disadvantages of different existing plastic waste management methods such as land filling, incineration, and recycling for treatment of solid wastes generated from the plastics use. It elaborates the importance of the research work along with the objectives. The chapter subsequently presents detailed literature review that include thermal and catalytic pyrolytic decomposition of waste plastics, thermal and catalytic dehydrochlorination (DHC), co-processing of waste plastics, thermal and catalytic pyrolysis/decomposition kinetics analysis of polymers, thermal and catalytic decomposition mechanism, sensitivity analysis and optimization methods such as hybrid genetic algorithm.

1.1. Introduction

Plastic with its exclusive qualities of being light yet strong and economical, has invaded every aspect of our day-to-day life. It has many advantages: it is durable, light, easy to mould, and can be adapted to different user requirements. Once hailed as a 'wonder material', plastic is now a serious worldwide environmental and health concern,

essentially due to its nonbiodegradable nature. Plastics have use in all sectors of the economy–infrastructure, construction, agriculture, consumer goods, telecommunications, health care, transportation, defense, and packaging. Plastics are so versatile in use that their impacts on the environment are extremely wide ranging. Careless disposal of plastic bags chokes drains, blocks the porosity of the soil, and causes problems for groundwater recharge. Plastic disturbs the soil microbe activity, and once ingested, can kill animals. Plastic bags can also contaminate foodstuffs due to leaching of toxic dyes and transfer of pathogens [1]. Low income countries have the lowest percentage of urban populations and the lowest waste generation rates ranging between 0.4 to 0.9 kg per capita per day. The countries with middle-income range have waste generation rates ranging from 0.5 to 1.1 kg per day. The high income countries show the greatest generation rates which vary from 1.1 to 5.07 kg per capita per day [2]. India will probably see a rise in waste generation from less than 40,000 metric tonnes per year to over 125,000 metric tonnes by the year 2030 [3]. Table 1.1 shows the plastic generation trend in India [4]. The waste fractions considered are the combustible and recyclable or compostable fractions of municipal solid waste (MSW) which includes food waste, newsprint, corrugated cardboard, mixed cardboard, polyethylene (PE), polypropylene (PP), polystyrene (PS), polyvinyl chloride (PVC) and polyethylene terephthalate (PET). Table 1.2 presents the demand scenario for key commodity plastics [4]. Packaging presents a major growth area where there has been an increasing demand for plastics and 52% of the plastics produced in India are utilized for packaging (Table 1.2) [4]. Among the commodity plastics, low-density polyethylene (LDPE) is used in the manufacture of carry bags and PET is used in packaging beverages like soft drink and mineral water. PET in particular presents a major

growth area in the years to come. Indian PET consumption has grown at an annual rate of 30% and the current PET consumption is estimated to be around 45,000 tones per annum and with this projected growth the Indian PET consumption will double in the next three years (Table 1.3) [5]. The LDPE consumption for the year (2001-2002) is 3, 03,000 tonnes and is expected to increase to 534, 000 tonnes in the year (2006-2007) [5].

The most common ways to treatment of the solid waste are land filling, incineration, and materials recycling. Waste is sometimes regarded as an alternative fuel. Therefore, it is necessary to identify advantages and disadvantages of the common methods for treatment of plastics waste which are discussed in the subsequent sections.

1.1.1. Land filling

Open dumping is the most commonly accepted way of disposing waste in India. Waste is collected and transported outside city limits and deposited along highways or low-lying areas. The unscientific and chaotic dumping of municipal solid wastes (MSW) has created overflowing landfills, serious emissions, and ground water pollution. The landfill gas contains 50-60% methane, which is a green house gas contributing significantly to global warming [6]. This is one reason for the policy in many countries to reduce land filling of organic materials. Yedla and Parikh [7] have proposed a system called purpose built landfill (PBLF) for the control of methane emissions from MSW. Based on certain theoretical considerations multivariate functional models (MFMs) are developed to estimate methane mitigation and energy generating potential of the proposed system. It has been found that the proposed methodology not only controlled methane emissions to the atmosphere but also could yield considerable energy in terms of landfill gas (LFG).

1.1.2. Incineration

Incineration is an alternative option that is widely practiced in developed countries with energy recovery popularly called Waste to Energy. Incineration with energy recovery is a feasible option in countries where material recycling is low and waste has a high calorific value. In the case of India, incineration with energy recovery may not be a feasible option, considering the fact that in India material recycling of plastics is as high as 60% and the MSW is characterized by its low calorific value, high moisture content, and high quantity of non-combustibles [8]. Moreover, incinerators pollute the environment with highly toxic substances like heavy metals, dioxins, and furans [9]. During 1980s an incineration plant was set up at New Delhi, India using Danish technology. It was also expected to generate power for local grid. But the operational experience of this plant was not satisfactory [10].

Modern incinerators are specifically designed to treat the hazardous waste generated by Hospital, Chemical, Pharmaceuticals/bulk drugs, and Pesticides units. The sensitive nature of the waste demands customized attention and the scheme has to be tailor made to meet the requirements of individual customers. M/s Thermax India Ltd. also introduced the volatile organic compounds (VOCs) range of incinerators to destroy the gaseous waste containing odourous VOCs. This range had been specifically developed initially for the U.K. market and is designed to meet the stringent norms set by its regulatory authorities [11]. The Gujarat-based Institute of Plasma Research is developing plasma based new incineration system in India. The Facilitation Center for Industrial Plasma Technology (FCIPT) has developed a new Hospital Waste Incinerator that can handle all types of hospital wastes and eliminates the need for segregation of waste into different

categories. Since over emissions of toxic pollutants is the major concern of this technology [9], further research is still needed in this direction to make it eco-friendly process. So, answer to the question "whether the energy from waste is viable or not" is that "energy recovery should be encouraged as an alternative to landfill, but not at the expense of practicable waste prevention, recycling and composting" [12].

1.1.3. Mechanical material recycling

In many countries, the legislative measures are being implemented which set clear guidelines for waste management to reduce the land filling of organic materials imposing land filling tax and causing emission from inclinator for recovery of energy by means of burning. Life cycle assessment (LCA) tool is used to compare different alternative waste treatment strategies. The simulation model Orware (organic waste research) for the material and energy flows in waste management based on life cycle assessment (LCA) was used in the quantification of emissions, energy use and financial costs. The results suggest the environmental preference of recycling over incineration over land filling [13]. Mechanical recycling mainly involves the melting and remodeling of waste plastic, which produce low grade plastic. Plastics' recycling rate is very high (60%) in India [8]. Efforts to improve recycling rates and to reduce household and commercial waste are led by the US Environmental Protection Agency (EPA). Today, the US recycles about 28% of its waste, which has almost doubled during the past 15 years. Recycling of specific materials has grown even more drastically: 42% of all paper, 40% of all plastic soft drink bottles, 55% of all aluminium beer and soft drink cans, 57% of all steel packaging, and 52% of all major appliances are now recycled. Figure 1.1 shows waste management scenario in European Union [14]. Recycling industry has emerged parallel to the virgin plastic

industry in India. There are more than 2500 recycling units with an average output of 350 tonnes per annum. These 2500 recycling units recycle 60% of the plastic waste generated in the country. The whole process of recycling, starting from sorting to the final reprocessing of plastic waste, is done by experience. The sorting of plastic scrap is done on the basis of colour, transparency, hardness, density and opacity. The sorted waste is sent to the granulators, which make granules from the plastic scrap. The converters are small industrial units that process the granules into finished products. One of the problems in reprocessing is that the source of plastic waste is difficult to be traced, and it is very likely that these may include bottles and packaging from pesticides also. In such cases, it may lead to major health and environmental problems. Wastewater is generated during the recycling process when the plastic scrap is cleaned to remove the dirt and foreign matter adhering to it. The wastewater has high pollution load in terms of biological oxygen demand (BOD), chemical oxygen demand (COD), and total suspended solid (TSS) depending on the material. This water needs proper treatment before disposal into the drains. Although PE and PET are less toxic than polyvinyl chloride (PVC), the incomplete combustion of PE releases carbon monoxide. Since toxic dyes and chemicals are used as additives during the recycling, the hygienic conditions of most reprocessing units in the informal sector are poor [5].

Thus, there are several issues of concern in plastic recycling that need immediate attention. These issues pertain to the health and hygiene of the workers involved in the reprocessing trade, upgrading of processing equipments used in the recycling of plastics, quality of the effluent from the recycling plants, and finally, the quality of the products from recycled plastics waste [5].

1.2. Importance of the work

Due to gradual depletion of world petroleum reserves and the impact of environmental pollution of increasing exhaust emissions, there is an urgent need for suitable alternative energy sources. The use of lesser amounts of fossil fuel and increased supply of energy can only be met by a planned harnessing of more renewable energy sources. Choosing the right options requires a critical understanding of the science and technologies involved. We need to know how our energy options affect the health of the planet and the human species, and impact on other life necessities. We need to know the way to produce and distribute energy. We also need to take into account of the social, ethical, economic, and political consequences of our choices. Finally, we need to question some of the most deeply held assumptions of the dominant model of unlimited unsustainable growth based on competition and market forces.

We can concentrate on the energy options that are most immediately available, the most promising and the most contentious i.e. nuclear, biofuels, wind, solar, and energy from wastes [1]. Analysis of Moh'd Abu Qudais et al [15] revealed that the average energy content of MSW is 2747 kcal/kg where energy content in waste plastic is 6662 kcal/kg. The utilization of solid waste such as waste plastic, paper, scrap tire in energy recovery is promising way of recycling. To overcome the associated demerits of land filling, incineration, and recycling; to develop value added products from waste plastics such as activated carbon, liquid fuel and gaseous product; and to recover monomer from the plastics; pyrolysis or catalytic cracking are the most popular alternative methods for treatment of solid waste [16]. In this process, waste plastics breakdown to give oil, wax, high calorific value gaseous product, and residual solid carbon [16-28]. There are some

valuable aromatic chemicals (limonene, indene, styrene, xylene and naphthalene) found in the oil that can be useful in petrochemical industries. The residual carbon is being upgraded to produce a high-grade activated carbon. The condensed liquids obtained from pyrolysis of urban solid waste in the form of scrap tire, waste paper and waste plastic were analyzed for their properties as fuels and compared with petroleum-derived products. The results showed that the pyrolysis of urban solid waste might be a potential source of liquid hydrocarbon fuel [17]. Various novel and innovative energy efficient and environmentally sound pyrolysis and gasification technologies have also been developed for disposal of waste [18-19].

The kinetics study of pyrolysis is important to know the decomposition mechanism, rate of reaction, reaction parameters and to predict the products distribution. This in turn helps in proper selection of reactor, optimization of the reactor design and operating conditions. Thermogravimetic analysis (TGA) coupled with model-fitting approach is commonly used for such studies to evaluate the apparent overall kinetic parameters such as activation energy, pre-exponential factor and the reaction model (kinetics triplet). In most of the reported literatures, model-fitting methods are applied to evaluate pyrolysis kinetics parameters using single heating rates and traditional n^{th} order reaction model. The traditional model-fitting kinetics analysis using single heating rates and single step n^{th} order decomposition model gives a single set of kinetics triplet, which is estimated after minimizing deviation between experimental and simulation data. However, presently, International Confederation of Thermal Analysis and Calorimetry (ICTAC) project, 2000 ruled out the validity of thermal kinetics analysis using single heating rate [29]. Modern model-fitting thermal kinetics analysis methods use multi-heating rates;

take care of multi-step reactions and incorporate possible partial diffusion, back reaction, branch reaction, etc. in the model equations [30-31]. Still the selection of appropriate model and initial guess of kinetics parameters are major drawback of model fitting methods [31]. Moreover, the kinetics triplet obtained by model-fitting technique from non-isothermal condition is highly uncertain. This uncertainty mainly comes from model incorrectness, experimental error, initial value approximations and the drawbacks associated with many optimization techniques to find out the global optimum. Vyazovkin model-free approach through use of isoconversion method is a trustworthy way of obtaining reliable and consistent kinetic information from nonisothermal data. It also helps to reveal the complexity of multiple reactions due to the dependencies of activation energy on the extent of conversion [30-38]. The present research work aims at investigating the thermal and catalytic decomposition behaviour of the commodity plastics and kinetics analysis methods to establish reliable and globally optimum kinetics triplet.

1.3. Objectives of the work

The present research project has been undertaken with the following objectives.

- To investigate the thermal decomposition behaviour of commodity plastics that include both virgin and waste PET, PE, and PP samples using thermogravimetry analyzer (TGA)
- To investigate the catalytic decomposition behaviour of the plastic samples using TGA over various commercially available and laboratory synthesized catalysts
- To find out the optimum catalyst percentage and catalyst reusability
- To analysis the products evolve during catalytic and noncatalytic pyrolysis

- To evaluate reliable and optimum overall kinetics parameters for both thermal and catalytic decomposition through improvement of existing and/or development of new kinetics analysis techniques

1.4. Literature review

This section describes published experimental and theoretical works relevant to the present work. It discusses in detail the thermal and catalytic decomposition behaviour of plastics, associated mechanism for decomposition and distribution of products out of such decomposition. It further elaborates the model-fitting and model-free methods employed for the analysis of the decomposition kinetics to evaluate of kinetics parameters. Finally it highlights the optimization procedures used during the kinetics analysis.

1.4.1. Thermal decomposition of waste plastic

Thermal pyrolysis has a great potential for utilization of plastic waste as a feedstock in petrochemical industry. This process mainly involves the chain scission mechanism to break the long chain polymer at very high temperature into gas, oil and residue under inert environment. The product composition depends on the process condition and type of plastics used. Tables 1.4-1.6 show the typical product yield of these three fractions obtained from the pyrolysis of different type of plastics at different pyrolysis conditions.

1.4.1.1. Thermal pyrolysis reactors and products

Various types of reactors are employed for catalytic multiphase reactions such as fixed bed with combustion zone (tickle bed reactor, monolith reactor (low pressure drop) and adiabatic fixed bed reactor), mechanically stirred tank rector or simply CSTR, and moving bed reactor (fluidized bed reactor (FBR) such as Bubbling FBR, Circulating FBR) along with regeneration unit. Various types of FBRs and fixed bed reactors were

employed for thermal degradation under nitrogen or hydrogen environment. But catalytic pyrolysis was mostly performed in a fixed bed reactor under nitrogen, steam and hydrogen environment. Most of the thermal and catalytic pyrolysis experiments were so far performed on virgin plastics as feed materials. Further experiments are needed for real plastics mixture in presence of novel catalyst, which is suitable for tickle bed reactor or fluidized bed reactors. Proper reactor selection ensure safety operation and make it environmental friendly process which gives higher conversion, maximum selectivity, high throughput, easy scale up and minimum overall process cost. To select proper reactor one must know the number and type of phases involved (Gas, liquid and solid), contacting pattern (counter-current, co-current, cross-current), reactions kinetics and the reaction parameters, operating temperature**,** RTD distribution (degree of mixing: high degree of mixing is advantageous for isothermal operation in FBR), reactor material properties, physical properties of reactants and products, temperature control and heat transfer rate (heat transfer co-efficient), catalyst deactivation (time, regeneration and deactivation mechanism such as sintering, poising, coking etc), energy requirements (pumping, heating etc), hydrodynamics of the reactors, reactor size, and scale up (fixed bed reactor easy to scale up than fluidized bed reactor) [39].

Municipal solid waste (MSW) pyrolysis in an externally heated fixed bed reactor showed that the pyrolysis derived oil is a potential source of liquid hydrocarbons [17]. Fluidized bed [23-26, 40-42] and internally circulating fluidized bed (ICFB) [24-25] reactors are employed for high heat transfer rate, uniform bed temperature, good control of operation and uniform product distribution. Typical product yield from fluidized bed pyrolysis, composition of liquid fraction cracking of waste plastics, gas composition, and aromatic

compounds from fluidized bed pyrolysis of waste plastics are reported in Tables 1.4-1.7 respectively. Umbetro et al [40] proposed an operating criterion to avoid defluidization. Laura et al [41] proposed a predictive model to estimate the occurrence of defluidization under different operating conditions taking into account the role of physical properties of the polymers and hydrodynamics variables of the reactor, together with that of the main operating parameters, like the process temperature and plastic waste feed rate for waste plastics treatment. Lower temperature and heating rate for carbonization reduce oil yield [25]. Poly(methyl methacrylate)(PMMA) was depolymerised to more than 98% of the monomer and polystyrene in feed gives up to 75% of styrene and 10% of oligomers in an indirectly heated fluidized bed at temperature of 450^{o}C using the Hamburg process [26]. Degradation of mixtures of the most common waste polymers (PE, PP, PS, Polyamide, Ethylene-propylene co-polymer, and polyrethene rubber) in a horizontal tube reactor showed increased volatile products both with residence time and pyrolysis temperature [28]. Table 1.5 shows the effects of temperature, residence time, and plastics mixture composition on formation of aliphatic and aromatic products. The yield of volatile products is increased both with increase in residence time and pyrolysis temperature. The aromatic content such as benzene and toluene is also increased with increase in temperature while styrene and ethyl-benzene content is decreased [28]. Pyrolysis and subsequent activation of PET from post consumer soft drink bottles at 925ºC under CO_2 atmospheres produced microporous with low porosity carbon materials having BET surface area up to 2468m^2g^{-1} [20-21]. Preliminary analysis on potential applicability of these materials showed that removal of phenol adsorption and polycyclic aromatic hydrocarbons (PAHs) was highly satisfactory and comparable to the retention attained

with commercial activated carbons. Moreover, the hydrogen adsorption capacities of the activated PET waste compare favourably well with those attained with high-value carbon materials [20-21]. Effect of reaction pressure on the thermal degradation behavior of PE showed that reaction pressure took part directly in the scission of C-C link during thermal degradation of waste plastics. The flash pyrolysis of PS carried out in a free fall reactor under vacuum maximized the liquid yield around 750ºC and the styrene yield at 825ºC [43].

1.4.1.2. Thermal dehydrochlorination (DHC)

Thermal pyrolysis of real waste plastic mixture leads to the production of chloroorganic compounds due to presence of PVC. The feedstocks obtained from waste plastic should contain less than 10 ppm of chlorine for use in petrochemical industry. The first step of thermal decomposition of PVC occurs at temperature around 300-330ºC with elimination of HCl and leads to the formation of conjugated double bond. The degree of conversion of chlorine from PVC into hydrogen chloride in the first step was about 99.6% [44]. A similar behavior was obtained for electronic scrap dehydrochlorination. Decomposition of organobromides in electronic scrap occurred at high temperature. A remarkable amount of bromine remains in the residue, possibly due to the reaction with copper or calcium carbonate forming copper and calcium bromide [44]. A continuous process, a cascade of well stirred reactors has been developed by Bockhorn et al. [45] that gives high heat transfer rate, high plastics hold up and good mixing. During stepwise pyrolysis of waste plastics containing PVC to recover valuable product in the first step hydrogen chloride from poly (vinyl chloride) was obtained, in the second step the monomer of polystyrene was formed and in the third step aliphatic compounds from polyethylene

decomposition were trapped [45-46]. The kinetic data from stepwise pyrolysis of waste plastics containing PVC confirms that different molecular structures of commodity plastics brought about different reaction mechanisms of thermal decomposition, different reaction rates, and different temperature dependencies of the decomposition rates [44, 47]. It is also found that the presence of PET in waste plastic mixture increased the formation of chloroorganic compounds in liquid fractions [48]. The chloroorganic compounds are the highest in liquid fractions from PP and PVC combination [44].

1.4.1.3. Thermal decomposition mechanism of polymers

Polymer decomposition mechanism, a complicated phenomenon, can often be described as occurring by a set of series or parallel chemical reactions via random scission mechanism, chain scission mechanism, etc. An initial stage of polymer decomposition is often accompanied by melting (or softening). At this step, the thermal decomposition can be controlled by the process of formation of a gas phase inside the polymer and by nucleation and nucleus growth in a heterogeneous medium [49-50]. Polymer decomposition by chain scission is a multi-step radical chain reaction involving initiation, propagation, branching, and termination steps. Initiation reactions are of two basic types: (1) random-chain scission and (2) end-chain scission. Both of course, result in the production of free radicals. The random-chain scission, as the name suggests, involves the breaking of a main chain bond. End-chain initiation involves the breaking off of a small unit or group at the end of the chain. These two types of initiation reactions may be represented by the following generalized reactions:

$P_n \Rightarrow R_r + R_{n-r}$ (random-chain scission)

$P_n \Rightarrow R_n + R_E$ (end-chain scission)

Where, P_n is the polymer containing n monomers, R_r is a radical containing r monomers and R_E refers to an end group radical.

Typical literature reported radical chain mechanism of thermal degradation of PE, is presented through Scheme 1. This scheme consists of six steps, namely: initiation by random scission of the polymer chain into primary radicals, *R*p (step 1); β-scission of these radicals to ethylene (step 2); intramolecular hydrogen transfer at lower temperatures producing more stable secondary radicals, *R*s (step 3); β-scission reactions leading to alkenes (reaction 4) and short primary radical and polymer with a terminated double bond (reaction 4′) (step 4); intermolecular hydrogen transfer (step 5); and termination reaction (step 6).

Scheme 2 presents the radical chain mechanism of the thermal degradation of PP. It is analogous to the mechanism of PE degradation (Scheme 1). After the bond scission into primary (*R*p) and secondary radicals (*R*s), tertiary radicals (*R*t) are formed via rearrangement reactions. Subsequent β-scission leads to volatile alkenes and the chain carrier, *R*s. A β-scission to the other side leads to a short secondary radical *R*s and a polymer chain with a terminated double bond. This short secondary radical is saturated via intramolecular hydrogen transfer and results in an alkane. Termination is assumed via combination, analogous to polyethylene degradation. The rate of decomposition of the polymer should be equivalent to the formed volatile products (VP*)* from reactions 4 and 6 [51].

The proposed mechanism of the thermal decomposition of PET investigated by Holland and Hay [52] are presented through Schemes 3 and 4. The thermal degradation of PET has been rationalised into two degradation processes, intramolecular back-biting and β-

C–H hydrogen transfer (Scheme 3) and formation of nonvolatile residue (Scheme 4). The intramolecular back-biting process leads to formation of cyclic oligomers.

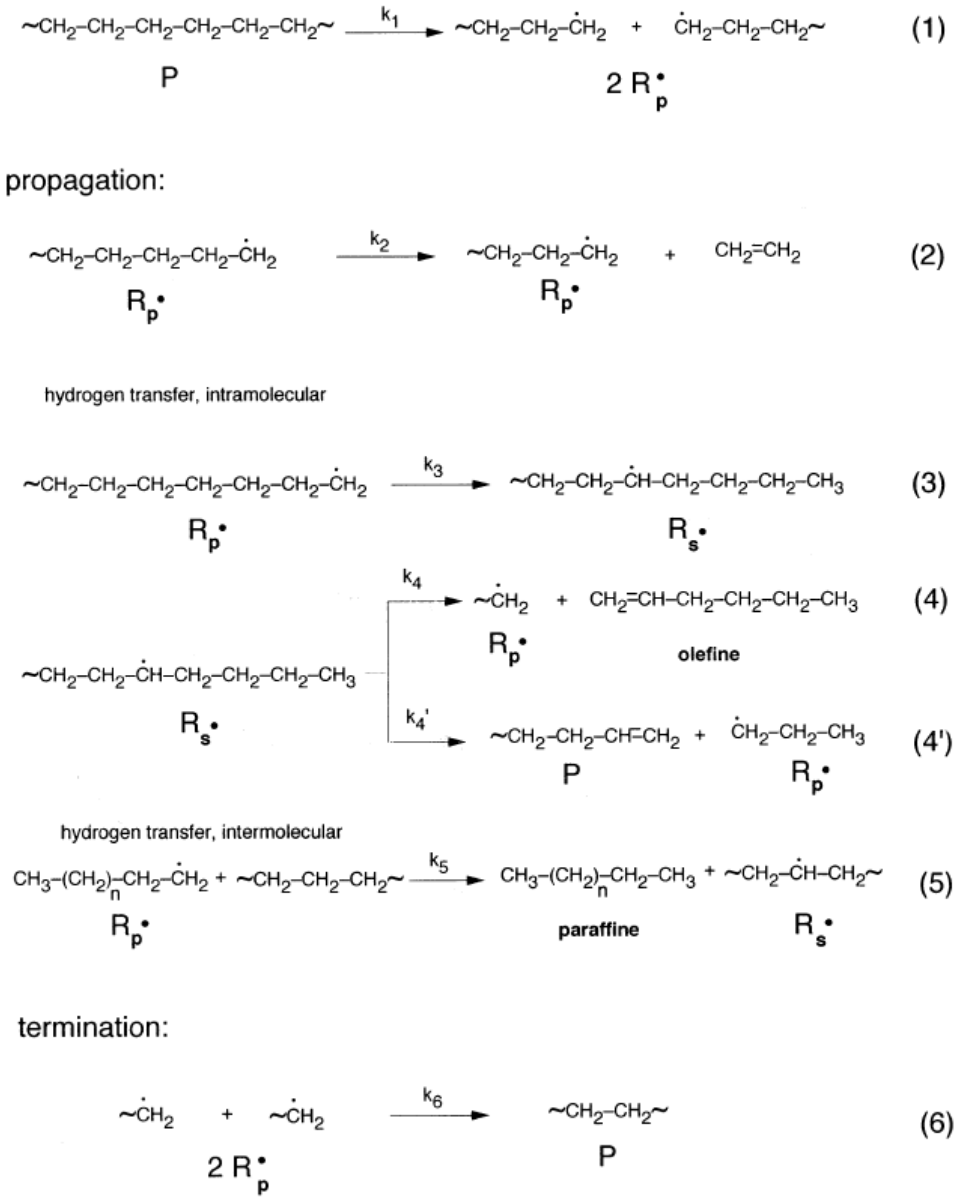

Scheme 1. Radical chain mechanism of the thermal degradation of polyethylene [51]

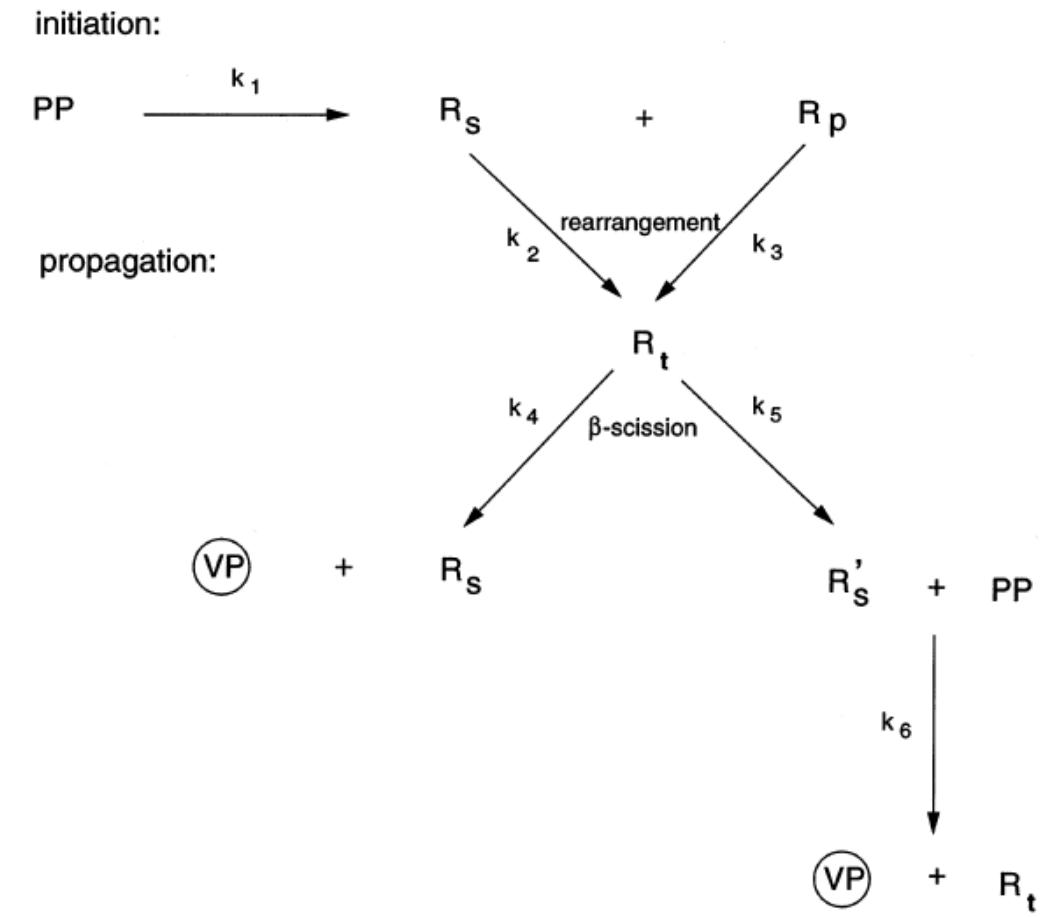

PP	polypropylene	R'_S	short secondary radical
R_p	primary radical	R_t	ternary radical
R_S	secondary radical	(VP)	volatile product

Scheme 2. Radical mechanism of the thermal degradation of polypropylene [51]

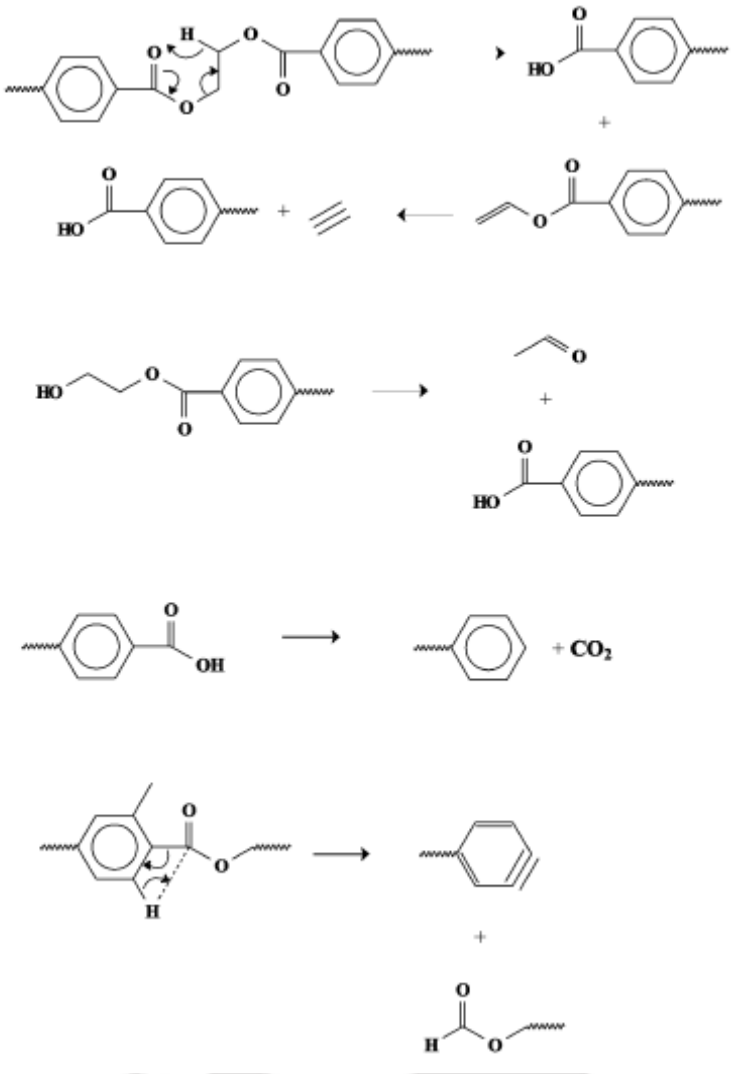

Scheme 3. Possible mechanism of thermal decomposition of PET [52]

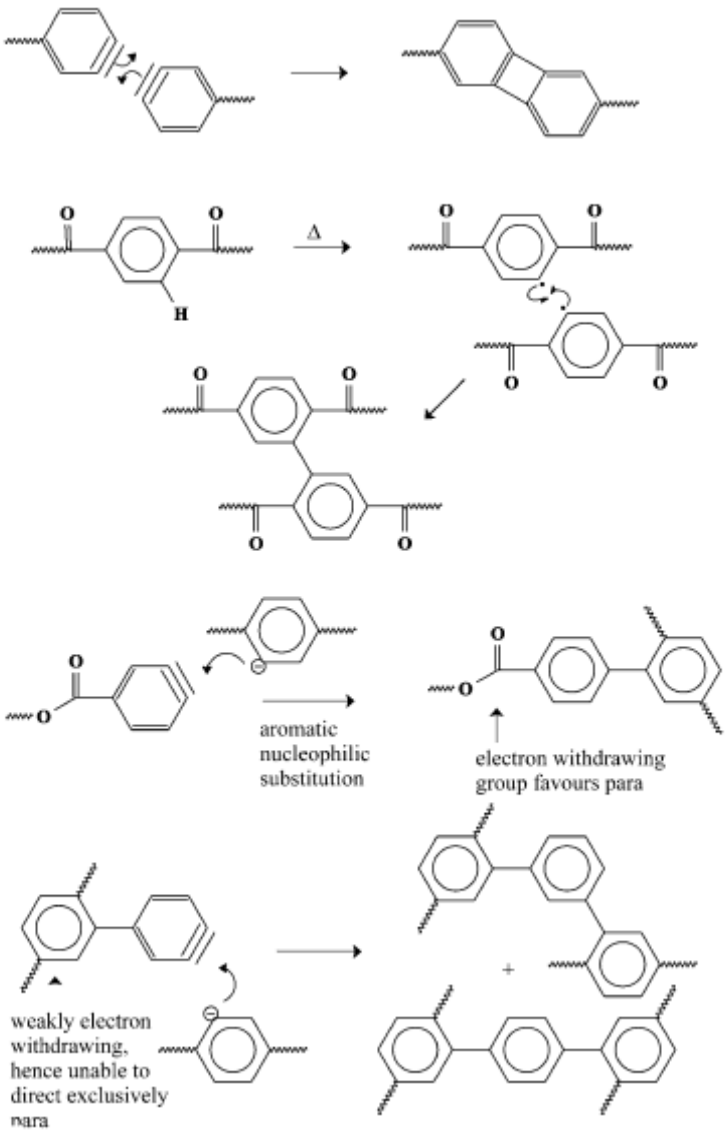

Scheme 4. Possible mechanism of formation of aromatics network in PET decomposition residue [52]

1.4.1.4. Co-processing of waste plastic

Copyrolysis is also an advanced and environmental friendly recycling route for processing of plastic wastes. Wastes are heterogeneous mixtures, which give rise to fluctuation in quality, availability, and composition. Thus it is necessary to develop a versatile technology that can help to reduce the problems of quality, composition and

availability. The co-processing of MSW with coal could help overcoming such problems [53].

Ha´jekova´ and Bajus [54] studied a new recycling route for the production of petrochemical feedstock. LDPE and PP were thermally decomposed individually in a batch reactor at 450°C to produce oil/wax products. Then these products were dissolved in primary heavy naphtha to obtain steam-cracking feedstock. The amount of benzene and toluene yields and coking were found similar to naphtha cracking.

Sharypov et al. [55] studied the interactions between coal and natural polymer with plastic waste and the thermal behavior of mixtures of PP (or PE)/brown coal from Kansk-Achisk (Siberia) in hydrogen atmosphere and using iron ore catalysts. There are mutual beneficial effects of coal–polyolefin blends during their hydro-pyrolysis where polymer plays the role of hydrogen donor and enhances the coal conversion. There is also a drastic reduction of olefinic contents in catalytic conditions (from 20% to 3%) and a sensible reduction of polyaromatic compounds in the heavy liquids.

1.4.2. Catalytic decomposition of waste plastics

Catalytic pyrolysis of waste plastics is drawing more and more interest on the perspective of solid waste management since they are an alternative source of energy or chemical raw materials. In general, thermal pyrolysis is a high temperature process but catalytic degradation reduces the process temperature, is selective towards certain desired range of hydrocarbons, and improves the quality of products. The major focus in the literatures till date has been to find the pyrolysis product distribution. Zeolite based catalysts such as ZSM-5 [56-64, 90], ZSM-12 [60], DeLaZSM-5 [61-62], DeZSM-5 [62], LaZSM-5 [62], nanocrystalline n-ZSM-5 [63, 93-94], BEA [64], MOR [64], HZSM-5 [65-73, 89],

PZSM-5 [65, 72], nanocrystalline n-HZSM-5 [66, 93-94], nanocrystalline H-beta [69], HMOR[70], HUSY [67,70,73], US-Y [56-57,59,61,74-75, 91-92], SAPO-37 [76-77], H-gallosilicate [78, 97] and Beta [63,79], H-beta [94] have been employed for catalytic decomposition of several plastics such as linear low density polyethylene (LLDPE), low density polyethylene (LDPE), high density polyethylene (HDPE), polystyrene (PS) and polypropylene (PP). These catalysts reduce decomposition temperature, decrease activation energy, and produce more gaseous / lighter products including the light olefins and aromatic fractions. Mesoporous catalysts such as silica-alumina [89], MCM-41 [59, 70, 80-81], Al-MCM-41(hydrothermal) [63], Al-MCM-41(sol-gel) [63, 66, 71], HMCM-41 [93-94], Al-SBA-15 [63], SAHA [70] accelerate the degradation process with production of low proportion of aromatics and a higher content of olefin and paraffin species. Other catalysts such as various types of FCC catalysts [56-58, 74-75,82-85, 96] (E-CAT, CATA-1, CATA-2, E-Cat (A), E-Cat B, Cat-C, Pt-catalysts), base promoted Fe catalysts (Fe-K/Al_2O_3, Fe-Ba/Al_2O_3, Fe-Zn/$Al_2O_{3,Fe}$-Mg/Al_2O_3, Fe_2O_3, Al_2O_3, Fe/Al_2O_3) [86], Ni-REY [87-88], barium oxide [95], clay type catalysts, and hybrid catalysts ZSM-5/MCM-41 [71] have also been used to find out the product distribution in different cases for decomposition of plastics. It has also been shown that the catalysts such as 5A, 13X, Y-zeolites, and metallic catalysts like $ZnCl_2$ and Fe_2O_3 have no influence on the conversion, product yield, and composition [98].

During catalytic cracking of waste plastics over Ni-REY catalysts, yield of liquid products, gas and residual wax were about 74, 22 and 4wt% respectively. Ni-REY catalyst showed high activity and higher selectivity (78%) than that of MFI type zeolite

(35%) towards gasoline for cracking of heavy oil obtained from degradation of waste plastics [87-88].

Decomposition of a polymer mixture over HZSM5 and orthophosphoric acid modified (PZSM5) zeolite catalyst showed increased amount of gaseous product [65]. The gaseous products contained a large C_3 fraction, while aromatic content increased in liquid product. C_{10}-C_{12} isoparaffins were the main compounds produced by decomposition over PZSM5 at temperature of 450-480ºC while C_6-C_9 naphtha were the main class of compound at temperature of 420-440ºC. The global reaction temperature reduced from 600-700ºC to 420-450°C. Waste samples of PE and PS being cracked thermally or in the presence of the catalyst (Pt/Al_2O_3) and hydrogen in closed autoclaves, produces more than 90% yield of gas and liquid fraction in gasoline and diesel range boiling hydrocarbon [82]. Proper selection of process parameter makes it possible to control in the yields and composition of gas, gasoline and diesel oil fractions. Performance of zeolite based catalysts including US-Y, ZSM-5 and clay based (Saponite, Atos, Zenith-N and AZA) catalysts have been studied by Karishma and Gobin [56]. Because of the strong zeolite acidity, severe over cracking takes place resulting in increase in gaseous fraction. Commercial cracking catalyst produced heavier hydrocarbons rich liquid fraction due to lower acidity level. Clay based catalysts possess milder acidity than zeolites and have bimodal pore structure including mesopore as well as micropore. Plastic catalytic cracking over these catalysts results in much less degree of over cracking and higher liquid yield. Thermal degradation gives rise to a broad product distribution, where as catalytic cracking over Al-MCM-41 leads mainly to hydrocarbon within the gasoline range (C_5-C_{12}) with selectivity up to 80% [98]. Degradation of HDPE with silicoaluminophosphate catalysts (SAPO-37)

showed good catalytic activity with decrease in the activation energy for the process. When thermal degradation of HDPE gave a product distribution over a wide range of carbon number C_5-$C_{26,}$ the catalytic reaction (SAPO-37) led to mainly lighter products (C_2-C_{12}) [76]. Catalytic degradation of PP using catalyst MCM-41 showed a remarkable effect of the catalyst in accelerating the degradation process [80-81]. FCC catalyzed decomposition of LDPE produced the liquid products in gasoline range hydrocarbon rich in aromatic, highly olefinic C_3-C_4 gases and Coke residue [84-96].

Recently, mesoporous catalysts (Al-MCM-41) synthesized either by sol-gel or by hydrothermal method have been used for decomposition of HDPE and LDPE to analyze the decomposition products [63, 66, 71]. However, much less articles are referred to the effect of MCM-41 on PP [68]. Though MCM-41 possesses large surface area, the utilization of MCM-41 in catalysis is now restricted by its relative low acidity and low hydrothermal stability, in comparison with those of microporous zeolites. But incorporation of aluminium in the framework of MCM-41 creates Bro¨nsted acid sites solving the problem of the low acidity [68]. Therefore, recently a few studies using mesoporous catalyst such as Al-MCM-41 have been conducted showing excellent performance in catalytic pyrolysis of plastics. Garc´ıa et al. [71] showed that polyolefin cracking over ordered mesoporous Al-MCM-41 proceeds by a random scission mechanism due to its large pore size and mild acidity, yielding hydrocarbons within the gasoline and gas oil fractions. Aguado et al. [63] reported that the disadvantage of weaker acid properties was partly compensated by the presence of larger pores that reduced diffusional hindrances. Hydrothermal Al-MCM-41 showed the strongest acid character and exhibited the highest catalytic activity in comparison to sol–gel Al-MCM-41 and Al-

SBA-15 during catalytic decomposition of LDPE and HDPE. Serrano et al. [63] showed that Al-MCM-41 exhibited a catalytic activity comparable to n-HZSM-5, but significantly greater than that of larger crystal size micrometer zeolite. Further, Grieken et al. [99] reported that mesoporous aluminosilicates (Al-MCM-41, Al-MTS, Al-SBA-15) favored the oligomerization reactions, which is the important pathway for the production of higher molecular weight hydrocarbon useful as fuel. Several pathways are known for synthesis of Al-MCM-41. They differ mainly in the use of templates, reaction temperature, time, pH of the reaction mixture, and aluminum source [99-102]. Mesoporous catalysts (Al-MCM-41 and Al-SBA-15) that had shown high activity in catalytic cracking of virgin LDPE were practically inactive with waste plastic [103].

1.4.2.1. Catalytic dehydrochlorination (DHC)

Catalytic dehydrochlorination is one of the preferred methods for removal of organic chlorine compounds. The dehydrochlorination (DHC) of chloroorganic compounds from Municipal Waste Plastic (MWP) derived oil was carried out using various metal oxides such as iron oxide, MgO, ZnO and Red mud. Iron oxide and its carbon composite were found to be effective and stable in DHC of MWP derived oil [104]. The oil derived from PVC containing pure polymer mixture by thermal degradation contained a lower amount of chlorine than the oil obtained by using Red mud and other catalysts [105]. The Al-Mg showed a good catalyst activity in PVC degradation and lower Cl_2 content in oil [106]. Brebu et al. [107] studied the degradation behavior of PE, PP, PS, antimony oxide synergist (ABS-Br) and PVC over iron and calcium based composites. Iron oxy-hydroxide and Fe-C composite were found to be effective in removing bromine where as Ca-C composite and $CaCO_3$ were suitable for chlorine removal.

1.4.2.2. Catalytic pyrolysis mechanism of polymers

Ohkita et al. [89] showed that there exists a relationship between the acid strengths and the ratio of silica-alumina ratio in catalysts and product distribution during catalytic degradation of PE. Presence of large amount of Brönsted acid sites in HZSM-5 increase the gaseous products but decreases the liquid (oil) product. However, aromatics in the oil are enhanced. Similar observations were reported by Manos et al. [92] during cracking of PE over two natural clays and their pillared analogues. Clay type catalysts with less acidic character and larger pores yield more liquid products and alkenes due to lower occurrence of hydrogen-transfer secondary reactions compared to US-Y zeolite.

Manos et al. [90], in another paper, obtained a variety of products depending upon the chosen zeolite with high values as fuel, confirming catalytic degradation of polymers (HDPE) as a promising method of waste plastic recycling. In the medium-pore zeolites, the hydrocarbons formed were lighter than those formed with large-pore ones. Higher amounts of alkenes were produced as primary products due to the fact that secondary bimolecular reactions are sterically hindered in medium-pores. They found the order for the carbon number distribution as: (lighter products) ZSM-5 < mordenite < β zeolites< Y zeolites < US-Y (heavier products) and that for the bond saturation as: (more alkenes) ZSM-5 < mordenite < β zeolites < Y zeolites < US-Y (more alkanes). Manos et al. [91] again reported that the presence of catalysts was necessary to initiate the solid sate reactions that change the polymers (HDPE) structure, mainly by breaking of chains of low molar mass to smaller chains. Gaseous products were formed first near melting point and liquid products were formed first slightly above melting point. The product range was typically between C_3 and C_{15}. Isobutane and isopentane were the main gaseous

products. The liquid product fraction was alkane-rich, as alkenes rapidly undergo bimolecular hydrogen transfer reactions to give alkanes as secondary products.

Serrano et al. [94] reported that during catalytic cracking of a polyolefin mixture consisting of PP, LDPE and HDPE over HMCM-41, n-HZSM-5 zeolite, and HBeta zeolite, the high surface area, large pores, and mild acidic strength present in HMCM-41 are responsible for the high conversions, yielding waxes as the primary product. HMCM-41 promotes random scission that is responsible for formation of heavy hydrocarbon. Likewise, n-HZSM-5 due to presence of high external surface area enhances its cracking activity because the zeolite external acid sites are not sterically hindered for the conversion of the bulky polyolefin molecules. n-HZSM-5 produces C_3-C_5 olefins. These olefins undergo subsequent oligomerization and cyclization reactions leading to heavier aliphatic hydrocarbons. Likewise, hydrogen transfer reaction from aliphatic products to gaseous olefins lead to aromatic hydrocarbon and favor the transformation of olefin into paraffin. n-HZSM-5 shows the highest selectivity toward C_1-C_4 gaseous hydrocarbons (50 wt %), HBeta leads mainly to liquid hydrocarbons in the range C_5-C_{12} (60 wt %) and HMCM-41 yields both C_5-C_{12} (54 wt %) and C_{13}-C_{30} (32 wt %) fractions. They also reported that both dealumination and particle aggregation that take place during the regeneration treatment are responsible for a certain loss of activity of HMCM-41 catalyst.

Similar studies was carried out by Aguado et al. [93] to compare the product distributions between a mesoporous HMCM-41 and a n-HZSM-5 catalysts during decomposition of a plastic mixture consisting of PP, LDPE, and HDPE. The product distributions obtained with these two catalysts are completely different, which is related to the prevailing

cracking mechanism. n-HZSM-5 zeolite, with high external surface area and strong acid sites, promotes end-chain scission reactions of the polymers, leading to light hydrocarbons, with around 80-90% of the products in the range C_3-C_6 where as heavier products such as waxes (C_5-C_{12} and C_{13}-C_{22}) are obtained over HMCM-41.

Serrano et al. [66] in their recent paper reported that Al-MCM-41 exhibited a catalytic activity comparable to n-HZSM-5, but significantly greater than that of larger crystal size micrometer zeolite like ZSM-5. n-HZSM-5 exhibited the highest catalytic activity. Al-MCM-41, owing to its mesoporous character, the reduced acidity of this sample was counteracted by a greater accessibility to its internal acid sites. They also showed that acidic zeolites cause higher amount of carbon deposition over acid sites. Catalytic degradation of LDPE over micrometer and nanocystalline HZSM-5 zeolites generated a similar range of degradation products with a marked increase in the light olefins and aromatic fractions (e.g. benzene, toluene, xylene) and complete elimination of heavier olefin and paraffin hydrocarbons. This is due to cracking of large polymer molecules into C_3–C_5 olefins in the catalytically active acid sites, followed by oligomerization, cyclization and hydrogen transfer reactions. The high proportion of aromatics generated has been attributed to both the strong acidity and the shape selectivity properties of the HZSM-5 zeolite due to its three dimensional micropore structure, which reduces the occurrence of side reactions. Despite its high catalytic activity, mesoporous Al-MCM-41 exhibited no shape selectivity in the products generated with a low proportion of aromatics and a higher content of olefin and paraffin species.

Durmus et al. [64] reported that catalytic activity of BEA and MOR is better than ZSM-5 for PP decomposition. They showed that higher amount of coke deposition occurs over

same pore structure with higher the number of acid sites. It is reported that the initial step of the degradation reaction over catalytic sites was considered to occur by either the abstraction of hyride ion (by Lewis acid sites) from the oligomer chains, or the addition of proton (by Brønsted acid sites) to double bonds of the thermally degraded shorter molecules. Strong acid sites accelerate both cracking and deactivation reactions yielding higher amount of coke and acidic property is necessary to form carbanium ion. PP molecules are much larger than the pore size of zeolites; therefore, the catalytic degradation must be initiated on the external surface of zeolite particles. First chain scissions start on the external surface of the catalyst and then smaller chains can enter into the pores where most of the active sites are located. Further degradation into shorter hydrocarbons continues in the pores depending on acidic character of the catalyst. PP degradation over ZSM-5 is more difficult as degraded chain segments cannot easily diffuse through the channels due to pore structure of these catalysts.

Lin and Yen [70] reported that product distributions varied markedly depending on catalysts type and structure. The acidic zeolite catalysts, HZSM-5, HMOR and HUSY, catalysed degradation resulted in much more amounts of volatile hydrocarbons compared with degradation over non-zeolite catalysts (MCM-41 and SAHA). MCM-41 with large mesopores and SAHA with weaker acid sites resulted in a highly olefinic product and gave a wide carbon number distribution, whereas HUSY yielded a saturate-rich product with a wide carbon number distribution and substantial coke levels. Greater product selectivity was observed with HZSM-5 and HMOR as catalysts with about 60% of the product in the C_3-C_5 range and HMOR generating the highest yield of *i*-C_4 for all catalysts studied. The larger pore zeolites (12 ring channels) of HUSY and HMOR

showed deactivation in contrast to the more restrictive HZSM-5 (10 ring channel system). The selectivity of catalysts is influenced by changes in reactor conditions. Olefins and iso-olefins were produced by low temperatures and short contact times.

Takuma et al. [97] showed that catalytic degradation of LDPE, HDPE and PP over the gallosilicate yielded lighter hydrocarbon mixtures that were rich in valuable aromatic components, mostly benzene, toluene, and xylenes. The product distribution was influenced little by the structure of the polymers to be degraded. The degradation mechanism was explained by frequent skeletal isomerization of the decomposed fragments. The unsaturated fragments, which were the most abundant and thereby the most important reaction intermediates, rapidly isomerized on the acidic gallosilicate, and the resulting isomers were distributed in thermodynamically equilibrated concentrations.

Aguado et al. [63] investigated the catalytic activity of six catalysts of varying acid and textural characteristics in the degradation of different plastic polymers (pure LDPE, pure HDPE and recycled polyethylene of urban and agricultural origins). The catalysts were three zeolitic materials (standard ZSM-5, nanocrystalline n-ZSM-5 and Beta) and three mesostructured solids (sol–gel Al-MCM-41 (sg), hydrothermal Al-MCM-41 (hy) and Al-SBA-15). Despite showing strong acid properties, standard ZSM-5 zeolite exhibited a very low catalytic activity on most plastics due to diffusional impediments that affected the access of the bulky polymer molecules to its internal active sites. Beta zeolite and n-ZSM-5 exhibited strong catalytic activity due to combination of strong acid properties and large external surface area. Mesostructured Al-MCM-41 (hy) exhibited one of the highest catalytic activities, largely surpassing the performance of crystalline solids with stronger acid properties. The catalytic activity of sol–gel Al-MCM-41 was comparable to

that of Al-SBA-15. Degradation of LDPE over standard ZSM-5 takes place over a much wider temperature range and presents a bimodal DTG curve suggesting the occurrence of a two stage process. In the case of n-ZSM-5, the larger availability of strong external acid sites is sufficient to permit complete degradation in the first stage of the process. Overall, n-ZSM-5 zeolite and, to a lesser extent, mesoporous Al-MCM-41 (hy) showed the strongest catalytic activities for the degradation of pure and waste polyethylenes.

Marcilla et al. [68] synthesized three catalysts with different chemical and physical properties. These were (one HZSM-5 zeolite and two ordered mesoporous aluminosilicates—MCM-41a and MCM-41b with different Si/Al ratio) and tested for the pyrolysis of four commercial polymers (LDPE, PP, PS and EVA copolymer). The HZSM-5 zeolite showed the lowest activity in the catalytic pyrolysis of the four polymers. The two mesoporous catalysts, with a greater pore size, were the most active materials in the catalytic pyrolysis of the polymers, and the MCM-41b sample, with higher acidity, was the most active. The MCM-41a with higher aluminum and acidity is the most effective catalysts for catalytic decomposition of LDPE. In spite of its relatively high acidity, activity of HZSM-5 is the lowest due to the lowest pore size which limits the diffusion of the reactants to the active sites. PP chains due to the presence of the methyl group present a greater cross-sectional area than LDPE. The presence of these methyl groups increase the number of tertiary carbons in the molecule, thus increasing the reactivity of the chain, and its temperature of thermal degradation is, therefore, lower than that corresponding to LDPE. However, the steric hindrance due to the presence of the methyl group affects the order of activity of the different catalysts with respect to that observed in the catalytic pyrolysis of LDPE. Marcilla et al. [67], in another paper,

reported that the degradation process is more complex with HUSY than that observed with HZSM5. HUSY possesses a large surface area and pore volume. Most of the surface area is located at the inner pores. Initially, the higher access windows of HUSY (7.4 A°) favours the catalytic degradation process, given that polymer chain ends can access easily to active sites. But the coke deposition is favoured in this type of zeolites due to their large pores, leading to a fast deactivation. Therefore, initially the cracking process is catalytic in the presence of this zeolite but as deactivation proceeds the thermal degradation takes place.

Marcilla et al. [69] studied the effect of nanocrystalline H-beta zeolite in the pyrolysis of commercial LDPE and compared with those obtained using a HZSM-5 zeolite. HZSM-5 produced lower carbon number (~C_3) but the H-beta zeolite showed higher selectivity to higher proportion of C_4 and C_5 compounds due to larger pore size. The mass fraction of isobutane is noticeably higher in the gas evolved in the presence of H-beta zeolite as compared with the HZSM-5 zeolite at the different temperature intervals studied. The isobutane mass fraction is decreased when the temperature is increased. This behaviour was explained considering that the catalytic cracking of hydrocarbons over acid solids follows a carbocationic mechanism, and these carbocations can undergo different bimolecular reactions which are more favoured in zeolites with large pore size such as HUSY. Higher amount of coke deposited over the H-beta zeolite than the HZSM-5 zeolite because the H-beta zeolite is a large pore zeolite with a 3D system of interconnected channels causing a free growth of coke molecules and a gradual activity drop. In the case of HZSM-5, the growth of the coke molecules is more hindered and, consequently, smaller coke retention is observed.

Catalytic degradation of waste polystyrene into styrene was studied by Zhang et al. [95] using solid acids and bases as catalysts. Solid bases, instead of solid acids, were emphasized to be effective for the selective degradation of polystyrene to both styrene monomer and dimer. Among the solid bases barium oxide was prone to be the most effective catalyst in that more than 85% of polystyrene was recovered as styrene monomer and dimer. The reaction mechanism of the degradation of polystyrene into styrene on solid bases was briefly discussed in terms of the depolymerization reaction, which starts with the elimination of a hydrogen atom on polystyrene by active basic sites on the solid bases to form carboanions. On the basis of these results, a design for disassembly of waste polystyrene was attempted by dispersing a small amount of barium oxide powder into polystyrene pieces when they were molded into polystyrene thin films. Puente et al. [96] to explore the feasibility of the current commercial FCC unit with minor change in technology for catalytic decomposition of polymers studied FCC catalysed decomposition of styrene-based polymers dissolved in benzene. Reaction times were up to 12 s in a discontinuous fluidized bed reactor at 550^{o}C. The major reaction products were ethyl benzene, benzene, toluene, and styrene, and production of coke was very significant. A simple scheme contemplating mainly oligomerisation, cracking, and hydrogen transfer reaction can explain formation of the most important products (benzene, toluene, and ethyl benzene) [96].

1.4.3. Pyrolysis kinetics analysis

Complex nature of polymer pyrolysis phenomena makes it difficult or virtually impossible to analyze separately the elementary reactions as well as to evaluate the quantitative contribution of each to the global degradation process. For these reasons,

even if the global or overall kinetics analysis of pyrolysis has no real significance with regard to the reaction mechanism, it is important to know the decomposition mechanism, rate of reaction, reaction parameters and to predict the products distribution. One of the main targets of kinetic study is to construct a model that can capture the essential chemistry of a system while maintaining a manageable model size. Mathematical modelling of thermal decomposition reactions helps in understanding the process being studied, in checking the validity of assumptions and in deducing quantitative conclusions there from. The latter is essential to achieve engineering calculations leading to the determination of the reactor size. Moreover, kinetic models with individual reaction steps lead to a great number of kinetic parameters, whose application for the simulation of industrial reactors is difficult [108-109].

1.4.3.1. Mechanistic model for kinetics analysis

Thermolysis or pyrolysis usually results in a complex mixture of many products, which can often be described as a continuous function (frequency distribution) of a property, such as molecular weight. In recent years, the use of mechanistic modeling to identify the kinetics of complex systems has increased greatly. Population balance-based models have been developed to model molecular weight changes and small molecule evolution simultaneously. A population balance model governs how the molecular-weight distribution (MWD) evolves in time and space. Distribution kinetics describes chemical or physical processes occurring in discrete or continuously distributed systems. McCoy and coworkers [110-124], and Kruse et al. [125-126] demonstrated the dynamics of MWDs using population distribution applied to polymer degradation. Rate coefficients are measured for the degradation of polymers by examining the time evolution of the

MWDs of the reacting polymers. The rate coefficients of the degradation reactions depend on the molecular chain length and thus on the molecular weight. The rate coefficient can be constant, linear, or quadratic. The time evolutions of MWDs can be determined by solving the governing population balance equations (PBEs), which are generally solved by moment techniques wherein the initial distribution is represented by a gamma distribution [110-126]. Further, the effects of different variables such as hydrogen donors, interaction of the polymers through hydrogen abstraction, effect of catalysts (Magnesium oxide), on the model results were explored. Depending on the particular polymer, hydrogen donors may increase, decrease, or have no effect on degradation rate [116]. A new approach to polymer pyrolysis kinetics is based on moments of a population balance equation describing chain-end and random scission and repolymerization. Two equations for the zero and first moments (moles and mass) are solved for isothermal and nonisothermal (linear T increase) thermogravimetric analysis (TGA) [117-124]. The majority of the models developed using this approach use global rate coefficients to quantify the kinetics. However, these models have been modified to describe the evolution of specific, low molecular weight products [126].

Mechanistic modeling requires many assumptions and is computationally intensive; therefore, whenever possible, it may be best that the kinetic data be estimated directly from experimental data. On the other hand, TGA is a good kinetic estimation tool; however, kinetic information obtained by TGA is characterized by errors due to certain restrictions such as heat and mass transfer limitations [109].

1.4.3.2. Thermogravimetric kinetics analysis

Thermogravimetic analysis (TGA) is widely applied to study the kinetics analysis of polymer pyrolysis. In addition, TG analysis is used for proximate analysis and getting important information of start, end and maximum decomposition temperatures. In most of the reported literatures, model-fitting methods are applied to evaluate pyrolysis kinetics parameters using single heating rates and chemical reaction models, which give a single set of kinetics triplet. Modern model-fitting methods are based on multi-heating rates taking care of different possible reaction mechanisms. Model-free method like Vyazovkin model-free approach, through use of isoconversion method, provides reliable and consistent kinetic information from nonisothermal data.

1.4.3.2.1. Model-fitting method of analysis for noncatalytic decomposition

Polymer pyrolysis kinetics is frequently described by either Prout-Tompkins model [127-128] or nth order reaction model [29-31, 50, 129-134]. The kinetic models in literature are broadly based on either representing the thermal analysis of the weight loss, traditional models or detailed reaction mechanisms. In absence of prior information about real kinetic mechanism, the reaction model can be chosen from a set of well-known reaction models to fit experimental data usually done in model-fitting techniques. Since, the thermal degradation of polymers corresponds to a set of successive and/or parallel chemical reactions, serious doubts arise about an accurate description of decomposition kinetics by using simplified equations expressing a rate of the process only via mass loss. Indeed, if information concerning a thermal degradation mechanism is obtained by an independent method, typical kinetic equations, and simple models can be insufficient for the description of the phenomenon. Nevertheless, the application of simplified models is

preferable. In a number of cases it is possible that the obtained kinetics triplet describes the rate-limiting step of the decomposition process and recommended that this approach is acceptable for Chemical Engineering applications [50, 131-132]. The activation energy of this process defines the response of a system against a change of temperature or time. Even if the formal approximation of kinetic data omits details of a chemical mechanism, its accuracy is often sufficient for technological estimations. Being fitted correctly, the constants in the Arrhenius equation allow a satisfactory approximation to be achieved. Unfortunately, the kinetics analysis is often complicated by the presence of several stages of decomposition, in particular, if the stages are not well resolved. Attempts to select realistic models seem to be more fruitful. If no information is accessible about the process, a manifold of models should be assumed in order to find the best model(s) both in terms of the minimum deviation between theoretical and experimental data and from the standpoint of physical/chemical sense [50].

Single heating rates and traditional chemical reaction models model-fitting technique:

In most of the reported literatures, model-fitting methods are applied to evaluate pyrolysis kinetics parameters using single heating rates and traditional n^{th}. order reaction model. This traditional analysis gives a single set of kinetics triplet that is estimated after minimizing deviation between experimental and simulation data. Bockhorn et al. [51] studied thermal degradation of PE and PP under isothermal conditions. They evaluated the kinetics triplet by model fitting method, proposed chain scission as possible mechanism of decomposition, and finally evaluated the rate constants for different steps of chain scission. They investigated the difference in kinetics triplet of the mixture from the single polymer decomposition kinetics triplet. In a recent paper, Faravelli et al. [135]

reported a satisfactory two-phase model to describe the thermal degradation of PE-PS mixture. The pyrolysis kinetics of various substances, including polyamide-6 (to recover ε-carprolactam) [136], electronic packaging materials at high temperature and in an oxidizing atmosphere [137], poly (vinyl chloride) [44, 46-47], and a mixture of PE and PS [51] has been reported in the literature. Thermal degradation of polymer is mostly described by random scission mechanism, which do not follow rigorously first order kinetics. Therefore, Gao et al. [134] established a relation for determining reaction order to avoid blind use of first order kinetics. The non-isothermal TGA kinetics of poly (trimethyl terephthalte) (PTT) and PET under argon, air and nitrogen atmosphere by Freeman-Carroll, Friedman and Chang methods to estimate the kinetics triplet [131] and PET thermal decomposition under strict pyrolysis condition and with different proportions of oxygen using TGA [129-130] were studied using chemical reaction model. Recently, artificial neural network technique [138] was also applied to study thermal decomposition kinetics.

Multi-heating rates and multi-step reactions modern model fitting technique:

Mamleev et al. [50] reported the kinetics modeling using multi heating rates and the traditional models for non-isothermal decomposition of polymer. In another paper, Mamleev et al. [131] reported cotton decomposition by modulated thermogravimetry (MTG) using single or multi heating rates and multi-step reaction mechanisms. Multi-parameter optimization applied during model-fitting analysis through minimization of the objective function such as square of the deviations between experimental data and calculated values (least square function) is frequently associated with uncertainty [30, 139] arising out of model incorrectness, experimental error, initial value approximations,

and the drawbacks associated with many optimization techniques to find out the global optimum. The unknown parameters of kinetic models are obtained by means of regression techniques from experimental data. Noise and processing error in variables and known parameters are propagated through the regression analysis to the uncertainties and processing error of unknown parameters and eventually in output variables.

Sensitivity analysis:

Sensitivity analysis is one approach to overcome such uncertainties and errors involved with the model-fitting technique [30-31, 33-37, 127-128, 139]. It identifies sensitive parameters and helps to develop a new objective function, which takes care of less sensitive parameters only. Sensitivity analysis is the technique used to investigate the propagation of parameters uncertainties into output variables uncertainties [139-140]. Statistical sensitivity analysis [141] approach is based upon Taylor series approximations for variance and expected value of the output variables of the model using the Direct Methods (DM) for first order sensitivity analysis of chemical kinetics systems. Dicknson and Gelinas [142] applied DM for both first order and second order sensitivity analysis of ordinary differential equations (ODEs). In the Green's Function Method (GFM), Green's function was used for auxiliary equations in the DM to obtain the sensitivity coefficients by integrating over Green's functions [143]. In the Decoupled Direct Method (DDM), extension of the DM, the auxiliary equations for sensitivity coefficients were solved separately from model equations [144]. Li and Petzold [145] investigated sensitivity analysis for differential algebraic equations (DAEs). The DDM was applied for first order and second order sensitivity analysis in case of multi-response parameters estimation using modified Newton scheme known as hybrid Newton/Gauss-Newton algorithm for

nonlinear ODEs [140]. First order, second and higher order sensitivity analysis and cross sensitivity analysis were applied for three dimensional air quality modeling using DDM and High-order Direct Decoupled Method (HDDM) [146]. Sandu et al. [147] extended the DDM to Rosenbrok stiff integration method and adjoint sensitivity analysis for chemical reactions system. The DM is advantageous due to the structural similarities between the model and sensitivity equation. But the method is unstable. The GFM method is efficient and advantageous for the systems of stiff ODEs where numbers of parameters are greater than the number of dependent variables. But the DDM has greater stability and efficiency. The HDDM is an extension to the DDM for efficiently calculating the higher order sensitivity coefficients. In case of statistical sensitivity analysis approach, the second order terms in the Taylor series approximations are strongly needed for more accurate analysis of nonlinear response [142, 146].

Recently, Automatic Differentiation (AD) technique is applied for atmospheric chemistry models such as tropospheric chemistry model and air quality model [148-149]. Sherman et al. [150] studied first and second order sensitivity derivatives using automatic differentiated incremental iterative scheme. A novel method for parametric sensitivity analysis based on singular value decomposition was applied by Zak et al. [151] in case of ordinary differential equation (ODE) models of biological oscillations. Zanfir and Gavariilidis [152] used parametric sensitivity analysis to investigate the influence of several design parameters of thermal behaviour and performance of a catalytic plate reactor. Sun et al. [153] applied sensitivity analysis in the case of colloid transport in the heterogeneous process media to study the identifiability of six colloid transport related parameters. In the recent publication, Salah et al. [154] applied uncertainty and sensitivity

analysis in order to asses the error margins and rank of the most influencing parameters involved in the performance of the nuclear power plant. Amongst all, DM is the simplest one and advantageous due to the structural similarities between the model and sensitivity equation though it is unstable in case of sets of stiff ordinary differential equations (ODEs).

1.4.3.2.2. Model-free (isoconversional) method of analysis for noncatalytic decomposition

The correctness of the pyrolysis kinetics heavily depends upon reliable evaluation of activation energy from the decomposition behavior under different conditions of temperature and/or atmosphere. However, selection of appropriate model and initial guess of kinetics parameters are major drawback of model fitting methods [31]. Moreover, the kinetics triplet obtained by model-fitting technique from non-isothermal condition is highly uncertain and cannot be compared with the kinetics triplet obtained from isothermal condition [33]. The aforementioned drawbacks of model fitting can be avoided with the use of isoconversional methods [31, 33-37]. Firstly, these methods allow the activation energy to be determined as a function of the extent of conversion and/or temperature. Secondly, this dependence is determined without making any assumptions about the reaction model. The basic assumption of the isoconversional method is that reaction model is not dependent on temperature or heating rate at same conversion for different heating rates. Kissinger method [64, 159-160], Ozawa method [134, 157, 159-160], and Vyazovkin model-free approach [33-38, 60, 76, 155, 158, 176, 178-180] are commonly used isoconversional i.e. model-free techniques. Vyazovkin model-free approach is a trustworthy way of obtaining reliable and consistent kinetic

information from both nonisothermal and isothermal data. It can also help to reveal the complexity of multiple reactions due to the dependencies of activation energy on the extent of conversion [37-38].

A few literatures dealt with the kinetics analysis using isoconversional methods such as thermal decomposition kinetics of solid like 1,3,5,7-tetraanitro-1,3,5,7 tetrazocine and ammonium dinitramide [33], ammonium perchlorate [34, 155], calcium carbonate [34], triphenylphosphine oxide [35] and desolvation kinetics of drug solvate, Sulfameter (5-methoxy sulfadiazine and dioxolane) [156]. Activation energy, E is expected to be a function of temperature and the extent of conversion (α) during polymer decomposition phenomenon. Isothermal kinetics data are mostly needed for practical application as most of the pyrolysis reactors operate at constant temperature. So, the simulation of isothermal kinetics can be performed using nonisothermal data by means of modern isoconversional method i.e. Vyazovkin model-free approach.

Apart from a few literatures dealing with the kinetics analysis using isoconversional methods for thermal decomposition of solids [33-35, 155-156], Lyon [157] proposed a new series solution for integration of the Arrhenius integral, obtained during isoconversional method of analysis of the kinetics. He used single step reaction from temperature scanning experiment and applied for decomposition of LDPE. Peterson et al. [158] studied thermal decomposition of poly (methyl methacrylate) using isoconversional method to evaluate the decomposition kinetics. Peterson et al. [38] in their subsequent research paper reported the thermal degradation kinetics of PS, PE and PP using isoconversional method. Gao et al. [134] used isoconversional method of Flynn-Wall-Ozawa method in case of HDPE decomposition to show the variation of activation

energy, E_α with α. They recommended that random scission does not rigorously follow first order reaction and first order reaction model should not be used blindly. Vasile et al. [161] reported thermoxidative decomposition of LDPE in nonisothermal conditions and applied isoconversional method of Friedmann to analyze dependency of E_α on α. They reported need of continuous modifications of reaction mechanism as different processes (decomposition paths, diffusions and volatilizations) are all influenced differently by the temperature change during heating.

1.4.3.2.3. Model-fitting method of analysis for catalytic decomposition

A few literatures have reported studies on the catalytic pyrolysis kinetics of plastics applying quantitative mechanistic kinetics model and evaluated the kinetics constants, which revealed reduction in the activation energy due to presence of catalyst [58-59, 80-81]. Nevertheless, catalytic pyrolysis is usually a multi-step reaction, which may not be appropriate to be represented by overall kinetics triplet using single heating rates. Marcilla et al. [58, 81] investigated the kinetics of the thermal and catalytic decomposition of PP over MCM-41, ZSM-5, and FCC catalysts. In another work, they investigated the kinetics of the thermal and catalytic decomposition of PE over MCM-41 catalysts [59, 80]. They applied model-fitting technique using quantitative mechanistic kinetics model and evaluated the kinetics constants, which revealed a reduction in the activation energy of the catalytic decomposition as compared to the thermal process.

1.4.3.2.4. Model-free (isoconversional) method of analysis for catalytic decomposition

Model free analysis technique is advantageous over model fitting analysis when the real kinetics mechanism is unknown. This becomes extremely important during catalytic decomposition since reaction mechanism may change drastically with type and

concentration of catalyst. Karishma and George [57] determined apparent activation energy for the overall polymer (LLDPE and Polystyrene) catalytic cracking process over zeolites, commercial cracking catalysts, clays and pillared clays using Ozawa method. The results showed that the activation energy increased with decrease in acidity of the catalysts. Thermal and catalytic degradation kinetics of PP have been studied over various catalysts such as silica gel, silica-magnesia, silica-titania, Mordenite, silica-alumina, silica-alumina at different heating rates [162]. The apparent activation energies were determined by the Kissinger equation using four different heating rates for catalytic pyrolysis of PP over BEA, ZSM-5, and MOR [64]. The apparent activation energy of the overall process of polymer catalytic cracking over USY, ZSM-5, and different clays has been estimated using Ozawa method at different heating rates [57]. The thermal and catalytic decomposition kinetics studies of HDPE over SAPO-37, and PP over ZSM-5 and ZSM-12 catalysts applying Vyazovkin model-free approach through use of isoconversion method [76, 60] showed variation of E_α with α and reduction in decomposition temperature and E_α. To the best of our knowledge no such literatures have reported variation of E_α with α during catalytic decomposition of LDPE using model-free technique. However, information on activation energy is useless without a method of calculation of kinetics curves. For description of multistage processes, the use of model-fitting methods is unavoidable [131]. It is worth mentioning that a good fit of experimental results is only one condition, but it should not be the unique one [163].

1.4.3.3. Optimization techniques for the kinetics analysis of TGA data

In model-fitting techniques, the model is to fit the experimental TGA data involves searching for the kinetics parameters that accurately describe the data as defined by an error criterion, which is generally the sum of the squares of the differences between the model predictions and the experimental data (least square function). Various traditional direct and gradient-based algorithms are applied to the optimisation of chemical systems and various techniques may be employed in order to adapt the standard algorithms to the chemical kinetics problem considered [164]. Microsoft excel solver 7.0 is used by Marcilla et al [58-59, 80-81] to evaluate the kinetics parameters for catalytic pyrolysis of polymers. The Microsoft Excel Solver tool uses the Generalized Reduced Gradient nonlinear optimization code developed by Leon Lasdon, University of Texas at Austin, and Allan Waren, Cleveland State University [Microsoft Excel help]. The kinetics parameters are determined though nonlinear regression analysis using various software such as 'non-parametric kinetics' (NPK), TA-KIN, NETZSCH [30, 29], and AKTS-TA used for nonisothermal and isothermal data in ICTAC project 2000 [29]. The (NPK) method uses the singular value decomposition (SVD) algorithm. TA-KIN software for thermal analysis used non-linear optimisation algorithm of Levenberg and Marquardt [29]. Similarly, the kinetics triplets are obtained through the minimization of objective function using nonlinear regression method of Levenberg and Marquardt algorithms [131]. The common gradient-based optimization routines such as Levenberg–Marquardt [MATLAB help] can identify a local optimum around the initial guess [165]. Sensitivity coefficients of the objective function with respect to the unknown parameters may be used to guide the gradient search. Most of the optimization techniques based on a

quadratic approximation of the objective function in parameters space, require the evaluation of gradient and Hessian matrix with respect to parameters. But the Hessian matrix is approximated by using only first order sensitivity coefficients or finite difference approximations. So, the coupling of first order and second order sensitivity analysis for the exact evaluation of Hessian matrix can possibly improve the efficiency of the exiting algorithms [140]. Various techniques to calculate the first order and second order sensitivity co-efficient with respect to parameters are reported in sub section Sensitivity analysis [139-154]. Additional coding for calculating the first order and second order sensitivity co-efficient, increased the computation time and burden. However, a major drawback of all gradient-based methods is the fact that they only converge to the next local optimum of the objective functions, which depends on the initial guess. On the other hand, direct search methods are usually slow and require many functions. They depend strongly on the initial guess. Therefore, frequently the evolution of kinetics parameters is associated with uncertainty. The uncertainty, as already discussed, mainly comes from model incorrectness, experimental error, initial value approximation and solution or optimization techniques. Moreover, the kinetics parameters are known to be strongly correlated giving rise to an objective function having the shape of narrow valley with lots of false global minima.

Recently, application of genetic algorithm (GA) or hybrid genetic algorithm (HGA) to overcome the above-mentioned problems for the estimation of kinetics parameters has attracted interest in chemical engineering, chemistry, and other fields [164-172]. Several authors report the complete description of genetic algorithm (GA). Genetic algorithms are population based stochastic search procedures based on the survival of the fittest

principle. Furthermore, GA does not require any of the gradient information of the fitness functions [164-165]. A population of randomly generated solutions, i.e. parameter values for this problem, is progressively modified using genetic operators such as crossover and mutation in order to improve the population's fitness as measured by their effectiveness in predicting the experimental data. It starts with a randomly initialised population of candidate solutions and implements a probabilistic, parallel search in the solution space using domain-independent genetic operators to form a new population of candidate solutions. The population undergoes a simulated evolution process. At each generation the relatively 'good' solutions reproduce, while the relatively 'bad' solutions die. To distinguish between different solutions one can use an objective (evaluation) function, which plays the role of an environment. Crossover and mutation operators produce new areas of the solution space to explore. The major advantage of GA is that GA do a multi-directional population based search. GA, based on natural selection, repeatedly modifies a population of individual solutions. Over successive generations, the population "evolves" toward an optimal solution. GA is considered to have better global optimizing properties than other heuristic optimization techniques, especially, in the case of discontinuous, non-differentiable, stochastic, and highly nonlinear problems having large search spaces with many local extrema [164-173]. However, GA employs a probabilistic approach and has better global optimizing properties but shows poor convergence to optimality. In order to search for the global optimum, hybrid techniques have been proposed where a genetic algorithm (GA) is used to identify initial guesses and then a local optimizer is used to determine the optimum. An additional feature of the hybrid methods is that, similar to the deterministic global optimizer, multiple low-lying local

solutions are determined. Therefore, hybrid methods using a GA to provide initial guess of the parameters followed by a traditional local optimization routine may be more efficient and improve in searching for a global optimum while overcoming the limitations of poor convergence and weak exploitation capabilities [164-173].

Table 1.1. Plastic waste generation (Figures in thousands tones) in India [4]

	1995-1996 (Actual)	2001-2002(Predicted)	2006-2007(Predicted)
Total polymers	1889	4374	8054
Process Waste (2%)	38	87	161
Post consumer Waste	870 (46%)	1966(45%)	3624(45%)

Table 1.2. Demand scenario for key commodity plastics (Figures in thousand tonnes) in India [4]

Polymer	1995-1996 (Actual)	2001-2002(Predicted)	2006-2007(Predicted)
Polyethylene (PE)	823	1835	3267
Polypropylene (PP)	340	885	1790
Polyvinyl chloride (PVC)	489	867	1287
Polyethyleneterephthalate (PET)	34	140	289
Others	203	647	1415
Total	1889	4374	8054
Plastics in Packaging	967	2272	4037
% of Plastics in Packaging	52%	52%	50%

Table 1.3. Indian PET market (tonnes) - current and projected [5]

Market Segment	2000	2003
Carbonated soft Drink	10,000	25,000
Mineral water	10,000	25,000
Country liquor	5,000	8,000
Edible oil	3,000	5,000
Jars (Tea, confectionery)	6,000	8,000
Small bottles (pharmaceuticals)	4,000	6,000
Others	7,000	13,000
Total	45,000	90,000

Table 1.4. Product yield from fluidized bed pyrolysis

Feedstock	Temperature ˚C	Residence time	Gas (wt %)	Oil (wt %)	Char (wt %)	Other	Source
Polyethylene PE	760		55.8	42.4	1.8 C		W.Kaminsky et al. 2004 [26]
Polyethylene PE	530		7.6	50.3	0.1	42 waxes	
Polypropylene PP	740		49.6	48.8	1.6 C		
Polystyrene PS	580		9.9	24.6	0.6	64.9styrene	
Mixtures of PE/PP/PS	750		52.0	46.6	1.4		
Polyester	768		50.8	40.0	7.1	2.1H_2O	
Polyurethane	760		37.9	56.3	0.5	5 H_2O+ 0.3HCN	
ABS copolymer	740		6.9	90.8	1.1	1.2HCN	
Polyamide PA	760		39.2	56.8	0.6	3.4HCN	
Polycarbonate	710		26.5	46.4	24.6	2.5 H_2O	
Phenolformaldehyde resins	780		14.4	28.1	49.5	8.0 H_2O	
Poly(methyl methacrylate) PMMA	450		1.25	1.4	0.15 C	97.2MMA	
Poly(vinyl chloride) PVC	740		6.8	28.1	8.8	56.2HCL	
Polytetrafluoroethylene PTFE	555		18.8	5.2	0.3		
Disposable syringes	720		56.3	36.4	5.8	1.5 Steel	
LDPE	797	400	92.9	5	2		B.J.Milne et al. 1999 [24]
	825	400	92.9	5	2		
	780	600	88	8	4		
	805	600	90	8	2		
LDPE	500		10.8	43.9		45.3 wax	P.T.Williams et al. 1999 [23]
	550		21.4	43.2		35.4	
	600		24.2	51		24.8	
	650		40.1	47.8		12.1	
	700		71.4	24.6		4	

Table 1.5. Composition of liquid fraction cracking of waste plastic [28]

Temperature (˚C)		500 ˚C			525˚C			550˚C		
Residence time (h)		**0.6**	**0.9**	**1.2**	**0.6**	**0.9**	**1.2**	**0.6**	**0.9**	**1.2**
(a) 40%PE +40%PP+20% ethylene-propylene copolymer										
Aliphatic	C_5-C_6	15.27	17.65	18.70	12.32	15.72	16.36	13.29	13.86	15.99
	C_7-C_9	27.99	29.42	31.90	30.07	28.61	31.92	30.20	29.18	30.12
	C_{10}-C_{12}	21.63	21.18	20.09	19.61	21.31	23.94	18.29	18.22	20.53
	C_{13}-C_{15}	15.27	13.25	17.13	19.17	14.64	16.08	19.46	17.03	15.86
	C_{16}-C_{18}	12.72	11.77	9.45	10.96	8.60	8.06	7.84	7.90	8.60
	C_{19}-C_{21}	4.90	4.71	1.50	3.99	6.14	1.36	2.91	6.26	3.58
	C_{22}-C_{24}	1.71	1.54	0.63	2.73	2.46	0.68	3.12	4.04	2.46
	C_{25}-C_{27}	0.00	0.00	0.00	0.63	1.21	0.00	1.21	1.26	0.62
	C_{28}-C_{30}	0.00	0.00	0.00	0.00	0.00	0.00	1.81	0.23	0.00
	∑Aliphatic	99.49	99.52	99.40	99.48	98.69	98.40	98.13	97.98	97.76
Aromatic	Benzene	0.09	0.12	0.11	0.08	0.16	0.18	0.05	0.09	0.13
	Toluene	0.00	0.00	0.06	0.04	0.06	0.10	0.10	0.18	0.11
	Ethyl-benzene	0.42	0.36	0.43	0.37	1.00	1.20	1.41	1.46	1.57
	Styrene	0.00	0.00	0.00	0.00	0.00	0.00	0.00	0.00	0.00
	o-Xylene	0.00	0.00	0.00	0.00	0.00	0.00	0.00	0.00	0.00
	m-Xylene	0.00	0.00	0.00	0.00	0.00	0.00	0.00	0.00	0.00
	C_{16}+	0.00	0.00	0.00	0.03	0.09	0.12	0.31	0.29	0.43
	∑aromatic	0.51	0.48	0.60	0.52	1.31	1.60	1.87	2.02	2.24
(b) 39%PE+49%PP+2%PA+2%PUR+8%PS										
Aliphatic	C_5-C_6	13.42	14.75	15.86	12.99	13.36	12.96	10.70	9.89	10.81
	C_7-C_9	22.08	22.83	24.79	24.37	23.24	23.03	24.12	22.93	23.78
	C_{10}-C_{12}	18.48	16.95	16.86	15.99	16.45	19.19	14.11	14.83	14.05
	C_{13}-C_{15}	12.65	15.95	15.86	11.99	10.65	13.44	14.59	13.84	13.41
	C_{16}-C_{18}	10.41	7.97	6.94	8.88	6.78	6.72	6.81	6.92	7.57
	C_{19}-C_{21}	3.70	2.99	1.98	3.50	4.84	1.92	2.63	3.95	3.24
	C_{22}-C_{24}	0.97	1.38	0.40	2.30	1.94	2.40	2.92	4.15	2.16
	C_{25}-C_{27}	0.00	0.00	0.00	0.60	0.95	0.00	0.97	0.96	0.54
	C_{28}-C_{30}	0.00	0.00	0.00	0.00	0.00	0.00	1.65	0.18	0.00
	∑aliphatic	81.71	82.82	82.69	80.61	78.21	79.65	78.50	77.65	75.57
Aromatic	Benzene	0.08	0.07	0.18	0.99	0.65	0.80	0.91	1.31	1.37
	Toluene	0.49	0.67	0.69	1.60	2.03	1.92	2.24	2.96	3.24
	Ethyl-benzene	0.70	0.70	0.61	0.81	1.00	1.23	1.69	1.85	2.31
	Styrene	10.70	9.77	9.91	10.59	11.33	9.00	10.70	10.18	9.84
	o-Xylene	1.65	1.00	1.27	1.30	1.74	1.14	1.36	1.94	2.59
	m-Xylene	0.39	0.30	0.29	0.28	0.77	1.15	0.39	0.65	0.86
	C_{16}+	4.28	4.68	4.34	3.82	4.26	3.9	4.18	3.46	4.22
	∑aromatic	18.29	17.18	17.31	19.39	21.79	20.35	21.50	22.35	24.43

Table 1.6. Gas composition from the fluidised bed pyrolysis of LDPE in relation to pyrolysis temperature [23]

Gas	Temperature (°C)				
	550	500	600	650	700
Hydrogen	1.05	0.23	0.22	0.68	0.66
Methane	0.83	1.52	3.03	4.22	11.76
Ethane	0.78	1.71	2.53	2.82	4.68
Ethene	2.19	5.33	6.84	10.81	26.86
Propane	0.76	0.84	0.83	0.83	1.25
Propene	1.82	4.79	5.64	9.10	18.59
Butane	0.50	0.55	0.21	0.55	B0.01
Butene	2.91	6.39	4.95	11.07	7.63

Table 1.7. Aromatic compounds in the oils from the fluidised bed pyrolysis of LDPE waste in relation to temperature of pyrolysis (ppm) [23]

Compound	Temperature (°C)				
	500	**550**	**600**	**650**	**700**
Benzene	nda	nd	14531	28213	76711
Toluene	nd	nd	8316	21780	43524
o-Xylene	nd	nd	946	3103	5039
m-Xylene	nd	nd	875	7885	6701
Dimethylbenzene	nd	nd	657	5442	19986
Trimethylbenzenes	nd	nd	nd	498	6570
Indane	nd	nd	nd	671	1079
Indene	nd	nd	nd	1837	16290
Methylindenes	nd	nd	nd	1088	9365
Naphthalene	nd	nd	nd	1197	28201
Methylnaphthalenes	nd	nd	nd	1100	12105
Ethylnaphthalene	nd	nd	nd	nd	189
Dimethylnaphthalene	nd	nd	nd	nd	426
Acenaphthylene	nd	nd	nd	nd	2901
Acenaphthene	nd	nd	nd	nd	429
Trimethylnaphthalenes	nd	nd	nd	nd	543
Fluorene	nd	nd	nd	nd	90
Tetramethylnaphthalene	nd	nd	nd	nd	87
Phenanthrene	nd	nd	nd	nd	519

*nd not detected

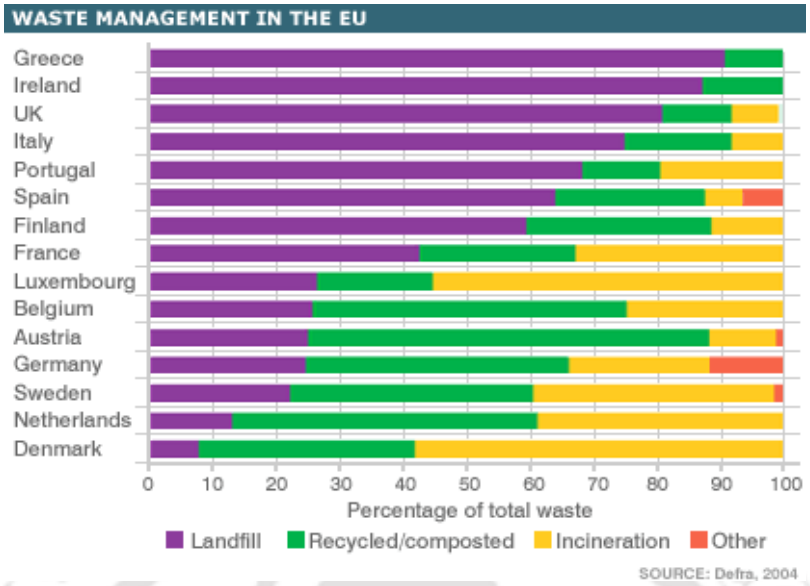

Figure 1.1. Waste management scenario in European Union [14]

2. Kinetics analysis

Kinetics analysis has two major objectives, namely probing reaction mechanism and parametrizing the reaction rates. Of these two objectives, the later has the foremost practical importance, because kinetic parameters are important to know the rate of reaction, predicting the experimental data, and scale up [174]. This chapter gives a complete description of the detailed development of various model-fitting and model-free kinetics analysis techniques for both the thermal and catalytic pyrolysis. The new direct integration techniques developed for integration of temperature integral, development of first order, second order, and second order cross sensitivity matrices and their computation methods are presented. It also describes the development of a new approach for the kinetics analysis technique to overcome the drawbacks of traditional model fitting methods and reliable evaluation of globally optimized kinetic parameters for both the TG decomposition of thermal and catalytic pyrolysis employing model-free coupled model fitting technique and hybrid genetic algorithm. Simulation procedures for prediction of the TGA data both for thermal and catalytic decomposition of plastics used are also discussed in this chapter.

2.1. Single step kinetics model

The kinetics model equations combined with the Arrhenius approach of the temperature function of reaction rate is expressed as:

$$\frac{d\alpha}{dt} = k_0 \exp\left(-E/RT\right) f(\alpha) \qquad (1)$$

where t is time (in minutes), T the temperature (in Kelvin), α the conversion of the reaction [$\alpha = (W_0 - W)/(W_0 - W_\infty)$, where W_0 is the initial weight of the sample, W the sample weight at any temperature T, and W_∞ the final sample weight [(all sample weight given in milligrams)], $d\alpha/dt$ the rate of reaction (min^{-1}), and $f(\alpha)$ the reaction model (Table 2.1). The terms k_0, represents the pre-exponential factor (K^{-1}), and E, the activation energy (kJ mol^{-1}), are the Arrhenius parameters. R is the universal gas constant (kJ mol^{-1} K^{-1}). The reaction model may take various forms based on nucleation and nucleus growth, phase boundary reaction, diffusion, and chemical reaction [29-31, 33-38, 181, 183]. In the present investigation, we applied fifteen such well-known models (Table 2.1) for estimating the best fitted overall kinetics parameters (k_0 and E) except n^{th} order reaction model, where we obtained the best fitted kinetics triplet (order of chemical reaction n, k_0, and E) for all the three types of polymers. Initially, for a few cases, we used single heating rate and later (in most of the work) we have used multi-heating rates. At a constant heating rate under non-isothermal conditions the explicit temperature/time [33-38, 175-183], dependence in Eq. (1) is eliminated through the trivial transformation

$$\beta \frac{d\alpha}{dT} = k_0 \exp(-E/RT) f(\alpha) \qquad (2)$$

Where, $\beta = \frac{dT}{dt}$ is the heating rate (K min^{-1}) and $\frac{d\alpha}{dT}$ is rate of reaction (K^{-1})

Brief discussions of the various techniques used to obtain kinetics parameters are given below

2.1.1. Model-fitting methods of kinetics analysis using TGA experimental data

Thermogravimetic analysis (TGA) is widely applied to study the pyrolysis kinetics of polymers. The traditional model-fitting kinetics analysis using single heating rate and

single step n[th] order decomposition model gives a single set of kinetics triplet, which is estimated after minimizing deviation between experimental and simulation data.

2.1.1.1. Model-fitting method for isothermal experiments [33, 175, 177]

For isothermal TG experiments, Eq. (1) can be rewritten as

$$\frac{d\alpha}{dt} = k(T) f_m(\alpha) \tag{3}$$

$$g_m(\alpha) = \int_0^{\alpha} \frac{d\alpha}{f_m(\alpha)} = k_m(T) \int_0^{t} dt = k_m(T) t \tag{4}$$

The subscript m corresponds to the reaction model selected. For each reaction model, the rate constants are evaluated at several temperatures, T_i and the Arrhenius parameters are determined from Eq. (5). The various forms of $g_m(\alpha)$ are presented in Table 2.1 and $k_m(T)$ can be expressed as $\ln k_m(T_i) = \ln k_{0,m} - \frac{E_m}{RT_i}$ (5)

Akaike's Information Criteria (AIC) [177, 181-184]

Akaike's Information Criteria (AIC), discussed below is applied to choose the appropriate reaction model.

$$AIC = N.\ln\left(\frac{SS}{N}\right) + 2K \tag{6}$$

Where N is number of data points, K is number of parameters plus one and SS is sum of square of vertical distance of the points from the centre. The corrected AIC for small number of data points is obtained from Eq. (7).

$$AIC_c = AIC + \frac{2K(K+1)}{N-K-1} \tag{7}$$

Thus for two reaction models A and B,

$$\Delta AIC = AIC_{C,B} - AIC_{C,A} \quad (8)$$

$AIC_{C,B}$ is corrected AIC for model B and $AIC_{C,A}$ is corrected AIC for model A.

2.1.1.2. Model-fitting methods for nonisothermal experiments using single heating rate

Nonisothermal or dynamic TG experiment is widely applied kinetics method to study the pyrolysis kinetics of polymers. The advantages of determining kinetic parameters by non-isothermal methods rather than by conventional isothermal studies are as follows.

(1) The nonisothermal kinetics can be established over wide temperature range in a continuous manner.

(2) It gives other kinetics information such as start, end and maximum decomposition temperatures.

(3) When a sample undergoes considerable reaction in being raised to the target temperature, the results obtained by isothermal methods are questionable because some decomposition may occur during the pre-heating period, particularly when the temperature of onset of reaction is considerably lower than the target temperature of the isothermal experiments [108].

In case of nonisothermal experiments using single heating rate, Saha and Ghoshal [175] have already reported details of the model-fitting techniques, such as the nth-order model technique and the ASTM E698 technique, in recent publication. Wang et al.[133] elaborated on the other model-fitting methods, such as the Freeman-Carroll, Friedman, and Chang techniques.

2.1.1.2.1. n^{th} Order Model technique [175]

In this technique, the n^{th} order kinetic model equation [Eq. (2)] is linearised as follows.

$$\ln\left(\beta\frac{d\alpha}{dT}\right) = \ln\ k_0 - \frac{E}{RT} + n\ln(1-\alpha) \quad (9)$$

The above equation is used to fit the experimental TGA data by regression analysis and to obtain the kinetics parameters from single heating rate TG curve.

2.1.1.2.2. Friedman technique [133, 175]

Friedman technique is another method to calculate the kinetic parameters of thermal decomposition using single heating-rate TGA curve. The corresponding equation is

$$\ln\ k_0 = \ln\left(\beta\frac{d\alpha}{dT}\right) - n\ln(1-\alpha) + \frac{E}{RT} \qquad (10)$$

In this technique, values of (-E/R) and n are obtained from the plots of $\ln\left(\beta\frac{d\alpha}{dT}\right)$ vs. $1/T_{avg}$ and $\ln(1-\alpha)$ vs. $1/T_{avg}$ respectively. Here, $T_{avg} = (T_{i+1}+T_i)/2$. The subscript, i stand for data point counter. Values of (-E/R) and n so obtained are used to calculate $\ln k_0$ from Eq. (10) at T_m.

2.1.1.2.3. Freeman-Carroll technique [133]

Freeman-Carroll technique for a single heating rate TGA curve to obtain the kinetics parameters of thermal decomposition uses the equation $Y_1 = n - (E/R)X_1$ (11)

Where, $Y_1 = \dfrac{\Delta\ln(\beta\frac{d\alpha}{dT})}{\Delta\ln(1-\alpha)}$ and $X_1 = \dfrac{\Delta\left(\frac{1}{T}\right)}{\Delta\ln(1-\alpha)}$.

(-E/R) and n are obtained from the slope and intercept respectively of the plot Y_1 versus X_1. The above information is further used to calculate $\ln k_0$ at T_m (Temperature at which maximum decomposition occurs) using Eq. (10).

2.1.1.2.4. Chang technique [133]

Chang technique is also used for a single heating-rate TGA curve to obtain kinetics parameters from equation $Y_2 = \ln k_0 - \frac{E}{RT}$ (12)

Where, $Y_2 = \ln\left[\frac{\beta \frac{d\alpha}{dT}}{(1-\alpha)^n}\right]$

A plot of Y_2 versus $1/T_{avg}$ gives a straight line provided the order is chosen correctly. The slope and intercept can give (–E/R) and $\ln k_0$ respectively.

The above equations are used to fit the experimental data by linear regression analysis and to obtain the kinetics parameters directly. Freeman-Carroll and Chang techniques describe the behaviour of thermal degradation in the temperature range from [T_m- (30 – 60)] to T_m. However, the E value given by Friedman technique mainly indicates the thermal decomposition behaviour in the temperature range from [T_d- (20 – 40)] to T_d, in which the linear relation between $\ln\left(\beta \frac{d\alpha}{dT}\right)$ versus 1/T is available. The n^{th} order model technique uses wide range of temperature from T_{Wo} to $T_{W\infty}$ to calculate the kinetic parameters.

2.1.2. ASTM E698 technique [33, 175, 185]

ASTM E698 technique occupies an intermediate position between the model fitting and model free methods. It uses a model-free estimate for the activation energy, which is evaluated from Kissinger's plot of $\ln(\frac{\beta}{T_m^2})$ against $\frac{1}{T_m}$, where T_m is the mean

temperature (K) corresponding to the maximum of $\frac{d\alpha}{dT}$. However, the pre-exponential factor is evaluated on assumption of a first-order reaction as follows.

$$k_0 = \frac{\beta E}{RT_m^2}\exp(\frac{E}{RT_m}) \quad (13)$$

By definition of ASTM E698 method, the reaction order is set to unity.

2.2. Model-free isoconversional method [33-38, 60, 64, 76, 155-160, 176, 178-180, 185]

Model-free method calculates the activation energy with the progress of a reaction using multi-heating rates. The basic assumption of the model-free method is that reaction model is not dependent on temperature or heating rate. It is also called isoconversional method as it takes values of temperature for a particular conversion from different heating rates. There are various such isoconversional methods available to calculate the apparent activation energy with the extent of conversion using multi-heating rates such as Kissinger method[64, 159-160], Flynn-Wall-Ozawa method [157, 159-160], Friedman method [33], and nonlinear Vyazovkin model-free method [33-38, 60, 76, 155, 158, 174, 176, 178-180,185]. Nonlinear Vyazovkin model-free method has been used in the present work to obtain the kinetic information from nonisothermal data.

2.2.1. Model-free isoconversional method for isothermal condition

Based on the assumption of the isoconversional method that the reaction model is not dependent on temperature or heating rate, Eq. (1) under isothermal condition is integrated as follows.

$$g(\alpha) = \int_0^{\alpha} \frac{d\alpha}{f(\alpha)} = k_{\alpha}(T) \int_0^{t} dt = k_{\alpha}(T)t \tag{14}$$

For each conversion level, the rate constants are evaluated at several isothermal temperatures, T_i, and Arrhenius parameters are determined in the usual manner using the logarithmic form of Arrhenius equation,

$$\ln k_{\alpha}(T_i) = \ln k_{0,\alpha} - \frac{E_{\alpha}}{RT_i} \tag{15}$$

Under isothermal condition combining Eq.(14) and Eq.(15) we obtain

$$-\ln t_{\alpha,i} = \ln\left[\frac{k_{0,\alpha}}{g(\alpha)}\right] - \frac{E_{\alpha}}{RT_i} \tag{16}$$

Where, activation energy, E_{α} at a particular conversion, α is evaluated from the slope of the plot $-\ln t_{\alpha,i}$ against T_i^{-1}. Thus the dependence of E_{α} on α is obtained for the thermal decomposition under isothermal condition [33, 177].

2.2.2. Vyazovkin model-free kinetics technique for non-isothermal condition

For nonisothermal experiments there are several relationships used to compute Arrhenius parameters. Each one is based on an approximate form of temperature integral that results from rearrangement and integration of Eq. (1).

$$g(\alpha) = \frac{k_0}{\beta} \int_0^{T_{\alpha}} \exp\left(\frac{-E_{\alpha}}{RT}\right) dT = \frac{k_0}{\beta} I\left(E_{\alpha}, T_{\alpha}\right) \tag{17}$$

The isoconversional integral method proposed independently by Flynn and Wall and Ozawa using Doyle's approximation [159-160] is based on the equation:

$$\log \beta = \log \frac{k_0 E_{\alpha}}{R g(\alpha)} - 2.315 - 0.4567 \frac{E_{\alpha}}{RT_{\alpha}} \tag{18}$$

Thus, at same conversion level, the plot ln β versus ($1/T_\alpha$), obtained from TG curves at several heating rates, should be a straight line whose slope can be used to evaluate the apparent activation energy.

Vyazovkin developed an advanced nonlinear isoconversional method for a set of nonisothermal experiments which avoids inaccuracies associated with analytical approximations of the temperature integral. Because $g(\alpha)$ is independent of heating rates, Eq. (17) can be written for a given conversion and a set of n experiments carried out at different heating rates β_i (i=1,...,n) as

$$\frac{k_0}{\beta_1} I\left(E_\alpha, T_\alpha\right) = \frac{k_0}{\beta_2} I\left(E_\alpha, T_\alpha\right) = \ldots = \frac{k_0}{\beta_n} I\left(E_\alpha, T_\alpha\right) = \text{constant}$$
$$\text{or } \sum_{\mathrm{i}=1}^{n} \sum_{\mathrm{i}\neq\mathrm{j}}^{n} I\left(E_\alpha, T_{\alpha,i}\right) \frac{\beta_j}{\beta_i} / I\left(E_\alpha, T_{\alpha,j}\right) = \text{constant} \tag{19}$$

Thus,

$$\sum_{\mathrm{i}=1}^{n} \sum_{\mathrm{i}\neq\mathrm{j}}^{n} I\left(E_\alpha, T_{\alpha,i}\right) \frac{\beta_j}{\beta_i} / I\left(E_\alpha, T_{\alpha,j}\right) = \text{constant} \tag{20}$$

Here, the subscripts i and j represent ordinal number of two nonisothermal TG experiments under different heating rates. Since the T_α values are measured with some experimental error, Eq. (19) can only be satisfied as an approximate equality [37]. Consequently, Eq. (20) may be satisfied as a condition of minimum value. The activation energy (E_α) can be determined at any particular value of α by finding the value of E_α for which the objective function Ω (E_α) is minimized, where

$$\Omega(E_\alpha) = \sum_{i=1}^{n} \sum_{j\neq i}^{n} \frac{I\left(E_\alpha, T_{\alpha,i}\right)\beta_j}{I\left(E_\alpha, T_{\alpha,j}\right)\beta_i} \tag{21}$$

Using experimental values of T_α and β into Eq. (21) and minimizing the function $\Omega(E_\alpha)$, the value of the E_α at a given conversion, is obtained. The objective function, $\Omega(E_\alpha)$ minimization is done by numerical method in MATLAB using 'medium-scale: Quasi-Newton line search' algorithm. The 'fminunc' function for unconstrained problem is applied for the optimization [173].

Where, $I(E_\alpha, T_{\alpha i}) = \int_0^{T_{\alpha i}} \exp\left(\frac{-E_\alpha}{RT}\right) dT$ (22)

The temperature integral can be evaluated by several popular approximations and direct numerical integration discussed below.

2.2.2.1. Direct integration of temperature integral

As we understand that the temperature integral in Eq. (22) has no exact analytical solution, an alternative way to express the temperature integral is given below [178-180].

$$\int_0^{T_{\alpha i}} \exp\left(\frac{-E_\alpha}{RT}\right) dT = \frac{E_\alpha}{R} P(u) \quad (23)$$

where $u = \frac{E_\alpha}{RT}$ and

$$P(u) = \int_u^\infty \frac{\exp(-u)}{u^2} du = \frac{\exp(-u)}{u} - Ei(u) \quad (24)$$

Where $Ei(u) = \int_u^\infty \frac{\exp(-u)}{u} du$, exponetial integral

$$I(E_\alpha, T_\alpha) = \int_0^{T_{\alpha i}} \exp\left(\frac{-E_\alpha}{RT}\right) dT = \frac{E_\alpha}{R}\left[\frac{\exp\left(\frac{-E_\alpha}{RT}\right)}{\left(\frac{E_\alpha}{RT}\right)} - Ei\left(\frac{E_\alpha}{RT}\right)\right] \quad (25)$$

Initially, numerical integration of Eq. (22) was also carried out using a function called 'quadv' based on recursive adaptive Simpson Quadrature [173, 176]. Later stages,

calculation of exponential integral [Eq. (24), as reported by Cai et al. [186]] was carried out numerically by a function called 'expint' using MATLAB [173, 178-180].

2.2.2.2. Approximations for integration of the temperature integral

Several popular approximations such as Coats and Redfern, Gorbachev, Agrawal and Sivasubramanian and approximation of Cai et al. [186] discussed subsequently, are also used for integration of Eq. (22).

Coats and Redfern [187] first approximated the integral by the relation:

$$\int_0^{T_\alpha} \exp\left(-\frac{E_\alpha}{RT_\alpha}\right) dT = \frac{RT_\alpha^2}{E_\alpha}\left(1-\frac{2RT_\alpha}{E_\alpha}\right)\exp\left(-\frac{E_\alpha}{RT_\alpha}\right) \tag{26}$$

In 1975, Gorbachev suggested the more accurate approximation of the temperature integral by the relation [187]:

$$\int_0^{T_\alpha} \exp\left(-\frac{E_\alpha}{RT_\alpha}\right) dT = \frac{RT_\alpha^{\,2}}{E_\alpha}\left(\frac{1}{1+2RT_\alpha/E_\alpha}\right)\exp\left(-\frac{E_\alpha}{RT_\alpha}\right) \tag{27}$$

Gorbachev approximation is better than Coats and Redfern approximation for activation energy ranging from 40 to 250 kJ mol^{-1} over the temperature range of 300-1000 K [187].

Agrawal and Sivasubramanian [187] improved the temperature integral by the relation:

$$\int_0^{T_\alpha} \exp\left(-\frac{E_\alpha}{RT_\alpha}\right) dT = \frac{RT_\alpha^2}{E_\alpha}\left[\frac{1-\frac{2RT_\alpha}{E_\alpha}}{1-5\left(\frac{RT_\alpha}{E_\alpha}\right)^2}\right]\exp\left(\frac{-E_\alpha}{RT_\alpha}\right) \tag{28}$$

This approximation is proved to be superior to the other two approximations discussed above for activation energy ranging from 40 to 250 kJ mol^{-1} over the temperature range of 300-1000 K [187].

The proposed approximation of Cai et al. [186], which is superior to all the above approximations, is given by this relation:

$$\int_0^{T_\alpha} \exp\left(-\frac{E_\alpha}{RT_\alpha}\right)dT = \frac{RT_\alpha^2}{E_\alpha}\left[\frac{\frac{E_\alpha}{RT_\alpha}+0.66691}{\frac{E_\alpha}{RT_\alpha}+2.64943}\right]\exp\left(\frac{-E_\alpha}{RT_\alpha}\right) \quad (30)$$

2.3. Development of objective function (multi-parameter) for optimization of kinetics triplet using single and multi-heating rate(s)

The traditional model-fitting kinetics analysis using single heating rate and single step decomposition model gives only a single set of kinetics triplet, which is estimated after minimizing deviation between simulated data and experimental data. Now, for nonisothermal condition, m-th model, l-th heating rate and j-th data point, integral form of Eq. (2) can be written as:

$$g_m(\alpha_{j,l}) = \int_0^{\alpha} \frac{d\alpha}{f_m(\alpha_{j,l})} = (k_0/\beta)\int_0^{T_{\alpha_{j,l}}} \exp(-E/RT_{\alpha_{j,l}})dT = (k_0/\beta)I(E,T_{\alpha_{j,l}}) = x \quad (30)$$

This equation can also be solved for α in all 15 models (Table 1) by substituting $\frac{k_0}{\beta} = \exp(\tilde{K}_0)$ Where $K_0 - \ln(\beta) = \tilde{K}_0$ and $k_0 = \exp(K_0)$. Taking logarithm on the both side of Eq. (30)

$$\ln\left(g_m(\alpha_{j,l})\right) = \tilde{K}_0 + \ln\left(I(E,T_{\alpha_{j,l}})\right) \quad (31)$$

The objective function in case of single heating rates TGA curve to calculate optimum values of kinetics parameter should be based on the minimum values of the deviation $\Delta(E, K_0, n)$, which is expressed as

$$\Delta(E,K_0,n)=\sum_{j=1}^{J}\left[\ln(g_m(\alpha_j))-\tilde{K}_0-\ln\left(I(E,T_{\alpha_j})\right)\right]^2 \quad (32)$$

However, major emphasis in the present work has been evaluation of kinetics triplet from the experimental data using multi-heating rates as International Confederation of Thermal Analysis and Calorimetry (ICTAC) project, 2000 [29] ruled out the validity of thermal kinetics analysis using single heating rate.

Accordingly, the objective function, [Δ (E, K_0, n)] for total L heating rates, J data points, and m-th model to calculate optimum values of kinetics triplet is formed as

$$\Delta(E,K_0,n)=\sum_{l=1}^{L}\left[\sum_{j=1}^{J}\left[\ln(g_m(\alpha_{j,l}))-\tilde{K}_0-\ln\left(I(E,T_{\alpha_{j,l}})\right)\right]\right]^2 \quad (33)$$

These objective functions [Eqs. (32) and (33)] are used most frequently to obtain pyrolysis kinetics parameters for single and multi-heating rates respectively. But this three parameters optimization is problematic due to choice of initial guess of the parameters [31]. The parameters E, ln(k_0/β) and n are strongly correlated and therefore it is very difficult to find global minimum of these objective functions. So, with the help of sensitivity analysis we have reduced the three-parameter optimization into a simple but reliable single parameter optimization problem discussed subsequently.

2.4. Sensitivity analysis of pyrolysis kinetics

Sensitivity analysis investigates the effect of parameter change on the solution of mathematical models. In chemical kinetics, models are usually based on differential equations and the results are concentration-time curves, reaction rates, and various kinetic features of the reaction. Sensitivity coefficients arising out of sensitivity analyses provide information about the importance and interconnection of parameters and variables [188].

Sensitivity analysis can identify sensitive parameters and help to develop a new objective function, which takes care of less sensitive parameters only. It is the technique used to investigate the propagation of parameter's uncertainties into output variables uncertainties [139-141]. This approach is based upon Taylor series approximations, where the second order terms are strongly needed for more accurate analysis of nonlinear response. In this work, I have applied sensitivity analysis to reduce the three-parameter optimization problem into single-parameter optimization problem. The details of the development of first order, second order, and cross second order sensitivity matrices are given in Appendix I.

2.4.1. Computation of first order sensitivity matrix

The initial conditions for computation of the first order sensitivity matrix are at T= T_{w0}, $S_{\alpha p_j}^{\langle 1 \rangle}$ =0 for all cases of p_i. To determine the effect of parameters uncertainties upon the model output variable (α), Eq. (AI.7) is added to this matrix form of equations for first order sensitivity co-efficient, Eq. (AI.21 or AI.22) with same initial condition. Then the matrix is solved simultaneously by MATLAB® using *ode15s* solver to obtain the sensitivity coefficients ($S_{\alpha p_j}^{\langle 1 \rangle}$). The *ode15s* is a variable-order; multistep solver based on the numerical differentiation formulae (NDF). These are related to but are more efficient than the backward differentiation formulae, BDF (also known as Gear's method) [173].

The first order sensitivities are reported in semi-normalized form, which is the ratio of values of the sensitivity coefficients and the respective parameters, i.e. $\frac{S_{\alpha p_j}^{\langle 1 \rangle}}{p_j^*}$ where p_j^* is the nominal value of parameter or optimum parameters values, p_j (Table 2.2).

2.4.2. Computation of second order and second order cross sensitivity matrix

The initial conditions for computation of the second order and second order cross sensitivity matrix are at T= T_{w0}, $s^{\langle 2\rangle}_{p_i}$ and $s^{\langle 2\rangle}_{p_i p_j}=0$ for all the parameters. Eqs. (AI.7) and Eq. (AI.21 or AI.22) (first order sensitivity matrix) are added to this matrix form of equations (AI.53 or AI.53) with same initial condition to simultaneously solve by MATLAB using *ode15s* solver to obtain the second order sensitivity coefficients and second order cross sensitivity coefficient, $s^{\langle 2\rangle}_{p_i}$ and $s^{\langle 2\rangle}_{p_i p_j}$. Both $s^{\langle 2\rangle}_{p_i}$ and $s^{\langle 2\rangle}_{p_i p_j}$ are reported in semi-normalized form as $\frac{s^{\langle 2\rangle}_{p_i}}{p_i^{*2}}$ and $\frac{s^{\langle 2\rangle}_{p_i p_j}}{p_i^* p_j^*}$.

Unfortunately, the calculated optimum E and $\ln(k_0/\beta)$ are completely determined by a model used and can greatly differ for different models for all traditional model-fitting kinetics analysis techniques [50, 131, 177]. Thus, $\ln(k_0/\beta)$ can be linearly related with E through Eq.(31). The values of optimal E and $\ln(k_0/\beta)$ vary greatly with the shift of order of the reaction which is called as compensation effect [33, 50, 177]. Since the DTG curves of the polymers (Figs. 1 and 2) [177] are almost symmetric about the maximum decomposition temperature (T_m), we have written Eq. (31) for maximum decomposition temperature (T_m) and m-th reaction model as follows:

$$\ln\left(g_m(\alpha_{T_m})\right) = \tilde{K}_0 + \ln\left(I(E,T_m)\right) \tag{34}$$

Applying Cai et al., [186] approximation in Eq. (30) can be written as:

$$\ln k_0 = \ln\left(g_m(\alpha_{T_m})\right) - \ln\left[\frac{RT_m^2}{E}\left(\frac{\frac{E}{RT_m}+0.66691}{\frac{E}{RT_m}+2.64943}\right)\right] + \frac{E}{RT_m} + \ln\beta \tag{35}$$

The term $\ln\left[\frac{RT_m^2}{E}\left[\frac{\frac{E}{RT_m}+0.66691}{\frac{E}{RT_m}+2.64943}\right]\right]$ and $\ln\left(g_m(\alpha_{T_m})\right)$ vary slightly with different reaction models and can be considered as constants about T_m [50,131, 177]. First order sensitivity coefficient is estimated for 26 E values ranging within 150–400 kJmole^{-1} with an interval of 10 kJmole^{-1} for each value of n. The corresponding ln(k_0/β) or $\tilde{K}_0$ values for each case of E is obtained from the linear relation using Eq.(35). Here, we have used only nth order chemical reaction model. Several values of n within the range of 0.5–2.0 with an interval of 0.05 are also used for such estimation. Each case is studied for different heating rates. The ranges of E, ln(k_0), n, and β used for sensitivity analysis are 150-400 kJmol^{-1}K^{-1}, 19.47-61.039, 0.5-2, and 5-25 (Kmin^{-1}) respectively (Table 2.2). The values are so chosen because in general, the values of kinetics parameters for pyrolysis of polymers lie in these ranges.

2.5. Development of single-parameter objective function

Multi-parameter optimization through minimization of the objective function such as square of the deviations between experimental data and calculated values (least square function) using direct or gradient based optimization techniques is frequently associated with uncertainty [30-34, 139, 177]. Moreover, the three parameters (E, ln(k_0/β) and n) optimization is problematic due to choice of initial guess of the parameters [31]. The parameters are strongly correlated and the solution of this objective functions is very difficult to find its global minimum. Therefore, with the help of sensitivity analysis we reduced the three-parameter optimization into a simple but reliable single parameter optimization problem

2.5.1. Standard deviation minimization technique (SDMT) for non-isothermal condition using multi-heating rates [177]

Here, we concentrated on the one parameter optimization considering the least sensitive parameter, E as obtained by sensitivity analysis. Thus, a new objective function almost similar to the objective function proposed by Mamleev and Bourbigot, [50] is developed as follows.

Rewriting Eq. (31) for a particular heating rates and total J data points, $\ln(k_0/\beta)$ or $\tilde{K}_0$ can be calculated as

$$\ln\left(k_0/\beta\right) = \tilde{K}_0 = \frac{1}{J}\sum_{j=1}^{J}\ln(g_m(\alpha_j)/I(E,T_{\alpha_j})) \tag{36}$$

Now, the objective function becomes two parameter function for m-th model, total J data point and L heating rates after substituting the Eq. (36) into Eq. (33)

$$\Delta(E,n) = \sum_{l=1}^{L}\left[\sum_{j=1}^{J}\ln(g_m(\alpha_{j,l})/I(E,T_{\alpha_{j,l}})) - \frac{1}{J}\sum_{j=1}^{J}\ln(g_m(\alpha_{j,l})/I(E,T_{\alpha_{j,l}}))\right]^2 \tag{37}$$

Since n is the most sensitive parameter for n^{th} order chemical model, we fixed a certain value of n or in other words Eq. (37) reduced to one parameters objective function [Δ (E)].

$$\Delta(E) = \sum_{l=1}^{L}\left[\sum_{j=1}^{J}\ln(g(\alpha_{j,l})/I(E,T_{\alpha_{j,l}})) - \frac{1}{J}\sum_{j=1}^{J}\ln(g(\alpha_{j,l})/I(E,T_{\alpha_{j,l}}))\right]^2 \tag{38}$$

In this case, the order of reaction, n is varied from 0.5 to 2.0 using increments of 0.05. The optimal values of E are obtained for different values of n by minimizing Δ (E). The objective function minimization is done by numerical method using MATLAB7®. The nonlinear least-square solver function 'lsqnonlin' without constraint was applied to solve the problem using 'large-scale trust-region reflective Newton algorithm' [173].

Thereafter, average values of $\ln(k_0/\beta)$ is calculated from Eq. (35) using the optimum values of E for each value of n. Finally the optimum kinetics triplet is obtained for the value of n where $\Delta(E)$ value is either minimum or close to minimum and standard deviation between the experimental and computed data is minimum [177].

2.6. Simulation of TGA data

Most of the polymer pyrolysis kinetics is studied under nonisothermal condition in the literatures. The advantages are discussed in section 2.1.1.2. However, isothermal kinetics data are mostly needed for practical application as most of the pyrolysis reactors operate at constant temperature. Therefore, the optimum kinetics triplets found by several model fitting and model free techniques from nonisothermal experiments are used for simulation to predict the isothermal data at required level of temperature.

2.6.1. Nonisothermal data prediction

The n^{th} order kinetic model equation with initial condition $\alpha=0$ at $T=T_{w0}$ is solved numerically by Runge-Kutta 4^{th} order method using the kinetics parameters obtained by n^{th} order model techniques, Freeman-Carroll, Friedman, Chang and ASTM E698 techniques. On the other hand, the n^{th} order kinetic model equation can also be solved after transforming the Eq. (3) as follows. The n^{th} order and first order kinetic model equation can be also be solved by substituting $\frac{k_0}{\beta} = \exp(\tilde{K}_0)$ Where $K_0 - \ln(\beta) = \tilde{K}_0$ and $k_0 = \exp(K_0)$ and transforming Eq. (30) for nth order chemical reaction model as follows.

$$\text{For } n \neq 1,\ \alpha = 1 - \left[(\exp(\tilde{K}_0)) I(E,T)(n+1) + 1 \right]^{\frac{1}{(n-1)}} \tag{39}$$

$$\text{For } n=1,\ \alpha = 1 - \exp[-(\exp(\tilde{K}_0)) I(E,T)] \tag{40}$$

The kinetic parameters obtained from SDMT are used to simulate nonisothermal decomposition data using Eqs. (39) and (40). The temperature integral [Eq. (22)] can be evaluated by several approximations and by direct numerical integration as discussed in sections 2.2.2.1 and 2.2.2.2. This work is also reported in our recent publication [177].

2.6.2. Prediction of isothermal kinetics from nonisothermal data [33, 35, 60, 176, 177-180, 189]

For non-isothermal condition at a particular conversion, α

$$g(\alpha) = \frac{k_0}{\beta}\int_0^{T_\alpha} \exp\left(\frac{-E}{RT}\right)dT = \frac{k_0}{\beta} I\left(E, T_\alpha\right) \tag{41}$$

For isothermal condition at the same conversion, α

$$g(\alpha) = kt_\alpha = k_0 \exp\left(\frac{-E}{RT}\right)t_\alpha \tag{42}$$

The reaction mechanism is assumed to remain same for both the non-isothermal and isothermal conditions. Therefore, at a particular value of α, the values of g(α) for both the non-isothermal and isothermal conditions are same. The evaluation of E_α dependence is sufficient to predict the isothermal kinetics from nonisothermal data. This is formalized by following equation.

$$t_\alpha = \frac{I\left(E_\alpha, T_\alpha\right)}{\beta \exp\left(-E_\alpha / RT_0\right)} \tag{43}$$

From this equation, time at which a given conversion will be reached at an arbitrary temperature T_0 is computed [33, 35, 60, 176, 178-180, 189]. Because predictions using this method can be made without knowledge of reaction model (and pre-exponential factor), they are referred as "model-free predictions."

The same expression can be used for isothermal data prediction from non-isothermal model-fitting techniques.

2.6.3. ASTM E698 prediction [33, 175,177]

ASTM E698 predictions for the isothermal kinetics are based on the assumption that a reaction obeys first-order kinetics. Time at which a given conversion will be reached is given by following equations [33,175, 177].

$$t = \frac{-\ln(1-\alpha)}{A\exp(E/RT)} \tag{44}$$

$$A = \frac{\beta E}{RT_m^2}\exp\left(\frac{E}{RT_m}\right) \tag{45}$$

2.7. Multi-steps and multi-heating rates model-fitting method for nonisothermal experiments [29, 50, 131-132, 177, 181-183]

The kinetics model equations combined with the Arrhenius approach of the temperature function of reaction rate constant for m-th model, i-th step and l-th heating rate is expressed as:

$$\frac{d\alpha_{i,l}}{dt} = k_{0i}\exp\left(-E_i/RT_{i,l}\right) f_{m,i}(\alpha_{i,l}) \qquad 1 \le l \le L,\ i = 1,2....5 \tag{46}$$

Where t is time (min), T, temperature (K), $\alpha_{i,l}$, conversion of reaction $(W_{0i,l}-W_{i,l})/(W_{0i,l}-W_{\infty i,l})$, $W_{0i,.}$, initial weight (mg), $W_{i,.}$, sample weight (mg) at any temperature T, $W_{\infty i,l}$, final sample weight (mg), $\frac{d\alpha_{i,l}}{dt}$, rate of reaction (min^{-1}), and $f_{m,i}(\alpha_{i,l})$, reaction model of i-th step and l-th heating rate. k_{0i}, the pre-exponential factor (K^{-1}) and E_i, the activation energy (kJ mol^{-1}) are the Arrhenius parameters. R is the gas constant (kJ $mol^{-1}K^{-1}$). The reaction model may take various forms based on nucleation and nucleus growth, phase boundary reaction, diffusion, and chemical reaction (Table 2.1). In the present

investigation, we have applied fifteen such well-known models (Table 2.1) for catalytic decomposition kinetics using single step and multi-heating rates.

At a constant heating rate and under nonisothermal condition, the explicit temporal/time dependence in Eq. (46) is eliminated through the trivial transformation

$$\beta_l \frac{d\alpha_{i,l}}{dT} = k_{0i} \exp\left(-E_i / RT_{i,l}\right) f_{m,i}(\alpha_{i,l}) \tag{47}$$

Where, $\beta_l = \frac{dT}{dt}$ is the heating rate (K min^{-1}) and $\frac{d\alpha_{i,l}}{dT}$ is rate of reaction (K^{-1}) of i-the step and l-th heating rate.

For each step, Eq. (47) can be integrated for m-th model, l-th heating rate, i-the step, and j data point as

$$g_{m,i}(\alpha_{i,j,l}) = \int_0^{\alpha_{i,j,l}} \frac{d\alpha}{f_{m,i}(\alpha_{i,j,l})} = [\exp(\tilde{K}_0)] \int_0^{T_{\alpha_{i,j,l}}} \exp(-E/RT_{\alpha_{i,j,l}})dT = (\exp(\tilde{K}_0))I(E, T_{\alpha_{i,j,l}}) = x \tag{48}$$

This equation can be solved for $\alpha_{i,l,j}$ using 15 different reactions models described in Table 2.1. Akaike's Information Criteria (AIC) [177, 181-184] is applied to choose the appropriate reaction model.

2.7.1. Multi-parameter optimization

The objective function most frequently used in case of multiple heating rates to calculate optimum values of Δ (E_i, K_{0i}, $f_{m,i}(\alpha_{i,l})$) for m-th model, total L heating rates i-the step and total J data points by minimization of square of deviation between experimental mass ($M_{exp}(T)$) and calculated mass ($M_{cal}(T)$) is given by Eq. 49.

$$\Delta(E_i, K_{0i}, f_{m,i}(\alpha_{i,l})) = \sum_{l=1}^{L}\left[\sum_{j=1}^{J}\left[M_{Exp,i,l,j} - M_{Cal,i,l,j}\right]\right]^2 \tag{49}$$

The values of $M_{Cal,i,l,j}$ calculated for each single value of $\alpha_{cal,i,l,j}$ are as follows:

$$M_{Cal,i,l,j} = M_{Exp,i,l,0} - \alpha_{i,l,j}(M_{Exp,i,l,0} - M_{Exp,i,l,\infty}) \quad (50)$$

Where $M_{Exp,i,l,0}$ is the initial point and $M_{Exp,i,l,\infty}$ is the final point of i-th independent step and l-th heating rate. However, in the present work all models except nth order reaction model involved two parameters optimization since in those models E_i, K_{0i} values are optimized for different models of $f_{m,i}(\alpha_{i,l})$ in Table 2.1.

However, as discussed earlier in section 2.5, the multi-parameter optimization strongly depends on the initial guess values of the parameters [31, 50, 177, 181-183] leading to possibility of achieving false minima, thus, may result unreliable values of the kinetics parameters.

2.7.1.1. Model-free coupled multi-parameters optimizations [182]

The use of modern nonlinear isoconversion method i.e. Vyazovkin model free technique not only obtains the activation energy as function of the extent of conversion but also helps to reveal the complexity of multi-step reaction and draw certain mechanic conclusions to over come the drawbacks associated with the traditional model fitting techniques. The initial guess for activation energy can be taken from the kinetics information from model-free kinetics analysis [31] for the new improved objective function [Eq. (49)] to calculate optimum values of kinetics triplet. For nth order chemical reaction model, I have used three initial guesses for n viz. 0.5, 1 and 1.5. Three initial guess values of E are taken for each initial guess value of n. These initial guess values of E are the average value of E_α i.e. $E_{\alpha,\,av}$ for the step obtained from Model-free analysis [179] and $E_{\alpha,\,av}$ ±5. Since the DTG curve [50, 131, 175, 177] is almost symmetrical around T_m with particular value of reaction order, n, the corresponding ln(k_0) or K_{0i} value for each case of initial guess values of E and n is obtained from Eq. (35). The

optimization of the objective function, after getting the initial guesses of the kinetics triplet, is carried out by direct search methods in MATLAB using 'fminsearch' function. The local minimization function (fminsearch) or LOA is generally referred to as unconstrained nonlinear optimization. This is a multidimensional unconstrained nonlinear minimization, by Nelder-Mead [173] direct search method.

2.7.1.2. Hybrid genetic algorithm (HGA) for three-parameter optimization [181-183]

The objective function, Eq. (49) for all 15 models (Table2.1), minimization is also done by HGA, discussed later, in MATLAB using 'fminsearch' as hybrid local search method in GA toolbox. Here, GA is used to provide initial guess values of the kinetics triplet for the LOA, the direct search method as above. General features of the GA are reported in Appendix II.

2.7.1.2.1. The structure of a hybrid genetic algorithm [169-173, 181-183]

GA employs a probabilistic approach and has better global optimizing properties but shows poor convergence to optimality. Whereas, HGA uses a typical basic GA with elitist strategy to reach near gradient or/ direct-based search method shows faster convergence to global optima. Therefore, often GA is hybridized using a LOA to improve its performance as a global optimization technique while overcoming the limitations of poor convergence and weak exploitation capabilities. The various kinds of hybridizations using LOA can be classified into three types:

Pre-hybridization [172]: Here the initial population of GA is generated using an LOA which reducing the solution space for GA and improving the efficiency. Such an approach seems to be well suited to the specific problem they addressed and does not seem to be suitable for general optimization.

Organic-hybridization [172]: In this case, an LOA is used as one of the operators of GA for improving each member of the population in each generation. Though the organic-hybridization is computationally more efficient than a GA, it offers little assurance of global minima and also lacks proper convergence criteria.

Post-hybridization [172]: In this case, GA is used to provide an initial design for LOA. This kind of hybridization seems to be the best way of combining the best characteristics of the two approaches as no compromise is made on the global and local optimizing characteristics.

2.7.1.2.2. Structure of HGA used for the present work [181-183]

In the present work, post-hybridization method i.e. GA coupled with LOA have been used. I have used the default initial population size (20), the default creation function 'Uniform' to create a random initial population with a uniform distribution, the stochastic options from the GA toolbox that chooses parents for the next generation, Gaussian function for mutation, scattered function for the next generation, forward migration option for the movement of individuals between subpopulations, default value of migration fraction (0.2) for migration of individuals between subpopulation, value of interval as 20 i.e. migration between subpopulations takes place every 20 generations, multidimensional unconstrained nonlinear minimization function 'fminsearch' as the hybrid function that uses the final point from the genetic algorithm as its initial point, and specified only the number of generation as stopping criteria.

Table 2.1. Various kinetics model functions and their integral forms

Kinetic Models	Kinetic Functions, Integral of kinetics function and calculation of α where, $x = (\exp(\tilde{K}_0))I(E_i, T_{i,l})$	Order	Model no
Nucleation and Growth	$f(\alpha) = (\frac{1}{n})(1-\alpha)(-\ln(1-\alpha))^{1-n}$	$n = 1/4$	1
		$n = 1/3$	2
	$g(\alpha) = [-\ln(1-\alpha)]^n$	$n = 1/2$	3
	$\alpha = 1 - \exp(-x^{1/n})$	$n = 2/3$	4
Phase Boundary Reaction	$f(\alpha) = n(1-\alpha)^{(n-1)/n}$	$n = 1$ (plate)	5
	$g(\alpha) = [1-(1-\alpha)^{1/n}]$	$n = 2$ (Cylinder)	6
	$\alpha = 1-(1-x)^n$	$n = 3$ (Sphere)	7
Diffusion	$f(\alpha) = 1/\alpha$	$n = 1$ (plate)	8
	$g(\alpha) = \alpha^2/2$		
	$\alpha = (2x)^{1/2}$		
Power law	$f(\alpha) = \left(\frac{1}{n}\right)\alpha^{1-n}$	$n = 1/4$	9
		$n = 1/3$	10
	$g(\alpha) = \alpha^n (0 < n < 2)$	$n = 1/2$	11
	$\alpha = x^{1/n}$	$n = 3/2$	12
Chemical reaction	$f(\alpha) = (1-\alpha)$	$n = 1$, 1st order	13
	$g(\alpha) = -\ln(1-\alpha)$		
	$\alpha = 1-\exp(-x)$		
	$f(\alpha) = (1-\alpha)^n$	$n = 2$, 2nd order	
		$n = n$, nth order	14
	$g(\alpha) = [1/(1-\alpha)^{n-1} - 1]/(n-1)$		15
	$\alpha = 1-[1+(n-1)x]^{1/(1-n)}$		

Table 2.2. Ranges of kinetics parameters used for sensitivity analysis

E ($kJmol^{-1}K^{-1}$)	$ln(k_0)$	n	β ($Kmin^{-1}$)
150-400	19.47-61.039	0.5-2	5-25

3. Experimental

This chapter presents polymer materials and their characterization, experimental procedure for nonisothermal and isothermal pyrolysis of polymers, and instruments used for this study. Next, it describes the catalysts synthesis, characterization of catalysts, catalytic decomposition procedure of plastics such as waste LDPE and PP. It also describes experiments on catalysts reusability and product analysis using gas chromatography. .

3.1. Polymer materials for noncatalytic pyrolysis

The nonisothermal decompositions were carried out for waste PET soft drink bottles, virgin PET (AS-40, bottle grade) supplied by South Asian Petrochem Limited, India, waste LDPE, coloured PE sample from poly pack, and PP (polypropylene homopolymer (PPHP), Trade name: Koylene ADL, Grade AS030N) supplied by Indian Petrochemicals Corporation Limited, Vadodara, India with melt flow index 3.0.

3. 2. Characterization of polymers

The polymer samples used for the present work were characterized by differential scanning calorimetry (DSC) analysis described subsequently.

3.2.1. Differential scanning calorimetry (DSC) analysis [185, 191, 178-180, 181]

Differential Scanning Calorimetry (DSC) is a thermal analysis technique, which is used to measure the temperatures and heat flows associated with transitions in materials as a function of time and temperature. The sample and reference materials are maintained at the same temperature by supplying heat to the sample during an endothermic process or

to the reference during an exothermic process. The amount of heat added to the sample or reference, ΔH, is recorded as a function of temperature to produce a DSC curve. Such measurements provide qualitative and quantitative information about physical and chemical changes that involve endothermic and exothermic processes, or changes in heat capacity. DSC can measure thermal events such as melting, recrystallization, decomposition, and glass transitions [185]. The DSC analysis of the PET, PE and PP samples under stagnant air atmosphere was performed using instrument, Mettler Toledo, Model No. DSC 821^e to measure the melting point and percentage crystallinity. All samples were shredded into very small pieces (mesh size of -40/60) and directly fed to the DSC instrument. DSC experiments were conducted in dynamic condition at a heating rate of 10ºC min^{-1}. Alumina crucible (with a capacity of 40 µL) was used as a sample holder. Total mass of samples taken was 4-7 mg for each run of the experiments.

3.3. Experimental procedure and instrument for thermal pyrolysis

3.3.1. Nonisothermal thermogravimetry experiments for polymer [175-183]

Nonisothermal or dynamic thermogravimetry experiments were carried out in a TGA instrument of Mettler TOLEDO with model no TGA/SDTA 851^e under nitrogen environment for a range of temperature 303-875 K. Nitrogen flow rate was maintained at 40-50 ml min^{-1} according to the specification of the equipment. All samples were shredded into very small pieces (mesh size of -40/60) directly fed to the TGA instrument. Thermal decomposition experiments were carried out in dynamic condition at different heating rates. Alumina crucible (with a capacity of 70 µL for the nonisothermal condition) was used as a sample holder for PET sample. Platinum crucible (150 µL) was used as sample holder for waste LDPE, waste PE, and PP. The experiments were

repeated three times at a heating rate of 10 K min^{-1}, to confirm the repeatability and authenticity of the generated data for all cases. The deviations observed are very little. However, the deviations are reported in terms of average relative deviation, $ARD(\%) = \frac{100}{N}\sum_{i=1}^{N}\left|\frac{x_i^{\exp} - x_{av,i}}{x_{av,i}}\right|$, Where $x_i^{\exp}$ and $x_{av,i}$ are the experimental values of the variables (temperature and normalized mass) and average values of the variables respectively. i=no. of data points for each experiment. Experimental conditions for TGA studies are given in Table 3.1.

3.3.2. Isothermal thermogravimetry experiments [176-178]

For isothermal thermogravimetry experiments, the temperature program was optimized to reach the preset temperature of experiments within maximum of 6.2 min when the sample temperature was regulated within ±1K of the set points. Four different temperatures were maintained to study the isothermal decomposition of both virgin and waste PET samples and three different temperatures were maintained to study the isothermal decomposition of waste PE samples. An alumina crucible (with a capacity of 900 µL for the nonisothermal condition) was used as a sample holder. The experiments were repeated three times at a target temperature of 685 K to test the repeatability of the experiments. Experimental conditions for isothermal TGA studies are given in Table 3.2.

3.4. Experimental procedure and instrument for catalytic pyrolysis of polymers [179-180, 182-183]

3.4.1. Polymer materials for catalytic pyrolysis

The nonisothermal catalytic decomposition was carried out with waste LDPE sample and PP (polypropylene homopolymer (PPHP), Trade name: Koylene ADL, Grade AS030N) supplied by Indian Petrochemicals Corporation Limited, Vadodara, India with melt flow index 3.0. The same samples were used during thermal pyrolysis experiments also.

3.4.2. Catalysts

The catalyst used was ZSM-5 supplied by Ranbaxy Laboratories Ltd., India; Fresh and spent FCC (fluid catalytic cracking) catalysts from India Oil Corporation Limited, Guwahati; laboratory synthesized Al-MCM-41 (sol-gel and hydrothermal) catalysts; and laboratory synthesized nanocrystaline n-HZSM-5 catalyst.

3.4.3. Catalysts synthesis

3.4.3.1. Synthesis of sol-gel Al-MCM-41 [99-100, 180, 183]

Sol-gel Al-MCM-41 catalysts of different amount of aluminum were prepared according to the room temperature method described in literatures [99-100] with template alterations. In the present case, N-cetyle-N, N, N trimethylammonium bromide ($C_{19}H_{42}BrN$) was used as template instead of tetradecyltrimethylammonium bromide or hexadecyltrimethylammonium bromide. The catalyst was synthesized using $C_{19}H_{42}BrN$ (98%, Loba Chemie, India), tetraethoxysilane (TEOS (98%), Merck, Germany); aluminium isopropoxide (>98%, Acros Organics, India), 25% ammonia solution ((99.5%), Merck, India), propan-2-ol (PrOH)((99.5%), Merck, India) and deionzied water. The low concentration (3.7%) solution of AIP in PrOH was prepared in a glass

tube by mixing in an ultrasonic bath for 10-15 min. The template (1.29g) was mixed with 69.2 g of water, warmed up until complete dissolution, and allowed to cool down before adding 5 mL of ammonia. To this, a mixture of 5 mL of TEOS with an appropriate volume of the AIP solution was added dropwise, while stirring, over a period of 15 min to achieve the required molar ratio. The molar composition of the gel was 1TEOS: 1/xAIP:0.147CTMABr:3.04NH_3:160H_2O:yPrOH, with y=2.89 for 100≥ x ≥ 15. The values of x, y and their corresponding compositions are reported in Table 3.3.

The suspensions were kept under stirring for 1 h. The synthesized products were recovered by filtration and washed with about 2 L of deionized water.

3.4.3.2. Synthesis of hydrothermal Al-MCM-41 [101, 183]

Hydrothermal Al-MCM-41 was synthesized according to the procedure described in literature [101]. NaOH (0.40 g) and $C_{19}H_{42}BrN$ (0.6 g) were dissolved in 32 mL deionized water. Tetraethoxysilane (TEOS (98%), Merck, Germany) (3.85 g) was added to the mixture. Aluminum sulfate (Al_2 $(SO_4)_3$.16 H_2O, Merck, India) (0.37g) was dissolved in 10 mL of deionized water in a separate beaker and was then added to the reaction mixture. Stirring was continued for about 105 min at ambient temperature. The resulting mixture was stirred and heated at 80ºC for 20 min. The mixture was further stirred overnight and then was transferred to a Teflon-lined autoclave at 150 ºC for 12 hr. The molar composition of the gel was 1.0SiO_2:0.031Al_2O_3:0.27Na_2O:0.089CTA^+:130H_2O.

3.4.3.3. Synthesis of n-HZSM-5 [193]

Nanocrystalline n-HZSM-5 is basically a micro-porous catalyst prepared by hydrothermal crystallization of clear supersaturated homogeneous synthesis procedure

described in literature [193]. Aluminum isopropoxide (>98%, Acros Organics, India) as aluminum source was first added to measured amount of 20% aqueous solution of TPAOH (Tetra-propylammonium hydroxide, 40wt.% Merck, India). Resulting solution was stirred at 0^oC till a clear solution is obtained. Then appropriate amount of tetraethoxysilane (TEOS (98%), Merck, Germany) (SiO_2/Al_2O_3 = 60) was added. The solution is further stirred at room temperature for several hours in order to hydrolyze TEOS completely. Then it is heated at 80^oC for 1-1.5 hours to remove water and alcohols. The concentrated solution was transferred to teflon-lined stainless steel autoclave, where it was crystallized by thermal treatment under autogenous pressure at 170^oC for about 72 hours.

3.4.3.4. Calcination

In both sol-gel and hydrothermal methods, the synthesized products were recovered by filtration and washed with about 2 L of deionzied water. After drying at 343 K, the samples were calcined at 823 K for 8-12 hour. Heating rate of 2 K min^{-1} was maintained during heating of the samples.

In case of n-HZSM-5, the formed solid product was separated by filtration and washed with about 1.5 L deionzied water. After that, washing was done several times. The washed sample was dried overnight at a temperature of 383 K followed by calcination in air at 550^oC for 8-9 hours maintaining a heating rate of 2 Kmin^{-1}

3.4.4. Catalysts characterization

3.4.4.1. X-ray diffraction method [179,-180, 182-183]

ZSM-5, fresh FCC, spent FCC, Al-MCM-41 and n-HZSM-5 catalysts were characterized by X-ray diffraction (XRD) analysis using Bruker AXS instrument using CuKα radiation

(40kV, 40mA) with step size of 0.05º (2θ) and time of 0.5 s per step. High angle XRD ranging 2-50º for ZSM-5, fresh FCC, spent FCC, n-HZSM-5 catalysts and angle ranging 2-30º for Al-MCM-41 catalysts were used.

3.4.4.2. Scanning Electron Microscopy (SEM)

Scanning Electron Microscope (SEM) micrograph (make: LEO, model: 1430VP) were taken for ZSM-5 [179], fresh FCC, spent FCC, and n-HZSM-5 catalysts samples to learn about their morphologies.

3.4.4.3. BET analysis [179,-180, 182-183]

Nitrogen adsorption isotherm at 77K was determined on SA 3100 surface analyzer from Beckman Coulter using helium (for dead space calibration) and nitrogen. The ZSM-5 sample was out gassed for two hours at 250ºC and Al-MCM-41, FCC and n-HZSM-5 samples were out gassed for three hours at 300ºC under nitrogen flow.

3.4.5. Catalytic decomposition

3.4.5.1. Experimental procedure and equipment [179-180, 182-183]

Catalytic decomposition experiments were carried out in a TGA instrument of Mettler TOLEDO with model no TGA/SDTA 851^e under nitrogen atmosphere for a range of temperature 303-873 K. Nitrogen flow rate was maintained at 40-50 ml min^{-1} according to the specification of the equipment. Platinum crucible (150 µl) was used as sample holder. Catalytic decomposition experiments were carried out with different of catalyst of fixed percentage (20 wt. %) at 10Kmin^{-1} for waste LDPE and PP samples over ZSM-5, Fresh FCC, Spent FCC, sol-gel Al-MCM-41 catalysts. Experimental conditions are summarized in Table 3.4. ZSM-5, sol-gel Al-MCM-41 containing the highest aluminum (Si/Al=15), and n-HZSM-5 have shown good catalytic effect in terms of reduction in T_m

on waste LDPE. Sol-gel Al-MCM-41 (Si/Al=30 and 15), n-HZSM-5, and Fresh FCC have shown promising catalytic effect on PP sample. Further catalytic decomposition experiments were carried out with different percentage of ZSM-5 catalyst (Table 3.5) at 10K min^{-1} for waste LDPE. Similarly, further catalytic decomposition experiments were carried out with different percentage of Al-MCM-41(hydrothermal), Al-MCM-41 (sol-gel) and n-HZSM-5 catalysts (Table 3.5) at 10 K min^{-1} for PP. Preliminary analysis showed that sol-gel Al-MCM-41 (Si/Al=30) was better performing than hydrothermal Al-MCM-41 in terms of reduction in T_m for PP. The optimum catalyst percentage was found around 20 wt % ZSM-5 on LDPE and 18.5 wt % sol-gel Al-MCM-41 and 50 wt% n-HZSM-5 on PP after which reduction in T_m with increase in catalyst percentage was not so significant.

Therefore, further catalytic decomposition experiments were conducted using 20 wt.% ZSM-5 on LDPE, and 18.5 wt % sol-gel Al-MCM-41 and 50 wt% n-HZSM-5 on PP at different heating rates of 5, 10, 15, 20, and 25 Kmin^{-1}. Platinum crucible (150 µL) was used as sample holder. The experimental conditions are summarized in Table 3.6.

3.4.5.2. Reusability of Al-MCM-41 (sol-gel) [183]

Reusability study of sol-gel Al-MCM-41 was carried out by reusing the catalyst at 17-wt% (close to optimum condition) for seven consecutive runs at 10 K min^{-1} maintaining identical experimental conditions. The experimental conditions are summarized in Table 3.7.

3.5. Products analysis

Product analysis of the gaseous substance coming out of all the thermal and catalytic pyrolysis experiments was carried out in a Varian 3800 Gas Chromatograph (GC).

Pyrolysis experiments were carried out in the TGA instrument (Mettler TOLEDO with model no. TGA/SDTA 851^e) at a heating of 10ºC min^{-1} for a range of temperature 303-875 K. Nitrogen flow rate was maintained at 40-50 ml min^{-1}. Total sample mass of around 30-45 mg were taken for all the cases. 20% wt catalyst was used for all the catalytic experiments. The evolved gaseous substance from TGA at around T_m (Table 3.4) was injected directly to the GC using gas-tight syringe (Hamilton, gas-tight, model no. 1005, 5ml) for each of the thermal and catalytic pyrolysis experiments. Chromatographic separation was performed on a mid-polarity column, VF-200ms (30 m length, 0.25-µm film thickness, 0.25 mm ID) composed of 100% trifluropropyl methyl siloxane phase. The GC was operated at constant helium flow of 1.0 ml min^{-1} with 1:50 split ratio. The oven temperature was programmed as heating to 50 ºC and hold for 2 min. Then ramp heating at a rate of 6 ºC min^{-1} to 300 ºC and hold for 15 min. Standard samples such as pure propane gas supplied by Vadilal Gases Ltd; n-hexane, heptane, benzene, and toluene supplied Merck, India; indene, naphthalene, bi-phenyl, and fluorine supplied by Ranbaxy Laboratories Ltd, India were also injected maintaining the similar condition as to analyze their retention times. The liquid samples were injected using liquid syringe (Hamilton, Reno Nevada, model no. 701, 10µl).

Table 3.1. Nonisothermal experimental conditions for TGA studies

Sample	Nonisothermal Experiments				
Waste LDPE	**Initial mass (mg)**	**Heating rate (K min^{-1})**	**Temperature range(K)**	**% Residue**	**$T_{w0}/T_d/T_m/T_{w\infty}$ (K)**
Waste LDPE	7.76	5	303-873	2.02	551.1/621.3/734.2/805.5
	8.43	10	303-873	1.92	551.3/634.3/748.4/800.4
	11.19	15	303-873	2.29	549.0/648.2/754.0/800.4
	8.66	20	303-873	2.35	549.4/646.8/763.3/802.5
	10.96	25	303-873	1.23	576.5/680.2/770.4/809.6
Waste PET (M/s. Coca-cola bottles)	7.80	5	303-873	11.59	622.0/642.1/700.2/784.6
	8.12	10	303-873	13.56	623.2/653.2/710.4/785.1
	9.36	15	303-873	14.84	623.1/661.4/720.6/782.7
	9.52	25	303-873	14.13	623.8/671.8/734.8/786.1
Waste PET (M/s. Pepsi bottles)	8.732	10	303-873	14.65	626.5/656.6/710.1/784.6
	8.0991	15	303-873	12.37	626.6/658.3/716.8/784.5
	7.5857	25	303-873	13.71	626.5/674.5/727.7/784.8
PP	19.77	5	303-873	1.49	533.6/596.9/706.8/773.9
	20.32	10	303-873	0.88	526.9/670.0/723.1/749.8
	20.67	15	303-873	0.51	527.8/684.6/731.4/777.6
	19.78	20	303-873	0.73	527.5/684.8/736.8/770.2
	19.41	25	303-873	0.70	527.1/696.6/742.9/785.7
Virgin PET	16.74	5	303-873	12.17	619.2/642.9/709.0/788.9
	14.59	10	303-873	12.40	623.3/653.3/719.5/789.7
	14.63	15	303-873	12.21	621.5/662.9/728.2/792.4
	14.034	25	303-873	12.205	621.6/670.2/741.1/794.5

Table 3.2. Isothermal experimental conditions for TGA studies

	Isothermal			
	Initial mass (mg)	**Sample temperature (K)**	**Total experimental time (min)**	**% Residue**
Waste PET samples	45.9978	685	0-84.3	16.85
	52.4871	693	0-94.4	17.06
	42.1638	703	0-94.4	16.03
	29.6361	711	0-94.6	13.59
Virgin PET samples	14.64	687	0-94.25	13.07
	16.53	699	0-84.15	13.51
	13.92	708	0-64.33	12.51
	15.83	718	0-64.67	12.11
Waste color PE sample	10.28	699	0-103.95	15.19
	10.32	708	0-103.95	14.9
	10.20	718	0-103.95	15.75

Table 3.3. The composition of Al-MCM-41 catalysts containing different amounts of aluminum

Al-41-P(X)	TEOS, ml	AIP, mg	C_{19}TMABr, gm	NH_4OH, gm	H_20, gm	PrOH, (3.7%wt)gm
Al-41-P(100)	5.00	50.02	1.31	1.24	69.18	1.28
Al-41-P(60)	5.00	83.37	1.31	1.24	69.18	2.14
Al-41-P(30)	5.00	166.73	1.31	1.24	69.18	4.27
Al-41-P(15)	5.00	333.46	1.31	1.24	69.18	8.55

Table 3.4. TGA experimental conditions of catalytic decomposition of LDPE and PP over various commercial and synthesized catalysts for 20 wt% catalysts

Samples	Total Initial Mass (mg)	T_m (K)
Catalytic pyrolysis of waste LDPE		
Waste LDPE	8.43	748.4
Waste LDPE+n-HZSM-5	7.19	694.2
Waste LDPE +Al-41-P(15)	2.86	703.6
Waste LDPE +Al-41-P(30)	3.41	708.1
Waste LDPE +Al-41-P(60)	4.19	719.7
Waste LDPE +Al-41-P(100)	6.99	725.5
Waste LDPE +ZSM-5	7.53	678.9
Waste LDPE +Fresh FCC	6.83	734.2
Waste LDPE +Spent FCC	6.02	739.1
Catalytic pyrolysis of PP		
PP	20.32	723.1
PP+n-HZSM-5	13.14	604.8
PP+Al-41-P(15)	14.29	626.8
PP+Al-41-P(30)	10.796	619.6
PP+Al-41-P(60)	13.15	650.5
PP+Al-41-P(100)	12.24	702.9
PP+ZSM-5	13.03	701.7
PP+Fresh FCC	14.54	689.0
PP+Spent FCC	13.65	709.1

Table 3.5. Experimental conditions for TGA studies using different percentages of catalysts

Catalysts	Catalysts Percentage %	Total Initial Mass (mg)	T_m (K)
ZSM-5+Waste LDPE	0	8.43	748.4
	5	17.76	719.9
	11.8	10.63	697.6
	17.6	8.98	681.6
	20	7.57	677.8
	22	9.79	679.4
	31	9.83	672.3
	35.3	10.77	657.1
	40	9.38	662.6
	50	9.89	657.0
Al-MCM-41+PP (Sol-Gel)	0	20.32	723.1
	7.7	9.53	652.5
	13.1	12.19	636.9
	16.4	19.09	625.8
	18.5	10.81	619.6
	21.6	10.7	616.7
	24.6	10.54	611.6
	32.5	12.11	608.9
Al-MCM-41+PP (Hydrothermal)	0	20.32	723.1
	5.1	9.69	677.4
	10.9	9.85	674.4
	17.1	10.44	658.8
	20.8	9.81	666.8
	25.5	10.28	654.7
	33.2	9.92	655.1
n-HZSM-5+PP	0	20.32	723.1
	10	14.54	644.8
	20	13.24	604.8
	30	13.99	591.4
	40	13.18	572.2
	50	13.46	561.6
	60	13.5	561.1

Table 3.6. Experimental conditions for TGA studies using optimum catalysts percentages

Sample	Nonisothermal Experiments			
	Initial mass (mg)	**Heating rate(K min^{-1})**	**Temperature range(K)**	**$T_{w0}/T_d/T_m/T_{w\infty}$ (K)**
Waste LDPE+ZSM-5(20%wt)	5.57	5	303-873	470.4/575.4/659.9/777.9
	7.55	10	303-873	462.7/586.9/678.4/769.9
	9.64	15	303-873	462.2/590.6/679.9/769.9
	7.83	20	303-873	471.1/599.1/686/779.7
	7.51	25	303-873	462.2/604.1/693.9/779.5
PP+Al-MCM-41 (18.5%wt)	7.48	5	303-873	489.3/535.1/608.6/669.9
	10.35	10	303-873	473.2/576.6/619.6/682.3
	13.59	15	303-873	461.7/596.3/637.6/700.9
	10.80	20	303-873	464.4/605.2/640.7/717.5
	9.09	25	303-873	461.9/607.9/649.0/711.0
PP+n-HZSM-5 (50% wt)	12.78	5	303-873	373.5/413/545.9/874.1
	12.58	10	303-873	373.3/401.6/561.6/874.9
	12.96	15	303-873	373.9/398.6/581.5/875.6
	12.31	20	303-873	373.8/391.3/599.0/877.5
	13.06	25	303-873	373.3/386.3/601.4/877.7

Table 3.7. Experimental conditions for reusability test

Run No	Mass of PP (mg)	Mass of Al-MCM-41(sol-gel) (mg)	% Cat	T_m (K)	ΔT_m (K)
1	15.84		17.0	625.8	0
2	16.29		16.6	627.4	1.6
3	15.95	3.25	16.9	631.5	5.7
4	15.89		17	633.7	7.9
5	15.87		17	643.8	18.0
6	16.19		16.7	643.9	18.1
7	15.97		16.9	649.9	24.1

4. Results and discussion

This chapter presents the results and discussion of the research work under the following topics.

- Characterization of catalysts and polymers
- Isothermal and non-isothermal experiments for thermal pyrolysis of plastic samples, kinetics analyses of these experimental results using model-free and model-fitting techniques, and simulation of the kinetics model for prediction of the experimental data
- Non-isothermal experiment for catalytic pyrolysis of plastics samples at the universal heating rate of 10 $Kmin^{-1}$ with variation of catalyst concentration, estimation of optimum catalyst concentration, further experiments at several heating rates, kinetics analyses of these experimental results using model-free and model-fitting techniques, and simulation of the kinetics model for prediction of the experimental data
- Reusability study of the catalyst
- Analyses of the products in the gaseous substance coming out of all the thermal and catalytic pyrolysis experiments through gas chromatography

4.1 Characterization of the polymers used

Results of characterization of the polymer samples used for the present work by differential scanning calorimetry (DSC) analysis are discussed in this section.

4.1.1. DSC analysis

Figures 4.1-4.5 present the DSC analysis of waste PET, Virgin PET, waste LDPE, waste PE, and virgin PP samples respectively. Each curve exhibits one endothermic peak, which is responsible for melting process. The melting initiates at start of the peak and finished at end of the peaks. Peak temperature is called melting points. The area under the peak represents the heat of fusion of the sample which is proportional to the amount of crystals present in the sample. The percentage crystallinity is calculated by comparing the measured heat of fusion of the sample with the theoretical heat of fusion of 100% crystalline standard sample. The melting point, percentage crystallinity, and purity (in terms of residue) of the samples are summarized in Table 4.1. Melting points of respective standard polymers are also reported in Table 4.1 for comparison.

4.2. Thermal pyrolysis of plastics

This section discusses the experimental results obtained during nonisothermal and isothermal decompositions of the plastics in the thermogravimetic analyzer (TGA) at several heating rates.

4.2.1. Nonisothermal decomposition

Pyrolysis of the waste LDPE and the PP samples were carried out at five different heating rates (5, 10, 15, 20, and 25 K min^{-1}), waste PET sample (from Coca-cola bottle) and virgin PET sample were carried out at four different heating rates (5, 10, 15, and 25 K min^{-1}), waste PE sample was carried out at four different heating rates (10, 15, 20, and 25 K min^{-1}), and waste PET sample (from Pepsi bottle) was carried out at three different heating rates (10, 15, and 25 K min^{-1}). The temperature at which $\alpha=0$ (T_{w0}), the temperature at which decomposition starts and $\alpha\approx0.01$ (T_d), the temperature at

which the maximum weight loss rate occurs (T_m), and the temperature at the end of the pyrolysis step ($T_{W\infty}$) are reported in Table 3.1 for each case of experiments. Figures 4.6-4.10 represent variations of conversion, α with temperature, T (thermogravimetric, TG curves) during pyrolysis of waste LDPE, waste PE, PP, waste PET (from Coca-cola bottle) and virgin PET, and waste PET (from Pepsi bottle) samples respectively at several heating rates. Figures 4.11-4.15 show the variations of the rate of conversion, $\frac{d\alpha}{dT}$ with T (derivative thromogravimetric, DTG curves) during pyrolysis of waste LDPE, waste PE, PP and virgin and waste PET (from Coca-cola bottle), and waste PET (from Pepsi bottle) respectively at several heating rates. It is observed from the figures (Figs. 4.6-4.15) that the curves show constant pattern behaviour at different heating rates. A quick thermal decomposition is observed in the range of T_d to $T_{W\infty}$ (Figs. 4.6-4.15) and the highest decomposition rate is observed at around T_m (Figs. 4.11-4.15). After this quick increase, the solid continues to decompose smoothly and slowly until the end of the experiment. Higher heating rate finishes the decomposition phenomenon faster (Figs. 4.6-4.10). The thermal decomposition behavior of all of samples is almost similar, except the difference in T_m. The constant pattern behaviour is attributed to the fact of similar reaction mechanism, which is the basis of isoconversional (model-free) approach for kinetics analysis [33-38]. We can clearly notice the single peak in all the DTG curves (Figs. 4.11-4.15). It is worth mentioning here that the single peaks that are observed in Figs. 4.11-4.15 though apparently indicate existence of single-step reaction, need not necessarily be the same rather it can be combination of several reactions taking place during pyrolysis [50, 133, 163, 175, 177, 181].

4.2.2. Isothermal decomposition

It is evident from the nonisothermal experiments (Table 3.1) for waste PET and waste PE samples that the thermal decomposition starts in the temperature range of 639-672K [175-177] and 702-718K [178] respectively. The maximum decomposition temperature lies between 703K and 738K for waste and virgin PET [175-177] and between 745K and 768K for waste PE sample [178] depending upon the heating rate. Also at $10Kmin^{-1}$, the universal heating rate, the maximum decomposition temperatures are 715 K and 719.5 K for waste and virgin PET respectively [175-177] and 745K for waste PE sample [178]. Therefore, the four different temperatures viz. 685K, 693K, 703K, and 711K of isothermal experiments for waste PET [176-177] and 687K, 699K, 708K, and 718K of isothermal experiments for virgin PET [177] were chosen with an approximate interval of 10K. Similarly, the three different temperatures viz. 699K, 708K and 718K of isothermal experiments for waste PE were chosen with an approximate interval of 10K [178].

The thermal decomposition behaviour of the virgin PET varies significantly from that of waste PET samples (Fig. 4.16). It is already reported by Holland and Hay [52] that the isothermal decomposition temperature for virgin PET is 643–683K. Therefore, the observed variation in the present study can be attributed to fact that in contrary to waste PET sample, very fast decomposition occurs in case of virgin PET samples while reaching the target temperature (685–718K). The percentage loss of waste and virgin PET samples before reaching the target temperature in different conditions is reported in Table 3.2 [177]. For each isothermal experiment with waste PET samples, 82-85% weight loss is observed within 62.5-67 minutes after reaching the preset isothermal temperature (6-6.2 minutes). After this quick loss of weight, the solid continues

decomposing smoothly and very slowly to the end of experiment [176-177]. It is also found from Table 3.2 that the residue left for waste PET sample is within 13-17 % and that for virgin PET sample is within 12-14%. Holland and Hay [52] reported 18-20% residue for different PET samples under isothermal conditions (643–683K). The marginally lower value of residue in the present work is possibly due to study at relatively higher temperature (685–718K).

In case of waste PE samples, a very quick (84-85%) (Fig.4.17) is observed within 38-67 minutes after reaching the preset isothermal temperature (6.3 minute) for each of the isothermal experiments. The initial weight, temperature, total time, percentage loss of total weight, t_{w0}, and $t_{w\infty}$ are presented in Table 3.2 [178]. After this quick weight loss, the sample continues decomposing smoothly and very slowly till the end of experiment. I have taken W_0 at t_{w0} when the preset temperature is reached and W_∞ at $t_{w\infty}$ when weight loss is about 99.5% of total weight loss for the calculation of α (Figs. 4.16-4.17) [176-178].

4.3. Characterization of catalysts

Results of characterization of both commercially available and laboratory synthesized catalysts by X-ray diffraction (XRD) analysis; Scanning Electron Microscopy (SEM); and nitrogen adsorption study are discussed in this section.

4.3.1. Characterization of ZSM-5 catalyst [179]

The XRD pattern (Fig. 4.18) shows that the ZSM-5 catalyst is crystalline without any evidence of another phase. The morphology of the catalyst is reported through Fig. 4.19 in the form of Scanning Electron Microscope (SEM) micrograph. Table 4.2 summarizes the surface area and pore volume of ZSM-5 sample used. The textural properties (Table

4.2) of ZSM-5 shows lower external surface area due to micrometer crystal sizes present in sample, which is also evident from SEM picture (Fig. 4.19). Fig. 4.20 shows the nitrogen isotherm of ZSM-5 sample. The pore size distribution calculated using Barrett, Joyner and Halenda (BJH) method (Fig. 4.21) indicates only the presence of the mesopores in ZSM-5 not the micropores, which should be more in ZSM-5 zeolite catalyst. The isotherm (Fig. 4.20) is Brunauer Type I with wide range of pore sizes, which is also supported by the BJH pore size distribution (Fig. 4.21). The nature of the isotherm indicates a continuous progression with increasing loading from monolayer to multilayer adsorption and then to capillary condensation.

4.3.2. Characterization of Fresh FCC and spent FCC catalysts

The XRD patterns for fresh FCC and spent FCC are shown in Figs. 4.22-4.23. The EDX of the fresh and spent FCC catalysts shown through Figs. 4.24-4.25 indicates stronger acid character of fresh FCC catalysts due to the presence of substantially higher amount of aluminium in fresh FCC than in spent FCC catalysts. The morphology of the catalyst is reported through Figs. 4.26-4.27 in the form of Scanning Electron Microscope (SEM) micrographs. It can be observed from the figure (Fig. 4.27) that pores of spent catalyst are already blocked and should not be useful for the catalytic decomposition of the polymers. Accordingly, almost no catalytic effect of spent FCC was observed (discussed later). Table 4.2 summarizes the surface area and pore volume of both the fresh and spent FCC samples used. The pore size distribution is calculated using BJH method. Figure 4.28 showing the nitrogen isotherms of the FCC samples indicate the Brunauer Type I isotherm. The nature of the isotherm indicates a continuous progression with increasing loading from monolayer to multilayer adsorption and then to capillary condensation.

Again, the nitrogen adsorption for spent FCC, as expected, found to be significantly lower than the fresh FCC catalyst (Fig. 4.28).

4.3.3. Characterization of Al-MCM-41 catalysts

The XRD patterns of both hydrothermal Al-MCM-41 and sol-gel Al- MCM-41 catalysts containing different amounts of aluminum Al-41-P(x) (x=100, 60, 30, and 15) exhibit the low angle and intense diffraction peak between $2\theta = 2.1\text{-}2.40^{o}$ indicating the reflection of 1 0 0 plane [192] and are presented through Figs. 4.29 and 4.30 respectively. This peak is also being assigned to the presence of a hexagonal mesopore array [71]. No peak at higher angle is observed indicating the absence of any crystalline phase containing aluminum. Nitrogen adsorption isotherms at 77 K of both sol-gel and hydrothermal calcined Al-MCM-41 catalysts are shown in Figs. 4.31 and 4.32. Both the Al-MCM-41 catalysts present a type IV isotherm according to IUPAC classification, typical of good quality mesoporous materials [71, 100, 192]. In case of Al-MCM-41(hydrothermal) nitrogen isotherm is completely reversible but Al-MCM-41(sol-gel) for which desorption points are shown exhibit a pore filling step within a fairly narrow range of P/P^{0}, indicating size uniformity of the tubular unidirectional mesopores [71, 100]. Table 4.3 compares the textural properties and chemicals used as raw materials for Al-MCM-41 catalysts prepared by sol-gel and hydrothermal methods between present case and literatures. BET surface areas and pore volumes of the Al-MCM-41 samples (1200–1550 $m^2\ g^{-1}$; 0.70–0.98 $cm^3\ g^{-1}$) are in the range of the expected values for these types of materials. Al-MCM-41(sol-gel) samples have higher Si/Al ratio and higher BET surface area than Al-MCM-41(hydrothermal). External surface area (by t-plot method) increases with increase in Si/Al ratio of sol-gel Al-MCM-41 catalysts samples. The highest BET

surface area and pore volume are obtained for the highest Si/Al ratio containing Al-MCM-41-or Al-41-P(100) samples and the lowest BET surface area and pore volume are obtained for Si/Al ratio of 36.5 containing sol-gel Al-MCM-41 or Al-41-P (30) samples. The pore size distributions are calculated using the BJH model applied to the adsorption branch of the isotherm, assuming cylindrical pore geometry. It is found that the pore sizes lie within 4 nm in both the cases (Fig. 4.33). The total distribution is not available due to limitation of the instrument to measure pore size below 3nm. However, Fig. 4.33 and Table 4.3 indicate that both the samples have pore size uniformity and considerable high pore volumes and surface areas. Pore volumes are determined from the nitrogen adsorbed volume at $P/P^0 = 0.98$.

4.3.4. Characterization of n-HZSM-5 catalysts

The crystallinity of the calcined catalyst samples was checked by powder XRD. Grieken at al. [193] reported that crystallinity of n-HZSM-5 increases with synthesis time. Several authors have shown that the mainly greater pore size and high external surface area favour the catalytic activity on polymers such as LDPE and PP [63-64, 66-69, 93-94]. Fig. 4.34 shows XRD the pattern of n-HZSM-5 zeolites. Fig. 4.35 shows the nitrogen isotherm of n-HZSM-5 sample. The XRD pattern of this zeolite (Fig. 4.34) clearly shows the presence of amorphous phase, which is also evident from SEM micrograph (Fig 4.36). In addition, a broad bottom reflection placed at 2θ ~ 20–23º corresponding to the possible contribution of amorphous material was observed in the sample. The broader and less intense diffraction peaks attribute to the facts that there is decrease in crystal size according to Scherrer law [194]. Table 4.2 also presents the textural properties of n-HZSM-5 samples. The nanocrystalline HZSM-5 sample has high external surface area

(364 m^2g^{-1}) due to its nanometric dimensions. The steep rise in adsorption (Fig. 4.35) at higher relatives pressures (P/P0 > 0.90) is due to the high reported pore volume value of 0.89 cm^3 g^{-1} at P/P0 = 0.98 (Table 4.5). This fact suggests the existence of interparticular mesoporosity/macroporosity among the primary nanocrystals forming the n-HZSM-5 samples [194]. The SEM picture of n-HZSM-5 presented through Fig. 4.36 agrees well with the literature SEM micrograph (Fig. 4.37) [192].

4.4. Comparison of Catalytic activities of different catalysts determined by TG analysis

Several studies have been conducted describing the cracking of pure polyolefins over different acid solids like zeolites [56-94], clays [56, 57] and mesostructured materials [59, 63, 66, 70-71, 80-81, 89]. Differences in the catalytic activities of these catalysts have usually been related to their acid properties, primarily the strength and number of the acid sites. Surface area, particle size and pore size distribution have also been reported to play key roles. These properties control the accessibility of bulky plastic molecules to internal active sites of the catalysts. Most of the reported works on the catalytic cracking of plastics have been conducted using pure polymers. In the present investigation, we have used eight different catalysts such as ZSM-5, n-HZSM-5, four mesoporous sol-gel Al-41 P(x) (x=100,60,30, and 15), fresh and spent FCC catalysts to determine the their activity on waste LDPE and pure PP, which in future can be useful to evaluate their potential application in commercial feedstock recycling processes.

4.4.1. Catalytic activities of different catalysts on waste LDPE

Figures 4.38–4.39 illustrate the TG and DTG plots resulting from the catalytic decomposition of waste LDPE over various types of catalysts (with 20 wt% catalyst). The

activity of each catalyst is related to its capacity to shift the TG curves to lower temperatures. The experimental results are summarized in Table 3.4. The results show that the fresh FCC and the spent FCC catalysts remain almost inactive on waste LDPE as there is little change in T_m observed. A marked reduction in the degradation temperature is observed when the process was conducted in the presence of acid catalysts such as ZSM-5, n-HZSM-5, and Al-P(30) with higher alumina content, although significant differences were observed depending on the characteristics of the catalysts. The strongest acid character, standard ZSM-5 showed the highest catalytic activity on the waste LDPE. T_m for the LDPE/ZSM-5 mixture was 679K, 70 K below that observed for the thermal cracking. Nanocrystalline n-HZSM-5 zeolite, and higher aluminum containing sol-gel AL-MCM-41 or Al-41-P(15) and Al-41-P(30) catalysts of comparable acid properties to standard ZSM-5 but having smaller crystal size, exhibited also very high catalytic activity for waste LDPE. The difference in the maximum decomposition temperature between thermal cracking and catalytic cracking, ΔT_m for the waste LDPE over n-ZSM-5, Al-41-P(15) and Al-41-P(30) are 54, 45 and 40K respectively. Though mesostructured solids exhibited weaker acid properties than crystalline zeolites, it is apparent that the comparatively weaker acid properties of these materials are partly compensated by their comparatively larger pore dimensions and surface area, which provide an easier accessibility to their internal acid sites. Sol-gel Al-MCM-41 [Al-41-P(15)] containing the highest amount of aluminum, the mesostructured solid with the strongest acid character, also exhibited the highest catalytic activity amongst the four Al-41-P(x) (x=100,60, 30, and 15) samples, reducing the temperature of maximum decomposition rate of waste LDPE by 45K.

4.4.2. Catalytic activities of different catalysts on pure PP

Catalytic conversion of pure PP over different types of catalysts is shown through Figs. 4.40 and 4.41. The catalytic effect on PP sample in terms of reduction in T_m of all the eight types of catalysts used is as follows:

n-HZSM-5>Al-41-P(15)≈Al-41-P(30)>Al-41-P(60)>FreshFCC>Al-41-P(100)>Spent FCC>ZSM-5.

The experimental results are summarized in Table 3.4. The results show that the spent FCC, lowest aluminum containing Al-41-P(100), and ZSM-5 catalysts remain almost inactive for the catalytic decomposition of PP. The n-HZSM-5 is the best one with ΔT_m= 118K. Different amounts of aluminum containing sol-gel Al-MCM-41 or Al-41-P(x) catalysts exhibited high catalytic activity for PP. Al-41-P (15) and Al-41-P (30) catalysts show almost similar and encouraging results (ΔT_m= 96 and 103K respectively) amongst the other mesoporous Al-MCM-41 catalysts. ΔT_m for the PP sample over Al-41-P (60) and fresh FCC are 73, and 34K respectively.

In case of catalytic decomposition, first chain scissions starts on the external surface of the catalyst and then smaller chains enter into the pores where most of the active sites are located. Further degradation into shorter hydrocarbons continues in the pores depending on acidic character of the catalyst. It is well known that thermal degradation of PP follows a radical mechanism and many oligomers are created by hydrogen transfer from the tertiary carbon atom along the polymer chain to the radical site. However, the carbanium ion mechanism was also offered for catalytic degradation of PP. The initial step of the catalytic decomposition reaction over catalytic sites was considered to occur by either the abstraction of hyride ion (by Lewis acid sites) from the oligomer chain, or

the addition of proton (by Brønsted acid sites) to double bonds of the thermally degraded shorter molecules [64].

PP molecules are much larger than the pore size of zeolites [64, 94]. Therefore, catalytic decomposition of PP over ZSM-5 is more difficult as degraded chain segments cannot easily diffuse through the channels due to relatively smaller pore size of the catalyst. EDX analysis (Figs. 4.24-4.25) shows substantial decrease in aluminum i.e. loss of acidic site in case of spent FCC in comparison to fresh FCC. SEM images (Figs. 4.26-4.27) indicates that most of the pore openings are blocked for the spent FCC catalyst. Thus, the two important catalyst characteristics being very low for spent FCC make it an almost inactive catalyst for PP decomposition and fresh FCC have shown relatively much better catalytic activity.

Although the number of the acid sites of the catalysts is mainly responsible for the catalytic decomposition of PP, pore size and structure are also important parameters for the same. The n-HZSM-5 catalyst sample with higher external surface area, pore size, and acidic nature accelerated the decomposition process of PP, as the diffusion hindrance reduces with increase in pore diameters of these catalysts sample. Similarly, mesoporous Al-41-P(30) and Al-41-P(15) catalysts with considerable amount of aluminium (acid site) showed very good effect on the catalytic decomposition of PP due to higher external surface area and pore size.

4.5. Individual Catalyst activity on plastics

This section discusses the activities of different catalysts in detail as observed from TG experiments for LDPE and PP decomposition.

4.5.1. Catalytic activity of ZSM-5 for waste LDPE decomposition

Table 3.1 reporting the comprehensive details on the temperatures T_{w0}, T_d, T_m, and $T_{w\infty}$ for each case of the experiments reflects that thermal decomposition of waste LDPE starts at around 640K and showed a maximum decomposition rate at T_m=748K at a heating rate of 10 $Kmin^{-1}$, which are shifted to much lower temperatures in the presence of catalyst. The maximum shift is observed to be 91 K at a catalyst percentage of 50 wt%. Figures 4.42 and 4.43 illustrate the TG and the DTG plots for the catalytic degradation of waste LDPE. It is observed from Fig. 4.43 that the shape of the DTG curves changes significantly due to different wt % of ZSM-5 catalyst. This change is very prominent at lower catalyst compositions. From catalyst composition of 18 wt% onwards, the curves are overlapping in nature though there are different peaks at different temperatures for different compositions. This behaviour indicates possibility of existence of different decomposition mechanism for different catalyst wt %. Therefore, meaningful correlation of these TGA data with different wt % of catalyst and without catalyst by a simple kinetics model using model-fitting techniques alone may be unreliable and unrealistic.

Since, the catalysts are expensive and, at the moment, there are no useful ways to improve their short life or to make effective recycling [58, 69], therefore, concentrated on getting the optimum catalysts percentage. Economically, optimum catalyst percentage should be decided based on the extent of decrease of decomposition temperature with catalyst percentage. Figure 4.44 and Table 3.5 show the effect of catalyst percentage on T_m of the waste LDPE sample. It is observed that T_m decreases exponentially with catalyst percentage. It is further observed that the optimum catalyst percentage could be around 20 wt %, since, after that reduction in T_m with increase in catalyst percentage is

not so significant. Hence using catalyst percentage more than this would not be economically effective. To illustrate quantitatively, it may be seen that for a change of catalyst percentage from 20 to 31 wt %, the further reduction in T_m is about 5°C, where as for a change of catalyst percentage from 12 to 20 wt %, the further reduction in T_m is about 20°C. Also, as discussed earlier, from the overlapping in nature of the DTG curves (Fig. 4.43) for catalyst composition of 18 wt% onwards, identification of 20 wt % catalyst may be a judicious selection. The reduction in maximum decomposition temperature is around 70 °C at 20 wt% catalyst. Thus, the optimum catalyst (ZSM-5) percentage is selected as 20 wt% [179, 182].

The exponential decrease in T_m for the LDPE catalytic pyrolysis with ZSM-5 can be explained in the similar line of Marcilla et al. [69], assuming that the large molecules have to react on the external surface of the zeolite catalyst, which could be the limiting reaction step. When more zeolite is added, more surfaces is available and more polymer molecules participate in the initial reaction step, until a situation is reached with an excess of zeolite, where there is not enough polymer to cover all the available zeolite active sites, thus not contributing this excess of zeolite to the initial reaction step of large macromolecules. Table 4.4 summarizes that literature available data for the catalytic effect on PE. Table 4.4 reflects that amongst the catalysts used for LDPE decomposition, Al-MCM-41 and MCM-41 shows similar reduction in temperature as have been observed in the present study with ZSM-5. But HZSM-5 performance is not at par with them, where the reduction in temperature is quite low. However, n-HZSM5 shows superior results in comparison to all [179]. But the n-HZSM5 synthesized in the present work performs somewhat lower than the ZSM-5 towards decomposition of LDPE, which might

be due to comparatively lower crystallinity and acid site. Therefore, further detailed study is performed in the present case only with ZSM-5 catalyst.

4.5.1.1. Catalytic nonisothermal decomposition at several heating rates

Nonisothermal decomposition of the waste LDPE sample was carried out at five different heating rates (5, 10, 15, 20, and 25 K min^{-1}) with the decided optimum percentage (20 wt %) of ZSM-5 catalyst. The nonisothermal noncatalytic pyrolysis yielded around 97-99% weight loss. The temperatures T_{w0}, T_d, T_m and $T_{w\infty}$ for the experiments are also reported in the Table 3.6. Variation of α with temperature for catalytic (20 wt %) decomposition at different heating rates are reported through Fig. 4.45. Variations of rate, dα/dT with temperature during nonisothermal pyrolysis using catalyst ZSM-5 (20 wt %) at different heating rates are reported through Fig. 4.46. It is observed from the tables (Tables 3.1, 3.5 and 3.6) and figures (Fig. 4.8 and Figs. 4.38-4.46) that catalytic decomposition starts and completes at much lower temperatures than that for noncatalytic decomposition. However, catalytic decomposition continues for a wider range of temperature than noncatalytic one leading to flatter α versus temperature curves. The slow decomposition behaviour in presence of catalyst is also evident from Fig. 4.46, where the rate of decomposition in most of the cases is much lower than that in absence of catalyst.

It has been reported that thermal decomposition of LDPE without catalyst occurs through random scission of original polymer chain into straight chain fragments of varying length generating radicals along the polymer backbone followed by scission of the molecule and hydrogen transfer resulting in formation of dienes, alkenes and alkanes [38,50-51,78,93, 97,134-135, 157-158, 178-179, 182]. But degradation of LDPE on the ZSM-5 catalyst takes place due to presence of strong zeolite acidic sites [59, 63, 66-69,71, 78, 93-94, 97,

179,182]. For both the cases of catalytic and non-catalytic decomposition of LDPE large polymer fragments are cracked on the external surface of the catalyst at the start of degradation forming smaller molecules and radicals via end-chain cracking pathway. These molecules in the subsequent stages, in case of catalytic decomposition, enter into the pores and participate in other reactions like isomerization and oligomerization [63, 66-69, 71, 78, 97]. Therefore, catalytic (ZSM-5) degradation of LDPE results in formation of aromatics, light parafins and olefins due to the reactions like oligomerization, cyclization, and hydrogen transfer reactions [179, 182]. Aromatics yield increased where subsequent steps of cyclization occurred at higher temperatures. The slowness of the catalytic decomposition over noncatalytic decomposition may be attributed to the different reaction mechanisms as discussed [179]. However, the products distribution depends on structure and steric effects of the zeolite catalyst [63, 66-69, 71].

4.5.2. Catalytic activity of sol-gel and hydrothermal Al-MCM-41 for PP decomposition

Experiments were conducted for catalytic dynamic decomposition of PP in TGA. The temperature at which maximum weight loss rate occurs (T_m) is reported in Table 3.5 for each case of the experiments. Reduction in T_m on application of catalysts (sol-gel and hydrothermal Al-MCM-41) is shown through the Table 3.6 and DTG curves (Fig. 4.47). It is observed from both the table and the figure that T_m reduces significantly, in comparison to noncatalytic decomposition, due to application of the catalyst. It is further observed that sol-gel Al-MCM-41 is much more effective compared to hydrothermal one in reducing the T_m for PP. Tables 3.5 and 3.6 reflects that the maximum shifts of T_m are observed to be 114K and 68K for sol-gel (32.5wt %) and hydrothermal (25.5wt %)

catalysts respectively. According to Aguado et al. [63], Hydrothermal Al-MCM-41 was more effective than sol-gel one towards decomposition of LDPE and HDPE. The reduction in maximum decomposition temperatures for LDPE and HDPE using hydrothermal AL-MCM-41 were reported to be 69 and 58 K respectively. They have used pure LDPE but in this present case, waste LDPE was used, which may differ by molecular weight as well as thermal stability. Moreover, different synthesis procedure of Al-MCM-41 (hydrothermal) (Table 4.3) may also differ the catalysts characteristics in terms of acidity, pore size, surface area, which are primarily responsible for the catalytic activity. Table 4.3 and Figs. 4.31-4.33 implies that the catalysts synthesized in the present study have almost the similar pore size and similar Si/Al ratio but they have widely different surface areas, which possibly makes the differences in the catalytic activities between the sol-gel and hydrothermal Al-MCM-41.

Again, Marcilla et al. [68] reported that Al-MCM-41 (sol-gel) should show better catalytic activity towards PP than LDPE. The present result is at par (Table 3.5 and Figs. 4.40-4.43) to the observations of Marcilla et al. [68]. It is worth mentioning that catalytic activity of mesoporous catalysts like MCM-41 towards polymer decomposition mainly depends on the mesopore size that allows the movement of the polymer chain in the pores, surface area that takes part in the decomposition reaction and the aluminium content (or number of acid sites), which is involved in such decomposition mechanism [68].

4.5.2.1 Determination of optimum catalyst (sol-gel Al-MCM-41) concentration

Since sol-gel Al-MCM-41 catalyst was found to perform better than hydrothermal Al-MCM-41, the optimum concentration of the sol-gel Al-MCM-41 catalyst only for

decomposition of PP sample was determined. Figures 4.48 and 4.49 illustrate the TG and the DTG plots respectively for the sol-gel Al-MCM-41 catalyzed decomposition of PP. It is observed from the figures that the shape of the curves changes significantly up to 15 wt% of the catalyst. From catalyst composition of 15 wt% onwards, the curves are overlapping in nature indicating less impact of the catalyst**.** Figure 4.50 shows the saturation effect of catalyst percentage on the change in T_m with respect to that for non-catalytic PP decomposition, ΔT_m. It is further observed that the optimum catalyst percentage could be around 18.5 wt %, since, after that reduction in T_m with increase in catalyst percentage is not so significant. The reduction in maximum decomposition temperature is around 103°C at 18.5 wt% catalyst. Thus, optimum catalyst (sol-gel Al-MCM-41) percentage was selected as 18.5 wt% [180, 183].

It is interesting to see from Fig. 4.48 that TG curves with and without catalysts are constant pattern in nature. Only shift in the TG curves towards lower temperatures are observed due to application of catalyst and increase in catalyst percentage. This shift of the curves also slowly reduced at higher percentages of the catalyst indicating less effect of addition of further catalyst in the polymer sample. However, this behaviour is contrary to the catalytic activity of ZSM-5 on LDPE [179, 182], as discussed in section 4.5.1., where catalytic decomposition continued for a wider range of temperature than noncatalytic decomposition leading to flatter TG curves. As discussed, this behaviour [68, 179, 182] suggested possible existence of different reaction mechanism due to the microporous zeolite catalyst compared to non-catalytic decomposition of LDPE resulting in formation of aromatics, light parafins and olefins due to the reactions like oligomerisation, cyclization, and hydrogen transfer reactions. Aromatics yield increased

where subsequent steps of cyclization occurred at higher temperatures [60, 64, 66, 69-70, 91, 94, 96-97, 179-180, 182, 183]. But in case of sol-gel Al-MCM-41 catalyzed decomposition of PP, the constant pattern behaviour of the TG curves possibly suggest existence of similar reaction mechanism both under catalytic and noncatalytic decomposition of mesoporous Al-MCM-41. Here, large polymer fragments are cracked on the external surface of the catalyst and then enters into the mesopores where they get cracked further leading mainly to the higher olefins and liquid products [66, 70, 179]. This can only be confirmed after thorough analysis of the decomposition products. However, presence of catalyst surfaces cracks the polymer into comparatively smaller fractions and at least makes the decomposition of PP energy effective [180, 183].

4.5.2.2. Catalytic nonisothermal decomposition at several heating rates

Figs. 4.51 and 4.52 represent the TG and DTG curves respectively for sol-gel Al-MCM-41 catalyzed decomposition of PP at five different heating rates of 5, 10, 15, 20, and 25 K min^{-1} with the optimum catalyst percentage (18.5 wt%). The other kinetics information such as T_{w0}, T_d, T_m and $T_{w\infty}$ are been reported in the Table 3.7 for each case of the experiments.

4.5.2.3. Reusability study of sol-gel Al-MCM-41 catalyst

Reusability of the sol-gel Al-MCM-41 catalyst was studied taking 17 wt% catalyst (close to optimum concentration 18.5 wt%) mixed with the PP sample. The same catalyst was repeatedly used for seven times to see the effect on decomposition behaviour. Figure 4.53 represents the TG plot for the repeatedly used sol-gel Al-MCM-41 (17 wt %) catalyzed decomposition of PP. It can be observed from Table 3.7 that the catalyst activity is reduced very slowly (also evident from Fig. 4.51), where T_m is increased from 353ºC

(first cycle) to 377 ºC (seventh cycle). This indicates that the catalyst is able to maintain its activity quite well even after seventh cycle which is also evident from the XRD plot of the catalyst after seventh cycle (Fig. 4.54). The XRD plots for both fresh sol-gel Al-MCM-41 catalyst and reused sol-gel Al-MCM-41 catalyst (Fig 4.54) after seven cycles are almost identical in nature. Thus, the present sol-gel catalyst is a promising one for industrial application point of view.

4.5.3. Catalytic activity of n-HZSM-5 for PP decomposition

Figures 4.55 and 4.56 illustrate the TG and the DTG plots for the catalytic degradation of PP over n-HZSM-5. It observed from Fig. 4.56 that the shape and height (rate of decomposition) of the DTG curves changes significantly due to different wt % of n-HZSM-5 catalyst during the catalytic decomposition of PP sample. This change is very significant at lower catalyst compositions. The rate of decomposition is very high at 10 wt % catalyst. Table 3.6 shows the effect of catalyst percentage on T_m of the PP sample. It is observed (Fig. 4.57) that the temperature decreases exponentially with catalyst percentage. It is further observed that the optimum catalyst percentage could be around 50 wt %, since, after that reduction in T_m with increase in catalyst percentage is not so significant. To illustrate quantitatively, it may be seen that for a change of catalyst percentage from 50 to 60 wt %, the further reduction in T_m is about 0.5°C, where as for a change of catalyst percentage from 0 to 10 wt %, 10 to 20 wt %, 20 to 30 wt %, 30 to 40 wt %, and 40 to 50 wt %, the further reduction in T_m are 78.3, 40, 13.4, 13.4, and 10.6°C respectively (Fig. 4.57). The reduction in maximum decomposition temperature is around 161°C at 50 wt% catalyst. Thus, the optimum catalyst (n-HZSM-5) percentage was selected as 50 wt%. HZSM-5 due to presence of high external surface area enhances its

cracking activity because the zeolite external acid sites are not sterically hindered for the conversion of the bulky polyolefin molecules [64, 93-94], and promotes end-chain scission reactions of the polymers [93]. First chain scissions start on the external surface of the catalyst and then smaller chains can enter into the pores where most of the active sites are located [64].

From the above study, it can be concluded here that n-HZSM5 shows the best result in terms of reduction in T_m among the catalysts used for decomposition of PP sample. However, requirement of n-HZSM-5 for the same is also much higher than sol-gel Al-MCM-41. So, further studies regarding reusability of the all the catalysts and analysis of the products coming out of the decomposition phenomena are very important and necessary to asses the target oriented suitable catalyst. This is the scope of future studies in this area of research.

4.5.3.1. Catalytic nonisothermal decomposition at several heating rates

Nonisothermal decomposition of the PP sample was carried out at five different heating rates (5, 10, 15, 20, and 25 K min^{-1}) with the decided optimum catalyst percentage catalyst i.e. n-HZSM-5 (50 wt %). The temperatures T_{w0}, T_d, T_m and $T_{w\infty}$ for the experiments are also reported in the Table 3.7. Variation of α with temperature for catalytic (50 wt %) decomposition at different heating rates are reported through Fig. 4.58. Variations of rate, dα/dT with temperature during nonisothermal pyrolysis using catalyst n-HZSM-5 (50 wt %) at different heating rates are reported through Fig. 4.59.

It is observed from the Figs. 4.8, 4.51, and 4.58 that the TG curves show constant pattern behaviour and higher heating rate finishes the decomposition phenomenon faster. The constant pattern behaviour is attributed to the fact of similar reaction mechanism (as

discussed earlier (sections 4.5.1.-4.5.2), which is the basis of isoconversional (model-free) approach for kinetics analysis [50, 131-133, 177]. This is also supported by the almost similar peak height and constant pattern behaviour of the DTG curves (Figs. 4.13, 4.51 and 4.59) both for the noncatalytic and catalytic decomposition of PP. Figures 4.13, 4.51 and 4.59 also clearly shows single peak in the DTG curves both for the catalytic and noncatalytic decomposition of PP.

4.6. Product analysis using Gas chromatograph (GC)

This section presents the first hand information on the kinds of products being formed during both thermal and catalytic pyrolysis of the plastic materials used in the present study. It discusses on the chromatograms obtained from the GC analysis of vapours coming out of decomposition at a particular temperature and also compares the results reported in the literatures.

4.6.1. GC analysis of standard samples

Available standard samples of different categories such as pure propane gas supplied by Vadilal Gases Ltd; n-hexane, heptane, benzene, and toluene supplied Merck, India; indene, naphthalene, bi-phenyl, and fluorine supplied by Ranbaxy Laboratories Ltd, India are injected in the FID column of the GC to analyse their retention times under the similar operating conditions as used during the analysis of the product of decomposition of pyrolysis. Figures 4.60-4.68 show the chromatograms of the respective standard standard samples. The retentions times observed for these samples are reported in Table 3.8.

4.6.2. GC analysis of thermal decomposition products

This section discusses on the products obtained during thermal decomposition of the plastics materials and compares with the literature results.

4.6.2.1. GC analysis of products from waste PET sample

Figure 4.69 presents the chromatogram of thermal decomposition of waste PET sample at 438ºC (close to T_m). It can be seen that the amount of lower hydrocarbon (<C_6, retention time less than 2.5min) is as good as 29% and presence of C_6 is very less. High percentage (30%) of the poly aromatic hydrocarbons (PAHs) that may include naphthalene (C_{10}) is observed. The rest of the major products are higher hydrocarbons. Martin-Gullon et al. [129] reported presence of biphenyl as the major PAHs obtained during PET decomposition at relatively much higher temperature (850ºC). According to Holland and Hay [52] thermal decomposition of PET is associated with intramolecular back-biting leading to cyclic oligomers and chain scission via β-C-H hydrogen transfer leading to vinyl ester and acid end groups.

4.6.2.2. GC analysis of products from waste LDPE sample

The chromatogram (Fig. 4.70) of thermal decomposition of waste LDPE at 470ºC (close to T_m) shows a wide range product distribution. The chromatogram shows very little amount of lower carbon number hydrocarbon that eluted at retention time less than 3 min. PAHs such as indene, naphthalene, biphenyl, and fluorene are also identified. The results agree well with that obtained by Predel and Kaminsky [27]. They also reported that very little amounts of light hydrocarbon (2.6%) produce during thermal pyrolysis of LDPE at 500ºC. Similar characteristic triplets are also observed consisting of alkane, alkene, and diene of a specific chain length [27]. It can also be observed that the present

chromatogram (Fig. 4.70) also closely matches with that given by Predel and Kaminsky and Serrano et al. [66] for the thermal decomposition of LDPE at 500^{o}C and 700^{o}C (Figs. 4.71-4.72) respectively. The product distribution depends primarily on decomposition temperature, heating rate, and the residence time [66]. Thus, the existing discrepancy in chromatograms are due to the operating condition of the thermal decomposition of LDPE; molecular weight and degree of branching of LDPE; and use of different GC columns and oven programs.

As discussed in chapter 1 under section 1.4.1.3., thermal decomposition of LDPE is generally described by the breaking of polymer chain and formation of hydrocarbon radicals of different number of carbon atoms. The β-scission and intramolecular hydrogen transfer mechanisms in the propagation step leads to formation of alkenes and alkanes respectively [23, 51, 66]. Secondary reactions via Diels-Alder type reactions are mainly responsible for higher hydrocarbons and PAHs formations [23].

4.6.2.3. GC analysis of products from PP sample

Figure 4.73 shows the chromatogram of thermal decomposition of PP sample at 440ºC (close to T_m). The chromatogram agrees well with the findings of Predel and Kaminsky [27] as well as that of Bockorn et al [51] who carried out thermal decomposition of PP at 550 ºC and 460 ºC respectively (Figs.4.74-4.75). The presence of the methyl groups in PP increase the number of tertiary carbons in the molecule. This results in increasing reactivity of the chain, and decreasing thermal degradation temperature as compared to LDPE [68]. Analogous to LDPE decomposition, chain scission and chain transfer mechanisms are important during thermal decomposition of PP. Substantial amount of lighter hydrocarbons are produced in comparison to that for LDPE sample (Fig. 4.73).

The highest amount of C_3 found in light hydrocarbon fraction is also reported through by Predel and Kaminsky [27]. PAHs such as indene, naphthalene, biphenyl, and fluorene are detected. It can also be observed from the chromatogram that heavy hydrocarbons production is reduced as compared to the pyrolysis of LDPE sample (Fig 4.73). This result is also in well agreement with the findings of Predel and Kaminsky [27].

4.6.3. GC analysis of catalytic decomposition products

This section discusses on the products obtained during catalytic decomposition of the plastics materials, LDPE and PP and compares with the literature results.

4.6.3.1. GC analysis of catalytic decomposition of waste LDPE and PP samples over fresh FCC catalysts

Figure 4.76 presents the chromatogram of waste LDPE over fresh FCC catalysts at 460ºC (close to T_m). The product distribution is almost similar to thermal decomposition of LDPE except formation of substantial amount of light hydrocarbon ($<C_6$), which might be due to cracking on the catalyst surface. Product distribution is also found to be more dispersed compared to thermal case, for example, C_6-C_7 ranges hydrocarbons are found here which are almost absent in thermal decomposition. Benzene is also present in the products. There is also an increase in amount of higher hydrocarbons (retention time >30 min) than thermal pyrolysis which is possibly due to the mesoporous nature of the catalyst. There is an overall decrease in PAHs production except indene.

Figure 4.77 presents the chromatogram for the catalytic decomposition of PP over fresh FCC catalysts at 416ºC. The product distribution is almost similar to thermal decomposition of PP except substantial decrease of light hydrocarbon ($<C_6$). Product distribution is again found to be more dispersed compared to thermal case. There is also

an increase in amount of higher hydrocarbons (retention time > 30 min) than thermal pyrolysis which is possibly due to the mesoporous nature of the catalyst. There is an overall decrease in PAHs production.

4.6.3.2. GC analysis of catalytic decomposition of waste LDPE and PP samples over ZSM-5 catalysts

Figure 4.78 presents the chromatogram of waste LDPE over ZSM-5 at 418ºC (close to T_m). It is evident from the figure that there is a sharp increase in light hydrocarbons ($<C_6$) due to the strong acidic properties as well as microporous nature of the catalyst. Production of C_3 ranges hydrocarbon increased drastically. C_6-C_7 ranges hydrocarbon also increased significantly. Production of PAHs decreased substantially. Higher hydrocarbons distribution became much narrower than thermal decomposition of waste LDPE. In case of ZSM-5, the presence of medium-pore zeolites sterically hinders the secondary bimolecular reaction, resulting in higher amounts of alkenes as primary products thereby reducing production of heavier hydrocarbons [90, 67]**.** The single ring aromatic hydrocarbon such as benzene and toluene are also found in the products, those are absent during thermal pyrolysis of waste LDPE. This results well agreed with the results (Fig. 4.79) obtained by Serrano et al. [66] due to the initial cracking of large hydrocarbon molecules into smaller olefins in the catalytically active sites followed by oligomerisation, cyclation and hydrogen transfer reactions that leads the formation of aromatics, light parafins and olefins [66]

Production of light hydrocarbons ($<C_6$) and C_6-C_7 ranges hydrocarbons are increased (Fig. 4.80) in case of ZSM-5 catalyzed decomposition for PP at 428ºC due to high acidic

nature of ZSM-5. Other products, though decreased in amount, are mainly lying in the retention time range of 20 – 30 minutes.

4.6.3.3. GC analysis of catalytic decomposition of waste LDPE and PP samples over Al-MCM-41 catalysts

It is evident from the chromatogram (Fig 4.81) of the catalytic decomposition of waste LDPE over Al-MCM-41 catalysts at 430ºC (close to T_m) that product distribution again narrows down and completely different from thermal decomposition of waste LDPE. The light hydrocarbon product ($<C_6$) increases compared to thermal one as observed in case of FCC catalyst also. Single aromatic ring such as benzene and toluene are almost absent. There is reduction in the PAHs compared to thermal decomposition of waste LDPE. Production of heavier hydrocarbons (retention time >30 min) increase significantly as compared to thermal decomposition. High surface area, large pores, and mild acidic strength present in the mesoporous Al-MCM-41 catalyst might be responsible for the high conversions, yielding high amount of heavier hydrocarbon. Moreover, Al-MCM-41 promotes random scission that is responsible for formation of heavy hydrocarbon [94]**.** The results obtained by Serrano et al. [66] during catalytic pyrolysis of LDPE over Al-MCM-41 exhibited a significantly lower proportion of aromatic species (benzene, toluene, xylene and other alkyl substituted benezene rings) and a greater proportion of heavier hydrocarbon compounds (Figure 4.82) [66].

Figure 4.83 presents the chromatogram of PP over Al-MCM-41 catalysts at 340 ºC. It is evident from the figure that product distribution narrows down. There is little increase in light hydrocarbons ($<C_6$). Presence of heavier hydrocarbons (retention time >30 min) is

almost negligible. The product is mostly lying within the range of retention time 20-30 min.

4.6.3.4. GC analysis of catalytic decomposition of waste LDPE and PP samples over n-HZSM-5 catalysts

Figure 4.84 shows the chromatogram of the catalytic pyrolysis of waste LDPE over n-HZSM-5 at 421ºC (close to T_m). There is enormous increase in the light hydrocarbon gases ($<C_6$) and subsequently thorough reduction in heavier hydrocarbon. n-HZSM-5 zeolite, with high external surface area and strong acid sites, promotes end-chain scission reactions of the polymers, leading to very high amount of light hydrocarbons. Presence of high external surface area enhances its cracking activity, because the zeolite external acid sites are not sterically hindered for the conversion of the bulky polyolefin molecules [66, 94]. Though PAHs such as naphthalene, biphenyl, and flurene are present in the products, their production is significantly decreased. The results are in well agreement with the reported one by Serrano et al (Fig. 4.85) [66, 93-94].

Figure 4.86 shows the chromatogram of the catalytic pyrolysis of PP over n-HZSM-5 at 330ºC. Similar type of product distribution such as sharp increase of light hydrocarbons ($<C_6$) and C_6- C_7 ranges hydrocarbons as is observed in case of n-HZSM-5 catalysed LDPE decomposition. Production of higher hydrocarbons (retention time <30min) and heavier hydrocarbons (retention time >30min) is reduced in comparison to the noncatalytic decomposition of PP. PAHs such as naphthalene, biphenyl, and fluorene are found in products except indene.

Thus, it may be concluded from the analyses of the products from noncatalyic and catalytic decompositions of LDPE and PP over various catalyst employed that PP

decomposition is difficult in ZSM-5 catalyst as decomposition chain segments finds diffusional hindrance due to smaller pore structure of the catalyst. But good catalytic activity of ZSM-5 is observed on waste LDPE sample. Moreover, the acidic character also plays an important role in the case of catalytic decomposition of polymers. The fresh FCC catalyst has less impact on the catalytic decomposition of waste LDPE samples. However, the good catalytic activity of FCC on PP sample is due to large pore sizes in the catalyst. Due to the presence of high external surface area, which can be easily accessible and strong acidic nature, n-HZSM-5 catalyst shows excellent catalytic activity on both the LDPE and PP samples. Both n-HZSM-5 and ZSM-5 zeolite, with strong acid sites lead to light hydrocarbons production, which is not the case with Al-MCM-41 and fresh FCC catalysts because of the presence of large pores and mild acidity in these catalysts. First chain scissions starts on the external surface of the catalyst and then smaller chains can enter into the pores where most of the active sites are located. Further decomposition followed by oligomerization, cyclation and hydrogen transfer reactions that result in the formation of shorter hydrocarbons such as aromatics, light parafins and olefins continues in the pores depending on acidic character of the catalyst [56, 60-69, 90, 93-94, 194].

4.7. Kinetics analysis of pyrolysis of plastics

4.7.1. Model-fitting methods for nonisothermal experiments using single and multiple heating rate(s)

4.7.1.1. n^{th} order model and ASTM E698 techniques [175]

One step nth order kinetic model is used to calculate kinetics parameters from one TGA curve for waste PET sample (from Coca-Cola and Pepsi bottles) using different

techniques as discussed earlier in Chapter 2 under Section 2.1.1.2. As mentioned earlier in Chapter 2 under Section 2.1.2, in ASTM E698 method, the decomposition order is assumed to be one (by definition) [33, 175, 185]. It can be observed from Table 4.5 that the calculated values of kinetics parameters by nth order model technique gives higher values of E and $\ln(k)$ than ASTM E698 techniques used. This can be attributed to fact that different calculating techniques, respectively, appropriate for the thermal degradation behaviours in different temperature ranges. As a matter of fact, kinetic parameters change more or less with temperature, even though we assume that they don't vary with temperature in every mathematical technique [133, 175]. In the present case the nth order model technique uses a wide temperature range starting from T_d to $T_{W\infty}$ and ASTM E698 method uses only T_m, which is much lower than $T_{W\infty}$. In case of nth order model technique, values of E, n and $\ln(k_0)$ are 322.3 kJ/mole, 1.72 and 54.76 respectively for Coca Cola bottle sample and 338.98 kJ/mole, 1.82 and 57.73 respectively for Pepsi bottle sample. Similarly, in case of ASTME698 method, values of E, n and $\ln(k_0)$ are 162.15 kJ/mole, 1.0 and 26.37 respectively for Coca Cola bottle sample and 210.64 kJ/mole, 1.0 and 34.81 respectively for Pepsi bottle sample. The difference in kinetic parameters between the samples may be due to difference in composition. The nth order model technique while compared with ASTM E698 method is expected to be more suitable one to describe the pyrolysis behaviours of the samples studied since it doesn't assume on values of n like the later method. This expectation is supported by the study of numerical simulation of the models described subsequently in section 4.7.3.

4.7.1.2. Freeman-Carroll, Friedman, and Chang techniques [177]

A single step reaction is assumed during non-isothermal decomposition of waste PET sample (from Coca-Cola bottle) and used a one-step chemical reaction model to calculate kinetics parameters from single heating rate TGA curves using different techniques as discussed earlier in Chapter 2 under Section 2.1.1.2. It may be observed from Table 4.6 that the Freeman-Carroll, Friedman and Chang methods give more or less constant values of kinetics parameters such as E, $\ln k_0$ and n., The n^{th} order model and ASTM E698 techniques (described in the previous section) give the highest and the lowest values of the kinetics parameters respectively (Table 4.6). This can be attributed to the fact that different calculating techniques respectively appropriate the thermal decomposition behaviours in different temperature ranges. Freeman-Carroll and Chang techniques describe the behaviour of thermal decomposition in the temperature range from (T_m- [30 - 60]) to T_m. The E value given by Friedman technique is somewhat lower mainly because the thermal decomposition behaviour is estimated in the lower temperature range from [(T_d- [20 - 40]) to T_d] than other techniques. [177]. n^{th} order model technique uses a wide temperature range starting from T_{w0} to $T_{w\infty}$. ASTM E698 method uses only T_m, which is much lower than $T_{w\infty}$. The kinetics triplet reported here by ASTM E698 method differs significantly from Table 4.5 to Table 4.6. This may be attributed to the use of different heating rates (5, 10 and 15 $Kmin^{-1}$ in the present case and 10, 15 and 25 $Kmin^{-1}$ in the previous case). In fact, this is the limitation of ASTM E698 method because in this method one point for each heating rate is taken for calculation of the kinetics triplet. Further, according to the ASTM E698 method [185], heating rate should be preferably within 20^oC.

4.7.1.3. Standard deviation minimization technique (SDMT) for non-isothermal condition using single and multi-heating rate(s) [177]

Table 4.6 shows that standard deviation values are much less while using SDMT for both single heating rate and multiple heating rate curves. It was also observed that standard deviation is minimum for n=1 using SDMT, when single heating rate is concerned. Therefore, n=1 is also considered for multiple heating rates. The dependency of exact and optimal $\ln(k_0/\beta)$ upon optimal E is shown in Fig. 4.87. Figure reflects that the first order model can be selected as the best model. Thus, this is similar to the observation by SDMT method with single heating rate curve using Agrawal and Sivasubramanian approximation discussed earlier in Chapter 2 under Section 2.2.2.2. So, the best kinetics triplet is obtainable with first order model and the corresponding optimal values of E and $\ln k_0$. Unfortunately, in the case of only one kinetic curve (one heating rate), the calculated optimum E and $\ln(k_0/\beta)$ are completely determined by a model used and can greatly differ for different models for all traditional model-fitting kinetics analysis techniques [50, 131]. Further, T_m changes with different heating rates and $\ln k_0$ becomes dependent on T_m. Therefore, different optimal kinetics triplets are possible for different heating rates. Therefore, to obtain a unique kinetics triplet for thermal decomposition of waste PET sample, SDMT method using multiple heating rate TGA curves should be applied since this technique only has the feature of using multi heating rates among the other model-fitting methods. However, the difference in optimum values of E and $\ln k_0$ obtained by single and multiple heating rate TGA curves in the present case is not significant for first order model (Table 4.6).

SDMT method for single parameter optimization (E) using multiple heating rate TGA curves was also applied for nonisothermal pyrolysis of waste PE sample. In this case also SDMT with n =1 showed minimum deviation from the experimental results. The kinetics triplet for PE decomposition using SDMT is 272.09, 43.24, and 1. In the present case, it is observed that AIC_c score for both PET and PE samples were found minimum for n=1. A sample calculation of AIC_c score using only n=0.5, 1 and 2 is shown in Table 4.7. Thus, it can be observed that the reaction orders obtained for PET and PE samples after single parameter optimization and by AIC criteria are same. This comparison finally justifies our new approach for evaluation of kinetics triplet. The optimized kinetics triplets for PET and PE samples are used to simulate nonisothermal decomposition data (Figs. 4.107-4.108) using Eqs. (89) and (90).

4.7.2. Model-fitting methods for isothermal experiments [177]

Model-fitting technique is also applied for isothermal kinetics analysis to obtain the kinetics triplet. Values of E and $\ln k_0$ obtained by model-fitting method for isothermal kinetics analyses are 196.96 $kJmol^{-1}$ and 28.515 for first order model and 210.25 $kJmol^{-1}$ and 31.81 for second order model. Further, Akaike's criterion analysis as discussed earlier (Chapter 2 under section 2.1.1.1.**)** shows that first order model is more likely. It was observed that for all the four temperatures of study, AIC_c is lower for first order model. Thus, like nonisothermal study, the isothermal study also indicates in favour of first order model reaction of thermal decomposition of waste PET sample.

The kinetics parameters obtained in the present work and from the literature, both under isothermal and nonisothermal condition, are reported in Table 4.8. It is observed from the table that the present results are in close agreement with the literature reported data [177].

4.7.3. Numerical simulation

The kinetics triplets obtained by different methods are used to simulate the kinetic model equation to predict the nonisothermal and isothermal experimental TGA data for the respective polymer samples.

4.7.3.1. Nonisothermal data prediction [177]

The n^{th} order kinetic model equation with initial condition $\alpha=0$ at T= 630 K is solved numerically by Runge-Kutta 4^{th} order method using the kinetics parameters obtained by n^{th} order model, Freeman-Carroll, Friedman, Chang and ASTM E698 techniques. The kinetic parameters obtained from SDTM techniques are used to simulate nonisothermal decomposition data using Eqs. (39) and (40). It is observed that though all the techniques predicted the experimental data fairly well; SDTM and n^{th} order model techniques predicted the nonisothermal experimental data better, which is evident from Figs 4.88, 4.89, and 4.90. This is further supported by the statistical analysis results reported in the form of standard deviations (Tables 4.6).

4.7.3.2. Isothermal data prediction [177]

The kinetics triplets obtained by several model-fitting techniques from nonisothermal experiments are used for isothermal predictions. Figure 4.91 represents isothermal prediction at 685 K by various model fitting kinetics analysis techniques at a heating rate of 10K min^{-1}. The figure indicates that Friedman and ASTM E698 are predicting the isothermal decomposition data better compared to the other all the techniques such as nth order, Freeman-Carroll, Friedman, Chang, and SDMT techniques. However, it is also interesting to observe that SDMT (for both the cases of single heating rate and multiple heating rates) predicted the experimental data well. Therefore, it may be concluded that

SDMT is likely to be the most versatile method of predicting the kinetics triplet for thermal decomposition of waste PET sample. Isothermal prediction of experimental data at 711 K also from SDMT is reported in Figure 4.92. The deviations observed in the figures may be attributed to the fact that PET degradation is a complex phenomenon, which involves many reaction steps. Broken values of n as reflected in Figure 4.87 also possibly indicated overlapping of reaction steps [177]. Thus, the degradation description in terms of a standard nth order model is not sufficient to cover wide operative conditions.

4.7.4. Sensitivity analysis

This section discusses the effects of first order, second order and second order cross sensitivity coefficients of the different kinetics parameters on the temperature of decomposition during nonisothermal pyrolysis.

4.7.4.1. First order sensitivity analysis

First order sensitivity analysis is carried out using several values of n ranging 0.5–2.0 with an interval of 0.05. Each case is studied for four different heating rates (5, 10, 15 and 25 $Kmin^{-1}$ for PET and 10, 15, 20 and 25 $Kmin^{-1}$ for PE respectively). The values and ranges of the kinetics triplet used are reported in Table 2.2. Variations of first order semi-normalized sensitivity coefficients with temperature for 26 E values and n = 1.5 and $\beta=10Kmin^{-1}$ are depicted in the Figs. 4.93-4.96. Figures show that while the parameter $\tilde{K}_0$, E and β are less sensitive, n is the highly sensitive one. Order of the sensitivity is n>> $\tilde{K}_0$ > β > E i.e. E is the least sensitive one. Similar natures (not shown here) are also obtained for other values of n and β. The results of second order sensitivity

coefficient and second order cross sensitivity coefficient studies give us more insight on the parametric dependence as discussed subsequently.

4.7.4.2. Second order sensitivity analysis

Figures 4.97-4.100 represent the variations of second order semi-normalized sensitivity coefficients with temperature for all the four parameters $\tilde{K}_0$, E, n and β. The figures again reflect that second order sensitivity is also maximum in case of n (absolute value lies between 0-0.4 (Fig. 4.98). For other parameters such as $\tilde{K}_0$, E and β the second order sensitivity (Figs. 4.97-4.98, and 4.100) is negligible with respect to that for n. Thus, analysis of second order sensitivity coefficient also indicates optimization of E to have kinetics triplet with the lowest possible error.

4.7.4.3. Second order cross sensitivity analysis

Second order cross sensitivity coefficients i.e. variations of first order sensitivity coefficient for parameter p_i with variation another parameter p_j are evaluated for different temperature ranges. The variations of second order semi-normalized cross sensitivity coefficient ($\frac{S^{\langle 2 \rangle}_{p_i p_j}}{p_i^* p_j^*}$) with temperature are shown in Figs. 4.101-4.106. From the Figures, it is again observed that association of n with $\tilde{K}_0$ and β (Figs. 4.102 and 4.106) gives higher second order cross sensitivity coefficient values. Association of E with β (Fig. 4.104) gives the lowest second order cross sensitivity coefficient values. This further supports the fact that E is the least sensitive one.

Thus, from the above analysis of the three types of sensitivity coefficients in case of pyrolysis characterized by n^{th} order rate equation, it is well understood that n is the

highest sensitive parameter and E is least sensitive parameter. The uncertainties in the solution of the optimization objective function come mainly from highly sensitive parameters. Hence, the evaluated kinetics triplet after optimization of single parameters objective function of E values will be more realistic and justified. The results will also contain the least error and the least uncertainty. The uncertainty and ambiguity associated with model and parameters can be overcome using multi-heating rate objective function of single parameter E only. This is also supported by the fact that use of isoconversion method, Vyazovkin non-linear model-free approach through using objective function of single parameter (E) is a trustworthy way of obtaining reliable and consistent kinetic information from nonisothermal data [33, 35]. Therefore, we have reduced the multi parameter optimization problem into single parameter optimization problem using a new approach called SDMT as discussed in chapter 2, sections 2.6 and 2.7.

4.7.5. Hybrid genetic algorithm (HGA) to find the best model and the globally optimized overall kinetics parameters for thermal decomposition of plastics

As discussed earlier, model-fitting methods that are exercised till date for evaluating the optimum overall pyrolysis kinetics parameters usually apply traditional gradient base optimization techniques but associated with major drawback of attaining global optimum due to uncertainties in selection of initial guess. To overcome such uncertainties and drawbacks, the modern evolutionary optimization method HGA technique is applied for fifteen models (Table 2.1) to attain the globally optimum kinetics parameters using the experimental TGA data and we did compare the experimental and simulated data to understand the possible mechanism occurring during pyrolysis. As case studies, thermal decomposition behaviour of waste PET, waste LDPE and PP is considered. The observed

single peaks in all the DTG (Figs. 4.11, 4.13-4.14) allowed approximating it as a single step reaction taking place. Accordingly the single step overall kinetics triplets (E, K_0 and n) are found out for pyrolysis of all three plastics by HGA applying all fifteen models using multi-heating rates. It is worth mentioning here that the single peaks that are observed in Figs. 4.11, 4.13-4.14 do not necessarily indicate a single-step reaction that is occurring during pyrolysis. The initial guesses are taken from the GA. The kinetics triplet data and the standard deviations, obtained from HGA based on 15 best data points for all the models and all types of plastics used are reported through Tables 4.9-4.11.

4.7.5.1. Prediction of experimental TGA data

As already discussed, AIC_c scores helps to identify the better reaction model for pyrolysis study. Lower the AIC_c scores for a reaction model, more correct is the model representing the system [177, 181-183, 184]. Therefore, the kinetics triplets [Tables (4.9-4.11)] obtained by HGA method employed in the present study are used in simulation to calculate the ACI_c scores for all the fifteen models considered. The AIC_c scores for all the models and the integral form of all kinetics models are presented in Tables 4.9-4.11. It is observed from Tables 4.9-4.11, for all the three plastics used, that the AICc score is minimum for nucleation and growth model with n = 2/3. The $n^{th.}$ order and first order models also show encouraging scores. But, according to the AICc criteria, the nucleation and growth model with n = 2/3 is likely to be the best of all the fifteen models for the all the polymers (LDPE, PET and PP) used in the present study. Thus, the pyrolysis kinetics equation was simulated using globally optimized kinetics triplet for all the three reaction models (nucleation and growth model with n = 2/3, first order and n^{th} order reaction model) to predict the experimental TGA data. Figures 4.107-4.109 show prediction of the

experimental TGA data by nucleation and growth model with n = 2/3 for different heating rates. It is observed from the figures that Nucleation and Growth (n=2/3) model successfully predicted the experimental TGA data particularly for LDPE and PET samples. In case of PP samples, it is observed that there is a significant deviation between experimental and predicted [Nucleation and Growth model (n=2/3)] data. From the agreement of Nucleation and Growth model (n=2/3), particularly for waste LDPE and waste PET samples, it is worth mentioning that an initial stage of polymer degradation is often accompanied by melting (or softening). At this stage, the thermal degradation can be controlled by the process of formation of a gas phase inside the polymer and by nucleation and nucleus growth in a heterogeneous medium [50].

Since, n^{th} order and first order models also show encouraging AICc scores, we compared the predictions of n^{th} order and first order models with experimental data and nucleation and growth model predictions and reported through Fig.4.110. It is a sample plot for waste LDPE. Similar behaviors are observed for waste PET and PP samples also and therefore not reported here. Figures show that though nucleation and growth model with n = 2/3 is marginally better than n^{th} order and first order models, they also closely predict the experimental TGA data. This fact is also supported by the AIC_c scores as discussed above. Therefore, suitability of both the Nucleation and Growth model and chemical reaction models for all the three samples indicates that both the mechanism (nucleation, growth and diffusion and chemical reaction) significantly controls the decomposition phenomena. It may be further added here that the proposed models may not fully describe particularly the decomposition phenomena of PP samples. Though single step kinetics from the single peak of DTG curves have been taken up, it may be possible that more

steps are involved in the reaction, which may possibly be taken care of by a new and different model. Therefore, further studies in this direction may help to estimate the more accurate kinetics expression for thermal decomposition of PP.

Table 4.12 summarizes the optimum model and the optimum kinetics parameters for all the polymers used in the present study along with the literature published data on the kinetics parameters of thermal degradation of waste LDPE, waste PET, and PP using different techniques. From the table, it is observed that most of the reported studies are based on first order model. Through the present work, it is shown that first order and n^{th} order models describe the thermal decomposition behaviour of the samples used well. At the same time, it established here that the nucleation and growth model with n = 2/3 is better suited for describing the thermal degradation kinetics of all the plastic samples used in the present study.

4.7.5.2. Hybrid genetic algorithm (HGA) for pyrolysis kinetics of Al-MCM-41 [183] and n-HZSM-5 catalyzed decomposition of PP

Single peak in the DTG curves (Figs. 4.13, 4.47, 4.49, 4.52, 4.56, and 4.59) is clearly noticed for both the noncatalytic and catalytic decomposition of PP over Al-MCM-41 (sol-gel) and n-HZSM-5 catalysts. These behaviours are different from our recent studies on ZSM-5 catalyzed decomposition of LDPE [179, 182], where the noncatalytic decomposition showed a single peak at various heating rates but catalytic one showed multiple peaks indicating possible existence of different reaction mechanism. Single peak at different heating rates for both catalytic and noncatalytic decomposition of PP allowed approximating it as a single step reaction taking place [175, 177]. Accordingly, the single step or overall kinetics triplet (E, K_0 and n) are found out by HGA applying all fifteen

models as mentioned in Table 4.13. The kinetics triplet data and the standard deviations, based on 15 best data points, for the noncatalytic and catalytic decompositions are reported through Table 4.14 for three best-fitted models in terms of AIC_c scores as described. The literature data of activation energies and ΔT_m over different catalysts are reported in Table 4.15.

Prediction of experimental TGA data

The kinetics triplets obtained by HGA method are used in simulation to predict the experimental TGA data using all fifteen models (Tables 2.1 and 4.13) both for catalytic and noncatalytic decomposition of PP. Corrected Akaike's Information Criteria [177, 181-184] is applied to choose the appropriate reaction model. According the to the AICc scores in Table 4.14, it is observed that Nucleation and growth model with n = 2/3 is the best one. The n^{th} order and first order models also show encouraging scores. These observations are also evident from the Figs. 4.111-4.113, where prediction of the experimental TGA data by the models is shown for five different heating rates. It is further observed from the figures and AIC_c test that Nucleation and Growth (n=2/3) model is the best one for both catalytic decompomposition of PP and accordingly the obtained kinetics triplets using the model predicted the experimental TGA data most successfully. An initial stage of polymer degradation is often accompanied by melting (or softening). At this stage the thermal degradation can be controlled by the process of formation of a gas phase inside the polymer and by nucleation and nucleus growth in a heterogeneous medium [50, 176]. Suitability of both the Nucleation and Growth model and Reaction model for both catalytic and non-catalytic decomposition of PP (Figs. 4.109 and 4.11) indicates that both the mechanism (nucleation, growth and diffusion and

chemical reaction) significantly controls the decomposition phenomena. Therefore, as opined by Marcilla et al. [163], a good fit of experimental results is not only the criterion to decide upon the decomposition mechanism. Further studies including infrared or mass spectroscopy, morphology study using SEM or TEM during such decomposition is very much needed to conclude upon the actual reaction mechanism that controls the catalytic decomposition behaviour of PP sample.

4.7.6. Model-free analysis

Nonlinear Vyazovkin model-free approach is applied to study the variation of activation energy with conversion for both noncatalytic and catalytic decomposition of plastics samples used in the present work.

4.7.6.1. Model-free analysis for waste PET sample [176]

A sample plot for E_α dependency on α obtained for nonisothermal decomposition for PET sample using Agrawal and Sivasubramanian approximation [187] is shown in Fig.4.114. For the other approximations such as Coats-Redfern and Gorbachev approximations exactly similar nature is obtained. The optimal E_α obtained by direct numerical integration is compared with that by using various approximation techniques. This is reported in terms of percentage deviation of E_α obtained by Agrawal and Sivasubramanian approximation (Fig.4.115) from direct numerical integration using recursive adaptive Simpson Quadrature scheme. All the approximations of temperature integral have all most same deviation from the results of direct numerical integration. The average relative deviation (ARD) values are 10.81, 10.82 and 10.83 for Coats & Redfern; Gorbachev; and Agrawal and Sivasubramanian approximation [187, 176] respectively. ARD is defined as $ARD(\%) = \frac{100}{N}\sum_{i=1}^{N}\left|\frac{E_{\alpha,i}^{DI} - E_{\alpha,i}^{j}}{E_{\alpha,i}^{DI}}\right|$, where $E_{\alpha,i}^{DI}$ and $E_{\alpha,i}^{j}$ respectively are

the activation energies calculated by direct integration method and jth approximation of temperature integral respectively. N is the number of data points. Application of model-free isoconversional method to isothermal and nonisothermal decomposition of waste PET samples to obtain E_α dependency on α is compared through Fig.4.116. It is observed from the figure that that E_α is weak but increasing function of α, though there are some fluctuations at the initial stages of conversions under nonisothermal condition. But E_α is a strong and continuously decreasing function of α in case of isothermal condition. These may be explained as follows.

According to Mamleev et al. [50], initial stage of polymer decomposition is often accompanied by melting (or softening). At this stage the thermal decomposition can be controlled by the process of formation of a gas phase inside the polymer and by nucleation and nucleus growth in a heterogeneous medium. Further, Vyazovkin and Wight [155] have reported that concentration of nuclei at fast heating rate, which is commonly the case for isothermal system (90 K min^{-1} for the present case) is very low and the isothermal decomposition is limited by nucleation only. But in case of non-isothermal decomposition, as the heating rate is low (5-25 K min^{-1} in the present case), it is limited by nuclei growth. They also added that nucleation and nuclei growth takes place at lower and higher activation energies respectively. Therefore, one may find decrease and increase in activation energies for isothermal and nonisothermal cases respectively at the initial stages (Fig. 4.116). In addition, it is also reported by Vyazovkin and Wight [155] and Flammersheim and Opfermann [30] that diffusion of the formed gas plays an important role to reduce the E_α in the subsequent stages of the decomposition phenomenon. Therefore, in case of isothermal decomposition one can observe continuous

decrease of E_α during the course of decomposition (Fig. 4.116). But in case of nonisothermal decomposition, the two opposite effects (nuclei growth and gas diffusion) may finally make E_α a weak function of α. It may further be observed in case of isothermal decomposition that at the later stage of the decomposition phenomenon, the E_α quickly falls with α. This may possibly be attributed to the fact that at the later stage formation of porous solid residue makes the diffusion faster leading to more decrease in E_α [176].

However, the optimum E_α dependencies from nonisothermal data have shown reliable prediction of isothermal data. The corresponding percentage deviations from experimental data are shown in Fig.4.117. The results show that 10°C min^{-1} heating rate (ARD%= 1.51) predicts the isothermal data better for all isothermal temperatures. ARD is defined as, $ARD(\%) = \frac{100}{N}\sum_{i=1}^{N}\left|\frac{t_{\alpha,i}^{\exp} - t_{\alpha,i}^{j}}{t_{\alpha,i}^{\exp}}\right|$, where $t_{\alpha,i}^{\exp}$ and $t_{\alpha,i}^{j}$ are the experimental time and time simulated by model-free method from nonisothermal experiment (Eq.43) respectively to reach the conversion, α [176].

4.7.6.2. Model-free analysis for waste PE sample [178]

A sample plot for E_α dependency on α obtained for nonisothermal decomposition for PE sample using direct numerical integration and approximation of Cai et al. [186], superior to all other approximations, is shown in Fig.4.118. It is observed from the figure that initially E_α is strong and increasing function of α for $\alpha \leq 0.1$, then decreasing for $0.1 < \alpha < 0.15$ and then again slowly increasing with decreasing slope for $\alpha \geq 0.15$. All the approximations of Coats and Redfern, Gorbachev, Agrawal and Sivasubramanian [187] and Cai et al. [186] used for integration of Eq. (22) showed almost similar result and similar deviations from the results with direct integration. Figure 4.119 represents

deviations from the results with direct integration. The average relative deviation (ARD%) [15] values are 0.04225, 0.01145, 0.00377 and 0.00104 for Coats & Redfern; Gorbachev; Agrawal and Sivasubramanian and new approximation respectively. Therefore, the other results obtained and presented subsequently are by direct integration only. [178]

Application of model-free isoconversional method to isothermal and nonisothermal decomposition of waste PE samples to obtain E_α dependency on α is presented through Fig.4.120. In case of nonisothermal decomposition of waste PE samples, similar nature was also observed for waste PET samples except a difference in slope of increase of E_α with α, which led to a cross over. The reported data of Lyon [157], Peterson et al. [38] and Gao et al. [134] are also compared with the present result through Fig. 4.121. It is observed from the figure that in all the cases except that of Lyon [157] the variation of E_α with α follows similar trend. In case of data reported by Lyon [157] for LDPE sample, E_α is almost independent of α after $\alpha \geq 0.2$. This apparent trend may possibly due to lack of sufficient data for different values of α and also due to application of new series solution for integration of the Arrhenius integral. Initial strong and increasing function of α for all the cases (Fig. 4.121), for $\alpha \leq 0.1$, can be attributed to the fact that the low values of E_α at low α are quite typical for degradation of polymers and usually associated with initiation at the weak links [38,134, 157, 158]. It is further observed that the values of E_α, $\alpha \geq 0.15$, are almost matching with that of Gao et al. [134] except at initial and final stages of decomposition but there is almost a constant difference between the present E_α values and that reported by Peterson et al. [38]. Table 4.1 shows that the present sample is a non-standard one having melting point closer to HDPE with certain amount of impurity. The

lower crystallinity data in comparison to standard LDPE and HDPE sample may possibly be due to recycling for several times. The close match of our E_α values with that of Gao et al. [134] indicates that the sample is possibly a HDPE sample. But the differences in values of E_α between the present work and that of Gao et al. [134] may be due to difference in structure and molecular weight. Similarly, the constant difference between the present E_α values and that reported by Peterson et al. [38] might also be due to difference in molecular weight [38] of the samples as well as chain branching. [178]

Thus, it may be concluded here that the sample used for the present study, a non-standard sample, follows neither perfectly the LDPE trend nor the HDPE trend. In practice, while going for solid waste management, most of the waste materials happen to be a non-standard one, particularly in developing countries. Therefore, the present study reflects that it becomes mandatory to study the decomposition behaviour of the waste materials before design of an incinerator and/or pyrolysis unit and one should not use blindly the information available for standard samples [178].

The thermal decomposition of PE occurs via initiation, propagation (intermolecular and intramolecular hydrogen transfer and β-scission) and termination [30, 38, 45, 51, 38, 134]. Vyazovkin [38] discussed that the shape of the increasing dependencies of E_α on α is found due to competing and some independent and consecutive reactions. The results agreed well with the thermal decomposition of PP and PE samples. Again Peterson et al. [38] reported that after the weak links are consumed, the limiting step of the degradation shifts towards the degradation initiated by random scission. Therefore, higher activation energy is observed at higher conversion. But according to Gao et al. [134], PE degrades via random chain scission, which doesn't depend upon heating rate. Degradation

temperature influences the size of the volatile products. As temperature increases, the minimum length of the fragments, which can evaporate under the prevailing conditions, increases. A higher heating rate leads to degradation at higher temperature, which results in a dependence of distribution of size of volatile products on heating rate and hence the variation of the E_α with α. Previously, it is already discussed that in case of nonisothermal decomposition of PET sample, the two opposite effects (nuclei growth and gas diffusion) may finally make E_α a weak function of α. But the difference in the slope of E_α vs. α under nonisothermal condition for PE and PET sample may be due to difference in chemical structure. [176,178].

E_α dependency on α presented in case of isothermal decomposition (Fig.4.120) is also quite interesting. Results show that at initial stage till ($\alpha<0.25$), E_α is weak and decreasing function of α and thereafter it is a weak but increasing function of α. Explanation for decrease in E_α at the initial stages is already discussed in case of PET sample in the previous section. Again, as discussed earlier, distribution of size of volatile products and the two opposite effects (nuclei growth and gas diffusion) are instrumental for the increase of the E_α with α [176].

A sample plot for the prediction of isothermal data by model free kinetics analysis technique at 708K is presented in Fig.4.122 for four different heating rates (10, 15, 20 and 25$Kmin^{-1}$) using direct numerical integration of temperature integral. The results show that amongst the others, 15$Kmin^{-1}$ heating rate (ARD (%) = 5.4928) very closely predicts the isothermal data. [178]

4.7.6.3. Model-free analysis for waste LDPE sample [179]

Dependency of E_α on α obtained for nonisothermal decomposition of the waste LDPE sample is presented through Fig.4.123. It is observed from the figure that in case of noncatalytic decomposition, E_α is almost constant (around 190 kJ mol^{-1}) with α. Almost similar values and similar trend were also observed by Lyon et al. [157] during non-isothermal noncatalytic decomposition of LDPE (Fig. 4.123). The reported data of Peterson et al. [38] is also compared with the present result through the same figure. It is observed from the figure that the trend of variation of E_α with α is similar with a substantial difference in E_α values. The constant difference between the present E_α values and that reported by Peterson et al. [38] might be due to difference in molecular weight of the samples as well chain branching [179].

4.7.6.4. Model-free analysis for PP sample [180]

Dependency of E_α on α obtained for nonisothermal decomposition of the PP sample is presented through Fig.4.124. It is observed from the figure that E_α is a slowly increasing function of α in the range ($0.1 \leq \alpha \leq 0.9$). Studies of Peterson et al. [38] and Filho et al. [60] on variation of E_α with α for the decomposition of pure PP are compared with the present result in the same figure. It is observed that the trends of variation reported by them are similar to that observed by us. The existing differences in the activation energy might be due to different molecular weights of the PP samples used for the different cases. In the present investigation, PP sample of melt flow index (MFI) 3.0 whereas Filho et al [60] used PP sample of much higher melt flow index 11.5. Higher MFI polymer has lower viscosity. Again, viscosity increase with molecular weight. Therefore, our PP sample have higher molecular weight, higher melting point and thermal stability (or

strength) than that of Filho et al [60]. Peterson et al [38] have used PP sample of average molecular weight 12000.

4.7.6.5. Model-free analysis for waste LDPE over ZSM-5

Dependency of E_α on α obtained for nonisothermal decomposition of the waste LDPE sample with and without catalyst is presented through Fig.4.123. In case of ZSM-5 catalyzed decomposition of the waste LDPE sample, it is observed that E_α is strong and increasing function of α except the plateau region for $\alpha = 0.15$ till $\alpha = 0.4$. The different reaction steps involved during catalytic decomposition is also obvious from the four steps observed in the variation of E_α with α (Fig. 4.123) during catalytic decomposition. Existence of wide range of pore sizes (Fig. 4.20 and Fig. 4.21) might also play important roles in the types of reactions taking place and the product distribution during catalytic decomposition of PE. The four-step process as evident from Fig. 4.123 goes on line with the reported discussion of Takuma et al. [78]. According to the scheme given by Takuma et. al. [78], these steps in sequence is thermal degradation of PE (step 1), catalytic cracking of the high molecular weight fragments to give liquid and / or gas (steps 2 and 3), and finally formation of aromatics through cyclization (step 4). However, higher activation energy indicates slowness of the reaction rate, which is also indicated through decreasing peak height in the DTG curves (Fig. 4.43) and in the flatter TGA curves (Fig. 4.42) for catalytic decomposition of LDPE sample.

4.7.6.6. Model-free analysis for waste PP over Al-MCM-41 [180] and n-HZSM-5

Dependency of E_α on α obtained for nonisothermal decomposition of the PP sample with and without catalyst is presented through Fig.4.124. It is observed from the figure that both for catalytic decomposition, E_α is a slowly increasing function of α in the range (0.1

$\leq \alpha \leq 0.9$) except for the case of n-HZSM-5 and ZSM-12 [60]. E_α for catalytic decomposition is much lower than that for noncatalytic one. It is also observed that the difference in E_α between noncatalytic and catalytic decomposition over Al-MCM-41 [Al-41-P(30)] (Laboratory synthesized) and ZSM-5 used by Filho et al. [60] is also slowly increasing with α. However, exactly similar trends for catalytic and noncatalytic cases for any value of α further justify the fact that similar reaction mechanism is followed for both the cases of decomposition. Thus, only effect of catalyst is observed in the form of reduction of the temperature and the activation energy. Studies of Peterson et al. [38] and Filho et al. [60] on variation of E_α with α for noncatalytic decomposition of pure PP are compared with the present result in the same figure. It is observed that the trends of variation reported by them are similar to that observed by us. The existing differences in the activation energy might be due to different molecular weights of the PP samples used for the different cases. Zeolite molecular sieve (ZSM) catalyzed results of Filho et al. [60] on PP are also compared with the present result in the same figure. It can be observed that our Al-MCM-41 is superior to the ZSM-5 catalyst used by Filho et al. [60] in terms of catalyst loading. Similar type of reduction of activation energy is obtained in the present case with much less catalyst (18.5 wt %) in comparison to ZSM-5 catalyst (50.0 wt %) used by Filho et al. [60]. Though ZSM-12 [60] and n-HZSM-5 are found to be better performing than Al-MCM-41 and ZSM-5 [60] catalysts, the catalyst percentage (18.5 wt %) used in the present case is much lower than that used by Filho et al. [60] and n-HZSM-5 (50 wt %). The strong and increasing values of E_α with α at the later part of ZSM-5 and ZSM-12 catalyzed decomposition [60] (Fig. 4.124) is just opposite to the

trend observed in case of our catalyzed decomposition for both the case of Al-MCM-41 and n-HZSM-5.

PP has greater cross-sectional area due to the presence of the methyl group that increases certain steric hindrance, which can affect the order of activity of the different catalysts [64, 68]. Hence, the catalytic decomposition of PP must start on the external surface of the catalyst and then enter into the pores where they get cracked further leading mainly to the higher olefins and liquid products [60, 64, 66, 68, 70, 179]. This is possibly a common phenomenon both for mesoporous and microporous catalysts. Thus, only effect of catalyst is observed in the form of reduction of the temperature and the activation energy at this stage of decomposition. At the later stage of ZSM-12 catalyzed decomposition, the reaction mechanism possibly takes different path for oligomerisation, cyclization, and hydrogen transfer reactions particularly in the micropores [60, 66]. The diffusional resistances become predominant for catalysts with comparable pore sizes i.e. the micropores. Therefore, it is expected that catalyst with wide pore size would give less diffusional resistance and would be more effective towards decomposition of PP. Further, according to Filho et al. [60] the used ZSM-12 catalyst, formed by a 12 ring member with 5.6A° X 6.0A°, had smaller cystallite size and greater external macropore and mesopore surface in comparison to the ZSM-5 used, formed by a 10 ring member with 5.3A° X 5.6A°. Therefore, the ZSM-12 catalyst has been more efficient in the degradation activity for PP in comparison to ZSM-5. This effect partly overcome by mild acidic Al-MCM-41 due to presence of much higher BET surface area and larger pore, which gives less diffusional resistance. Similarly, n-HZSM-5 catalyst in the present case, due to existence of larger external surface in it, also show the best catalytic activity in comparison to AL-

MCM-41,ZSM-12, and ZSM-5, for decomposition of PP. Again, Durmus et al. [64] reported that higher amount of coke deposition occurs over same pore structure with higher the number of acid sites. Si/Al ratio are quite low for both Al-MCM-41 (Si/Al=35.6) and n-HZSM-5 (Si/Al=60) catalysts than those of ZSM-5 (Si/Al=23.7) and ZSM-12 (Si/Al=29.3) used by Filho et al. [60]. Therefore, the increasing trend of activation energy both ZSM-5 and ZSM-12 catalysts with similar acidic strength [60] at the later stage of conversion (Fig. 4.124) might be due to their microporous activity and coke deposition occurring over pore, which is not the case for the mesoporous Al-MCM-41 and n-HZSM-5 catalysts.

4.7.7. Hybrid genetic algorithm (HGA) and model free coupled direct search methods for pyrolysis kinetics of ZSM-5 catalyzed decomposition of waste LDPE [182]

As discussed in Chapter 1 under section 1.4.3.2.2., model free techniques have a unique feature to reveal the complexity of multiple reactions due to the dependencies of activation energy on the extent of conversion [37-38]. Model free analysis gives the idea about the four different reaction steps involved during ZSM-5 catalyzed decomposition of LDPE as obvious from the four steps marked in the Figs. 4.125 and 4.126. The higher activation energy indicates slowness of the reaction rate, which is also indicated in the form of decreasing peak height in Fig. 4.43 and flatter TGA curves (Figs. 4.42 and 4.45) for catalytic decomposition of LDPE sample reported in our recent publication [177]. Start and end temperatures of catalytic decomposition in the different steps at various heating rates are summarized in Table 4.16. Table 3.1 indicates the start and end temperatures of noncatalytic decomposition, which shows a single step, at various

heating rates. Kinetics triplets (E, K_0 and n) for both catalytic and noncatalytic decomposition of LDPE are obtained by GA coupled with LOA, fminsearch (HGA) and by model free coupled with LOA, fminsearch. The initial guesses for the former method are taken from the GA and those for the latter method are taken from the model free analysis of activation energy variation with conversion.

In case of HGA, the kinetics triplet data and the standard deviations, based on 15 best data points, for the noncatalytic and catalytic decompositions are reported through Tables 4.17 and 4.18 respectively. Results show that except the fourth step in catalytic decomposition, in all other steps the standard deviations are quite low. It is also observed that the activation energy increases with the steps, which is indicative of the different reaction steps as discussed. In case of model free coupled with LOA, the kinetics triplet data and the standard deviations, based on 9 sets of guess values for each step for the noncatalytic and catalytic decompositions are reported through Tables 4.17 and 4.19 respectively. The guess values as discussed are decided from the model free data. In this case also it is observed from the tables that standard deviation in the fourth step in catalytic decomposition is considerably higher than other steps. This may be because of less number of data points towards the end of the decomposition experiments. The standard deviations are calculated using the inbuilt function (STDEV) in MS-Excel.

4.7.7.1 Prediction of experimental TGA data

The kinetics triplets obtained by both the methods employed in the present study are used in simulation to predict the experimental TGA data. Fig. 4.127 shows the prediction for catalytic and noncatalytic decomposition of LDPE at heating rate of 10 K min^{-1} using HGA predicted kinetics triplet. Similarly, Fig. 4.128 shows the prediction for catalytic

and noncatalytic decomposition of LDPE at heating rate of 10 K min^{-1} using the kinetics triplet data from model free coupled with LOA method. It is observed from both the figures that the obtained kinetics triplets predict very well the experimental TGA data. The standard deviations ranges 0.027-0.044 and 0.029-0.069 for HGA method and model free coupled with LOA method respectively in case of noncatalytic decomposition of waste LDPE at different heating rates. Similarly, the standard deviations ranges 0.03-0.007 and 0.011-0.009 for HGA method and model free coupled with LOA method respectively in case catalytic decomposition of waste LDPE at different heating rates.

Thus, it can be inferred that HGA (GA coupled with LOA) is a useful tool for determination of the kinetics triplet for pyrolysis. At the same time, model free method of analysis coupled with LOA predicts the experimental TGA data equally well. Therefore, either of these approaches can be effectively used for pyrolysis kinetics analysis. However, model free method happens to be useful also to understand the different reaction steps taking place during pyrolysis from the variation of activation energy versus conversion plots.

Table 4.1. Characteristics of samples (LDPE, PET, and PP)

Sample type	Melting point, K	Melting point of Standard PE samples [203]	Heat of fusion, Jg^{-1}	Heat of fusion, 100% crys., Jg^{-1}	Degree of crystallinity	Crystallinity of Standard PE samples [203]	Purity (Residual amount after TGA Experiment upto 600°C)
Waste PET	258.43	PET: 267	35.78	115	31.11%	-	10-15%
Virgin PET	246.55	PET: 267	46.85	115	40.74%	-	12.2-12.4
Colorless Waste LDPE	128.7°C	LDPE: 98-120°C	38.37	290	23.95 %	LDPE: 50-70%	Non-isothermal: 1-2%
Color Waste PE (non standard samples)	132.4°C	LDPE: 98-120°C HDPE: 127-135	13.23	290	23.95 %	LDPE: 50-70% HDPE: 80-95%	Non-isothermal: 10-15%
PP	175.69	PP: 165-171	62.38	190	32.83	82%	0.67-1.4%

Table 4.2. Textural properties of ZSM-5, FCC and n-HZSM-5

Sample	BET surface area ($m^2 g^{-1}$)	External surface area (by t-Plot surface Area) ($m^2 g^{-1}$)	Micropore volume (by t-Plot Surface Area)($cm^3 g^{-1}$)	Pore volume (at Ps/Po=0.9814, Adsorption) ($cm^3 g^{-1}$)
ZSM-5	342.36	166.88	0.084	0.207
Fresh FCC	121.23	47.4	0.03362	0.1633
Spent FCC	61.058	22.165	0.01731	0.0797
n-HZSM-5	695.58	364.44	0.13951	0.8877

Table 4.3. Chemical composition and textural properties of Al-MCM-41 (present work and literature data)

Sample	BET surface area ($m^2 g^{-1}$)	Pore volume (at Ps/Po=0.9814, Adsorption) ($cm^3 g^{-1}$)	X=Si/Al ratio	Al source	Si source	Template	Reference
Al-MCM-41(sol-Gel)	1547 1460 1202 1311	0.981 0.8804 0.7005 0.7778	104.1 62.4 35.6 15.6	Aluminium isopropoxide (AIP)	Tetraethoxysilane (TEOS)	N-cetyle-N, N, N trimethylammonium bromide ($C_{19}H_{42}BrN$)	Present work
Al-MCM-41(sol-Gel)	1441	1.023	40	Aluminium isopropoxide (AIP)	Tetraethoxysilane (TEOS)	Hexadecyltrimethyl ammoium chloride ($C_{16}H_{33}(CH_3)_3NCl$)	[102]
Al-MCM-41(sol-Gel)	960	0.51	26	Aluminium isopropoxide (AIP)	Tetraethoxysilane (TEOS)	n-Tetradecyltrimethyl ammonium bromide	[99]
Al-MCM-41(sol-Gel)	1034 1014 978 919	0.77 0.75 0.70 0.59	100.9 69.2 35.6 16.5	Aluminium isopropoxide (AIP)	Tetraethoxysilane (TEOS)	Hexadecyltrimethylammonium bromide	[100]
	988	0.72	26.8	aluminium sulfate (Al2(SO4)3. 18H2O	Tetraethoxysilane (TEOS)	Hexadecyltrimethylammonium bromide	
	1020	0.82	31.9	sodium aluminate	Tetraethoxysilane (TEOS)	Hexadecyltrimethylammonium bromide	
Al-MCM-41(sol-Gel)	1270	0.83(Ps/Po=0.98)	31	Aluminium isopropoxide (AIP)	Tetraethoxysilane (TEOS)	Hexadecyltrimethyl ammoium chloride ($C_{16}H_{33}(CH_3)_3NCl$)	[192]
Al-MTS(2)	1102	0.88(Ps/Po=0.6)	30	Aluminium isopropoxide (AIP)	Tetraethoxysilane (TEOS)	Hexadecyltrimethyl ammoium chloride ($C_{16}H_{33}(CH_3)_3NCl$)	[102]
Al-MCM-41(hydrothermal)	920	0.69	17.6	sodium aluminate	Silica Ludox and tetramethylammonium silicate (TMASi)	hexadecyltrimethylammonium chloride/ tetramethylammonium hydroxide (TMAOH)	[192]
	811	0.73	32	Alumina	Silica Cab-O-Sil and TMASi	Hexadecyltrimethylammonium chloride/ ammonia	
Al-MCM-41(hydrothermal)	1012.3	0.804	31.9	Aluminum sulfate ($Al_2(SO_4)_3$) ,16 H_2O	Tetraethoxysilane (TEOS)	N-cetyle-N, N, N trimethylammonium bromide ($C_{19}H_{42}BrN$)	Presnt work
Al-MCM-41(hydrothermal)	1100	0.84	30	$AlCl_3 \cdot 6H_2O$	Tetraethoxysilane (TEOS)	N-cetyle-N, N, N trimethylammonium bromide ($C_{19}H_{42}BrN$)	[101]

Table 4.4. Effect of catalysts on PE decomposition temperatures

Sample	Catalysts	Wt percentage	T_d(°C)	T_m(°C)	Reference
	-	0	420	-	Araujo et al. [76]
HDPE	SAPO-37	25	375	-	
LLDPE(Escorene)	-	0	-	485.2	
	MCM-41	9.31	-	406.4	
LLDPE(Borecene)	-	0	-	484.3	
	MCM-41	9.18	-	419.6	
LLDPE(Dowlex)	-	0	-	483.7	Marcilla et al. [80]
	MCM-41	9.38	-	423.5	
HDPE	-	0	-	486.0	
	MCM-41	8.98	-	408.1	
LDPE	-	0	-	482.4	
	MCM-41	8.67	-	407.6	
	-	0	425	477	
	n-HZSM-5	-	-	396	
LDPE	HZSM-5	-	-	443	Serrano et al. [66]
	Al-MCM-41	-	-	407	
LDPE	-	0	367	475.2	Present work
	ZSM-5	20	313.7	405.2	

Table.4.5. Kinetics parameters derived from experiments for waste PET [173]

Sample	Method	E, (kJ)	n	$\ln k_0$
Coca Cola bottles	*ASTM E698*	162.15	1	26.37
	n^{th} order	322.3	1.72	54.76
Pepsi bottles	*ASTM E698*	210.64	1	34.81
	n^{th} order	338.98	1.82	57.73

Table 4.6. Kinetic parameters using different non-isothermal model fitting techniques

Sample	Method	E (kJ)	n	$\ln k_0$	Standard deviation							
Waste PET Sample	*ASTM E698*	214.91	1	35.628	0.0241							
	Freeman-Carroll	288.99	1.2085	48.649	0.0140							
	Friedman	278.56	1.216	46.973	0.0199							
	Chang	287.87	1	47.903	0.0425							
	n^{th} order Model	322.3	1.724	54.76	0.0137							
	SDMT (single heating rate)	272.77	1	45.614	0.008794							
		384.63	2	65.472	0.01931							
	SDMT (multiple heating rates)	269.35	1	β(°C min^{-1})				β(°C min^{-1})				
				5	10	15	25	5	10	15	25	
				45.21	45.02	44.85	44.69	0.0094	0.0094	0.0069	0.0056	

Table 4.7. Akaike's criterion analysis for isothermal curve fitting

PET sample			PE sample		
AIC_c for n=0.5	**AIC_c for n=1**	**AIC_c for n=2**	**AIC_c for n=0.5**	**AIC_c for n=1**	**AIC_c for n=2**
-4.32	-165.5345	-97.46	-3.86	-96.31	-75.87
$\Delta AIC = AIC_{Ist\ order} - AIC_{n=0.5}$	$\Delta AIC = AIC_{Ist\ order} - AIC_{2nd\ order}$		$\Delta AIC = AIC_{Ist\ order} - AIC_{n=0.5}$	$\Delta AIC = AIC_{Ist\ order} - AIC_{2nd\ order}$	
-161.215, First order more likely	-68.0745, First order more likely		-92.45, First order more likely	-20.44, First order more likely	

Table 4.8. Present work and literature reported kinetic parameters

Sample	Kinetic parameters			Reference
	E $\left(kJ\ mol^{-1}\right)$	n	ln (k_0 / min)	
Non isothermal Experiment				
Waste PET sample from beverage bottles (M/s coca-cola)	322.3	1.724	54.76	(nth. order method)[173]
	162.15	1	26.37	(ASTM E698 method)[173]
	210.64*	1*	34.81*	
	256.4	1.05	36.88	(for main pyrolysis step) [129]
	271.6	1.09	41.98	(for main pyrolysis step) [130]
	269.35	1	44.94	Present work
Virgin PET sample	242	1	-	[195]
	238.7	1.15	18.00	[46]
	259.34	1	43.077	Present work
Virgin PET I sample	220±10	1	30.297	[196]
Isothermal Experiment				
Waste PET sample from beverage bottles	196.96	1	31.81	Present work
Virgin PET I sample	220±10	1	29.89	[46]
Virgin PET E and PET I sample	200±10	1	25.996	[52]
	220±10	1	29.29	
Virgin PET sample	214±2	1.15	15.2±0.04	[46]

Table 4.9. Average values of kinetic parameters for waste LDPE

Kinetic Models	Order	E(kJ mol^{-1})	Std.Dev in E(kJ mol^{-1})	K_o	Std.Dev in K_o
Nucleation and Growth	n=1/4	148.14	5.16E-06	23.01	3.75E-15
	n=1/3	151.44201	2.77E-06	23.53623	7.40E-15
	n=1/2	166.67	0	26.02636	7.42E-15
	n=2/3	189.06	2.94E-14	29.70	0
Phase Boundary Reaction	$n=1$ (plate)	69.17697	0	8.56174	0
	$n=2$ (Cylinder)	88.0816	0	11.46703	3.61E-15
	$n=3$ (Sphere)	106.76425	1.59E-14	14.38751	0
Diffusion	$n=1$ (plate)	161.35968	0	22.8995	7.35E-15
Power law	n=1/4	7.06097	0	-3.00337	0
	n=1/3	12.37652	0	-1.84356	0
	n=1/2	24.86678	3.71E-15	0.6511	1.16E-16
	n=3/2	115.36091	4.41E-14	16.20774	2.58E-06
Chemical reaction	$n=1$, 1st order	246.2922	2.93609E-06	39.045	4.8349E-07
	$n=2$, 2nd order	337.9255	5.83201E-14	54.5665	7.29001E-15
	$n=n$, nth ** order	242.425	0.1680986	38.385	0.02892788

** n=0.949, Std.Dev= 0.002917

Table 4.10. Average values of kinetic parameters for waste PET

Kinetic Models	Order	E(kJ mol^{-1})	Std.Dev in E(kJ mol^{-1})	K_o	Std.Dev in K_o
Nucleation and Growth	n=1/4	134.8427	0	21.7678	7.29E-15
	n=1/3	137.9391	2.92E-14	22.2816	1.0935E-14
	n=1/2	152.231	5.83E-14	24.728	3.65E-15
	n=2/3	173.3451	3.08E-05	28.3564	0
Phase Boundary Reaction	$n=1$ (plate)	51.49	9.96E-07	5.79	1.74E-07
	$n=2$ (Cylinder)	71.05	1.06E-06	9.01	1.82E-07
	$n=3$ (Sphere)	87.50	1.32E-06	11.70	2.20E-07
Diffusion	$n=1$ (plate)	119.777	2.95E-14	16.7591	3.69E-15
Power law	n=1/4	4.7957	1.82E-15	-3.4669	4.56E-16
	n=1/3	9	1.78E-18	-0.0025	4.46E-19
	n=1/2	85.53	1.32E-06	11.70	2.26E-07
	n=3/2	18.6717	2.24E-05	-0.3978	1.139E-16
Chemical reaction	$n=1$, 1st order	227.0584	5.83201E-14	37.5614	1.458E-14
	$n=2$, 2nd order	309.8936	5.83201E-14	52.3226	1.458E-14
	$n=n$, nth ** order	225	0.029018	37.2	0.004936

** n= 0.969, Std.Dev= 0.004693

Table 4.11. Average values of kinetic parameters for waste PP

Kinetic Models	Order	E(kJ mol^{-1})	Std.Dev in E(kJ mol^{-1})	K_o	Std.Dev in K_o
Nucleation and Growth	n=1/4	122.031	0	19.4421	3.66E-14
	n=1/3	123.0691	0	19.6025	3.65E-15
	n=1/2	131.9114	0	21.1064	3.65E-15
	n=2/3	146.6868	2.916E-14	23.6383	7.29E-15
Phase Boundary Reaction	$n=1$ (plate)	61.48	7.29E-15	7.6349	9.11E-16
	$n=2$ (Cylinder)	85.3717	2.92E-14	11.6102	1.82E-15
	$n=3$ (Sphere)	104.5035	0	14.7527	0
Diffusion	$n=1$ (plate)	146.1213	0	21.3854	0
Power law	n=1/4	132.9115	260.7238	17.35658	42.14982
	n=1/3	127.2946	240.1613	16.8	38.82339
	n=1/2	20.8227	0	0.0468	2.14E-17
	n=3/2	104.3377	1.46E-14	15.0636	3.65E-15
Chemical reaction	$n=1$, 1st order	186.6747	5.831E-14	30.48	3.65E-15
	$n=2$, 2nd order	247.31	2.92E-14	41.4	1.46E-14
	$n=n$, nth ** order	181.4567	0.061891	29.53	0.012581

** n= 0.9039, Std.Dev= 0.004667

Table 4.12. Present work and literature reported kinetics parameters (N_2 atmosphere)

Polymer	E(kJmol^{-1})	ln(k_o)	n	Method	Reference
Waste PET	322.3	54.76	1.724	n^{th} –order model	[173]
	162.15	26.37	1	ASTM E698	[173]
	256.4	36.88	1.05	n^{th} –order model	[129]
	271.6	41.98	1.09	n^{th} –order model	[130]
	269.35	44.94	1	SDMT-multiple heating rate	[175]
	242	-	1	First-order model	[195]
	180-210	-	-	Isoconversion model-free method	[174]
	173.3451	28.3564	2/3	Nucleation and Growth	Present work
Virgin PET	238.7	18.00	1.15	n^{th} –order model	[46]
	259.34	43.077	1	SDMT-multiple heating rate	[175]
	220±10	30.297	1	First-order model	[196]
	244±8	35.7±1.3	1	First-order model	[197]
PP	237±7	32.1±1.3	1	Random-chain dissociation model	[197]
	216	30.909	1	First-order model	[198]
	214.5	28.198	1	Random-chain dissociation model	[198]
	(138.1±3.8)[a]	(26.7099) [a]	1	Method of Ozawa, Flynn and Wall	[199]
	43.9	24.8664	0.90	n^{th} –order model	[200]
	150-250	-	-	Isoconversion Method	[38]
	146.69	23.64	2/3	Nucleation and Growth	Present work
LDPE	221	31.0944	1	First-order model	
	234.5	30.518	1	Random-chain dissociation model	
	241±10	34.6±1.7	1	First-order model	[197]
	244±12	32.2±2.1	1	Random-chain dissociation model	[197]
	(214.2,238.9, 200)[a]	(24.58,32.71, 25.476)[b]	-	Three-Reaction Model (Flexible Simplex Optimization Method)	[198] [201]
	272	-	0.14	Freeman and Carroll's Method	
	49.3	27.81334	0.63	n^{th} –order model	
	150-240	-	-	Isoconversion Method	[202]
	(200)[c]	(26.039) [c]	-	Integral method	[200]
	192- 263	-	-	Isoconversional method by Flynn	[38]
	201.5	28.1257±0.0185	0.55	Nucleation and Growth	[157] [134]
	189.05815	29.69583	2/3		Present work

a) At 10% weight-loss and values of E increase with the extent of degradation.
b) Three step mechanism is assumed
c) All most constant for alpha >0.2(130-200)

Table 4.13. Optimum kinetics triplet for PP decomposition with and without of Al-MCM-41 (sol-gel) using HGA

Average values of Kinetics parameters	PP+ Al-MCM-41 (sol-gel)	Std. Dev	PP+n-HZSM-5	Model	Std. Dev
E (kJ mol^{-1})	128.63	5.88E-14	97.848		2.95E-14
n	0.866	0	0.99962	n^{th} order	1.15E-16
K_0	23.737	7.35E-15	19.595	chemical reaction model	0
E (kJ mol^{-1})	134.37	0	97.858		2.92E-14
n	1	-	1	First order	-
K_0	30.698	7.3E-15	19.597	chemical reaction model	3.64E-15
E (kJ mol^{-1})	99.42	2.92E-14	76.573		2.92E-14
n	2/3	-	2/3	Nucleation and	-
K_0	18.08	0	14.998	Growth reaction model	3.64E-15

Table 4.14. The equations for calculation AIC_c results [31-32]

Kinetic Models	Kinetic Functions, Integral of kinetics function and calculation of α where, $x = (k_{0i}/\beta_l)I(E_i, T_{i,l})$	Order	Model no	AIC_c Score	
				PP+Al-MCM-41 samples	PP+n-HZSM-5 samples
Nucleation and Growth	$f(\alpha) = (\frac{1}{n})(1-\alpha)(-\ln(1-\alpha))^{1-n}$ $g(\alpha) = [-\ln(1-\alpha)]^n$ $\alpha = 1 - \exp(-x^{1/n})$	$n = 1/4$ $n = 1/3$ $n = 1/2$ $n = 2/3$	1 2 3 4	-573.672 2232.016 -2081.74 -2697.39	-3634.44 -4614.66 -6732.7 -8446.13
Phase Boundary Reaction	$f(\alpha) = n(1-\alpha)^{(n-1)/n}$ $g(\alpha) = [1-(1-\alpha)^{1/n}]$ $\alpha = 1-(1-x)^n$	$n = 1$ (plate) $n = 2$ (Cylinder) $n = 3$ (Sphere)	5 6 7	723.9327 -327.42 -1121.42	4433.269 3288.472 2562.463
Diffusion	$f(\alpha) = 1/\alpha$ $g(\alpha) = \alpha^2/2$ $\alpha = (2x)^{1/2}$	$n = 1$ (plate)	8	136.29	2798.571
Power law	$f(\alpha) = \left(\frac{1}{n}\right)\alpha^{1-n}$ $g(\alpha) = \alpha^n (0 < n < 2)$ $\alpha = x^{1/n}$	$n = 1/4$ $n = 1/3$ $n = 1/2$ $n = 3/2$	9 10 11 12	2367.908 2232.02 1874.391 234.7345	6200.819 6053.067 5703.012 3476.466
Chemical reaction	$f(\alpha) = (1-\alpha)$ $g(\alpha) = -\ln(1-\alpha)$ $\alpha = 1-\exp(-x)$	$n = 1$, 1st order	13	-2056.68	-7453.49
	$f(\alpha) = (1-\alpha)^n$ $g(\alpha) = [1/(1-\alpha)^{n-1} - 1]/(n-1)$ $\alpha = 1-[1+(n-1)x]^{1/(1-n)}$	$n = 2$, 2nd order $n = n$, nth order	14 15	-1181.07 -2054	-5759.89 -7454.1

Table 4.15. Activation energy and the effect of different catalysts on PP decomposition temperatures

Sample	Catalysts	E (kJ mol^{-1})	ΔT_m(K)	Reference
PP samples	MCM-41(16.3%)	209.07 (1st Step) 161.10(2nd Step) 41.68(3rd Step)	113.15	Model-fitting Method [81]
	E-Cat (86.1%)	204.4 (1st Step) 160.5(2nd Step) 53.5(3rd Step)	122.8	Model-fitting Method [58]
	ZSM-5 (87.3%)	246.3 (1st Step) 130.1(2nd Step) 121.9(3rd Step)	89.8	
	SM(93.5%)	94	19	
	ST(93.6%)	129	25	Model-fitting
	MO(89.8%)	121	139	Method [160]
	SALA(90%)	88	184	
	SAHA(92.5%)	82	184	
	ZSM-12(30%)	75-105	-	Model-free
	ZSM-5(50%)	112-130	-	method [60]
	Al-MCM-41 (sol-gel) (18.5%)	128.63 (n^{th} order) 128.89 (first order) 99.42 (Nucleation and Growth)	102.8	Present work Model-fitting method
	n-HZSM-5 (50%)	97.85 (n^{th} order) 97.86 (first order) 76.573 (Nucleation and Growth)	161.4	Present work Model-fitting method

Table 4.16. Start and end temperatures of different steps of ZSM-5 catalyzed waste LDPE sample

Step	Heating Rates									
	β=5K min^{-1}		β=10K min^{-1}		β=15K min^{-1}		β=20K min^{-1}		β=25K min^{-1}	
	T_{w0}	$T_{w\infty}$	T_{w0}	$T_{w\infty}$	T_{w0}	$T_{w\infty}$	T_{w0}	$T_{w\infty}$	T_{w0}	$T_{w\infty}$
First	470.4	651.3	462.7	657.8	462.2	665.7	471.1	671.4	462.2	674
Second	651.3	686.1	657.8	699	665.7	706.3	671.4	707.4	674	714.9
Third	686.1	714.9	699	728.4	706.3	729.6	707.4	737.8	714.9	738.6
Fourth	714.9	777.9	728.4	769	729.6	769.9	737.8	779.7	738.6	779.5

Table 4.17. Optimum kinetics triplet for LDPE decomposition in absence of ZSM-5

Optimization methods	**HGA algorithm method**			**Model free coupled direct search method**		
Kinetics parameters	E (kJ mol^{-1})	n	K_0	E (kJ mol^{-1})	n	K_0
Average values	242.43	0.949	38.39	235.34	0.845	37.17
Std. Dev.	0.168	0.003	0.029	9.761	0.145	1.673

Table 4.18. Optimum kinetics triplet for LDPE decomposition in presence of ZSM-5 using HGA

Average values of Kinetics parameters	First step	Std. Dev	Second step	Std. Dev	Third step	Std. Dev	fourth step	Std. Dev
E_i (kJ mol^{-1})	173.55	4.88E-06	253.71	7.70E-06	312.46	9.26E-06	492.84	0.22
n_i	0.541	2.3E-16	0.5306	2.3E-16	0.09	2.87E-17	0.977	1.23E-03
K_{0i}	31.33	2.58E-06	43.90	1.47E-14	51.66	5.07E-06	80.55	0.036

Table 4.19. Optimum kinetics triplet for LDPE decomposition in presence of ZSM-5 using Model-free method coupled with direct search method

Average values of Kinetics parameters	First step	Std. Dev	Second step	Std. Dev	Third step	Std. Dev	fourth step	Std. Dev
E_i (kJ mol^{-1})	173.55	3.01E-14	253.71	3.01E-14	312.46	0.000	468.20	24.38
n_i	0.541	0.000	0.5306	0.000	0.09	1.5E-17	0.818	0.1645
K_{0i}	31.33	3.77E-15	43.90	0.000	51.66	0.000	76.42	4.09

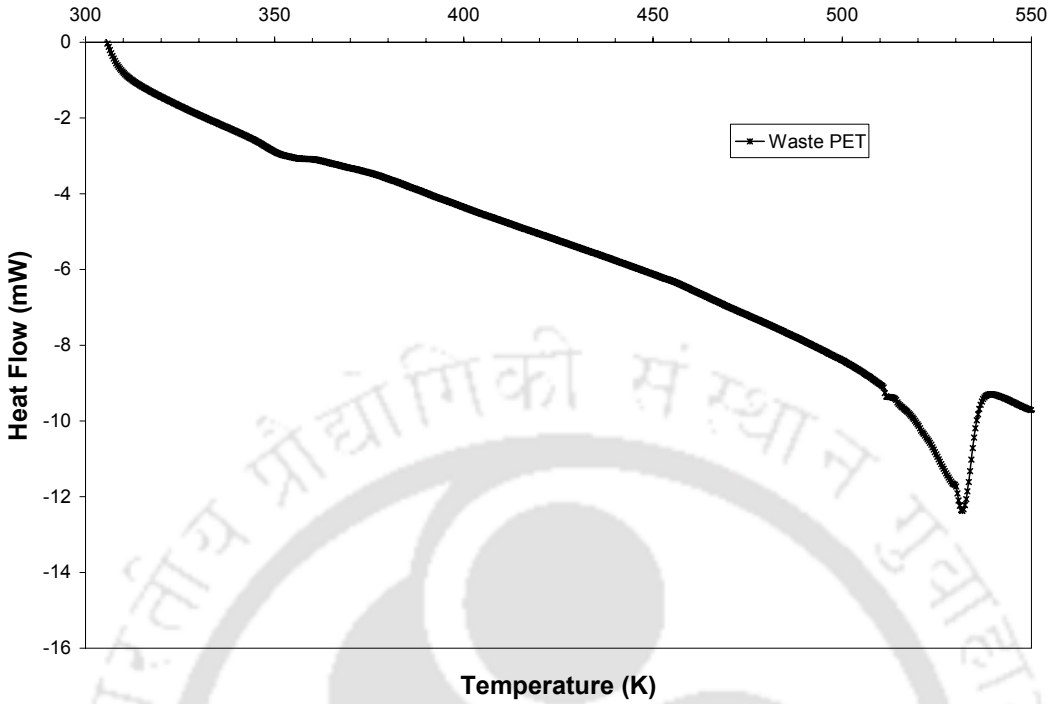

Figure 4.1. DSC analysis of waste PET sample

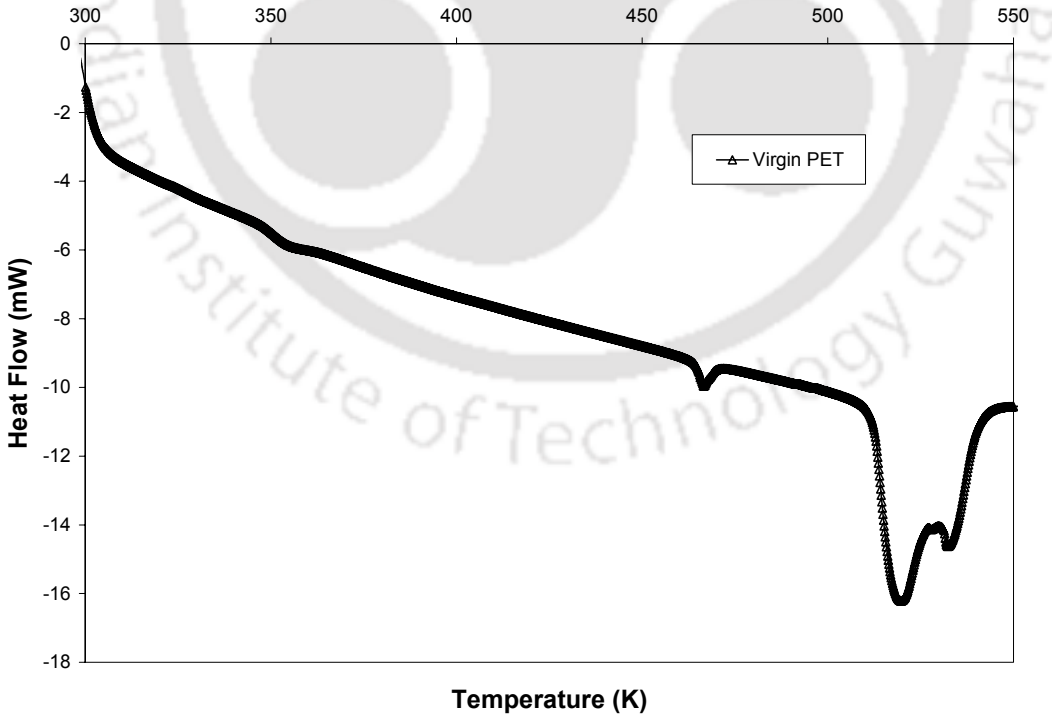

Figure 4.2. DSC analysis of virgin PET sample

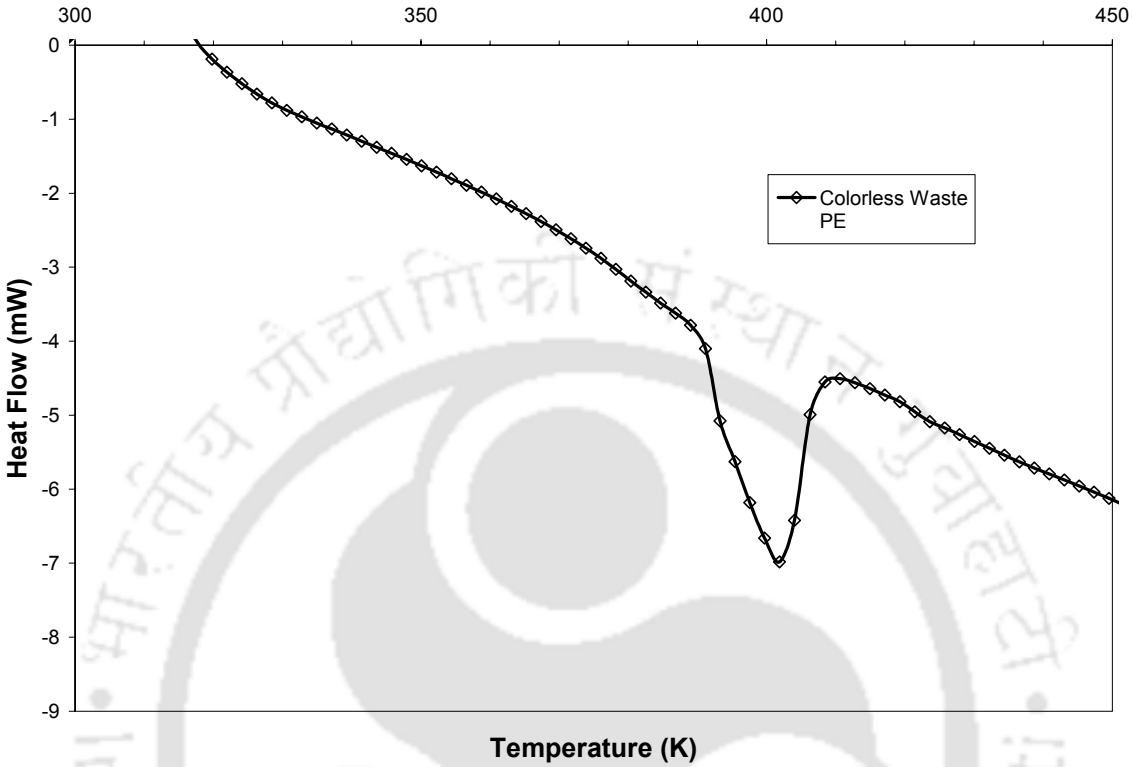

Figure 4.3. DSC analysis of colorless waste LDPE sample

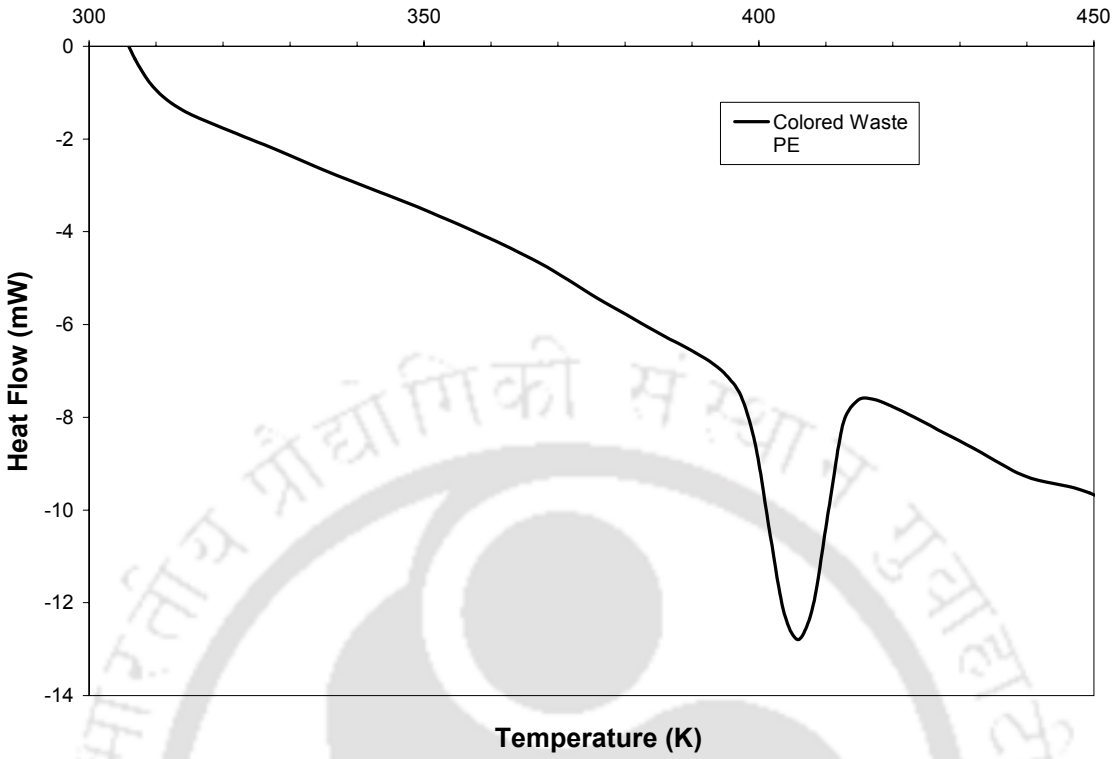

Figure 4.4. DSC analysis of color waste PE sample

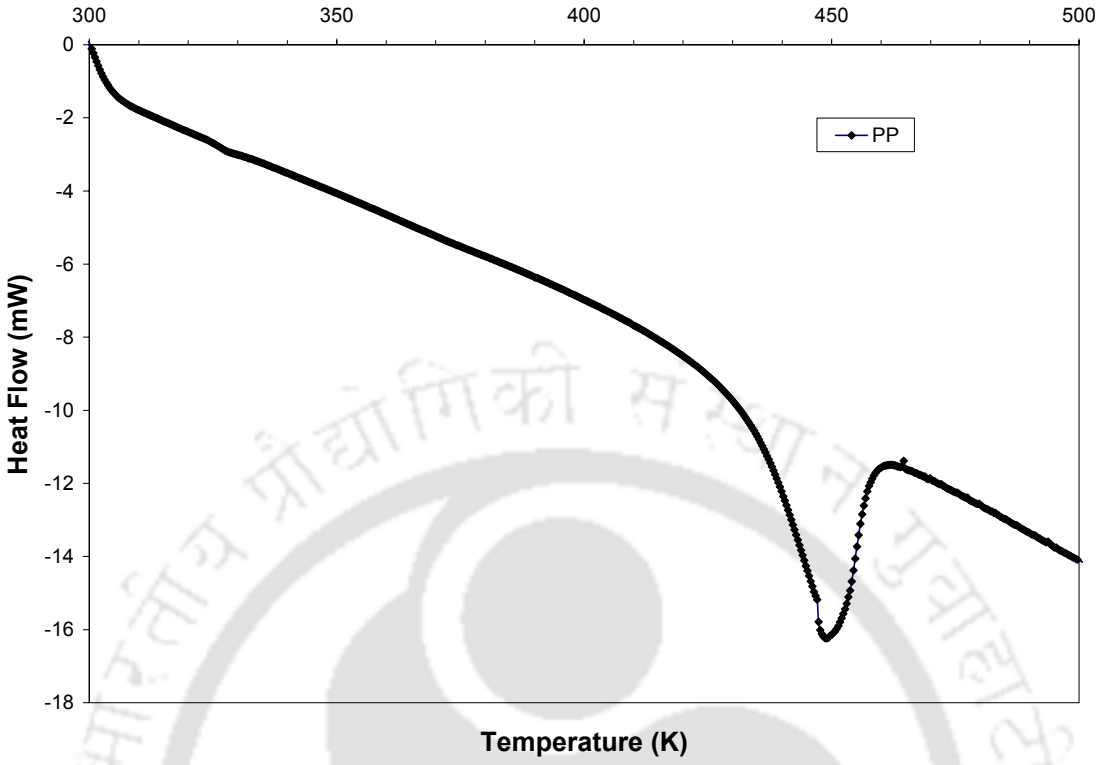

Figure 4.5. DSC analysis of PP sample

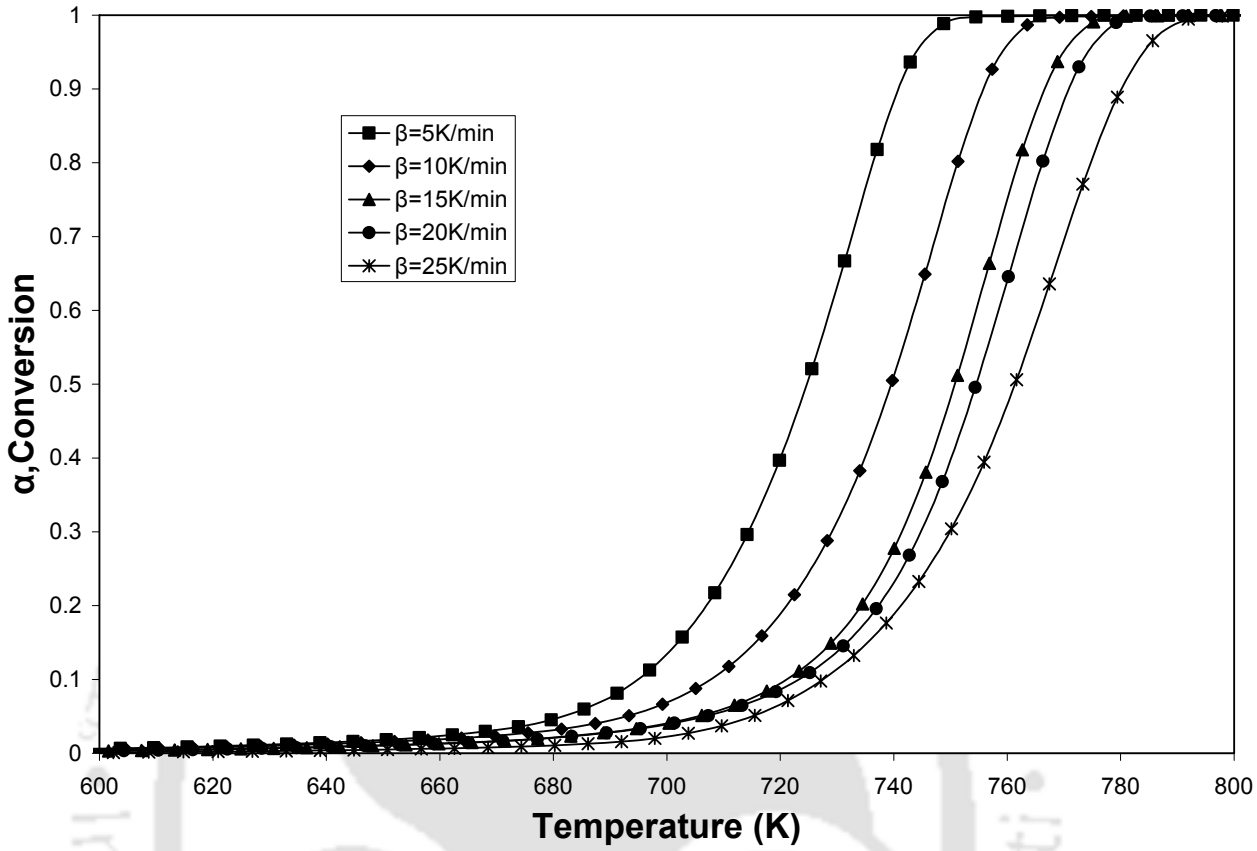

Figure 4.6. Variation of conversion (α) with temperature during non-isothermal pyrolysis of waste LDPE sample at multiple heating rates

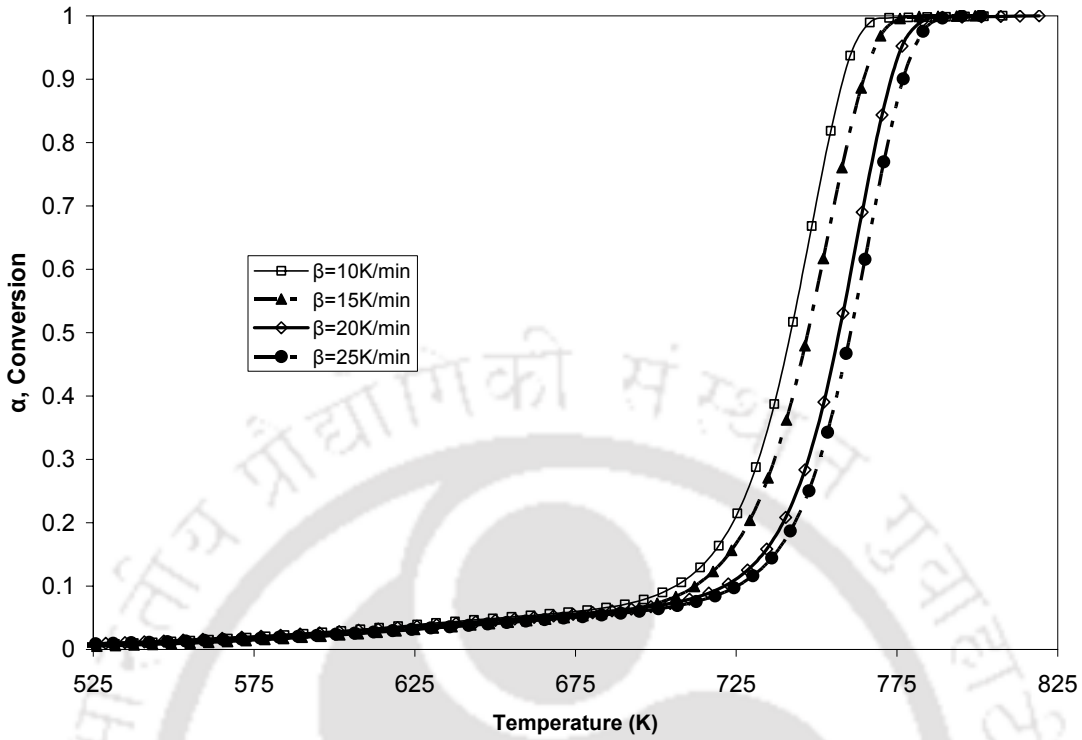

Figure 4.7. Variation of conversion (α) with temperature during thermal pyrolysis of waste PE samples

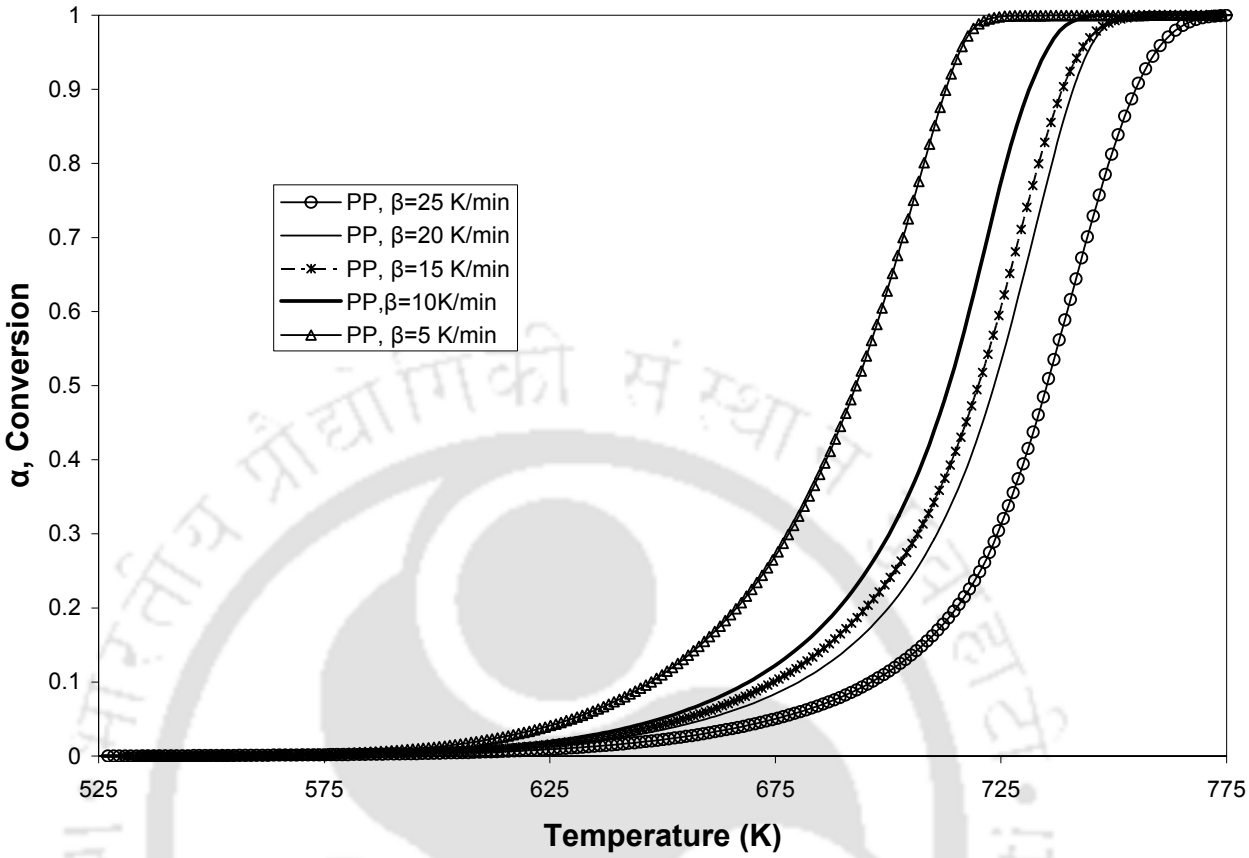

Figure 4.8. Variation of conversion (α) with temperature during non-isothermal pyrolysis of PP sample at multiple heating rates

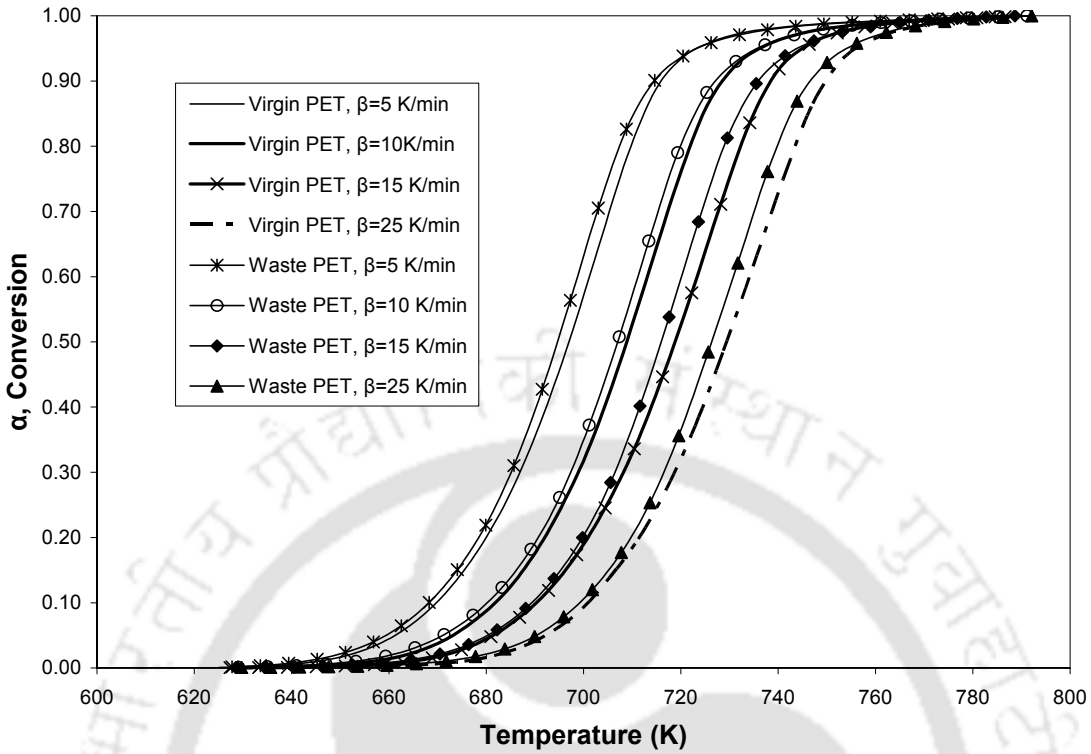

Figure 4.9. Variation of conversion (α) with temperature during nonisothermal pyrolysis of virgin and waste PET sample

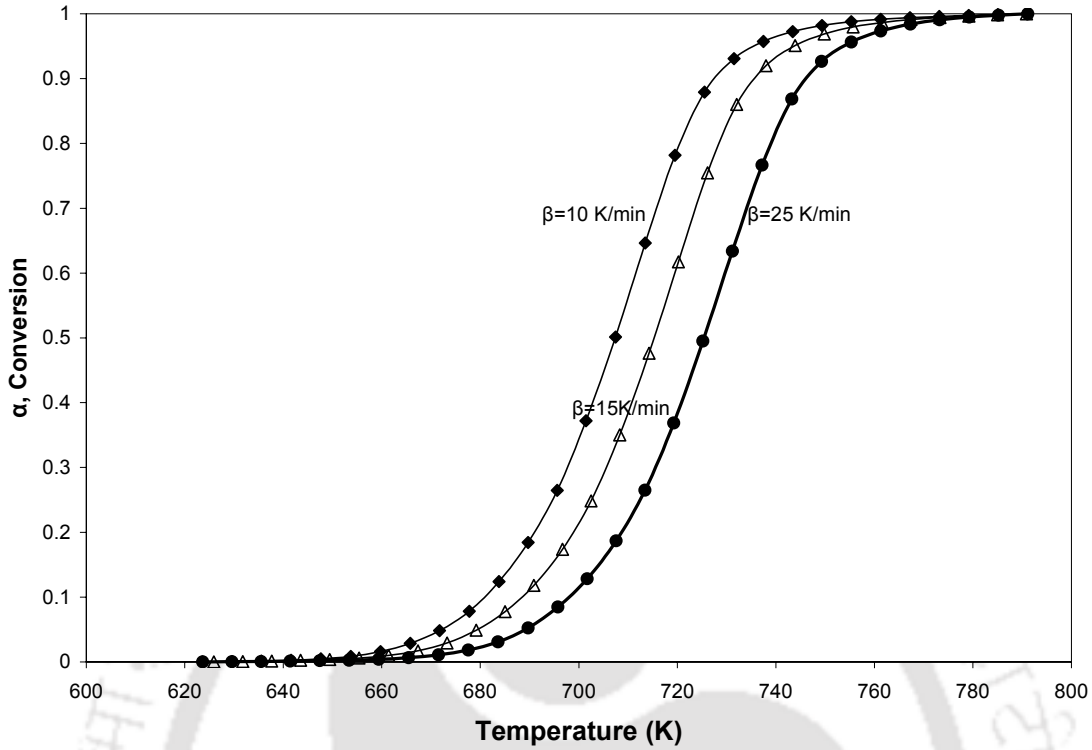

Figure 4.10. Variation of conversion (α) with temperature during pyrolysis of Pepsi bottles

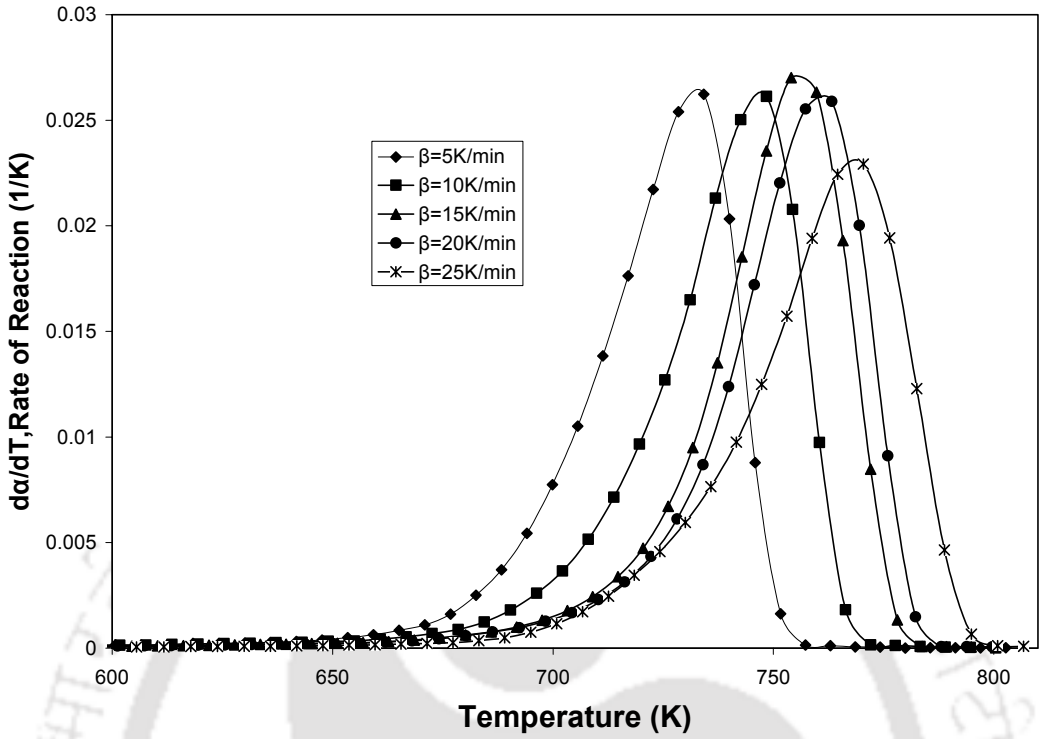

Figure 4.11. Variation of rate of decomposition (dα/dT) with average temperature during non-isothermal pyrolysis of waste LDPE sample at multiple heating rates

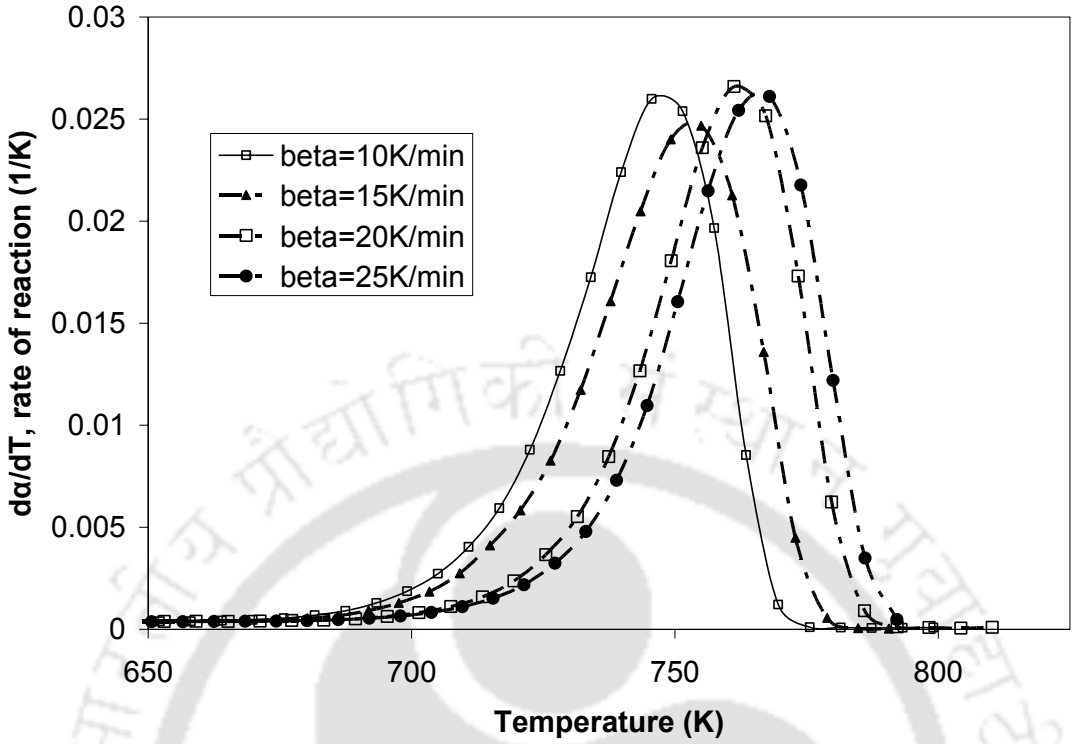

Figure 4.12. Variation of rate of decomposition (dα/dT) with average temperature during non-isothermal pyrolysis of waste PE sample at multiple heating rates

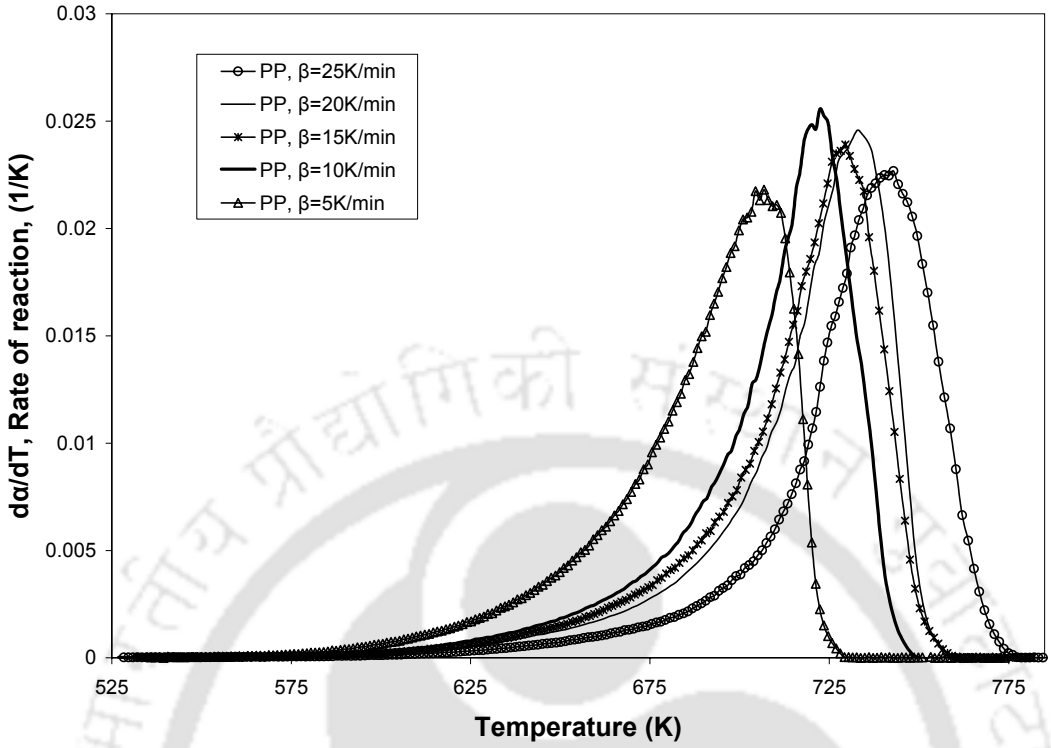

Figure 4.13. Variation of rate of decomposition (dα/dT) with average temperature during non-isothermal pyrolysis of PP sample at multiple heating rates

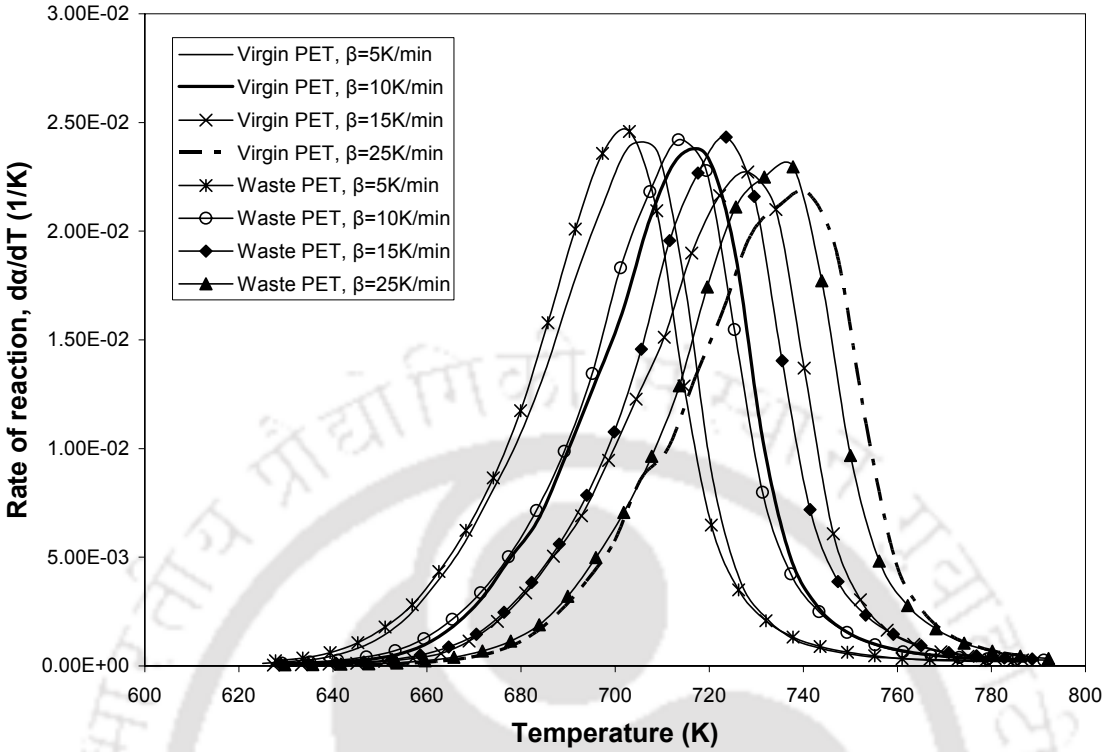

Figure 4.14. Variation of rate of reaction (dα/dT) with temperature during nonisothermal pyrolysis of virgin and waste PET sample

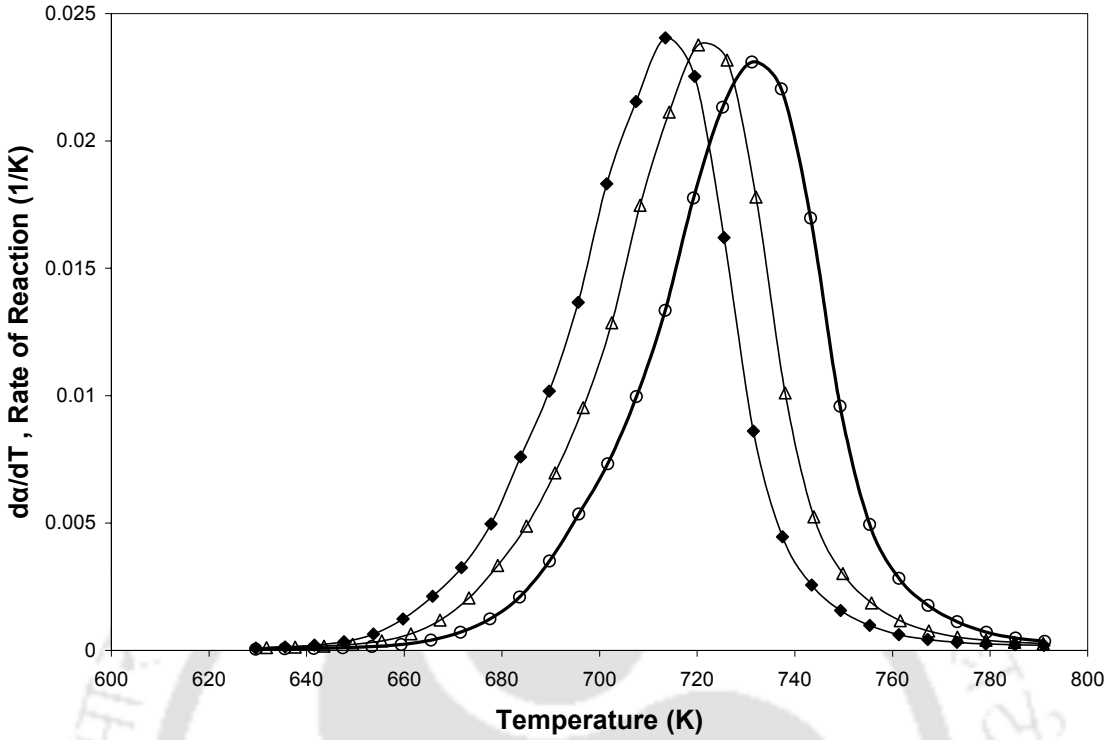

Figure 4.15. Variation of rate of reaction (dα/dT) with temperature during pyrolysis of Pepsi bottles

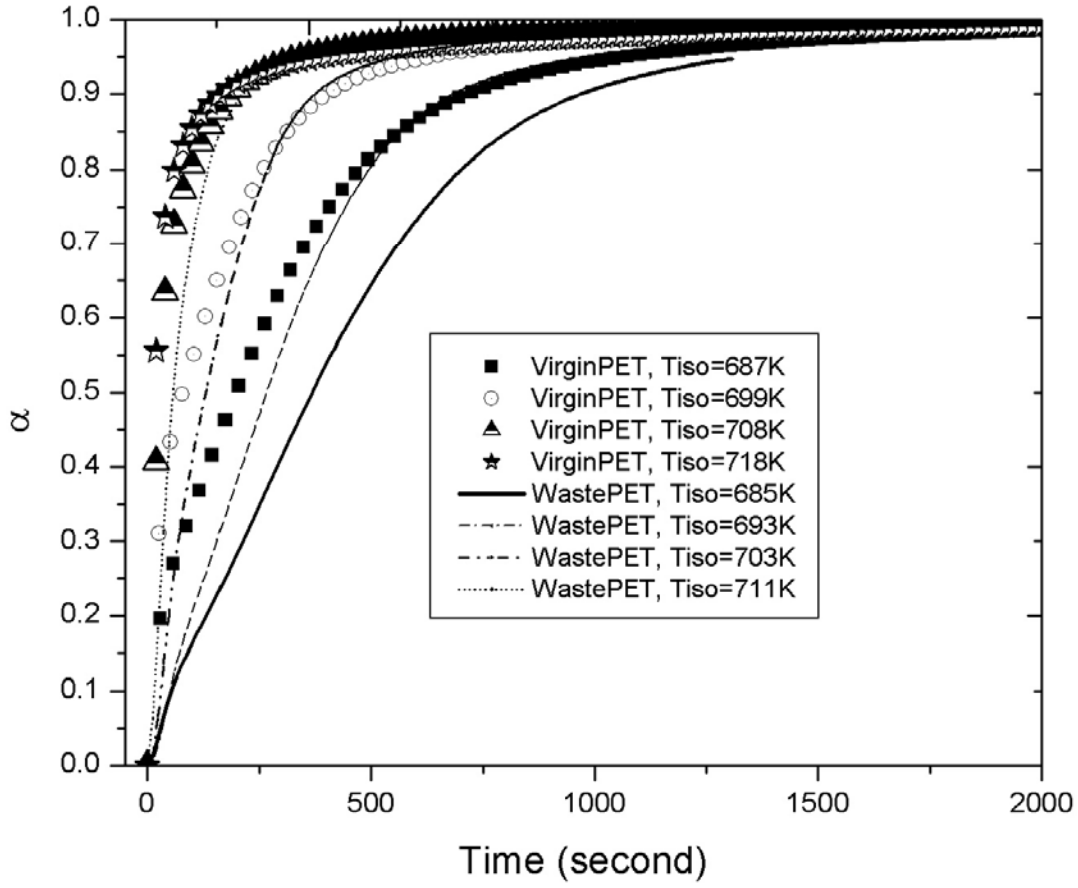

Figure 4.16. Variation of conversion (α) with time during isothermal pyrolysis of waste and virgin PET sample

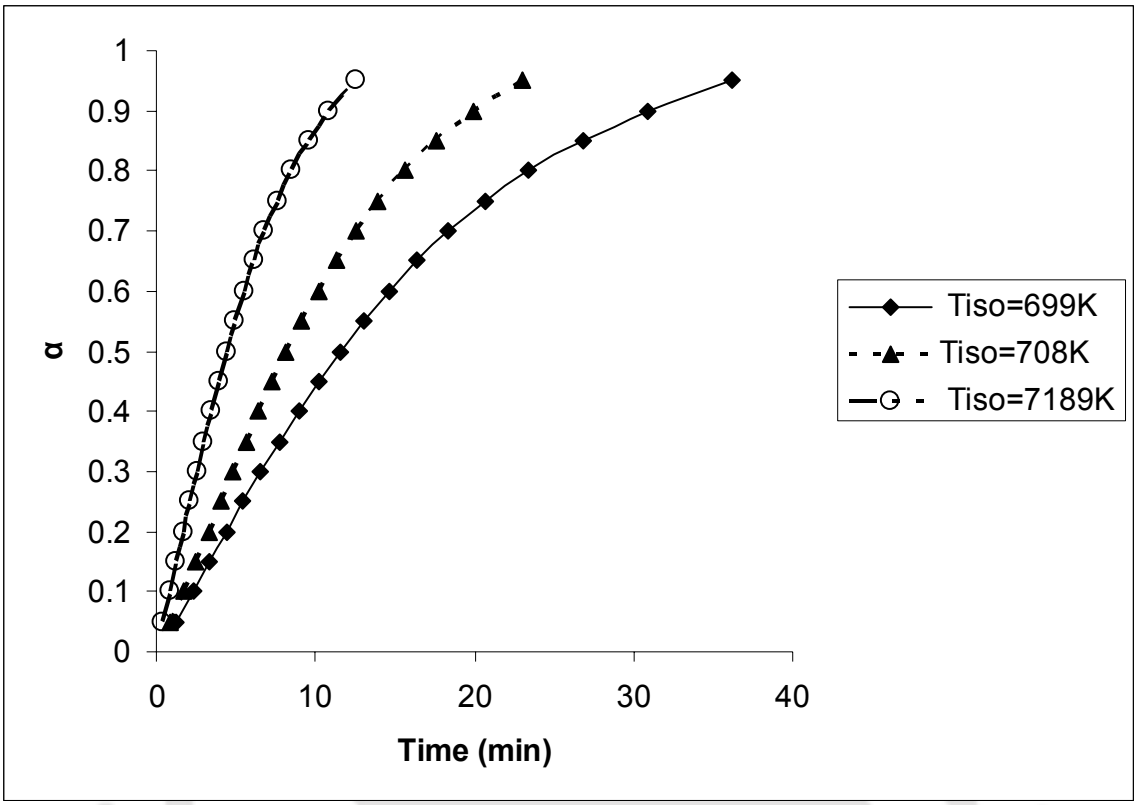

Figure 4.17. Variation of conversion (α) with time during isothermal pyrolysis of waste PE samples

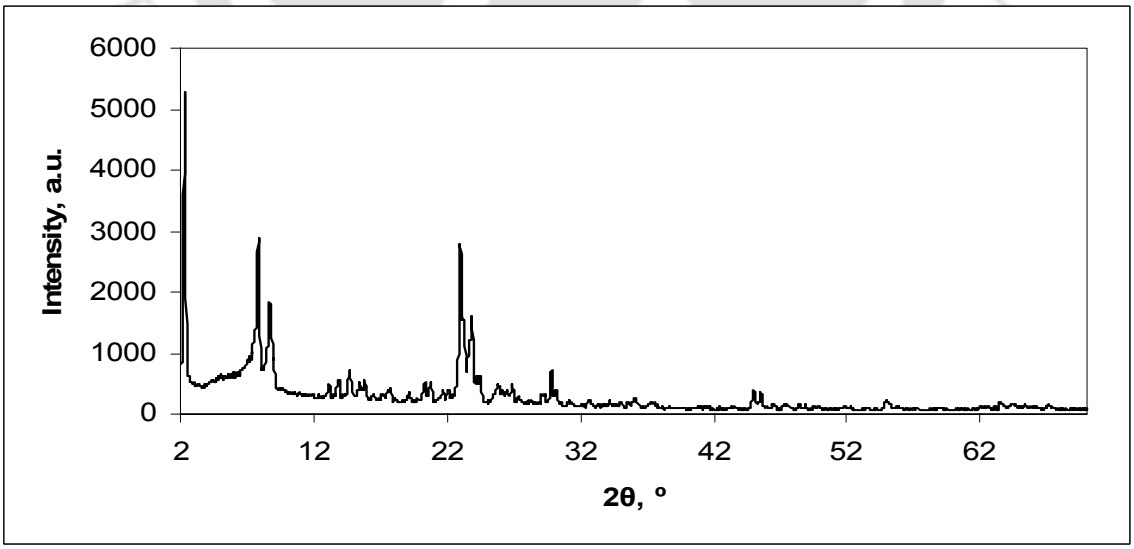

Figure 4.18. XRD pattern of ZSM-5 zeolite catalyst

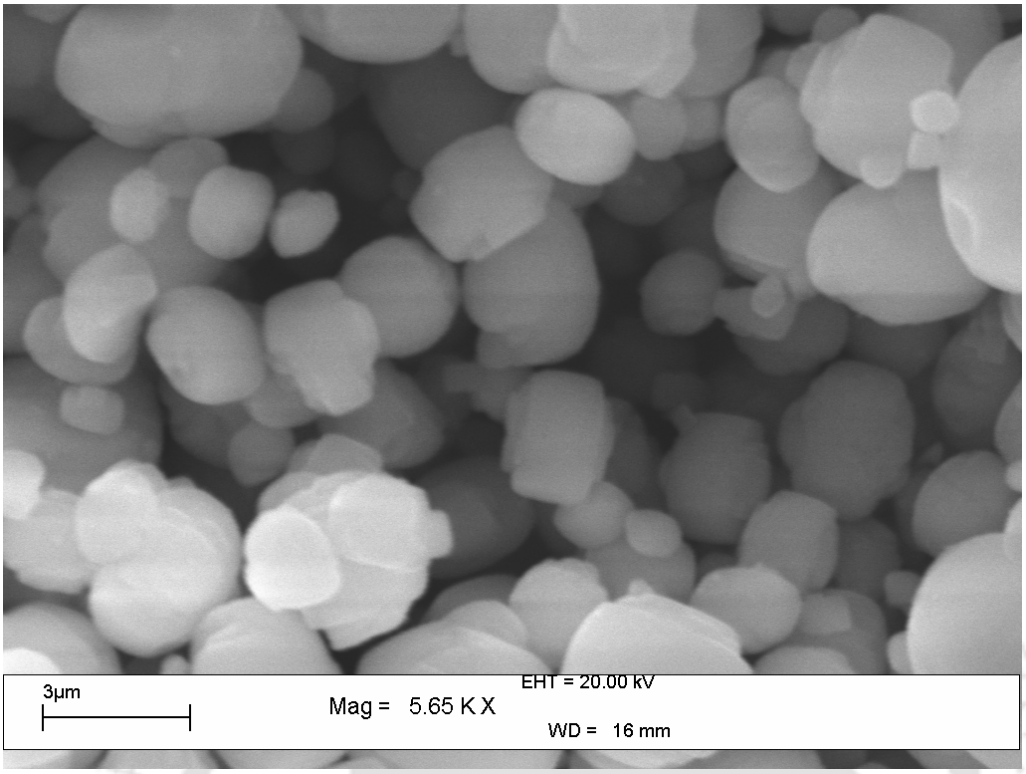

Figure 4.19. SEM micrograph of ZSM-5 zeolite catalyst

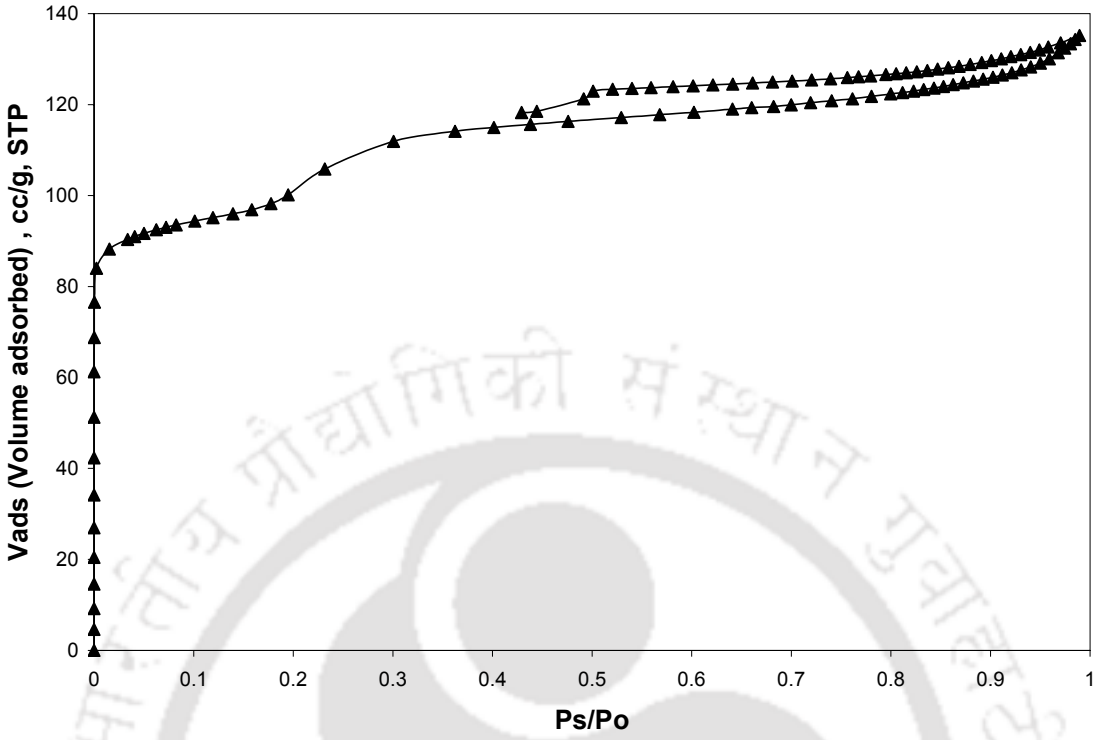

Figure 4.20. Nitrogen adsorption isotherm at 77 K of ZSM-5 catalysts

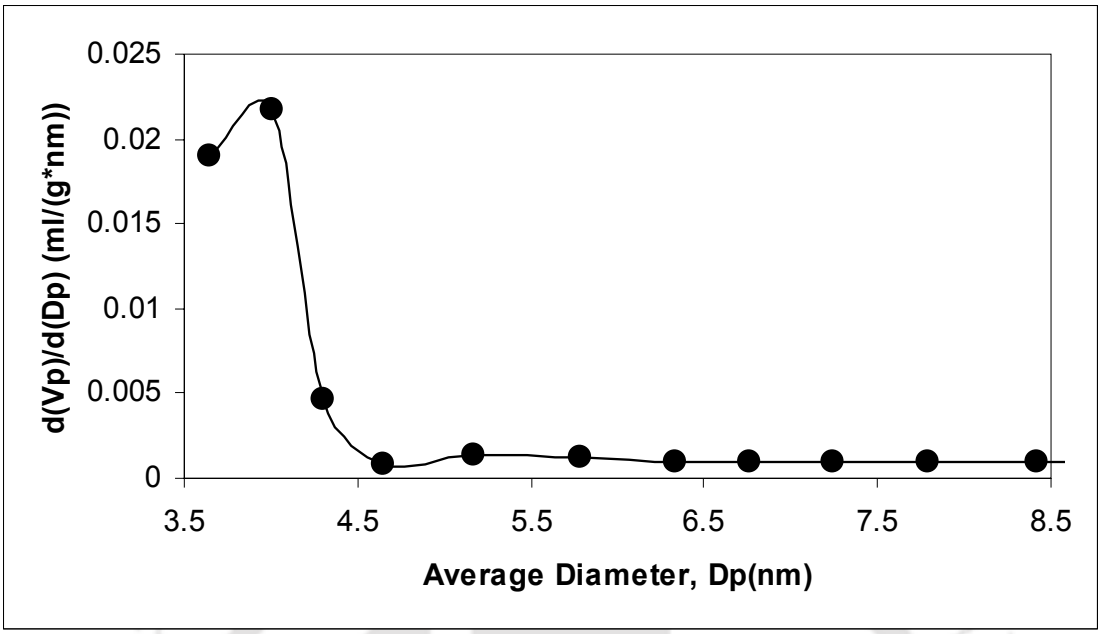

Figure 4.21. BJH (Desorption) pore size distribution of ZSM-5 catalyst

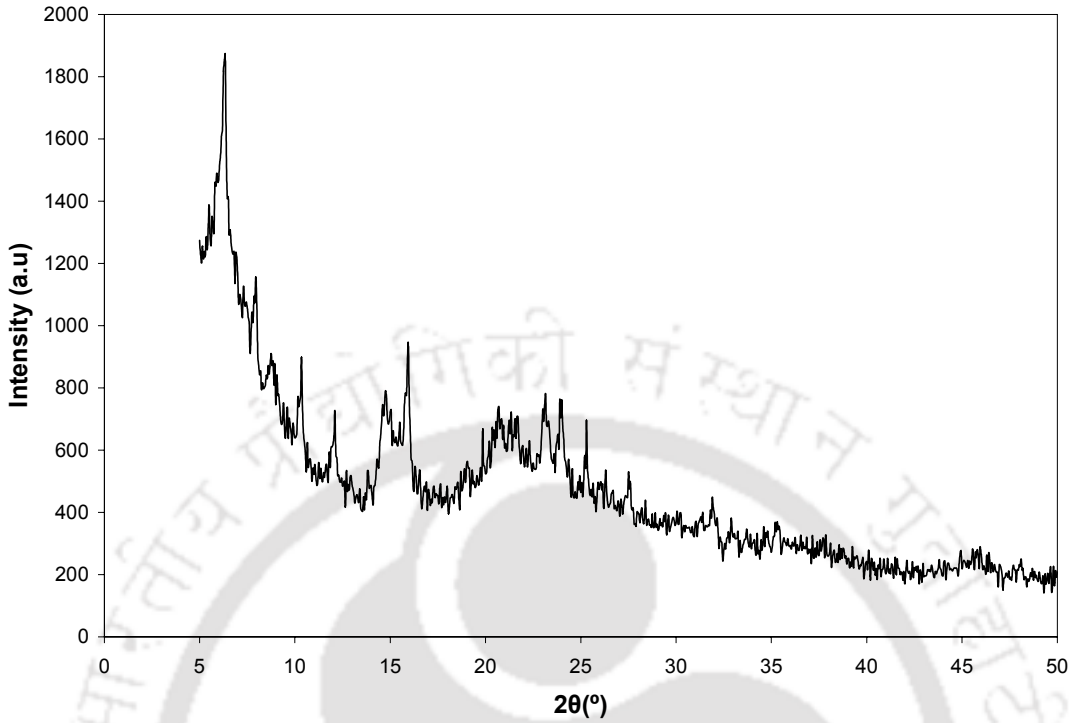

Figure 4.22. XRD pattern of fresh FCC catalysts

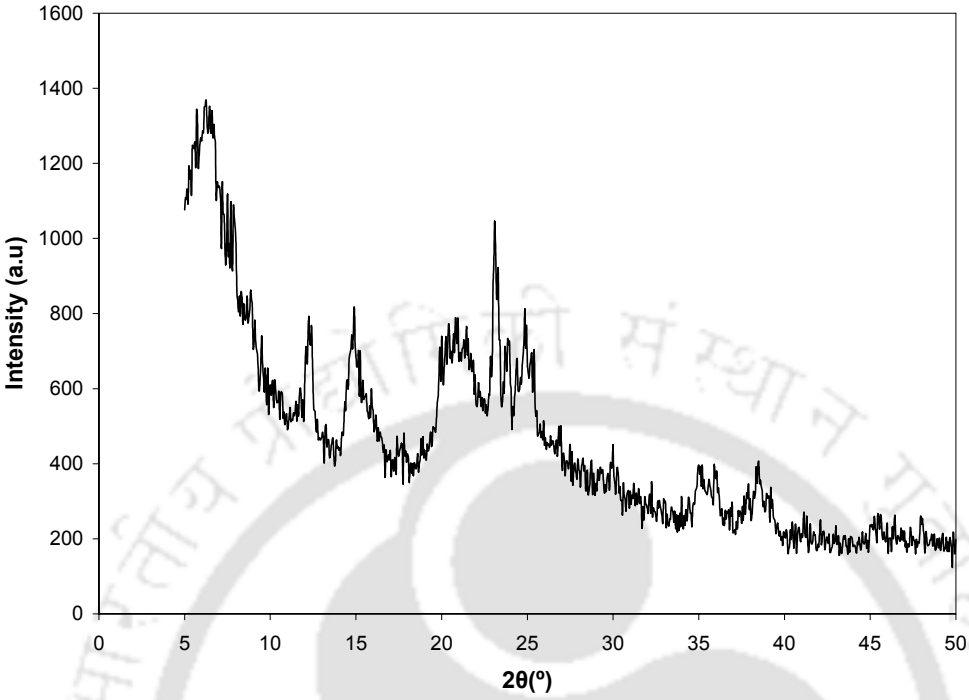

Figure 4.23. XRD pattern of spent FCC catalysts

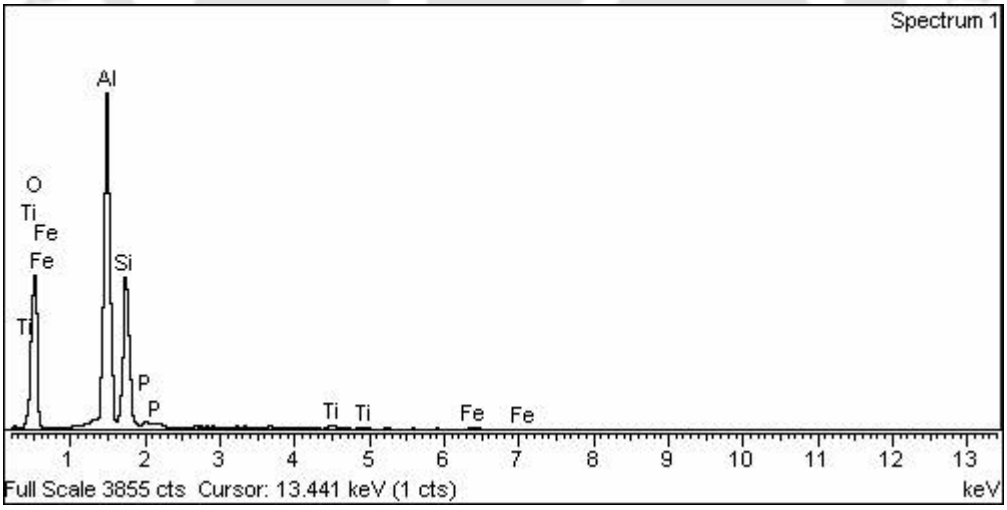

Figure 4.24. EDX of fresh FCC catalysts

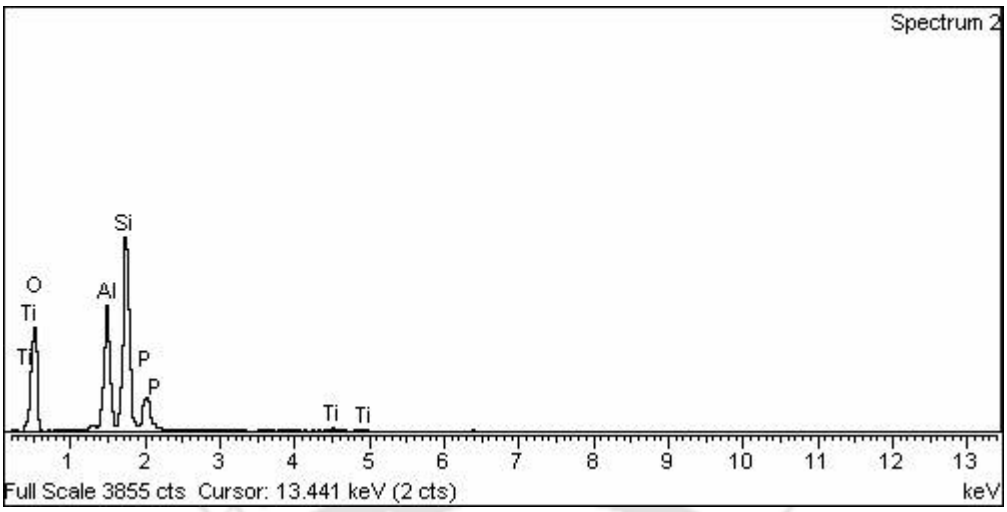

Figure 4.25. EDX of spent FCC catalysts

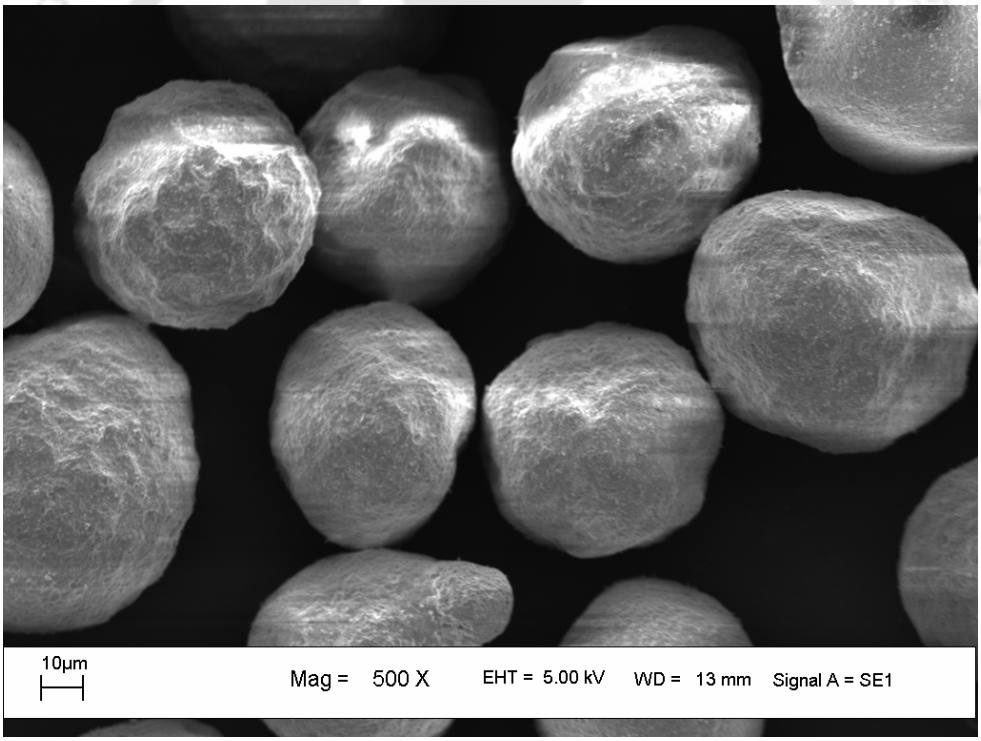

Figure 4.26. SEM of fresh FCC

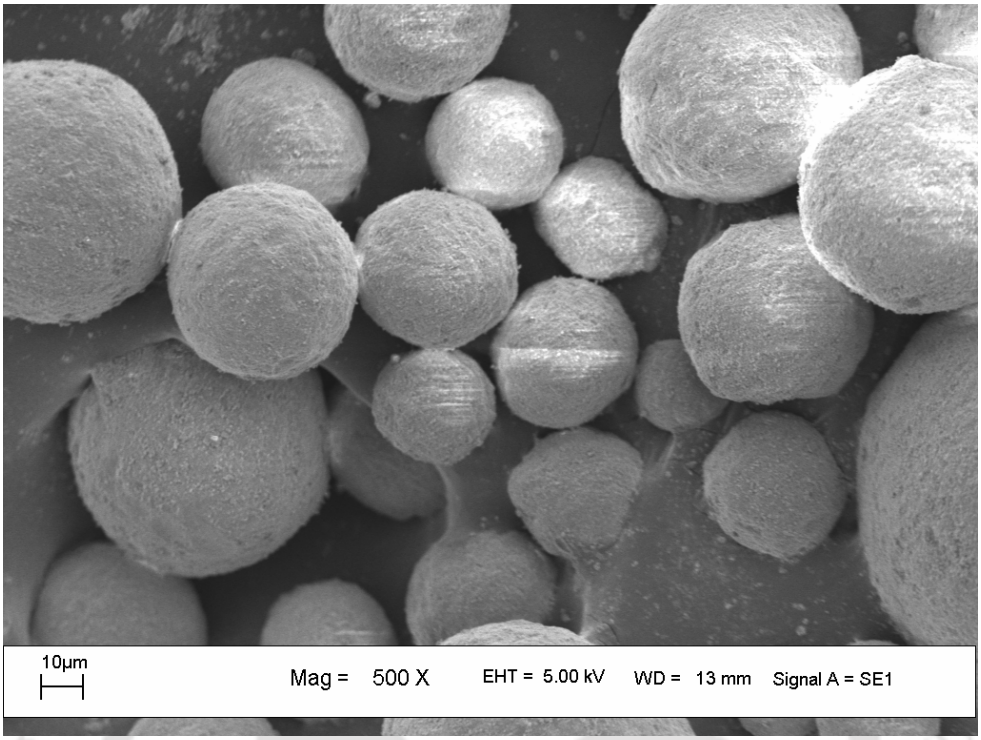

Figure 4.27. SEM of spent FCC

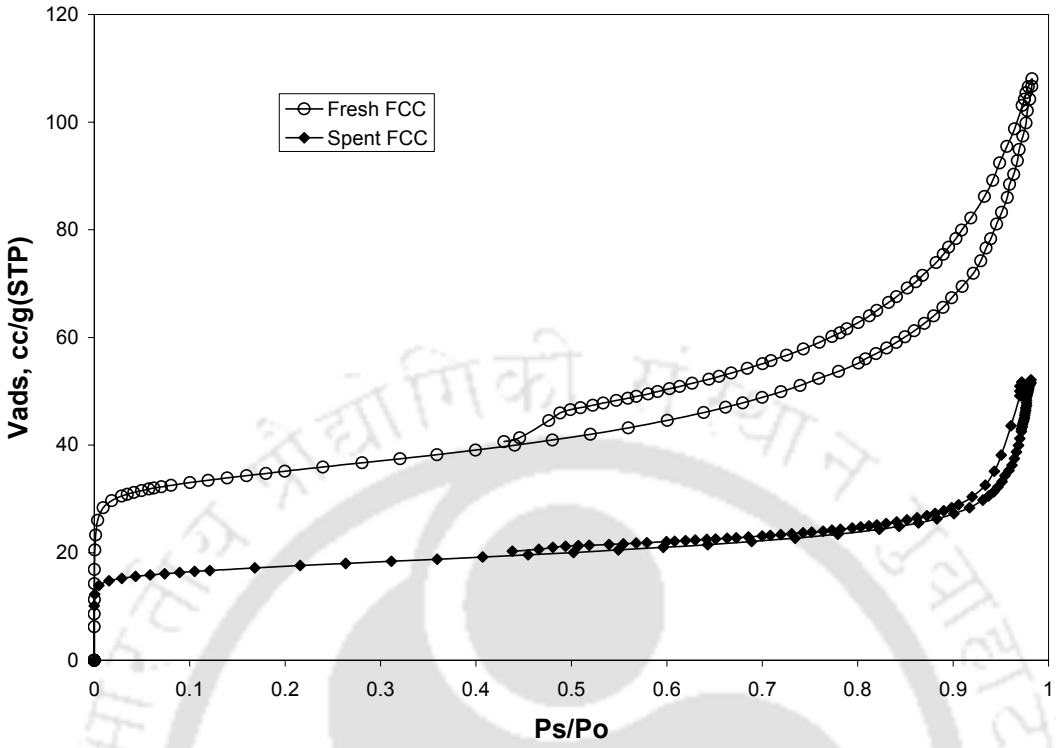

Figure 4.28. Nitrogen adsorption isotherm at 77K of FCC catalysts

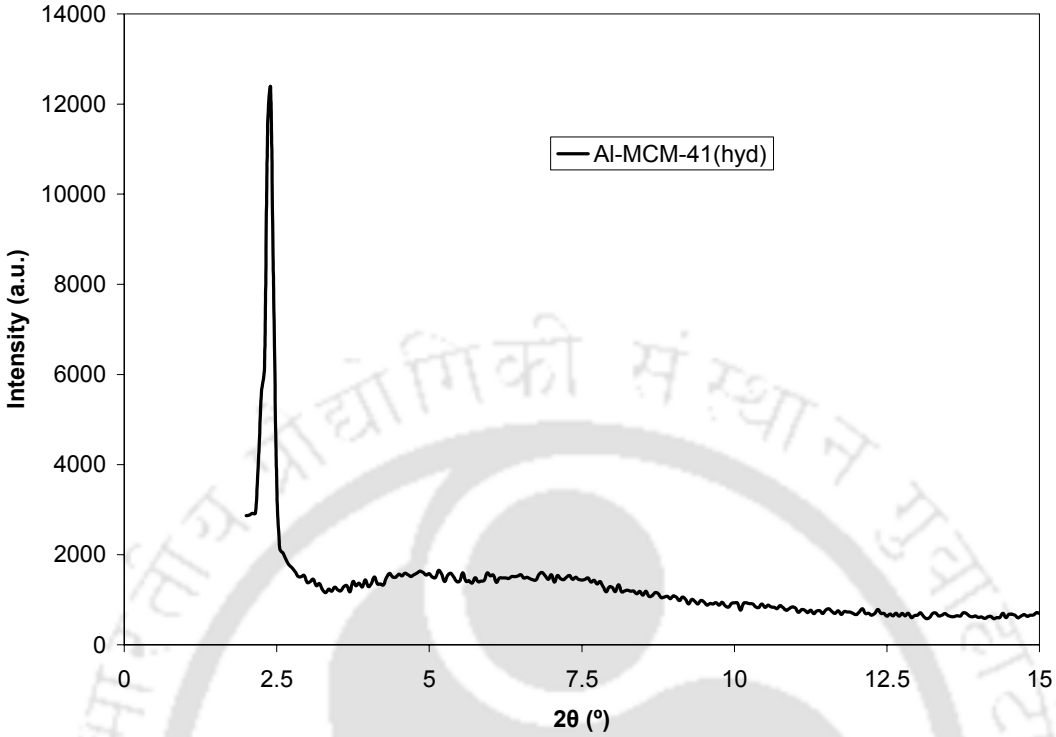

Figure 4.29. XRD pattern of Al-MCM-41 (hyd) catalysts

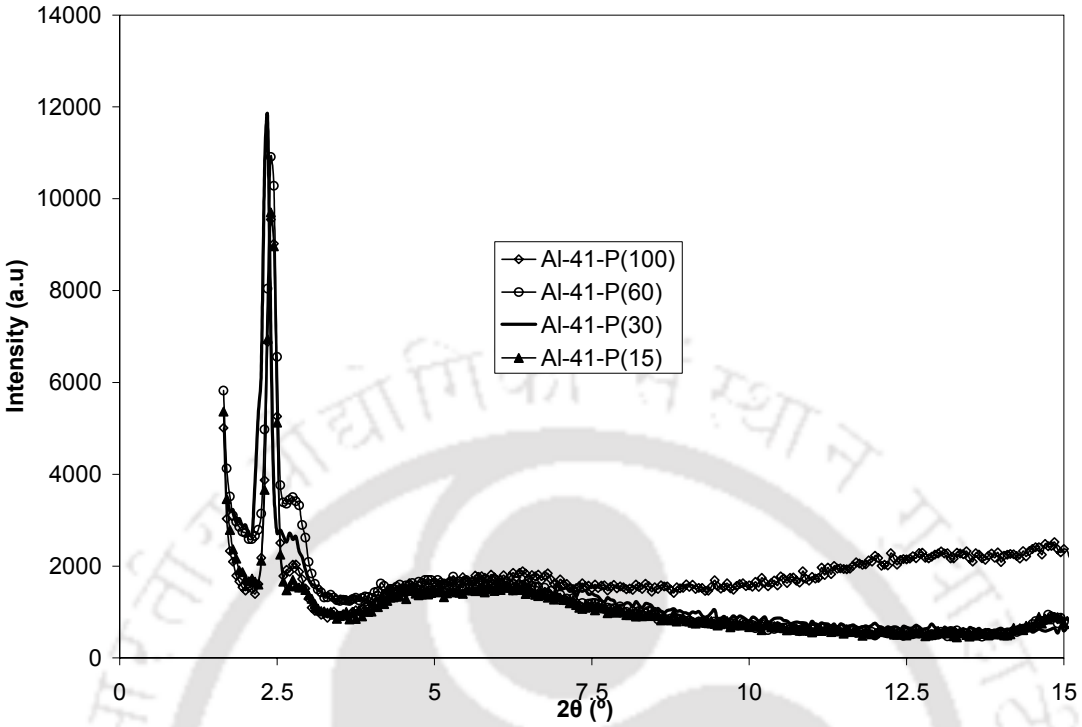

Figure 4.30. XRD pattern of Al-MCM-41 (sol-gel) catalysts

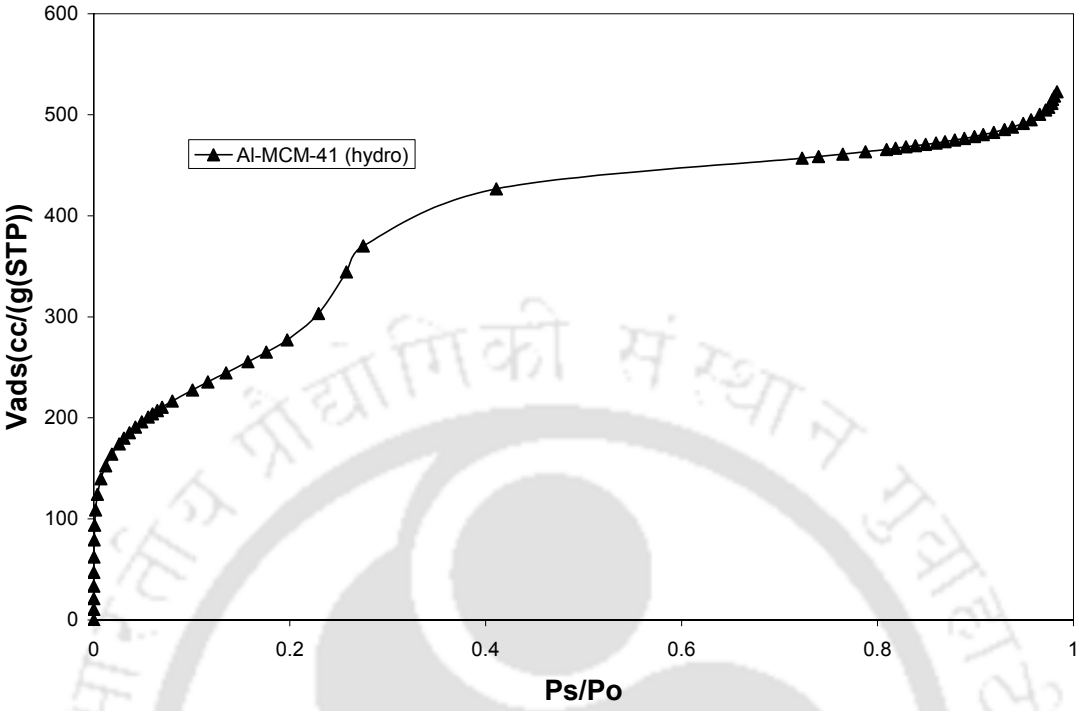

Figure 4.31. Nitrogen adsorption isotherm at 77K of Al-MCM-41 (hyd) catalysts

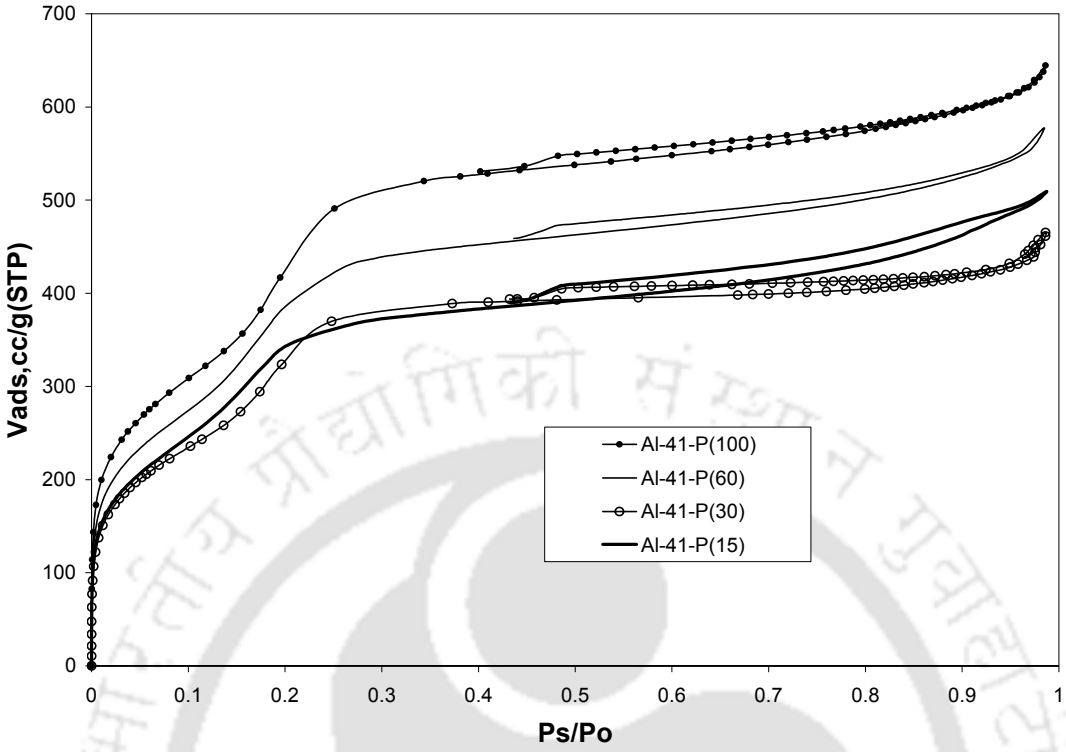

Figure 4.32. Nitrogen adsorption isotherm at 77K of Al-MCM-41 (sol-gel) catalysts

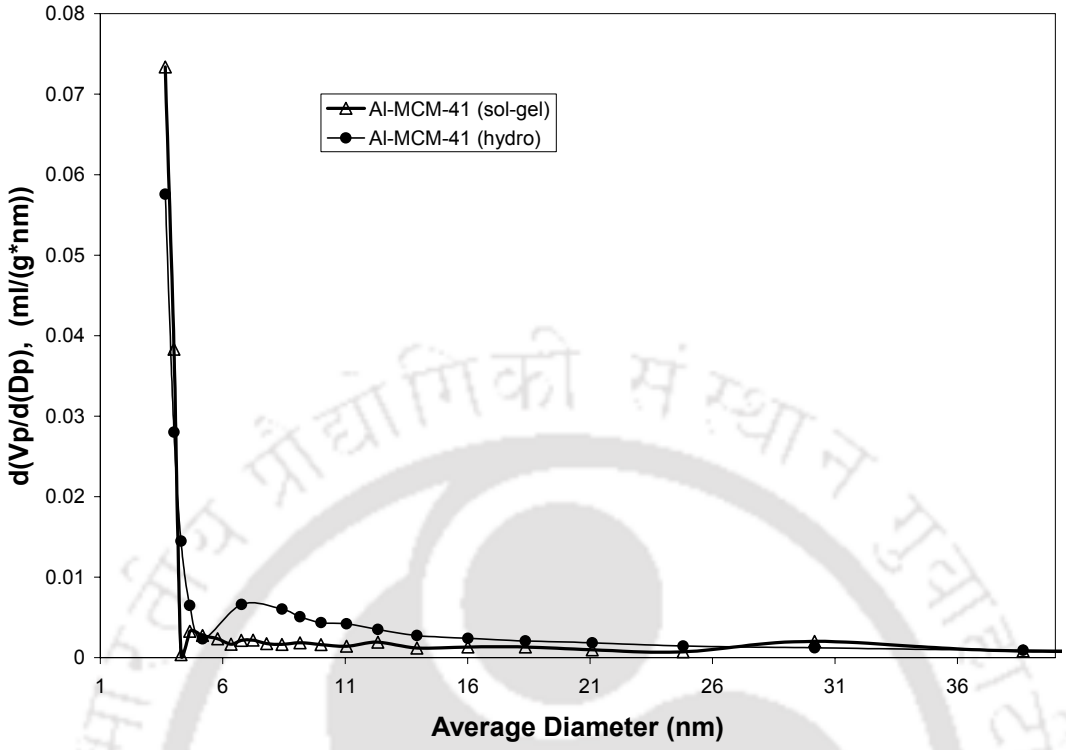

Figure 4.33. BJH (Desorption) pore size distribution of Al-MCM-41 catalyst

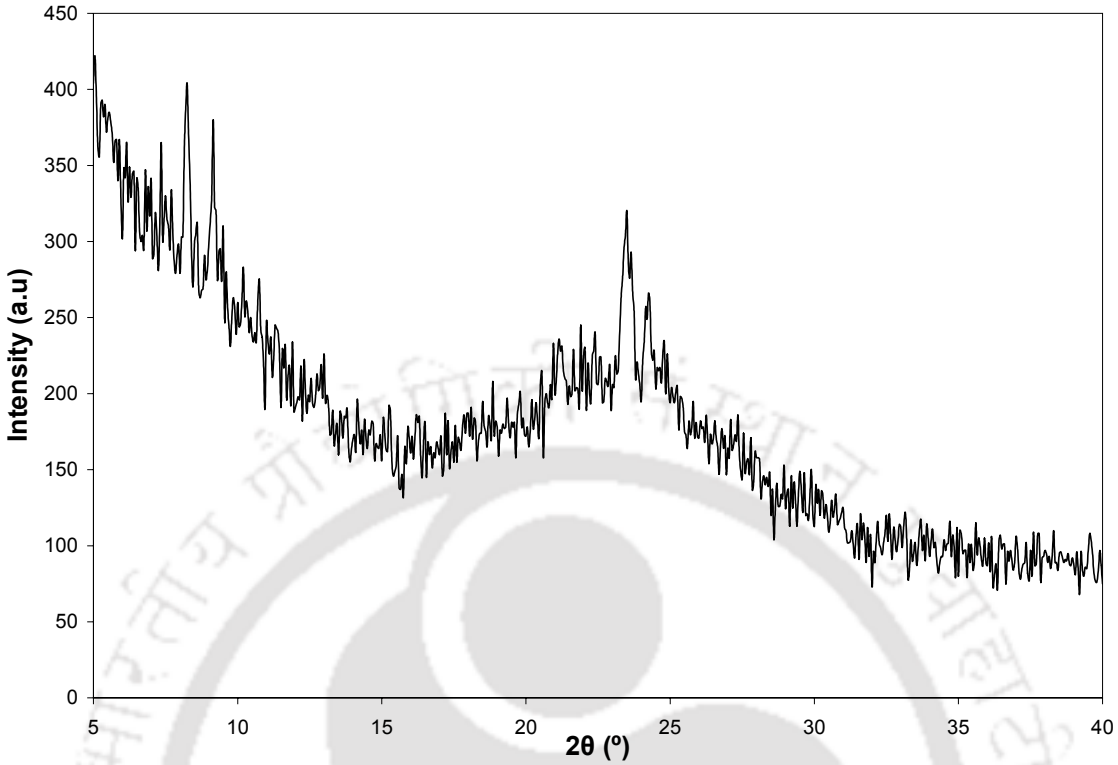

Figure 4.34. XRD pattern of n-HZSM-5 catalysts

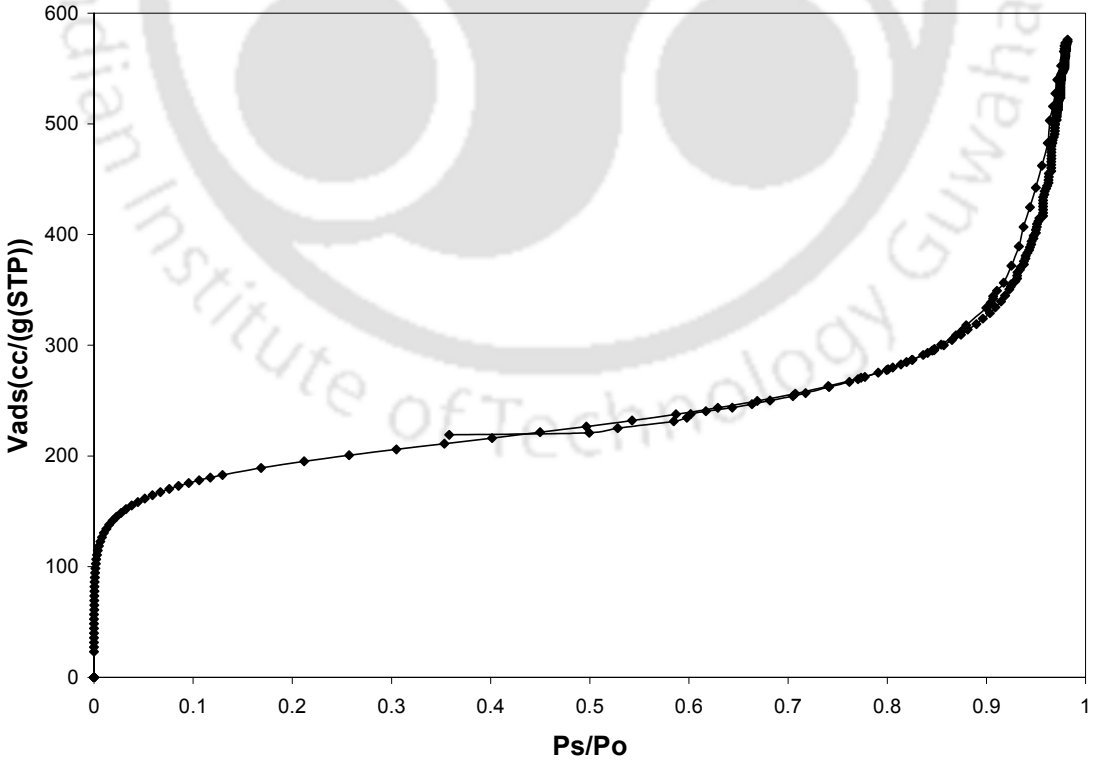

Figure 4.35. Nitrogen adsorption isotherm at 77K of n-HZSM-5 catalysts

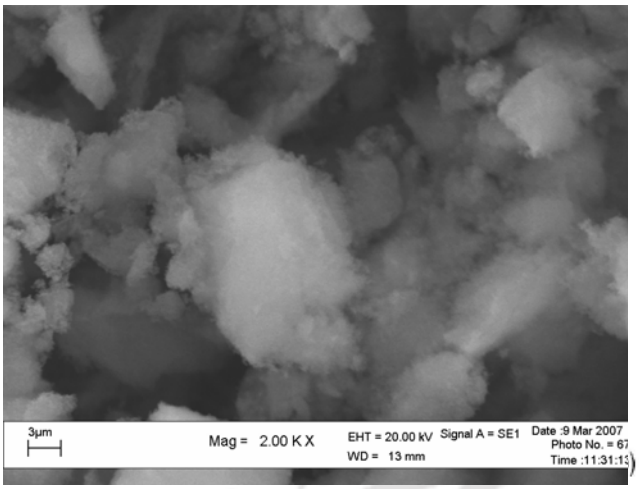

Figure 4.36. SEM micrographs of n-HZSM-5

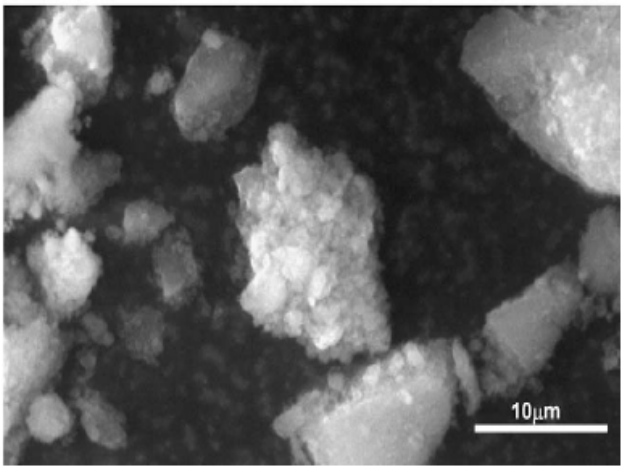

Figure 4.37. SEM micrograph of n-HZSM-5 [192]

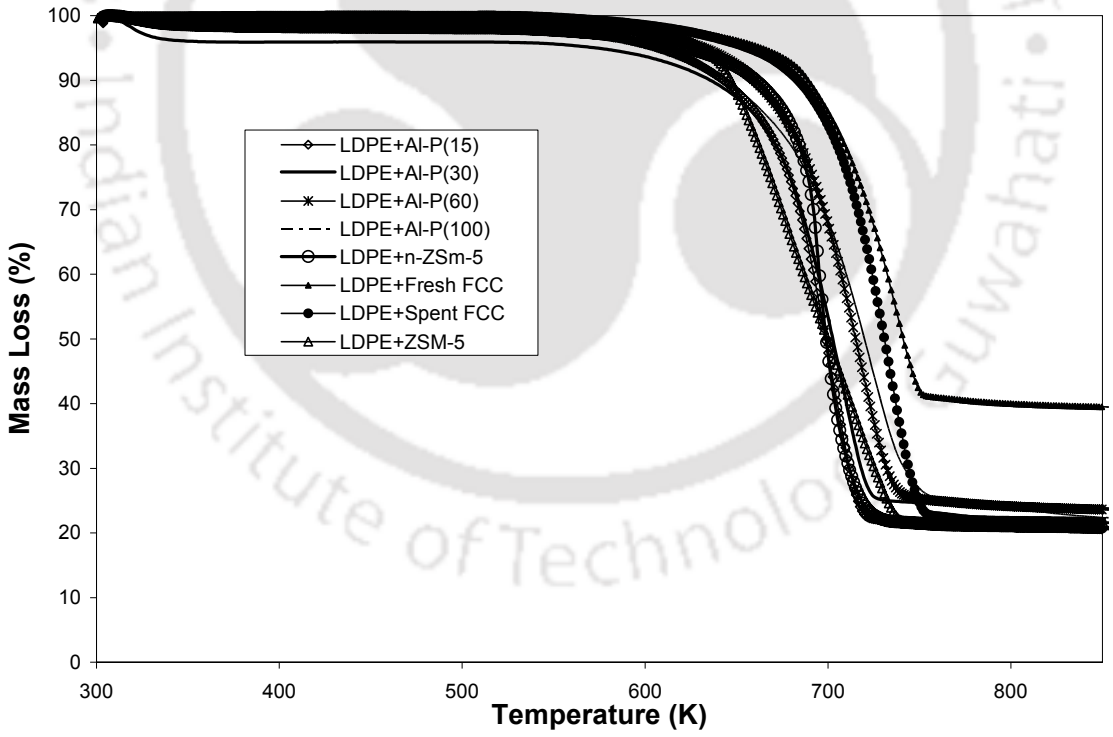

Figure 4.38. Experimental TG curves for the catalytic pyrolysis of waste LDPE with different catalysts at 20wt %

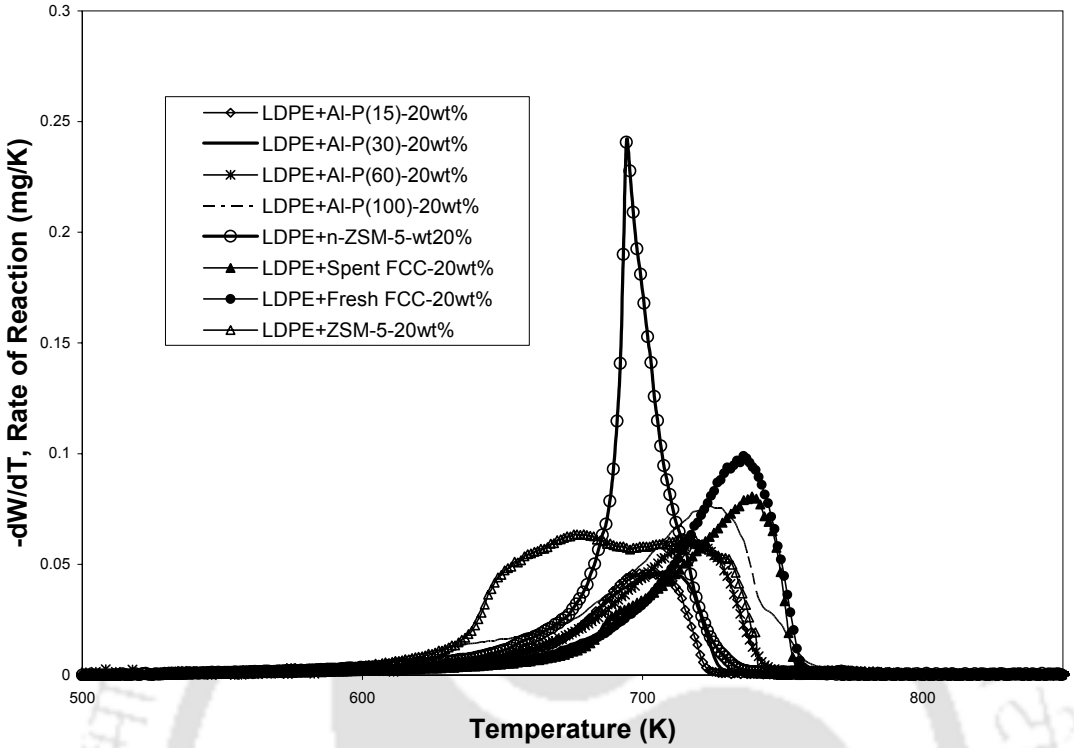

Figure 4.39. Experimental DTG curves for the catalytic pyrolysis of waste LDPE with different catalysts at 20wt %

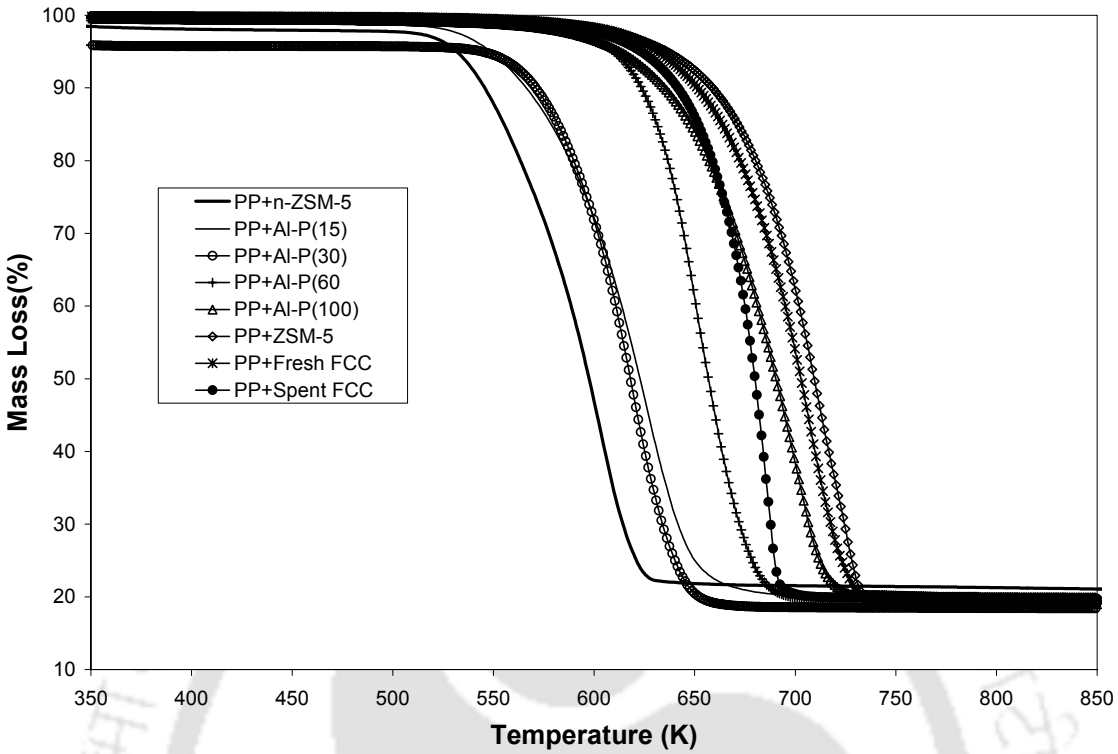

Figure 4.40. Experimental TG curves for the catalytic pyrolysis of PP with different catalysts at 20wt %

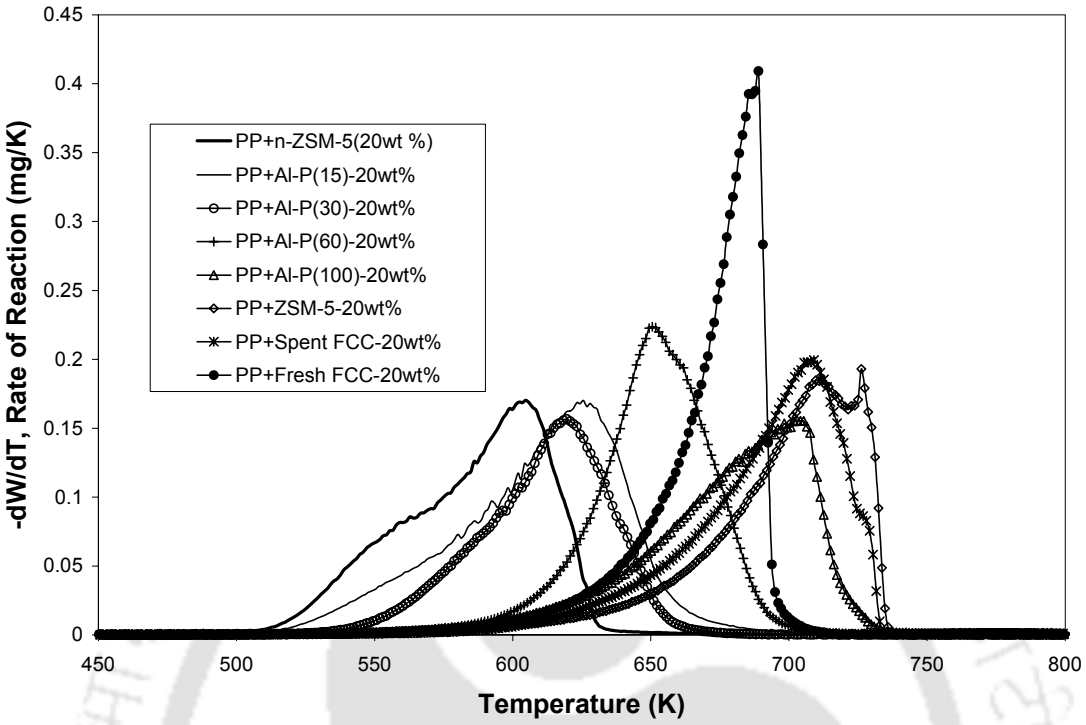

Figure 4.41. Experimental DTG curves for the catalytic pyrolysis of PP with different catalysts at 20wt %

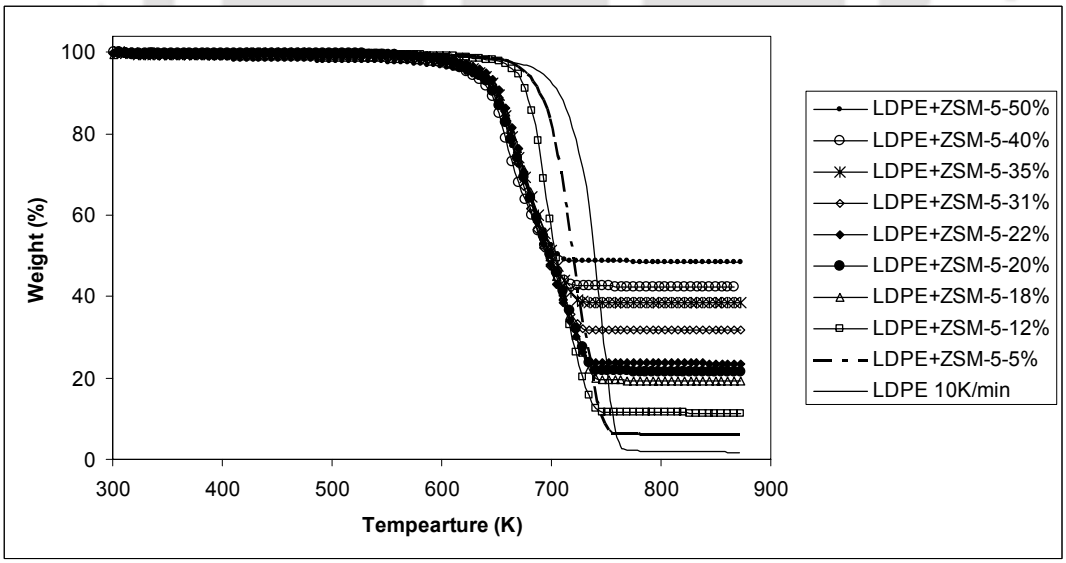

Figure.4.42. Experimental TG curves for the catalytic pyrolysis of waste LDPE with different catalyst (ZSM-5) percentage

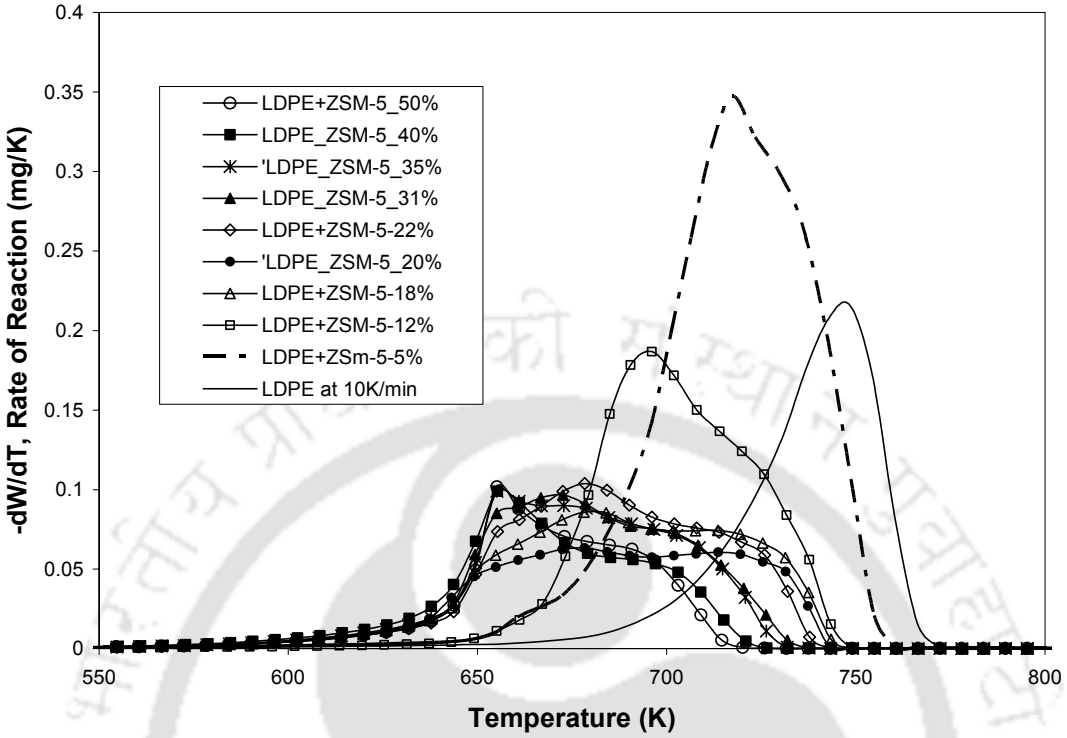

Figure. 4.43. Experimental DTG curves for the catalytic pyrolysis of waste LDPE with different catalyst (ZSM-5) percentage

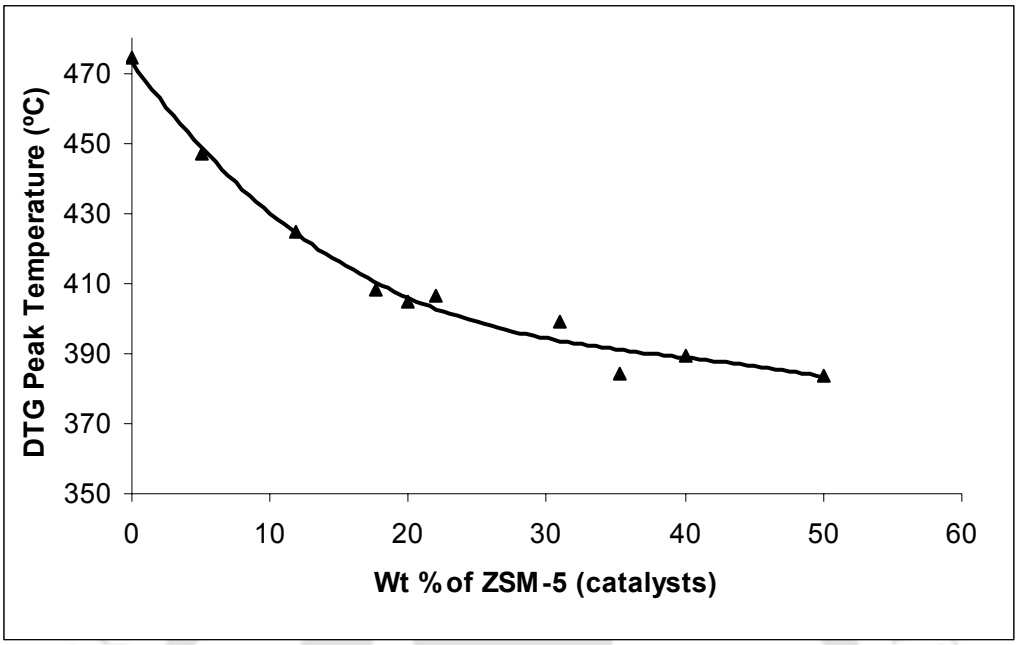

Figure 4.44. Effect of catalyst (ZSM-5) on the maximum decomposition temperature

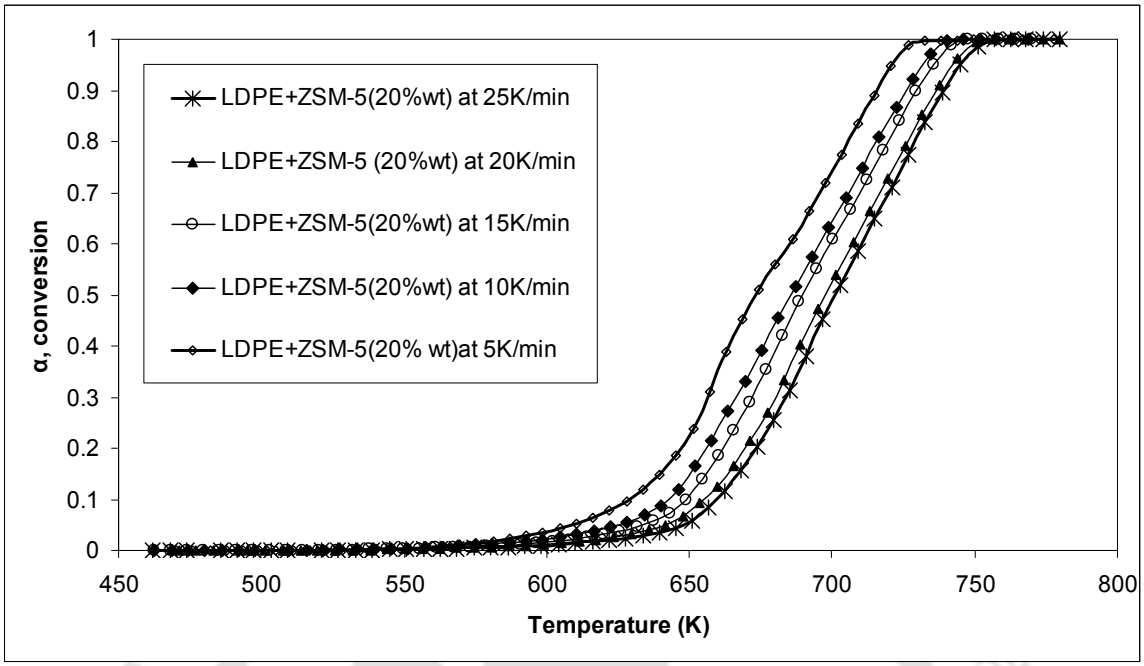

Figure 4.45. Variation of conversion (α) with temperature during catalytic nonisothermal pyrolysis of waste LDPE sample

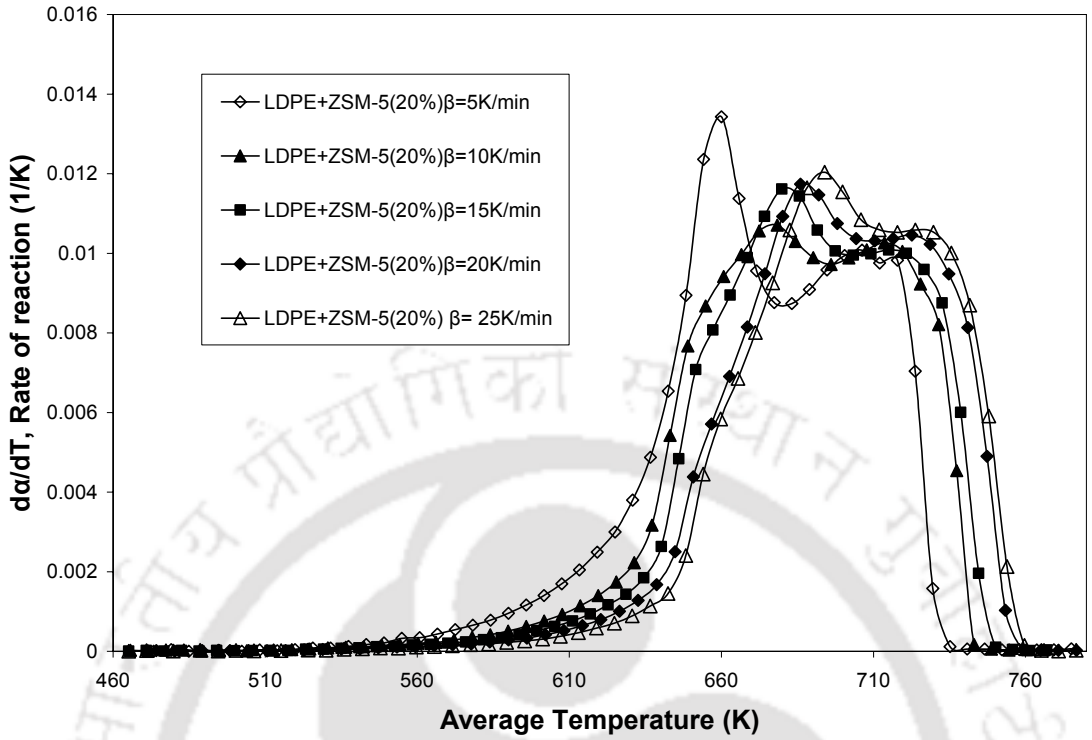

Figure 4.46. Variation of rate of decomposition (dα/dT) with temperature during catalytic nonisothermal pyrolysis of waste LDPE sample

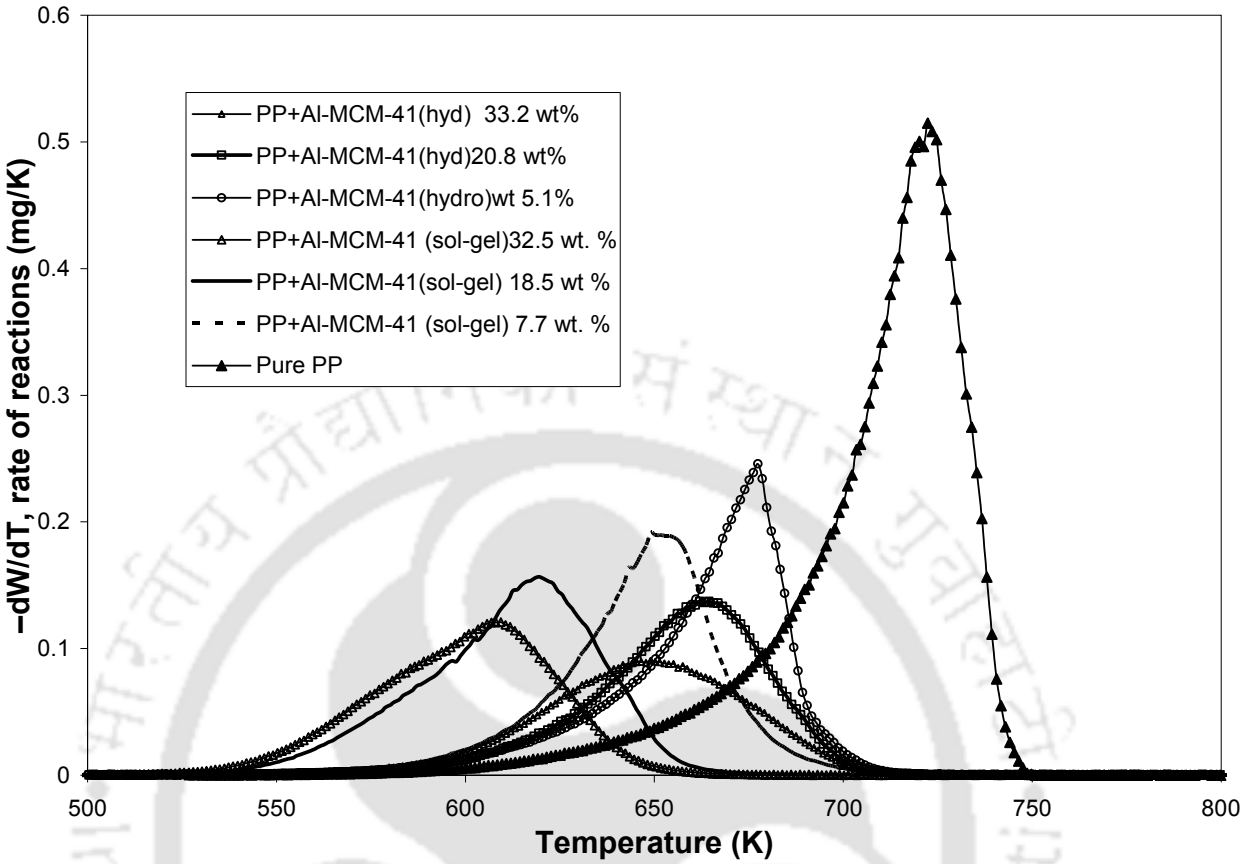

Figure 4.47. Experimental DTG curves for the catalytic pyrolysis of waste PP with different catalyst [Al-MCM-41(sol-gel) and Al-MCM-41(hyd)] percentage

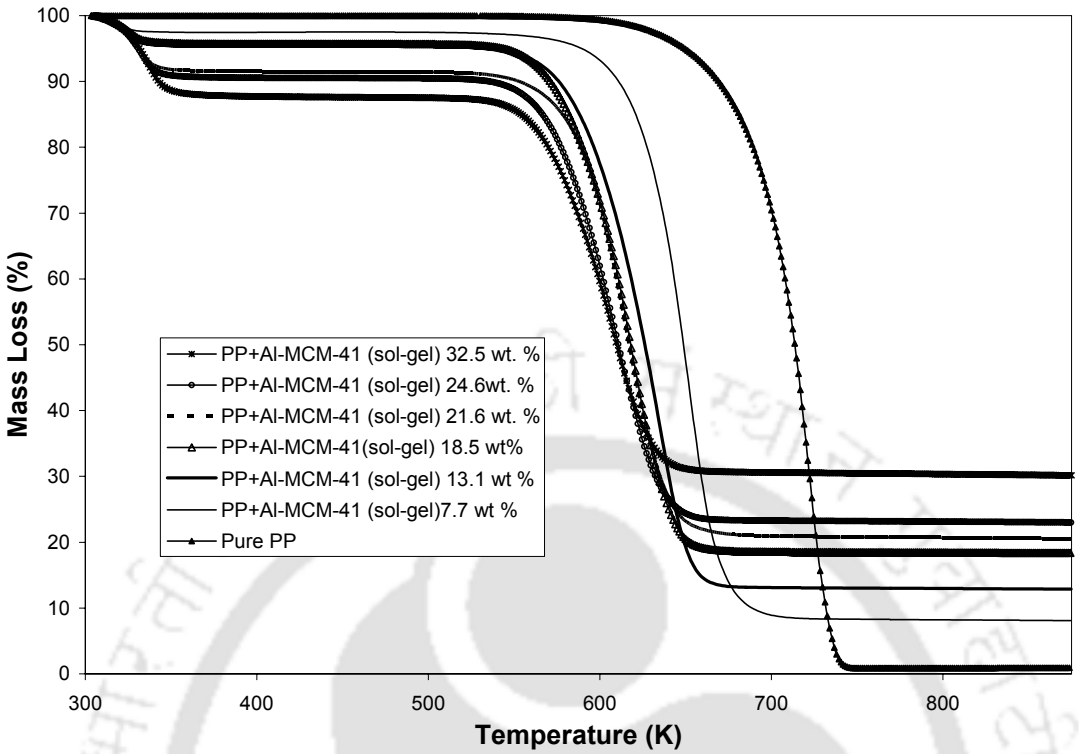

Figure 4.48. Experimental TG curves for the catalytic pyrolysis of waste PP with different catalyst (Al-MCM-41(sol-gel)) percentage

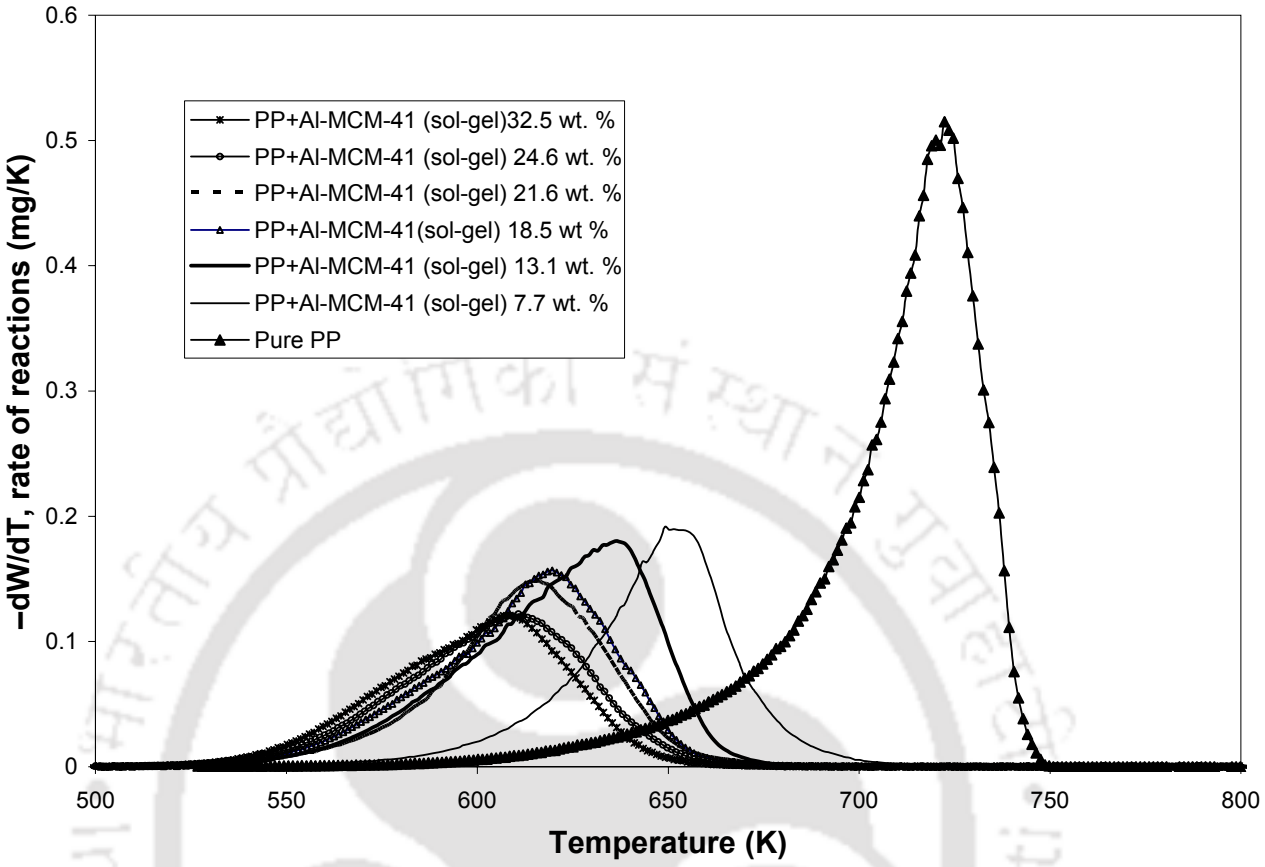

Figure 4.49. Experimental DTG curves for the catalytic pyrolysis of waste PP with different catalyst (Al-MCM-41(sol-gel)) percentage

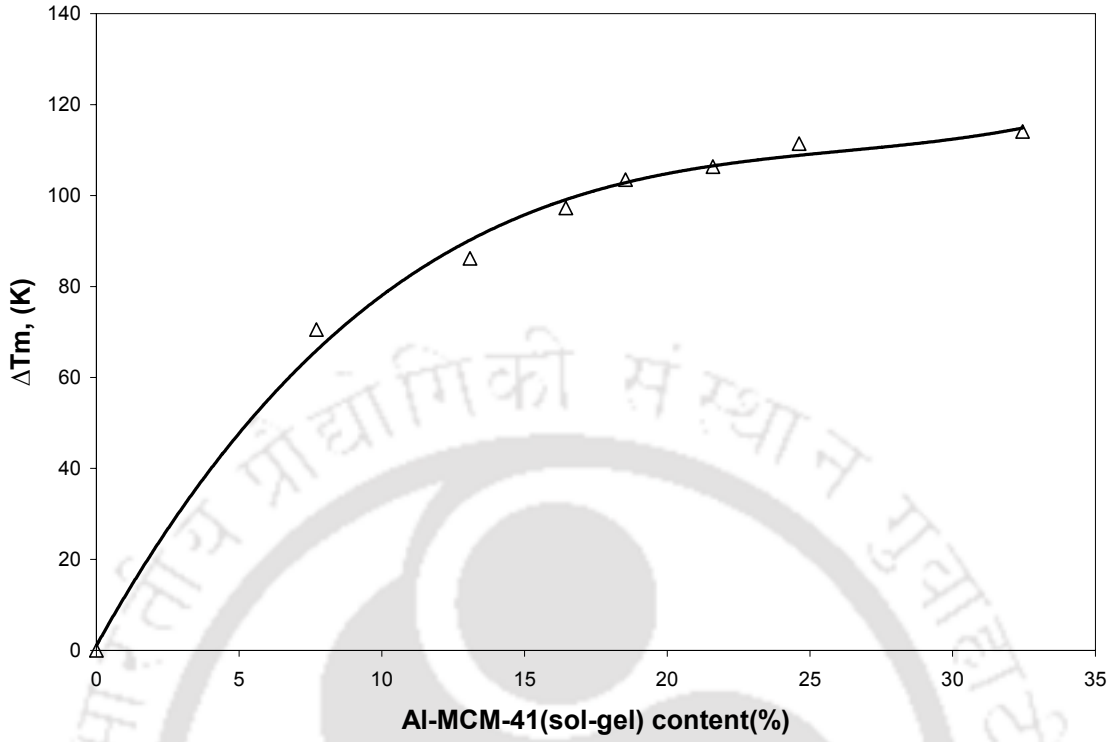

Figure 4.50. Effect of catalysts (Al-MCM-41) on reduction in maximum decomposition Temperature (ΔT_m)

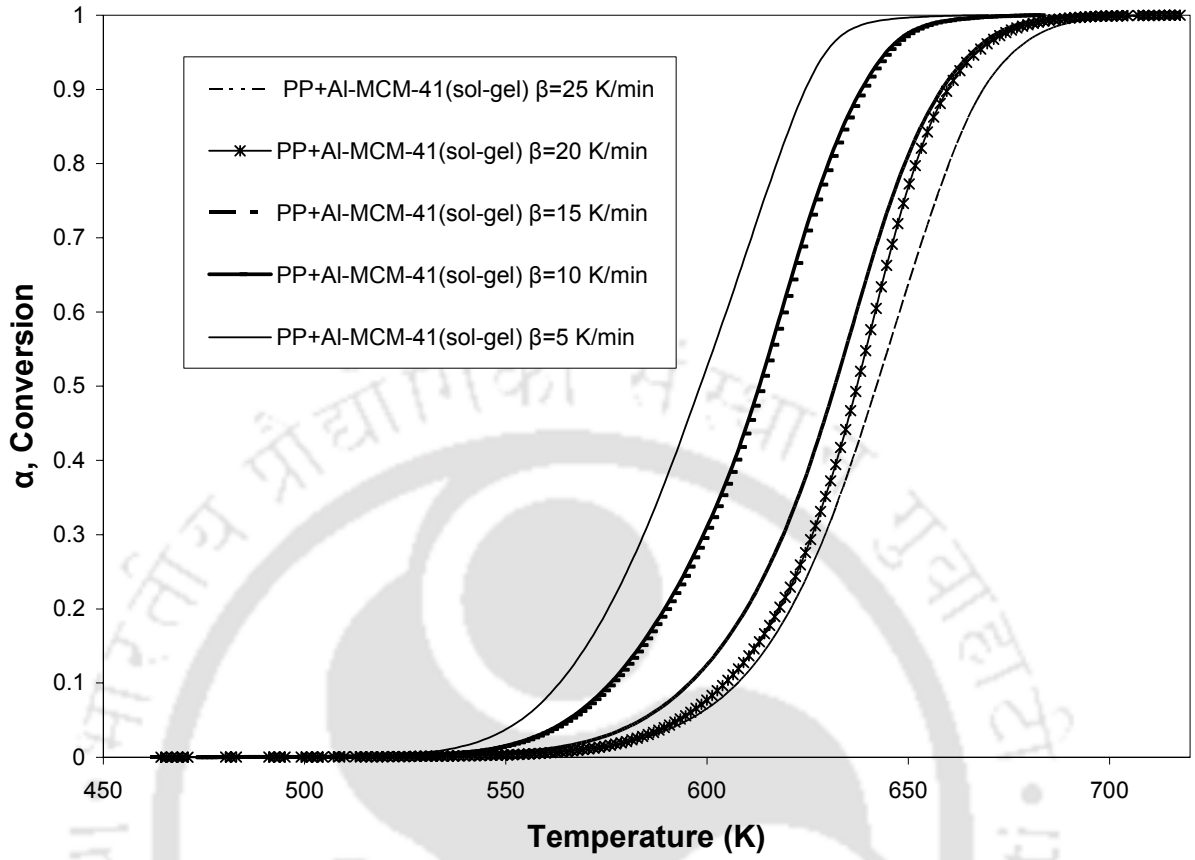

Figure 4.51. Variation of conversion (α) with temperature during catalytic nonisothermal pyrolysis (18.5 wt % catalyst) of PP sample

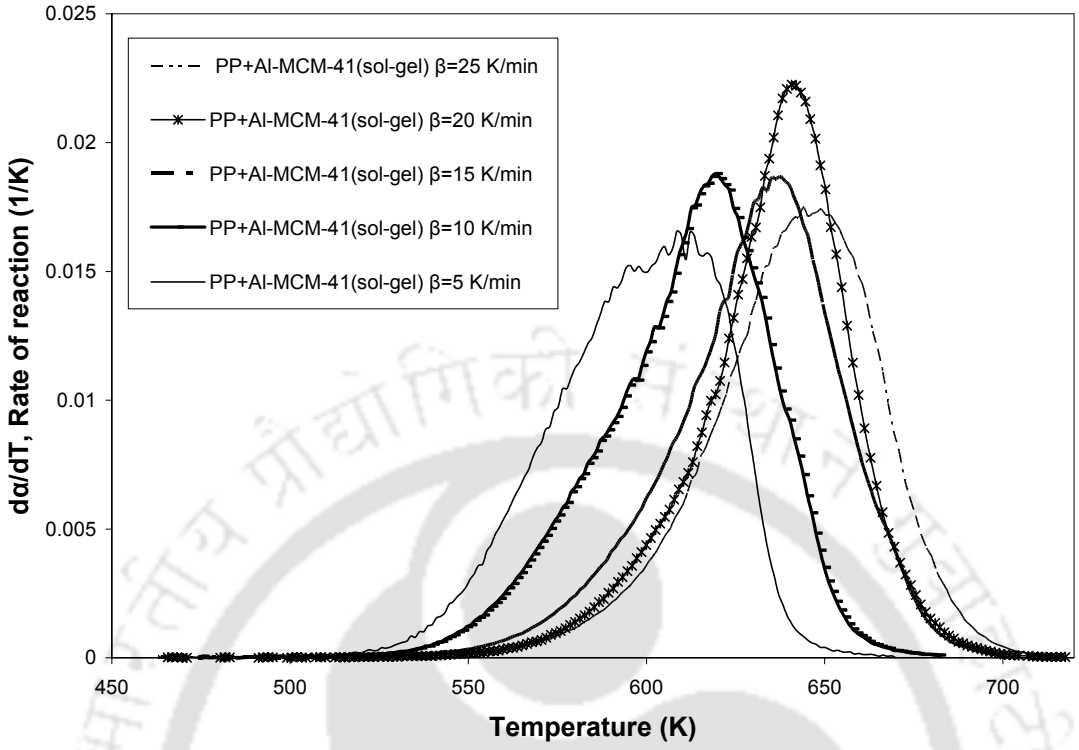

Figure 4.52. Variation of rate of decomposition (dα/dT) with temperature during catalytic nonisothermal pyrolysis (18.5 wt % catalyst) of PP sample

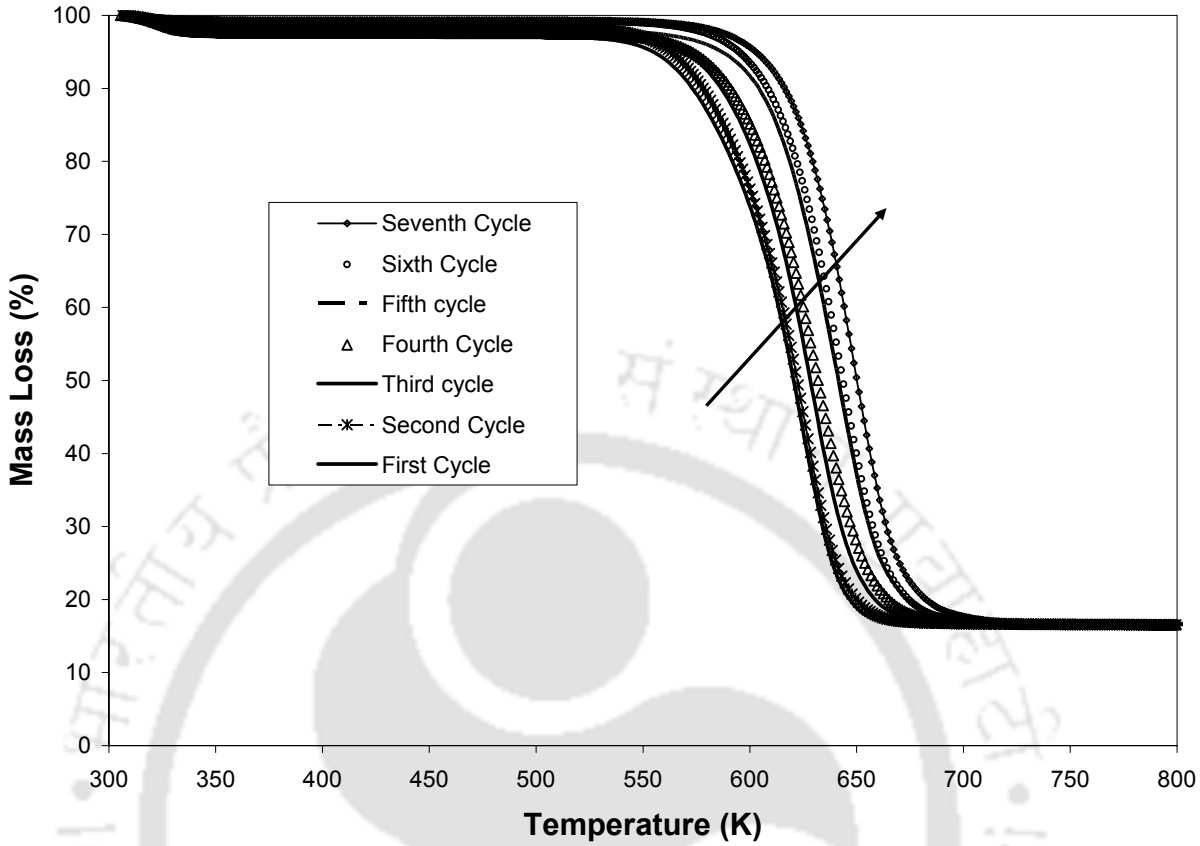

Figure 4.53. Experimental TG curves for the different cycles of catalytic pyrolysis of PP with 17% catalyst (Al-MCM-41(sol-gel)

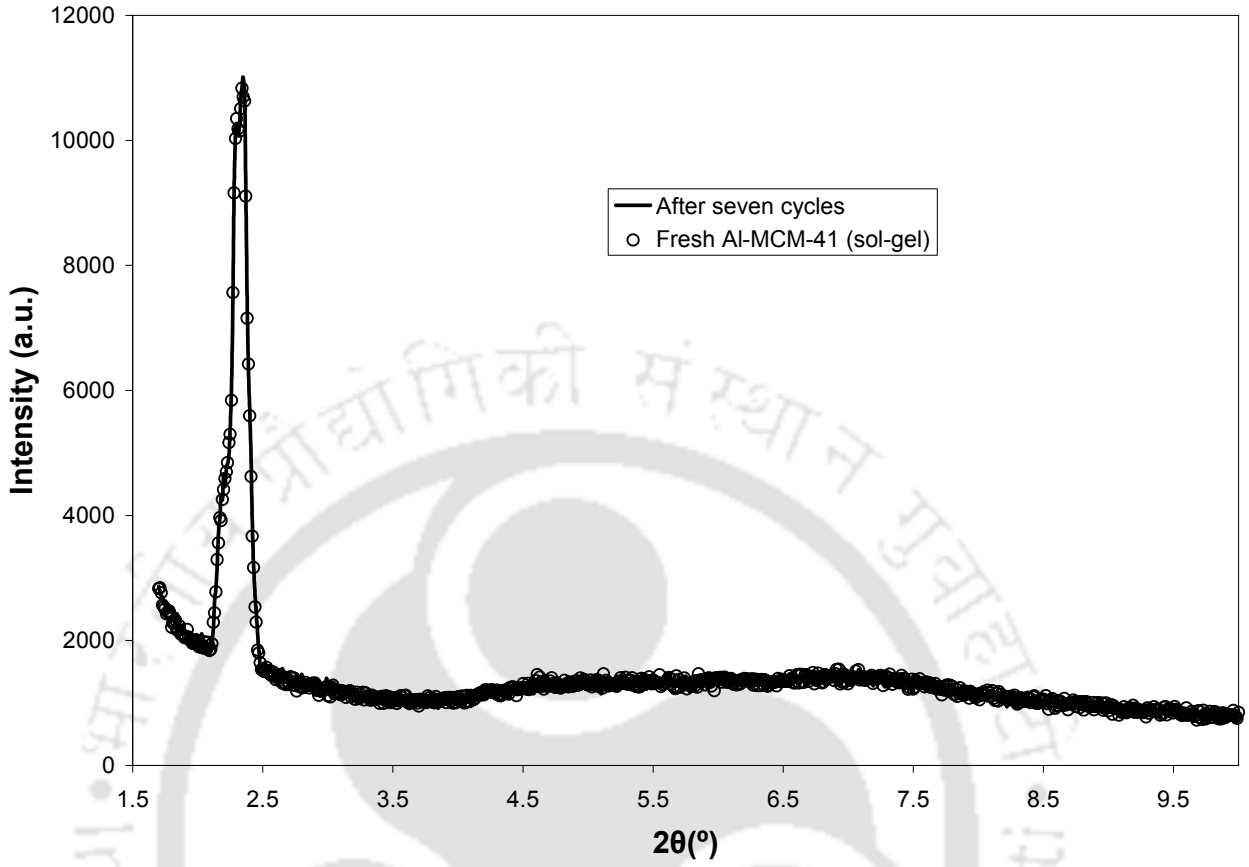

Figure 4.54. XRD pattern of Al-MCM-41(sol-gel) catalyst after seventh cycle (using Step Size=0.01º and Step time 0.5s)

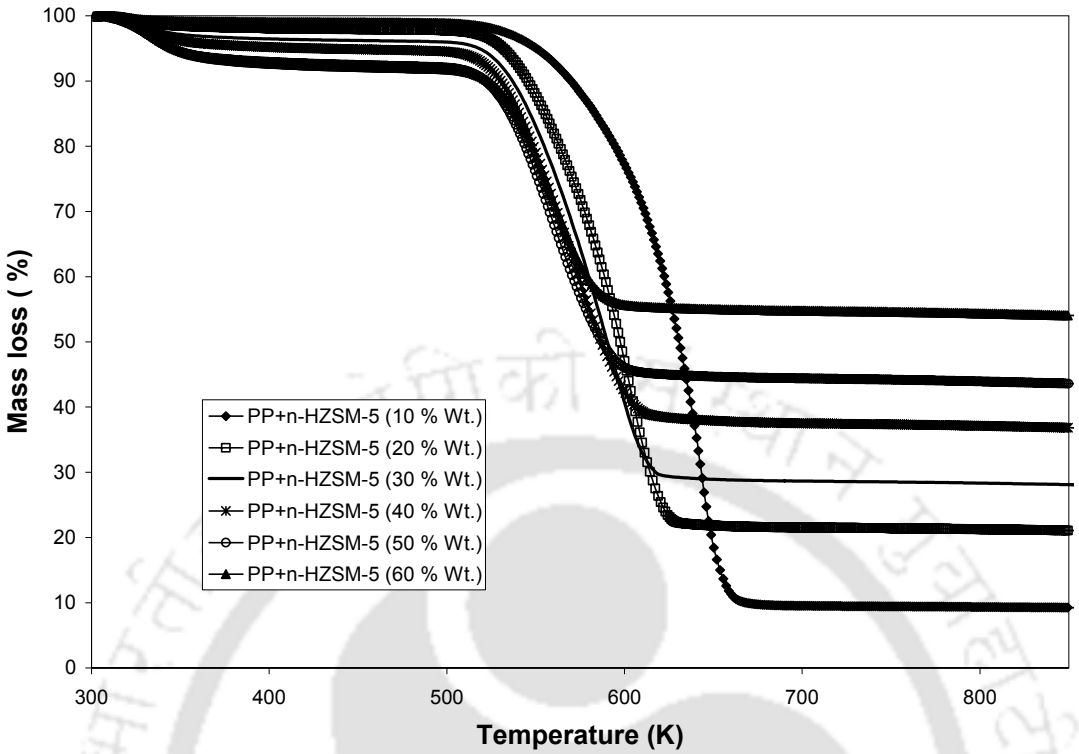

Figure.4.55. Experimental TG curves for the catalytic pyrolysis of PP with different catalyst (n-HZSM-5) percentage

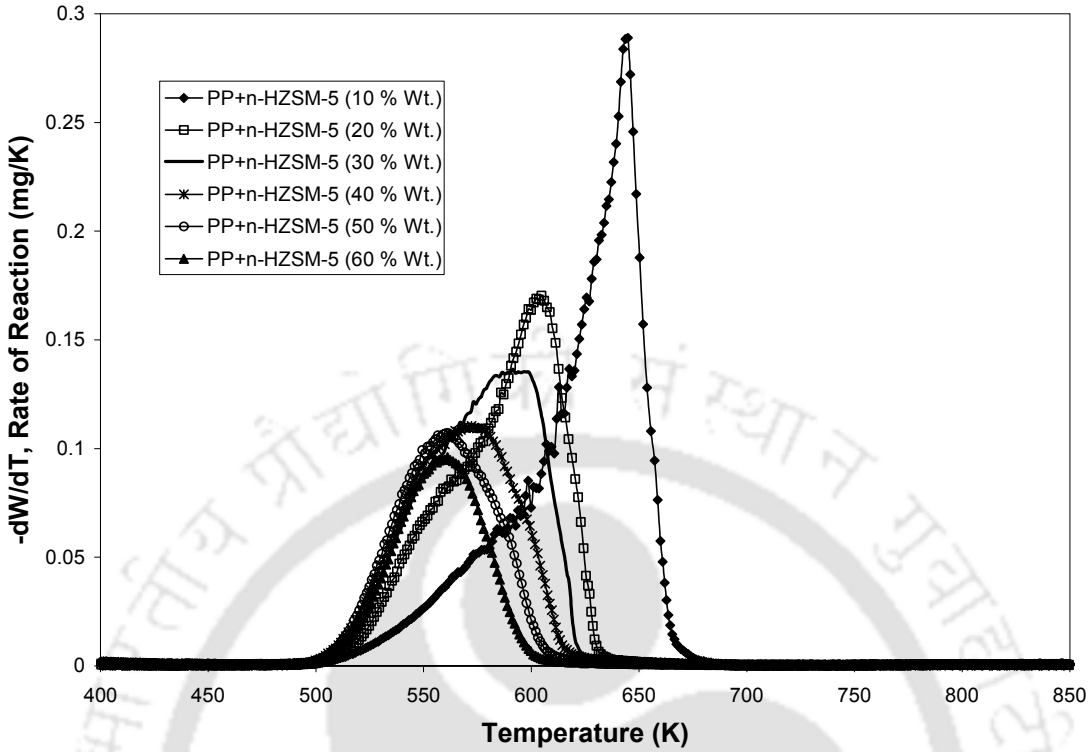

Figure 4.56. Experimental DTG curves for the catalytic pyrolysis of PP with different catalyst (n-HZSM-5) percentage

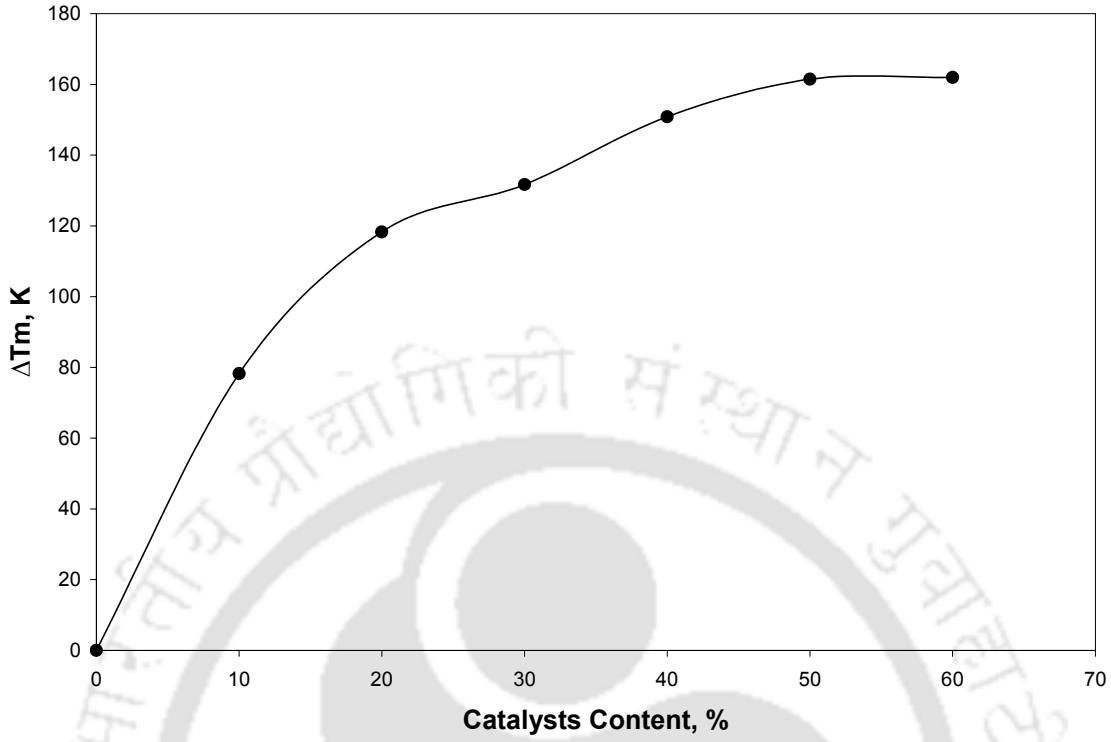

Figure 4.57. Effect of catalysts (n-HZSM-5) on reduction in maximum decomposition Temperature (ΔT_m)

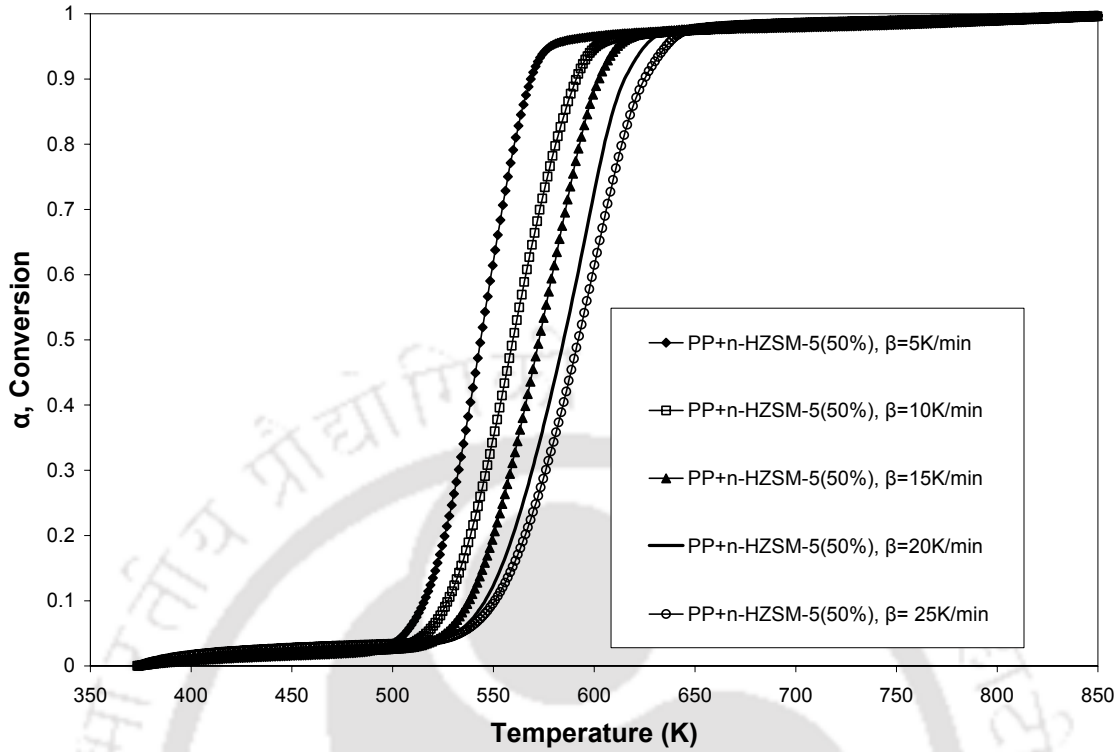

Figure 4.58. Variation of conversion (α) with temperature during catalytic nonisothermal pyrolysis (50 wt % n-HZSM-5 catalyst) of PP sample

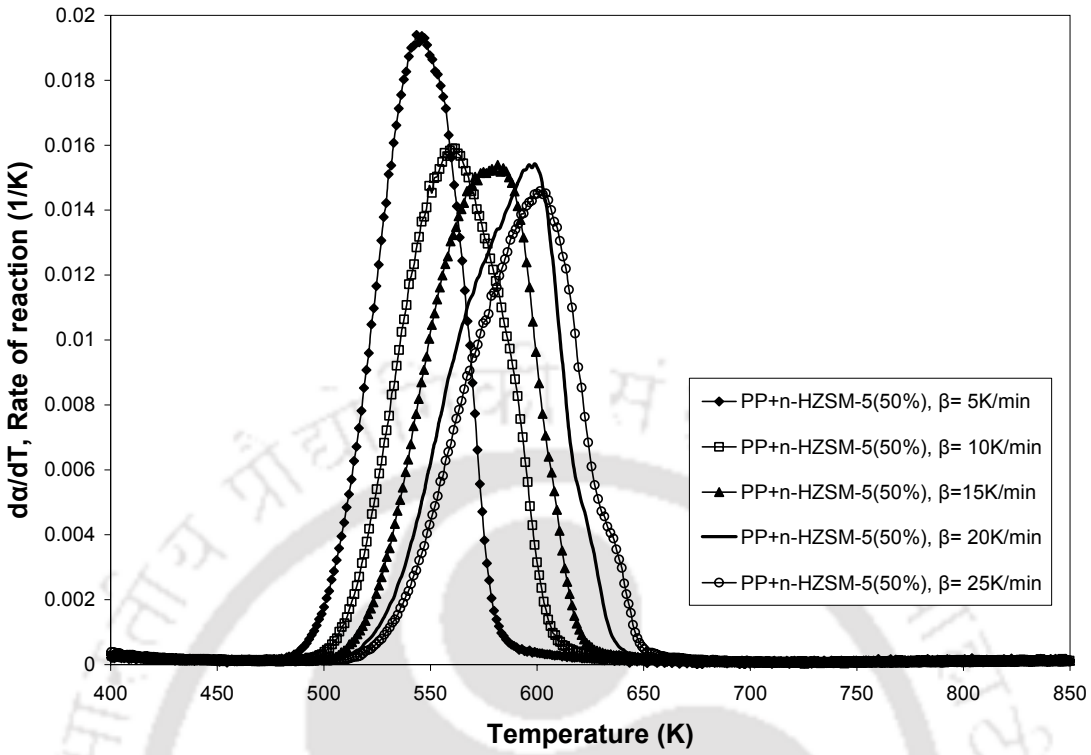

Figure 4.59. Variation of rate of decomposition (dα/dT) with temperature during catalytic nonisothermal pyrolysis (50 wt % n-HZSM-5 catalyst) of PP sample

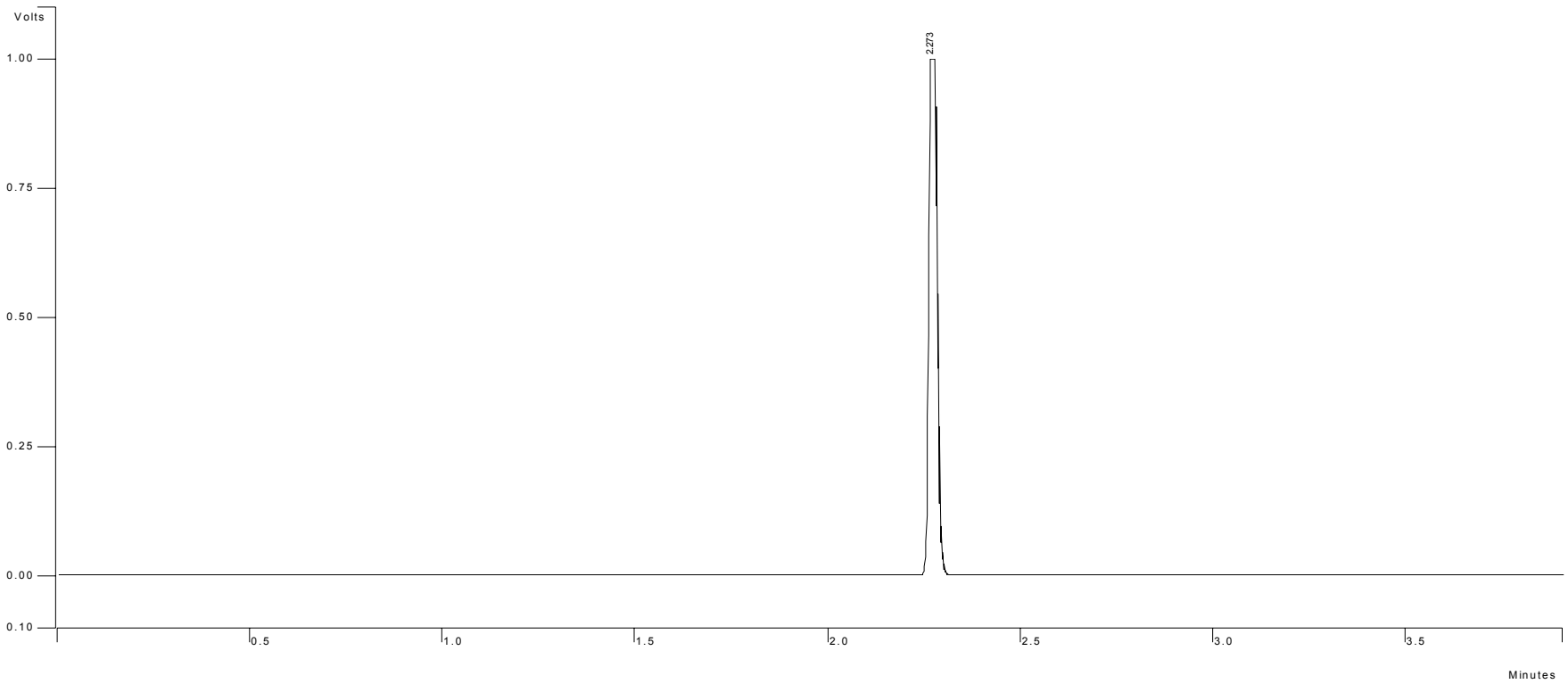

Figure 4.60. GC chromatogram for pure propane

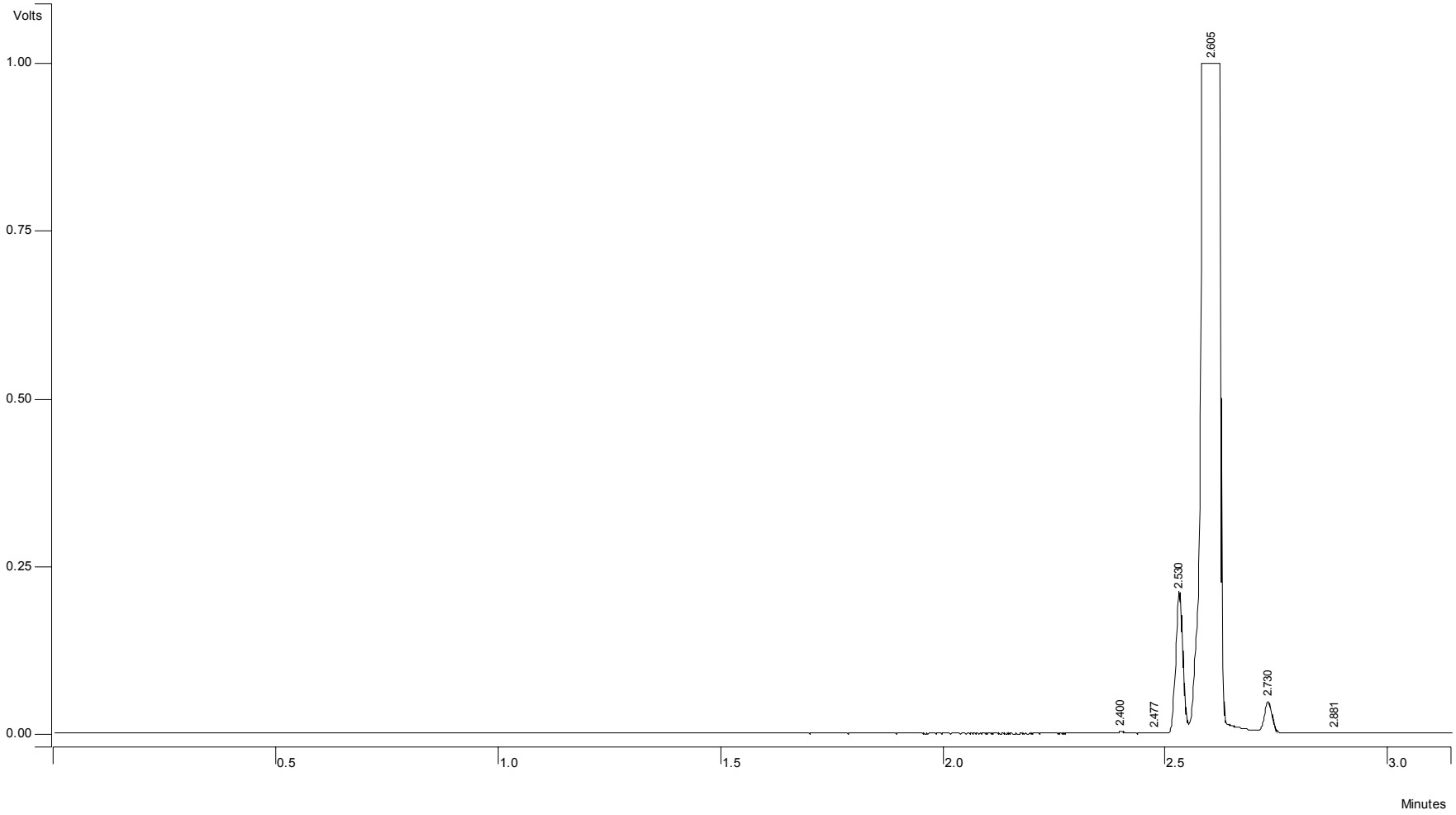

Figure 4.61. GC chromatogram for n-hexane

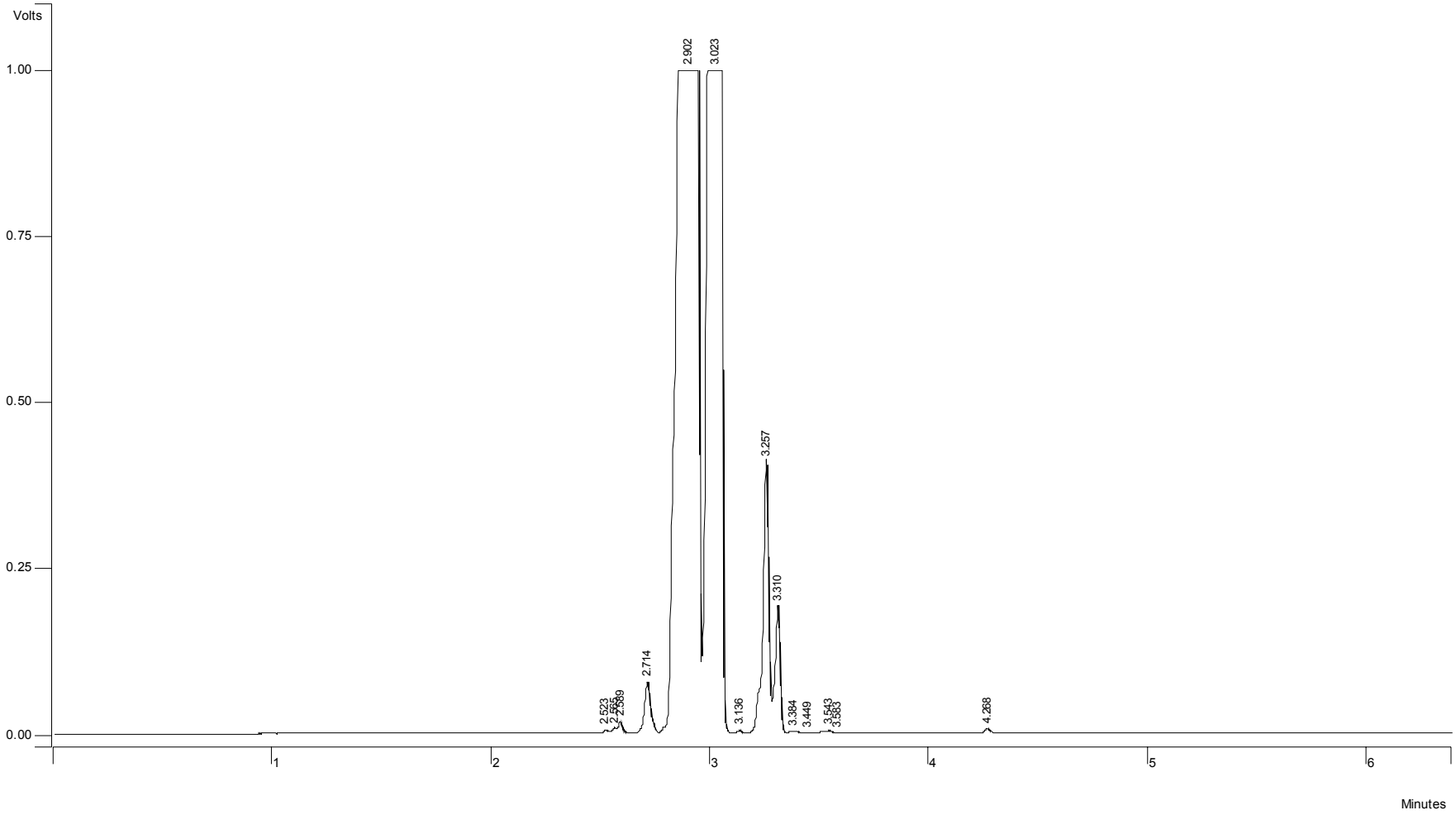

Figure 4.62. GC chromatogram for heptanes

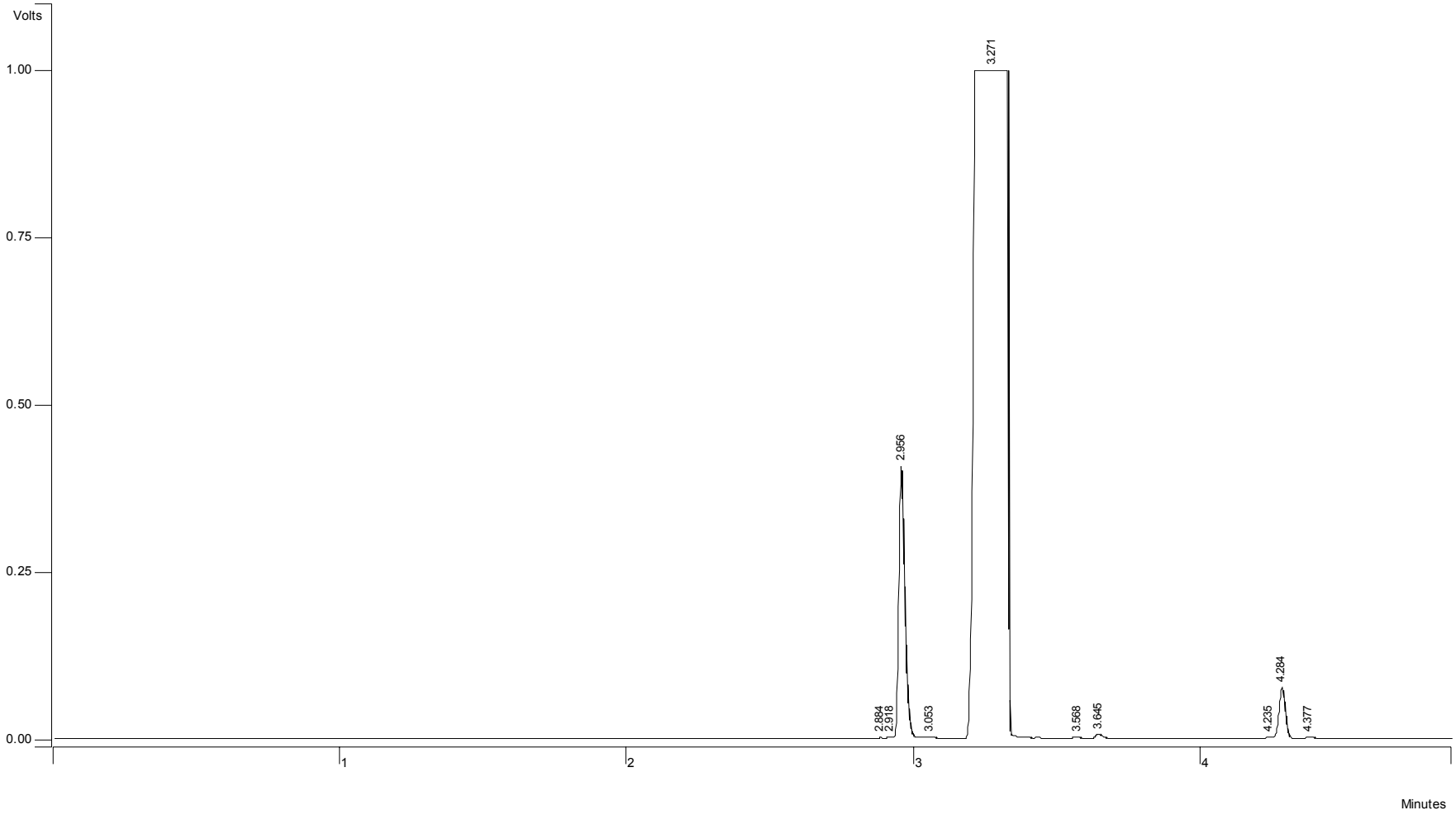

Figure 4.63. GC chromatogram for benzene

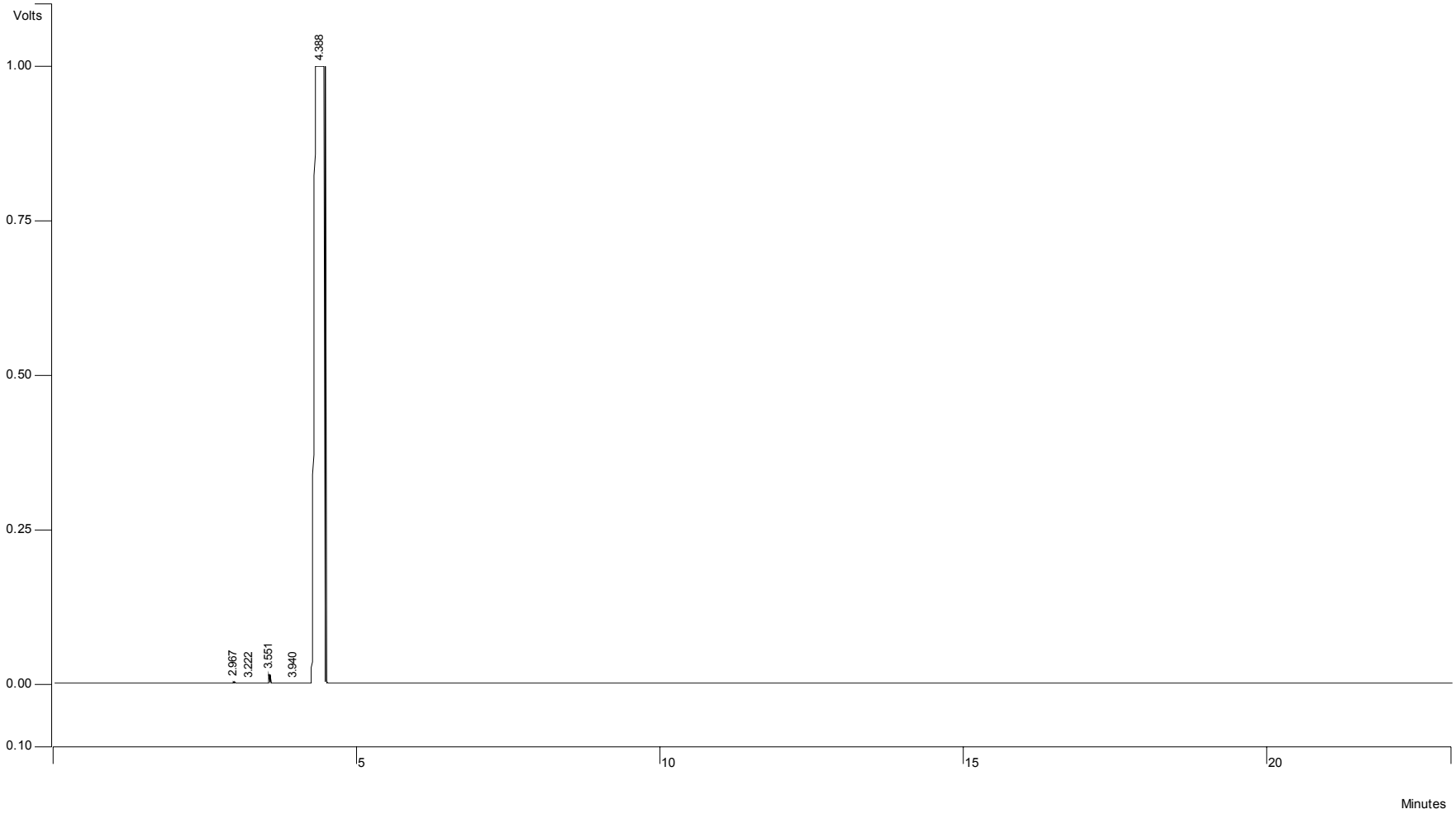

Figure 4.64. GC chromatogram for pure toluene

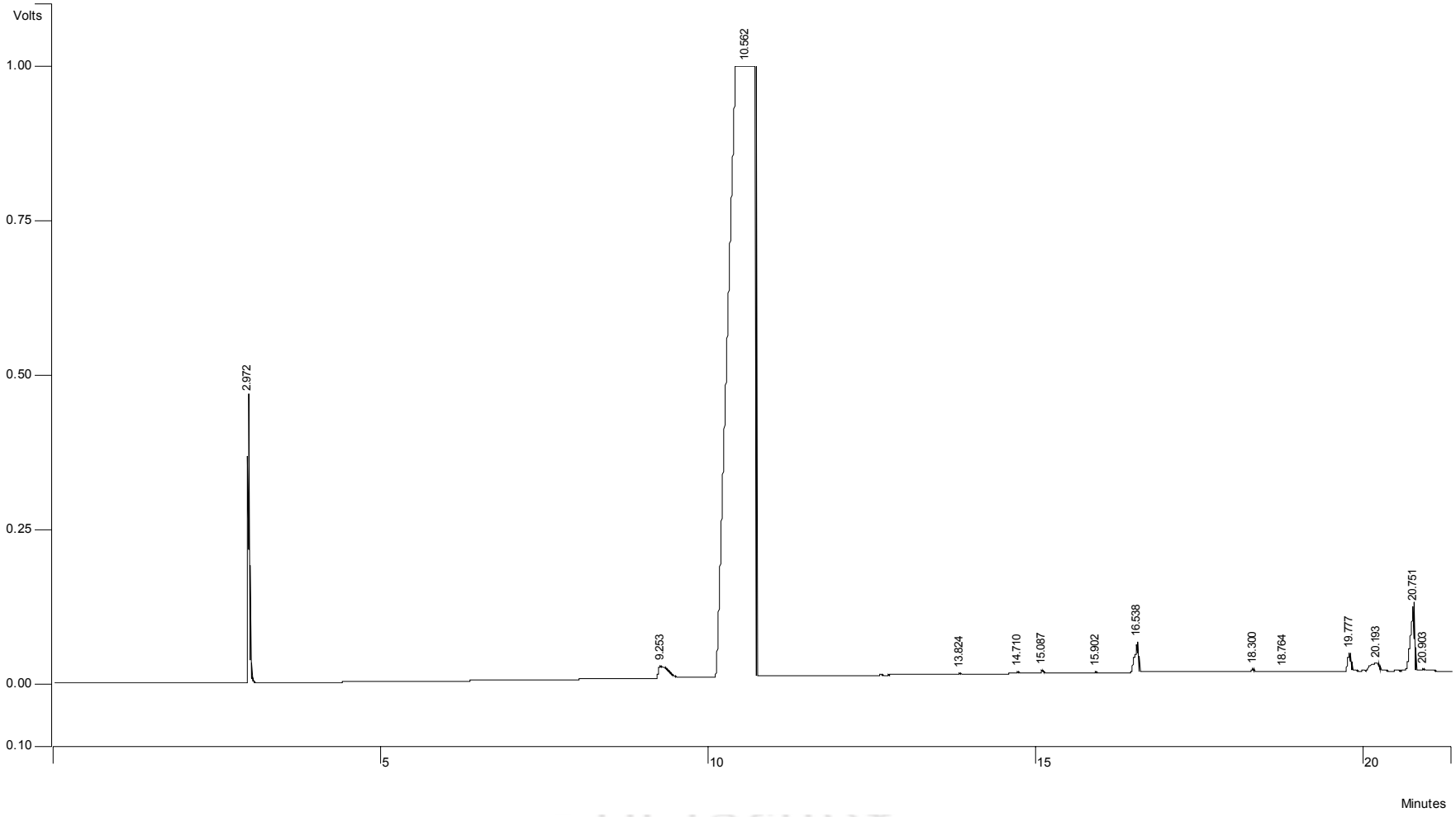

Figure 4.65. GC chromatogram for indene

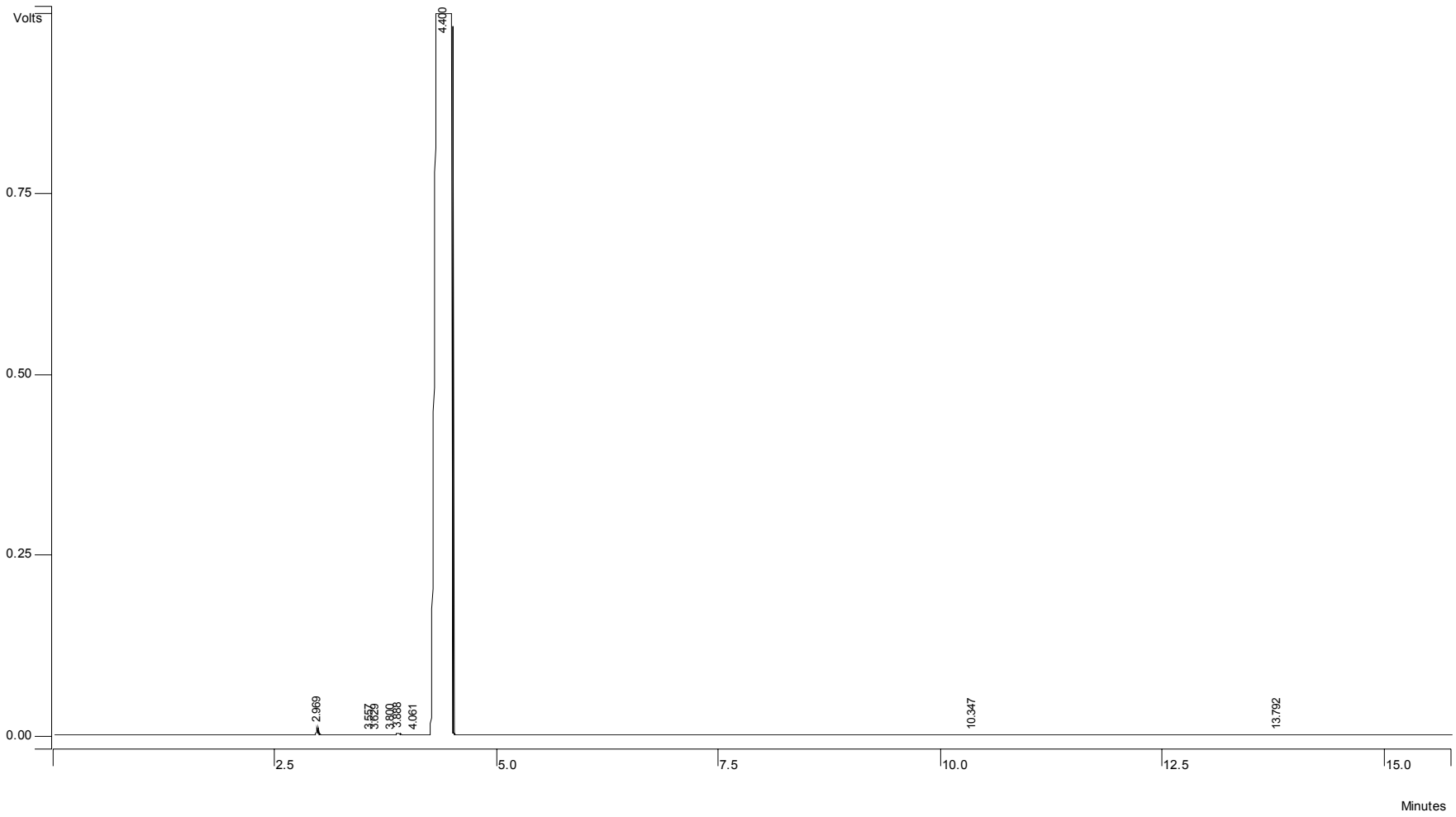

Figure 4.66. GC chromatogram for naphthalene (0.005% naphthalene, 99.99% toluene)

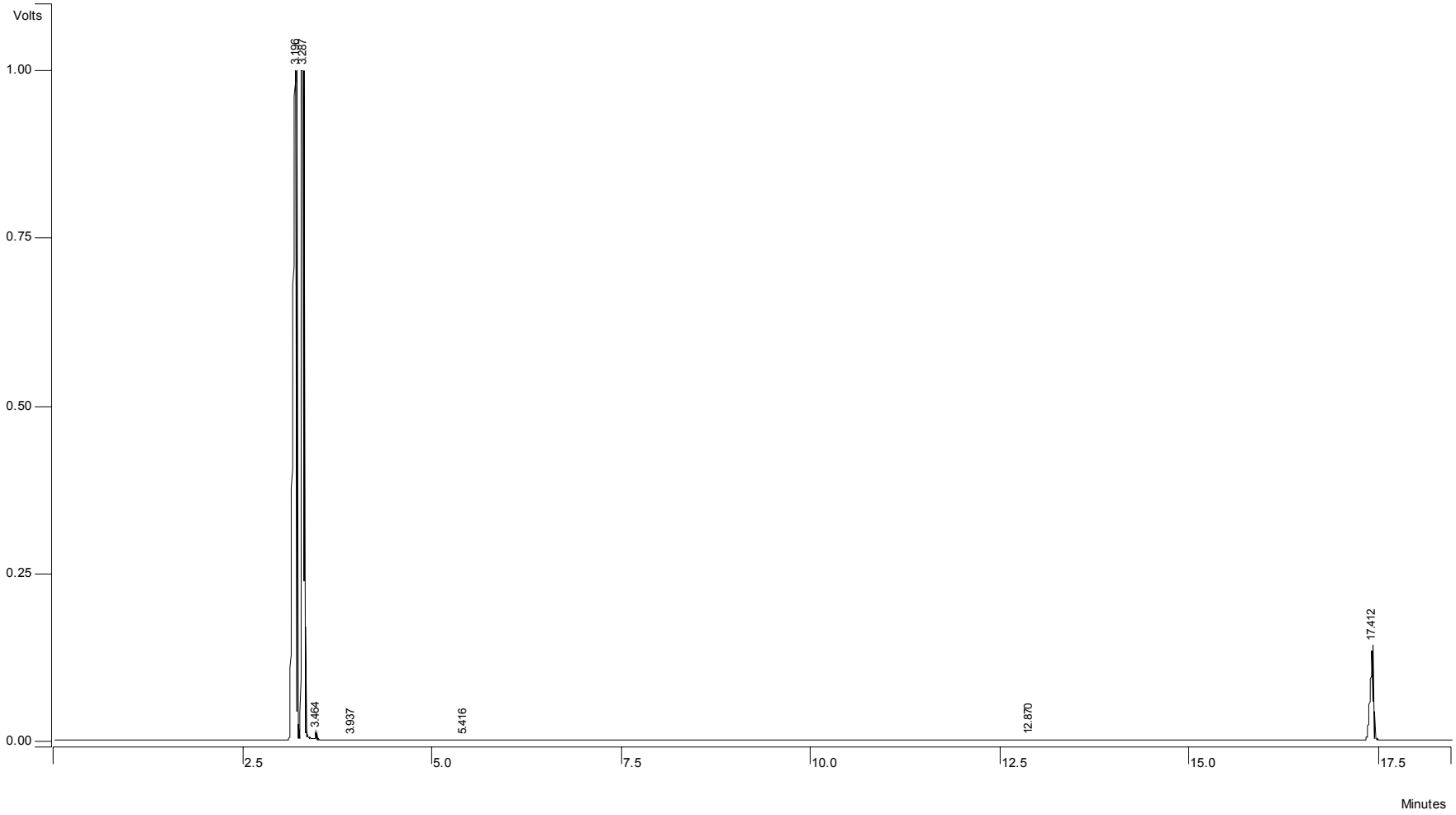

Figure 4.67. GC chromatogram for biphenyl (2% biphenyl, 49% acetonitrile, and 49% tetrahydrofuran)

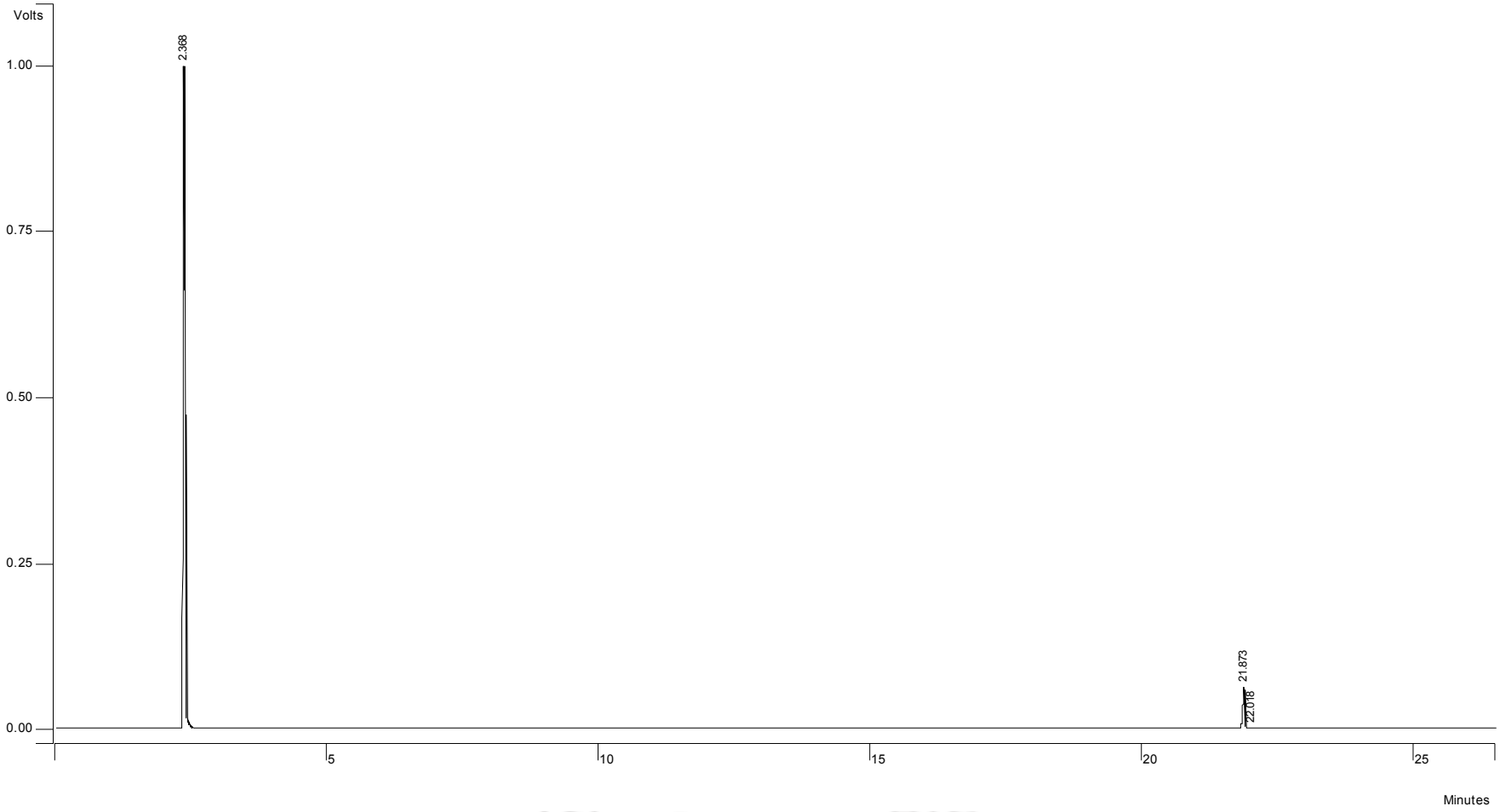

Figure 4.68. GC chromatogram for fluorene (0.5% fluorene, methanol 99.5%)

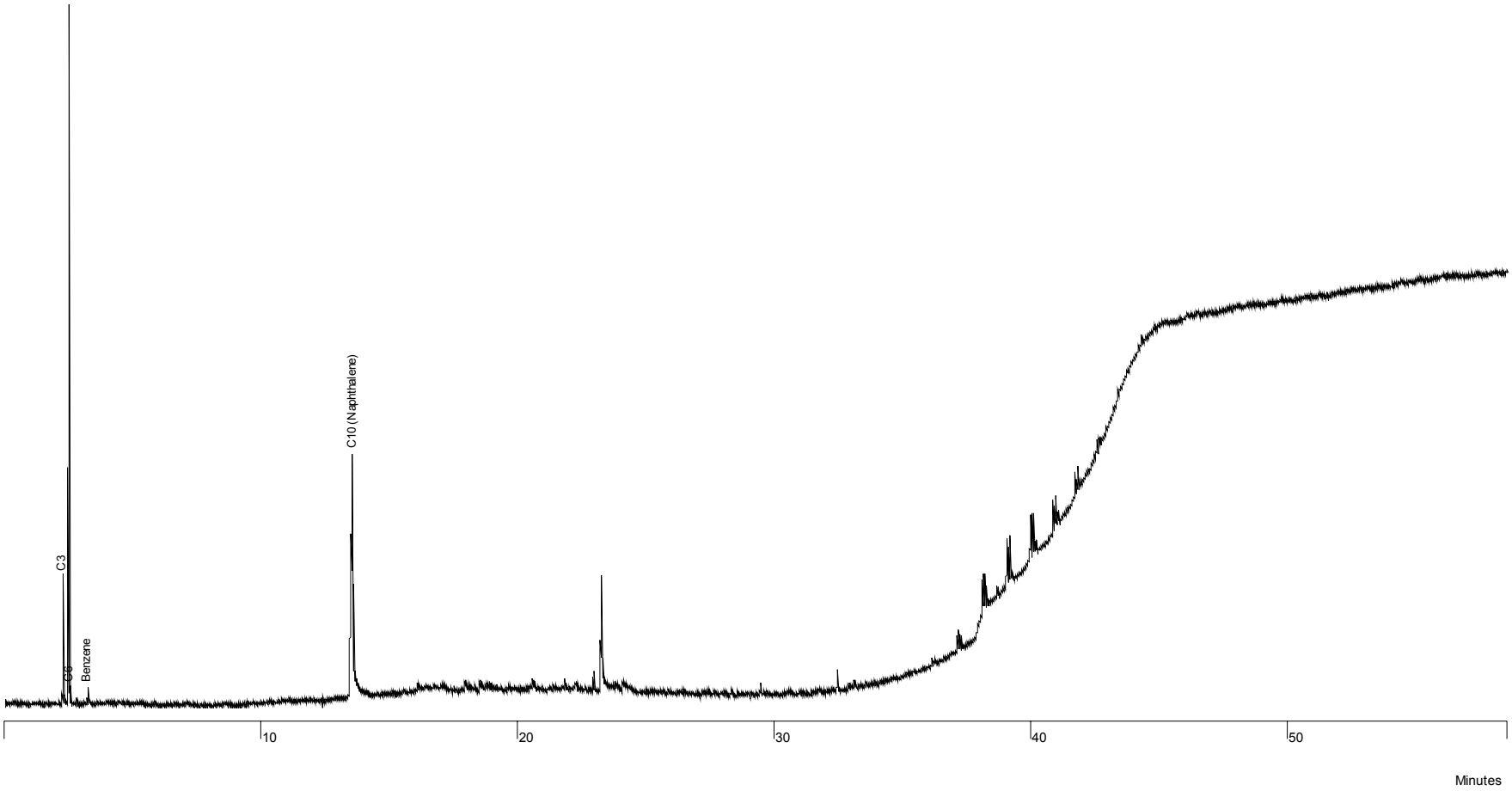

Figure 4.69. GC chromatogram for the thermal decomposition of waste PET

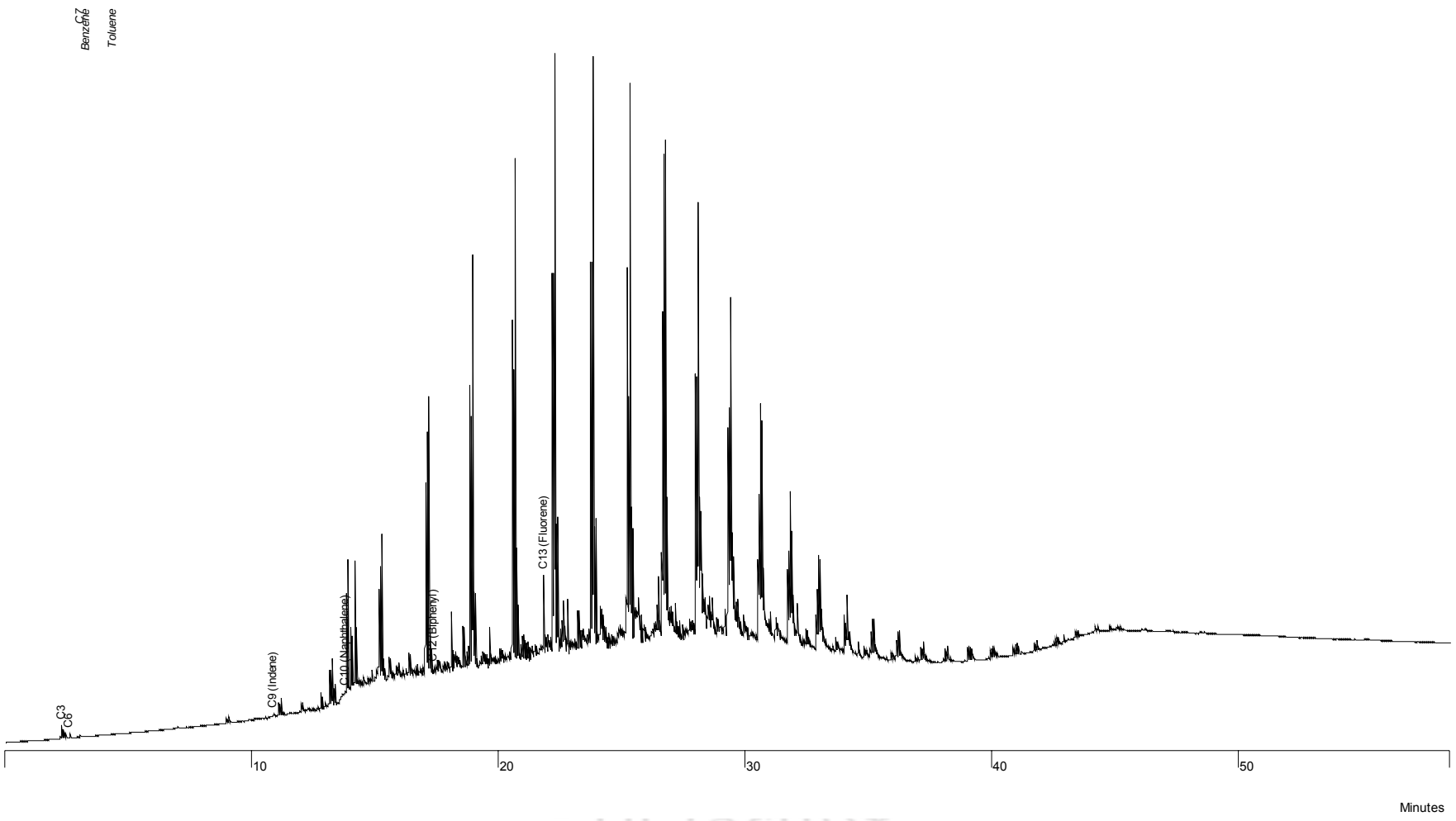

Figure 4.70. GC chromatogram for the thermal decomposition of waste LDPE sample

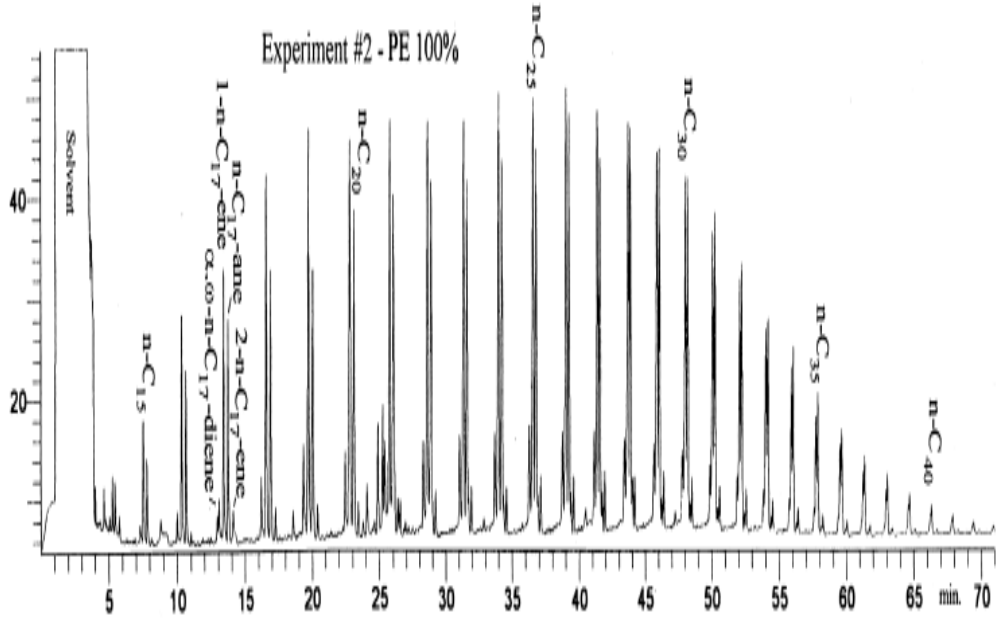

Figure 4.71. GC plot for the thermal decomposition of LDPE [27]

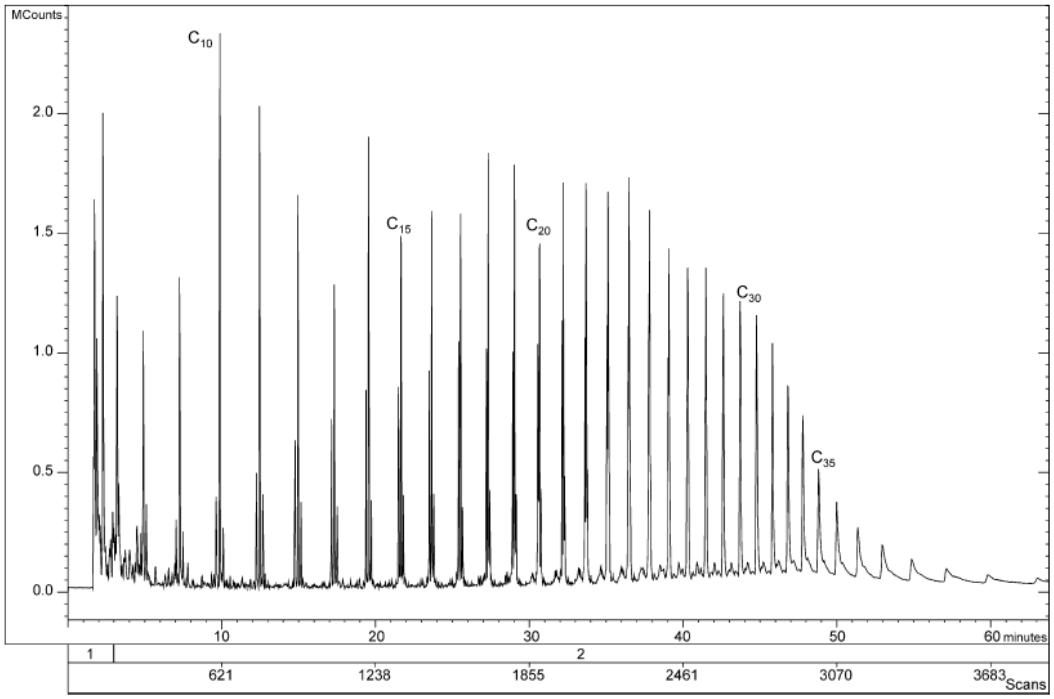

Figure 4.72. GC plot for the thermal decomposition of LDPE [**66**]

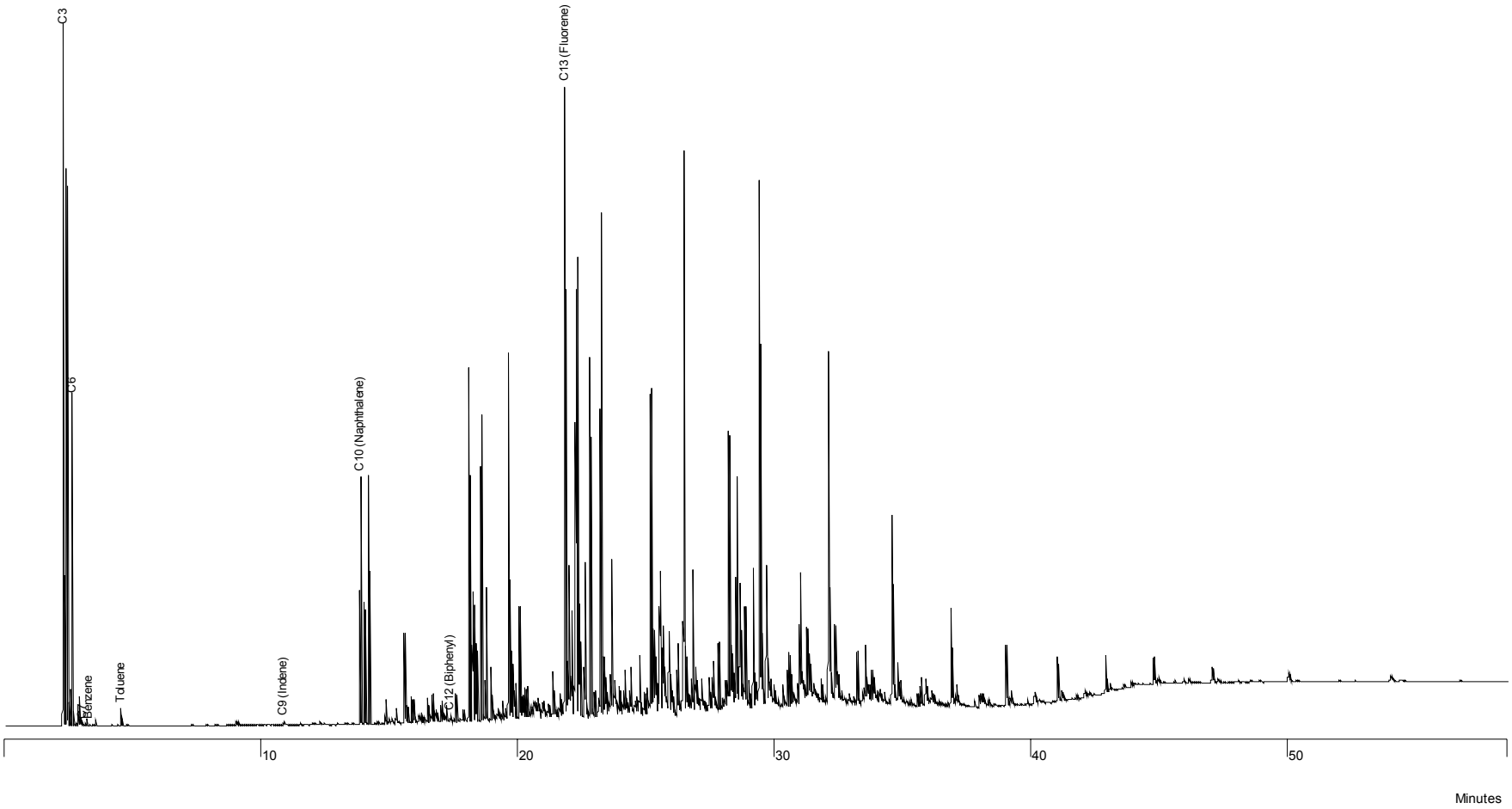

Figure 4.73. GC chromatogram for the thermal decomposition of PP sample

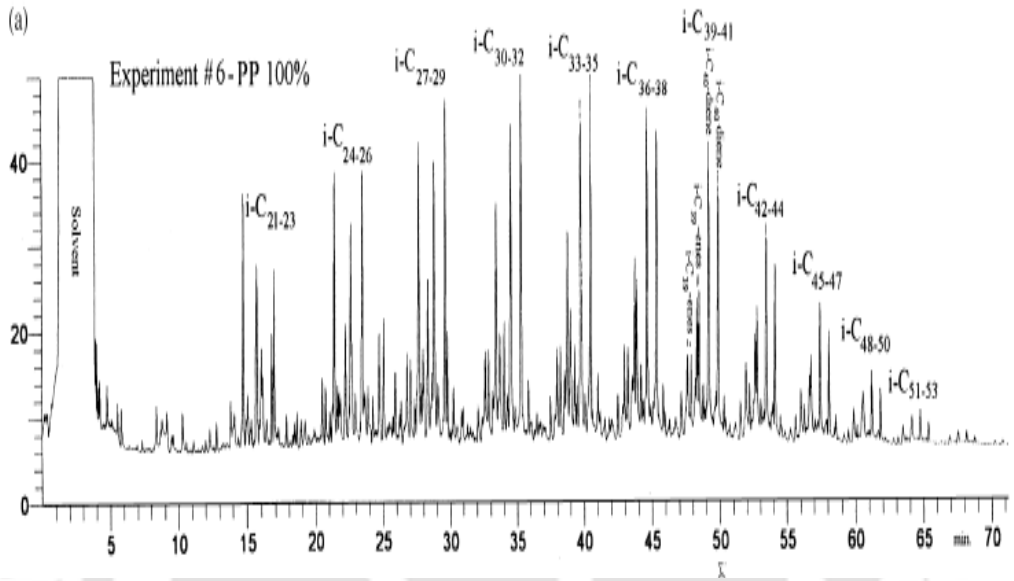

Figure 4.74. GC plot for the thermal decomposition of PP sample [27]

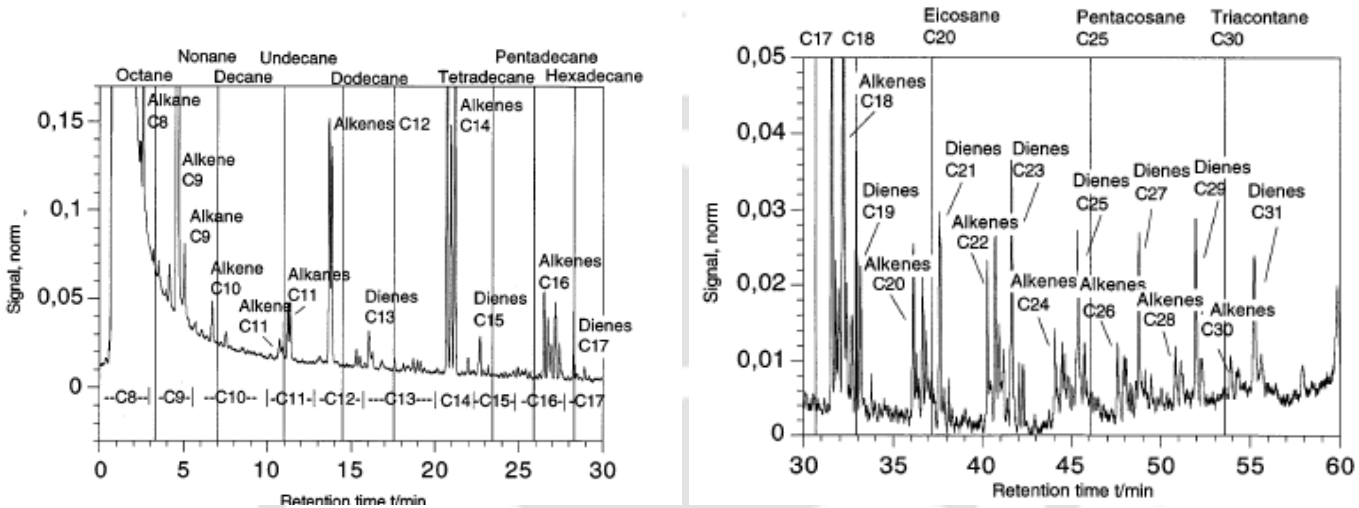

Figure 4.75. GC plot for the thermal decomposition of PP sample [51]

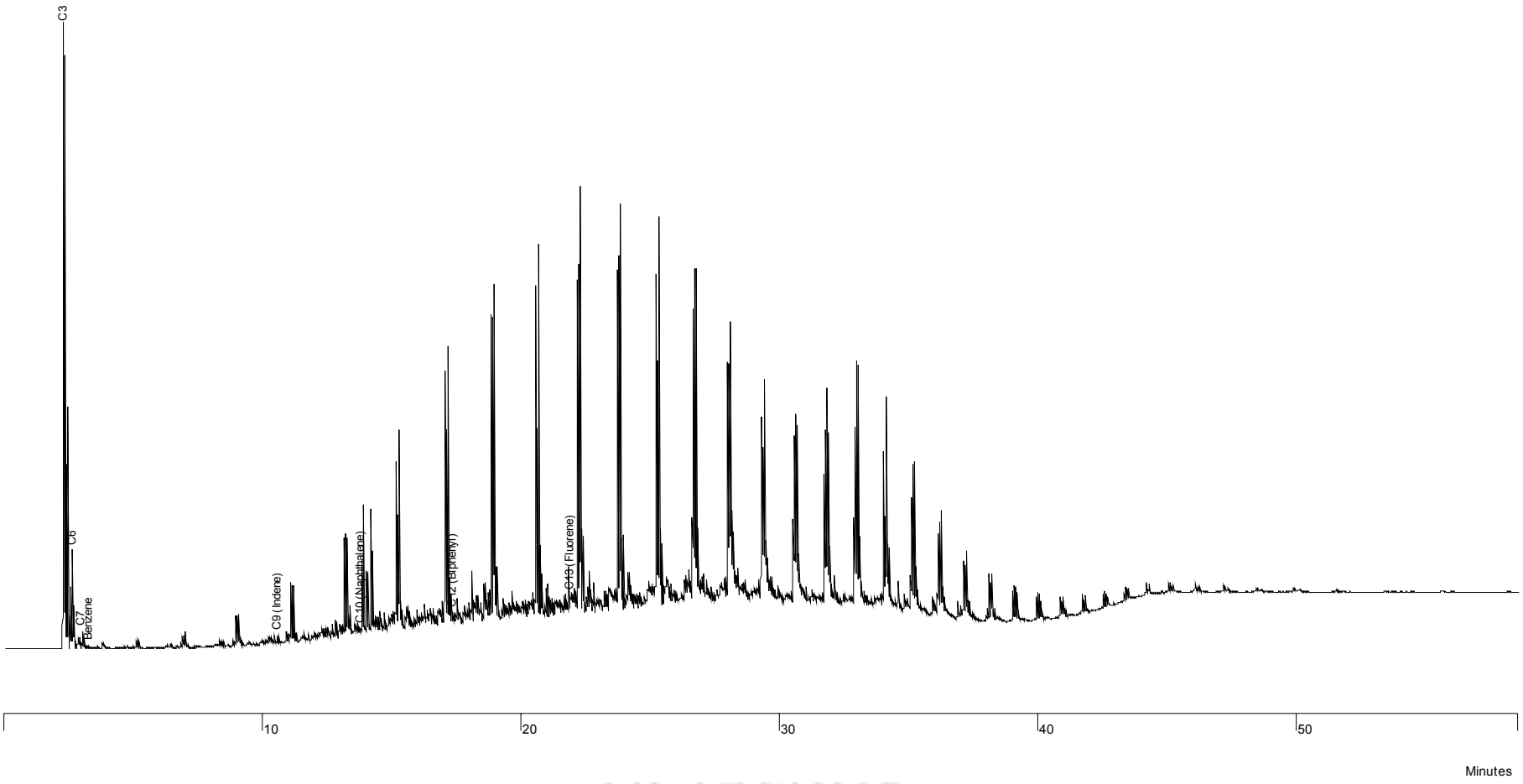

Figure 4.76. GC plot for the catalytic decomposition of waste LDPE over fresh FCC catalysts

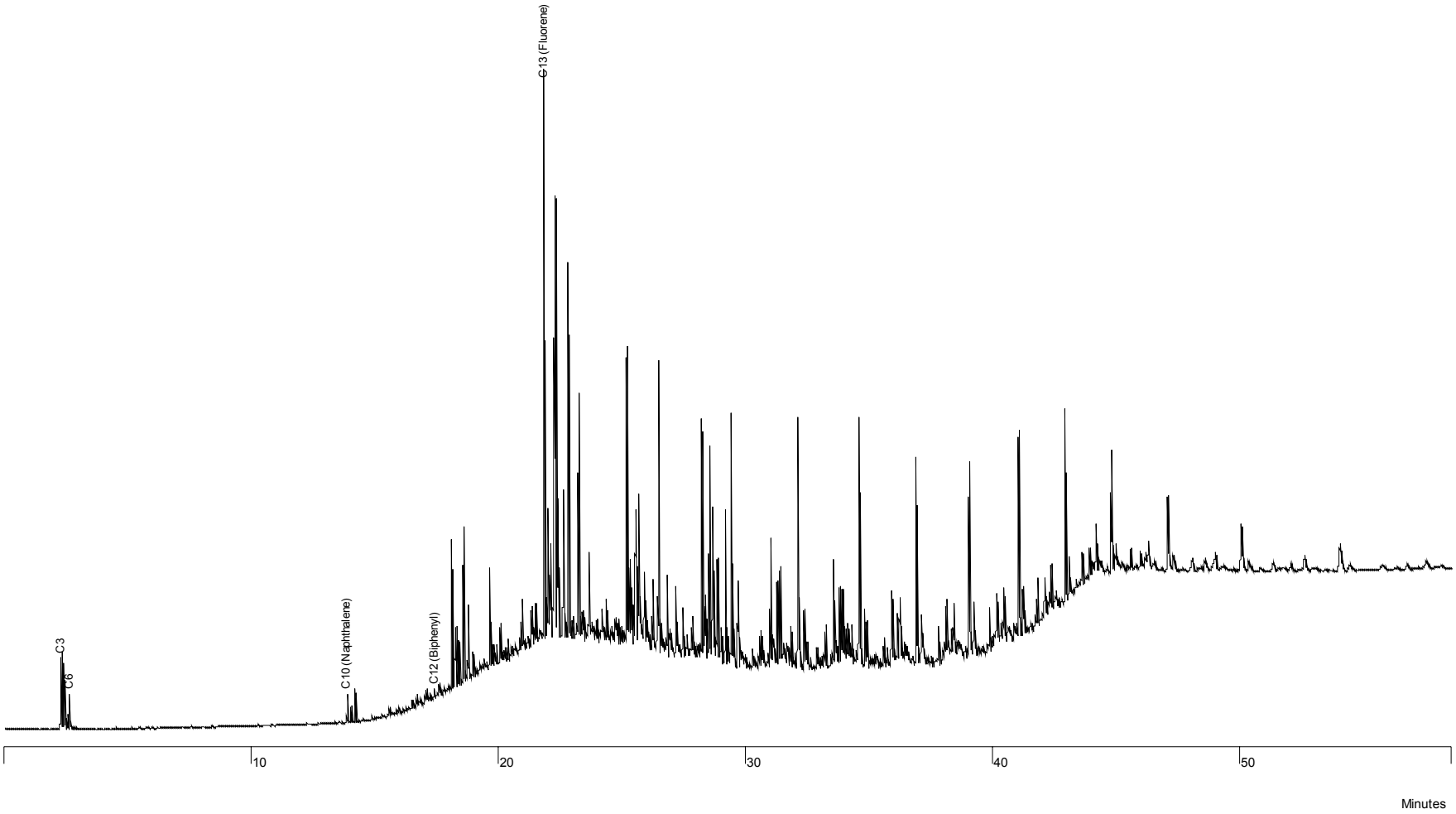

Figure 4.77. GC plot for the catalytic decomposition of PP over fresh FCC catalysts

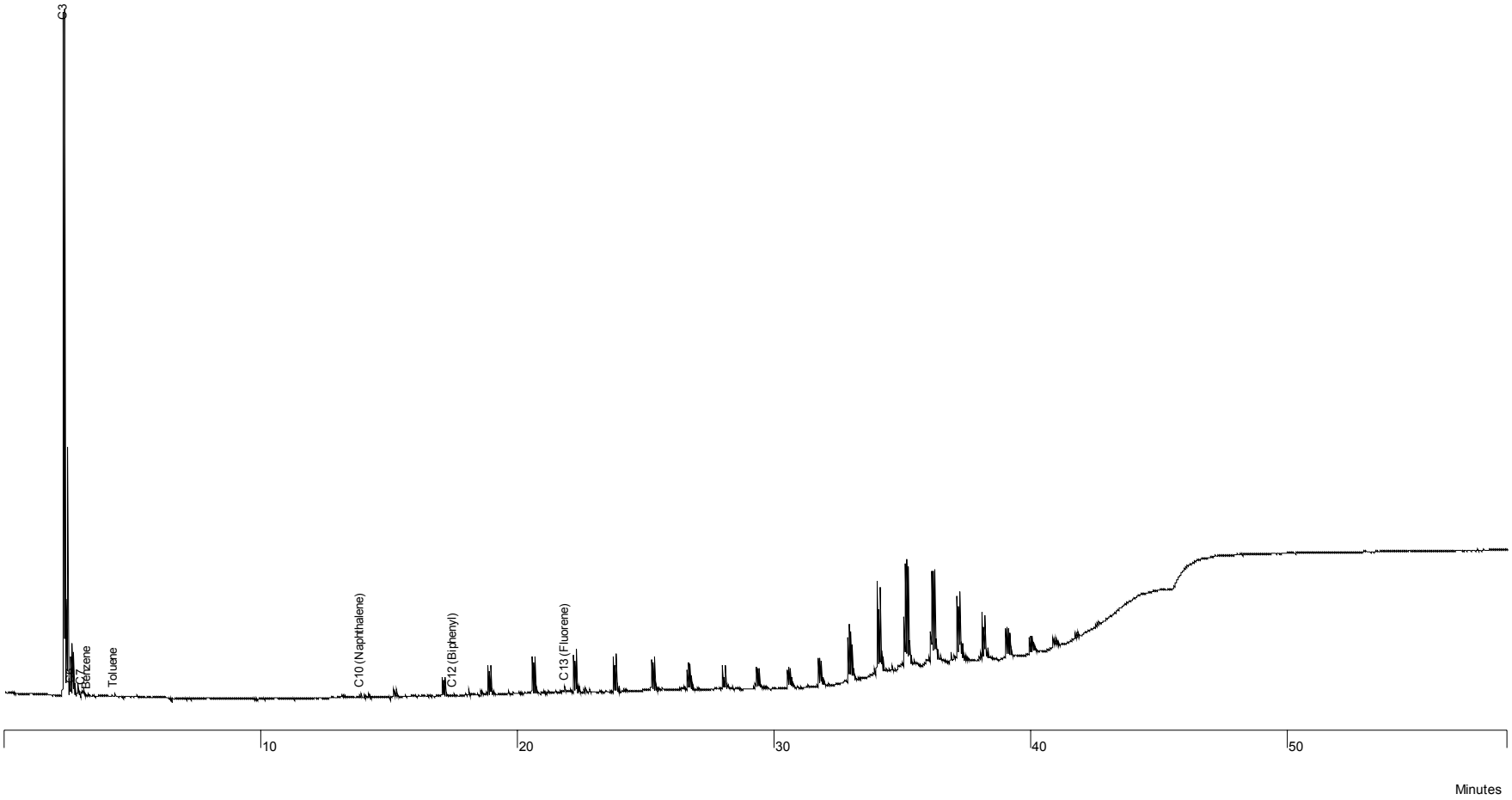

Figure 4.78. GC plot for the catalytic decomposition of waste LDPE over ZSM-5 catalysts

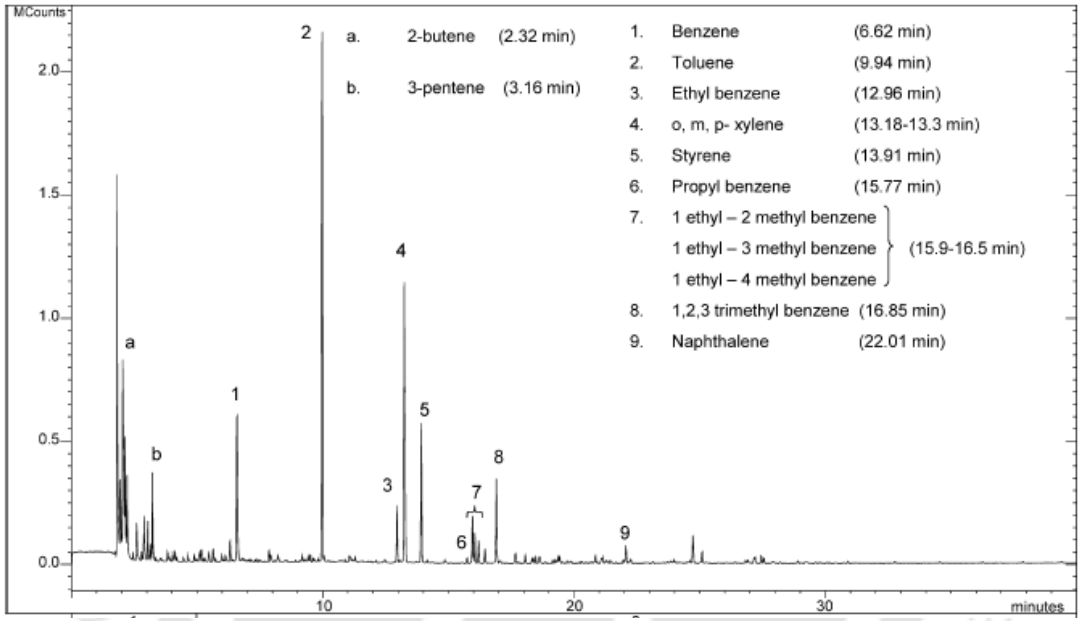

Figure 4.79. GC plot for the catalytic decomposition of waste LDPE over ZSM-5 catalysts [66]

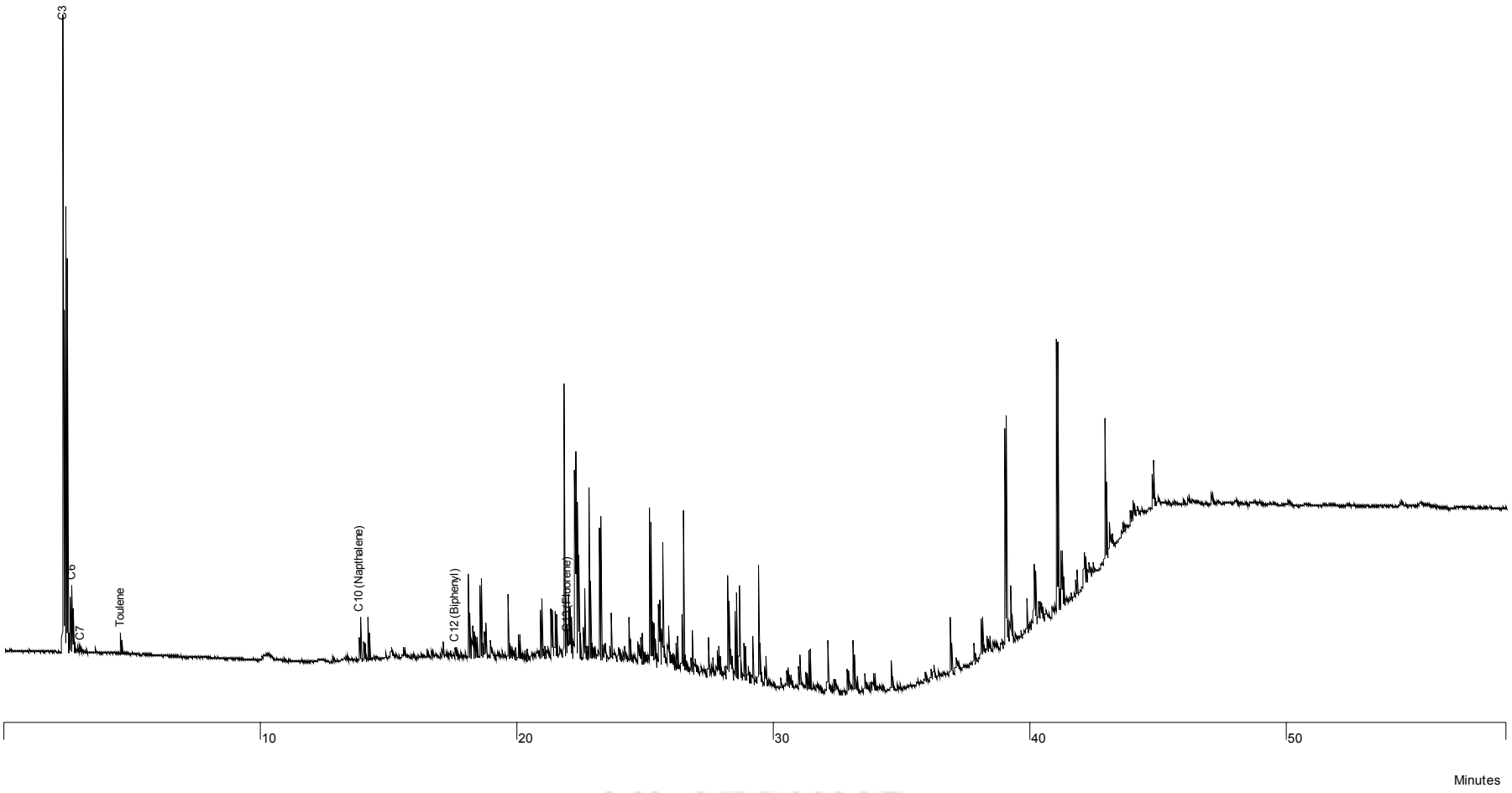

Figure 4.80. GC plot for the catalytic decomposition of PP over ZSM-5 catalysts

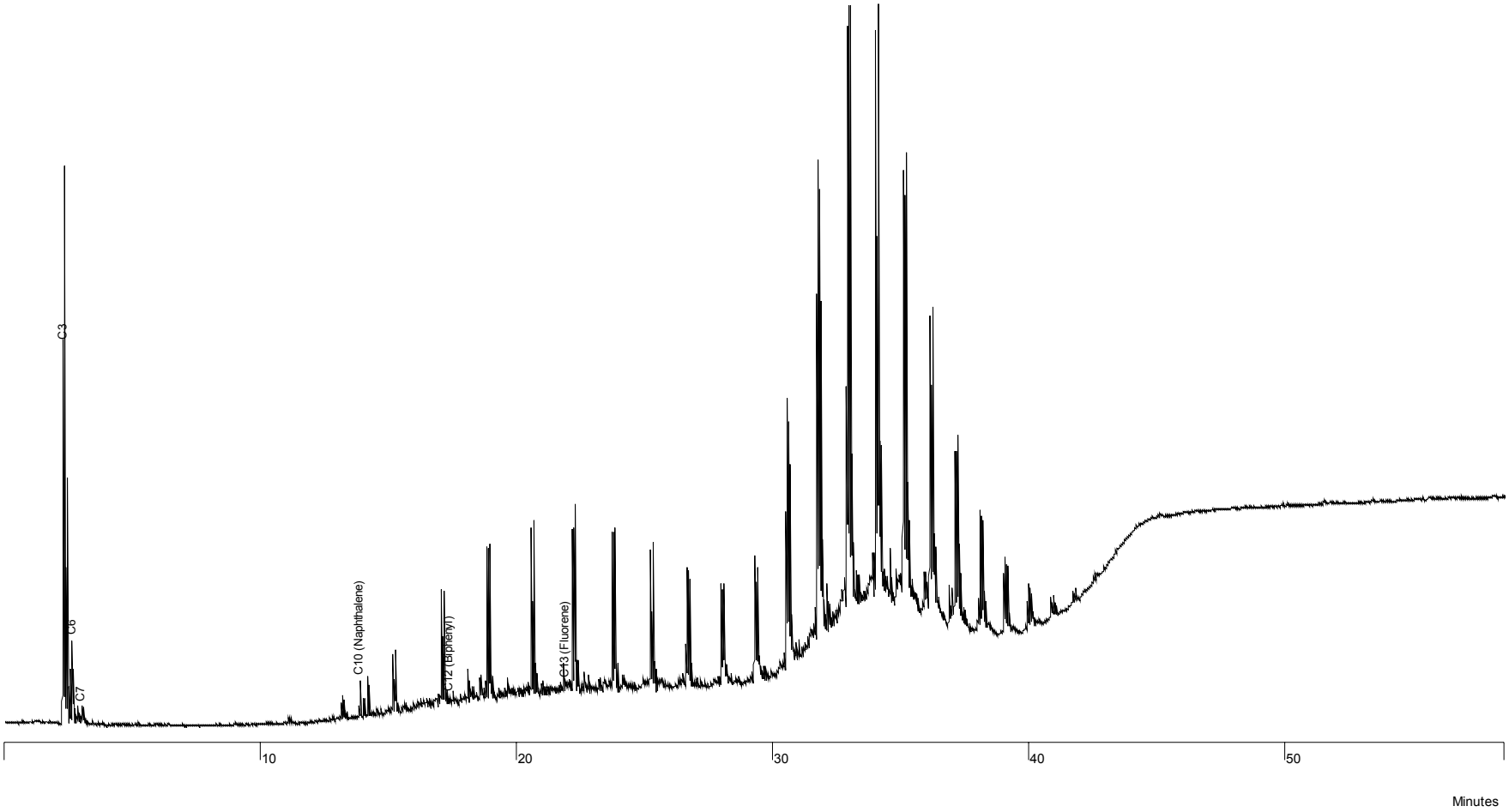

Figure 4.81. GC plot for the catalytic decomposition of waste LDPE over Al-MCM-41 catalysts

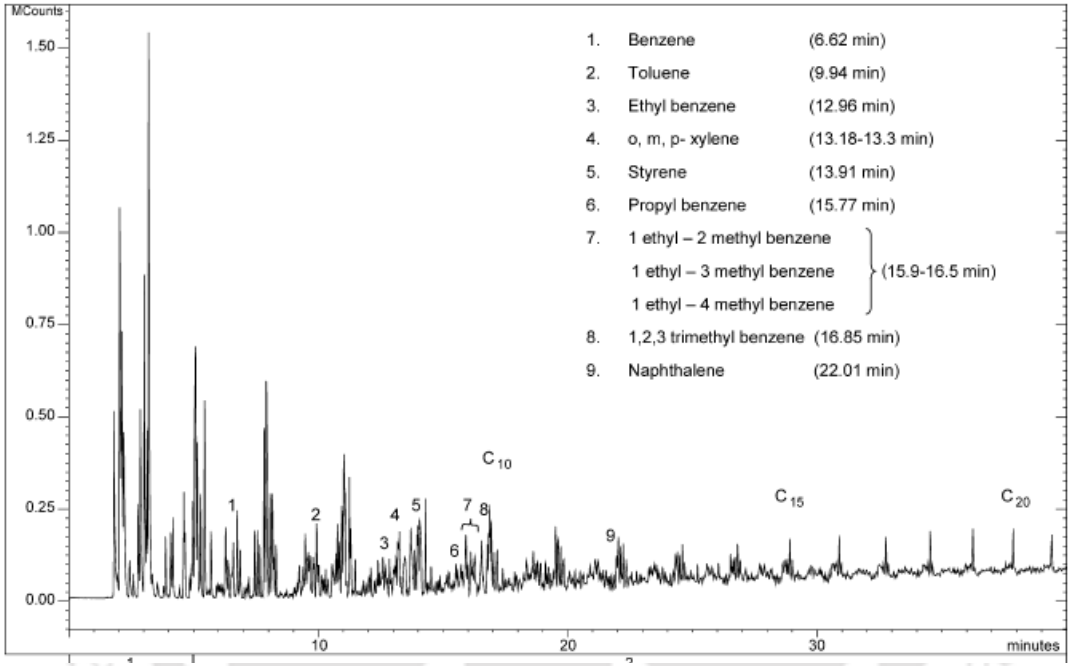

Figure 4.82. GC plot for the catalytic decomposition of waste LDPE over Al-MCM-41 catalysts [66]

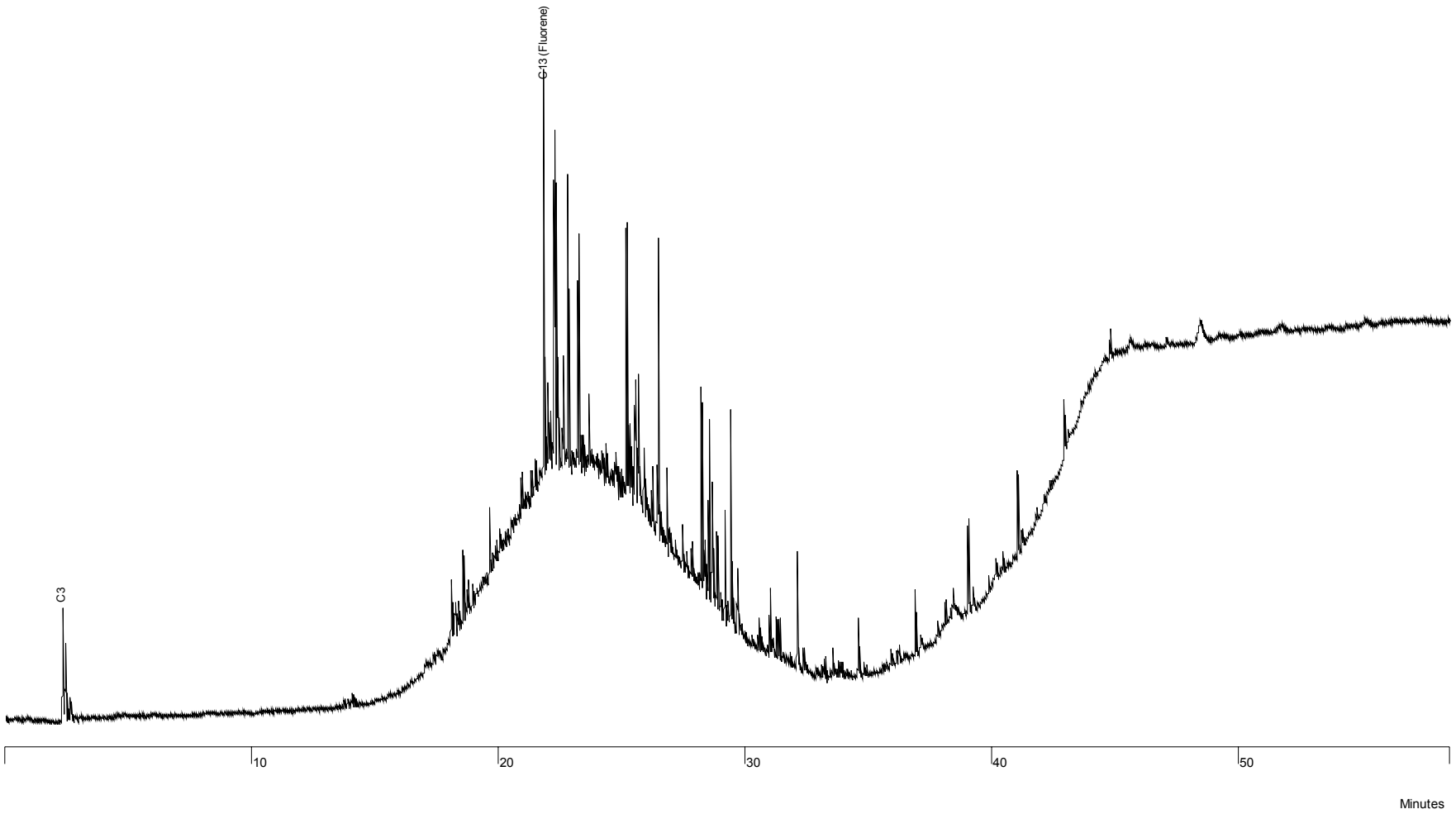

Figure 4.83. GC plot for the catalytic decomposition of PP over Al-MCM-41 catalysts

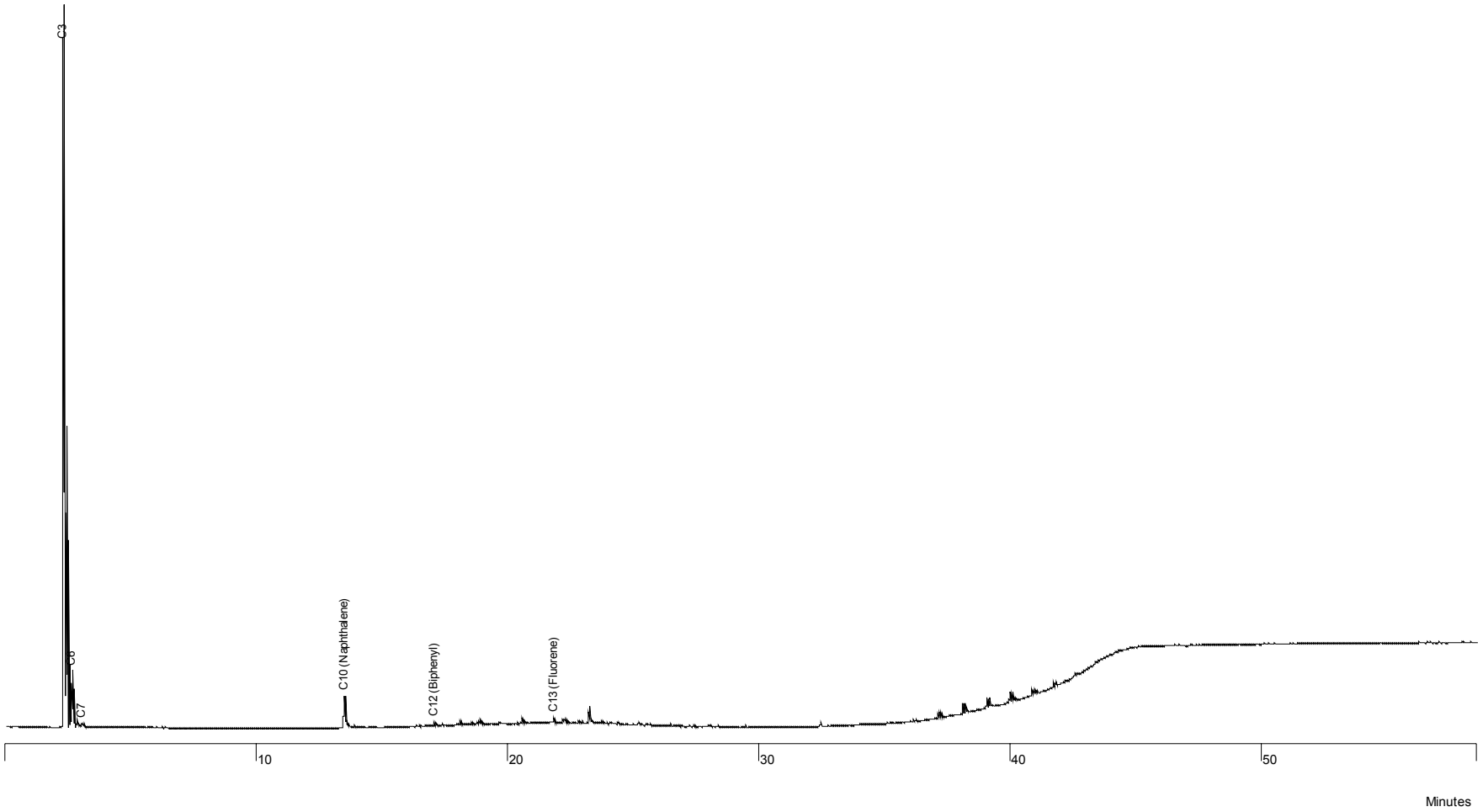

Figure 4.84. GC plot for the catalytic decomposition of waste LDPE over n-HZSM-5 catalysts

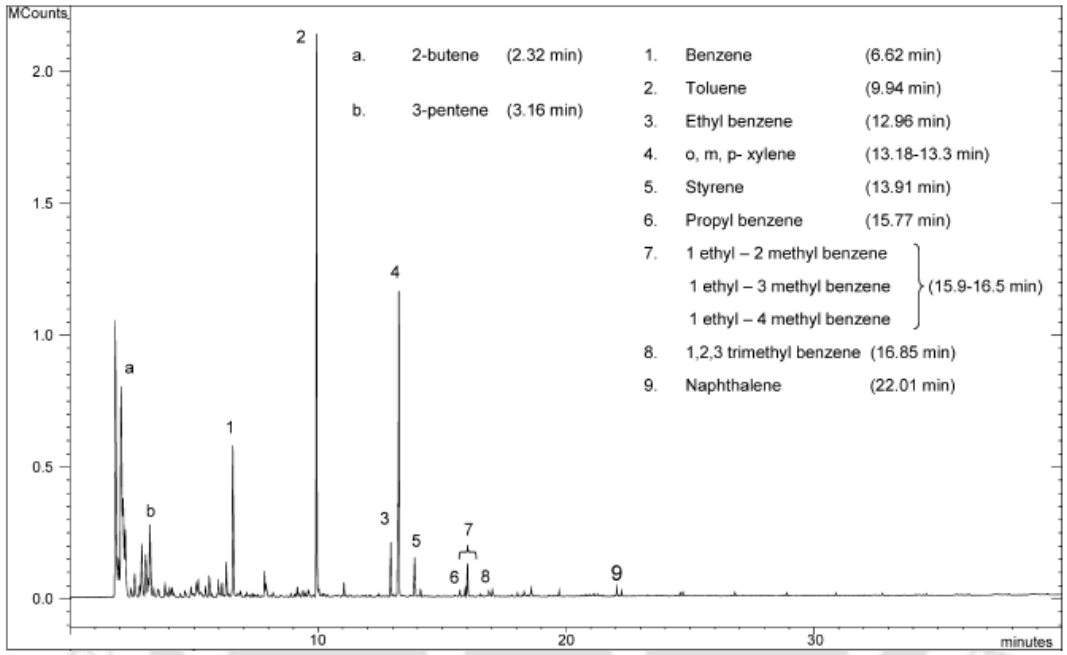

Figure 4.85. GC plot for the catalytic decomposition of waste LDPE over n-HZSM-5 catalysts [66]

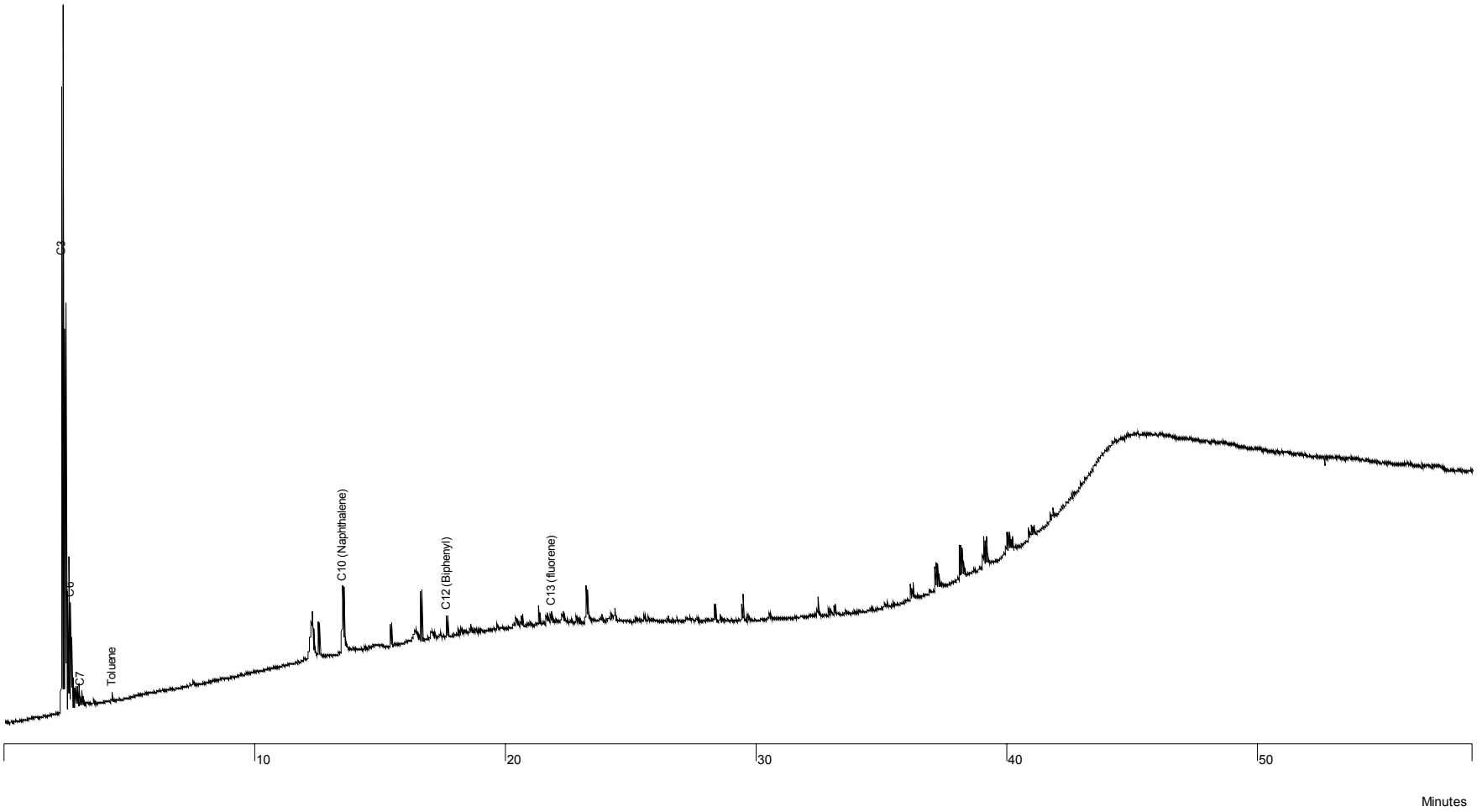

Figure 4.86. GC plot for the catalytic decomposition of PP over n-HZSM-5 catalysts

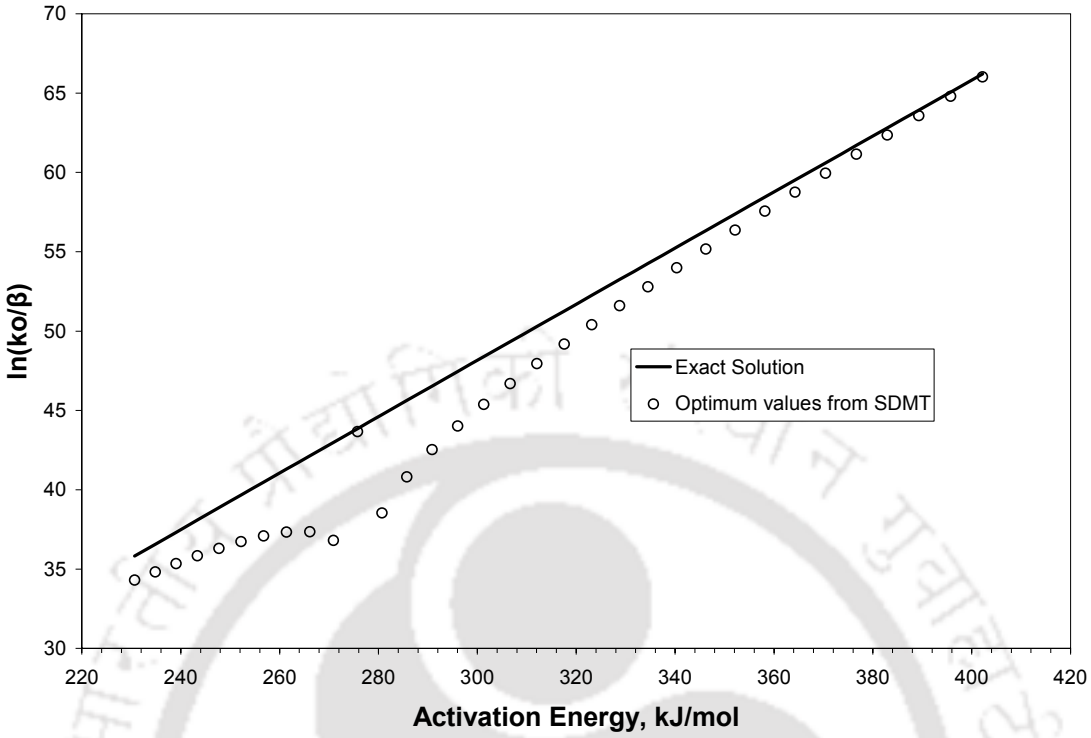

Figure 4.87. Dependency of exact and optimal $\ln(k_0/\beta)$ upon optimal E obtained from SDMT technique

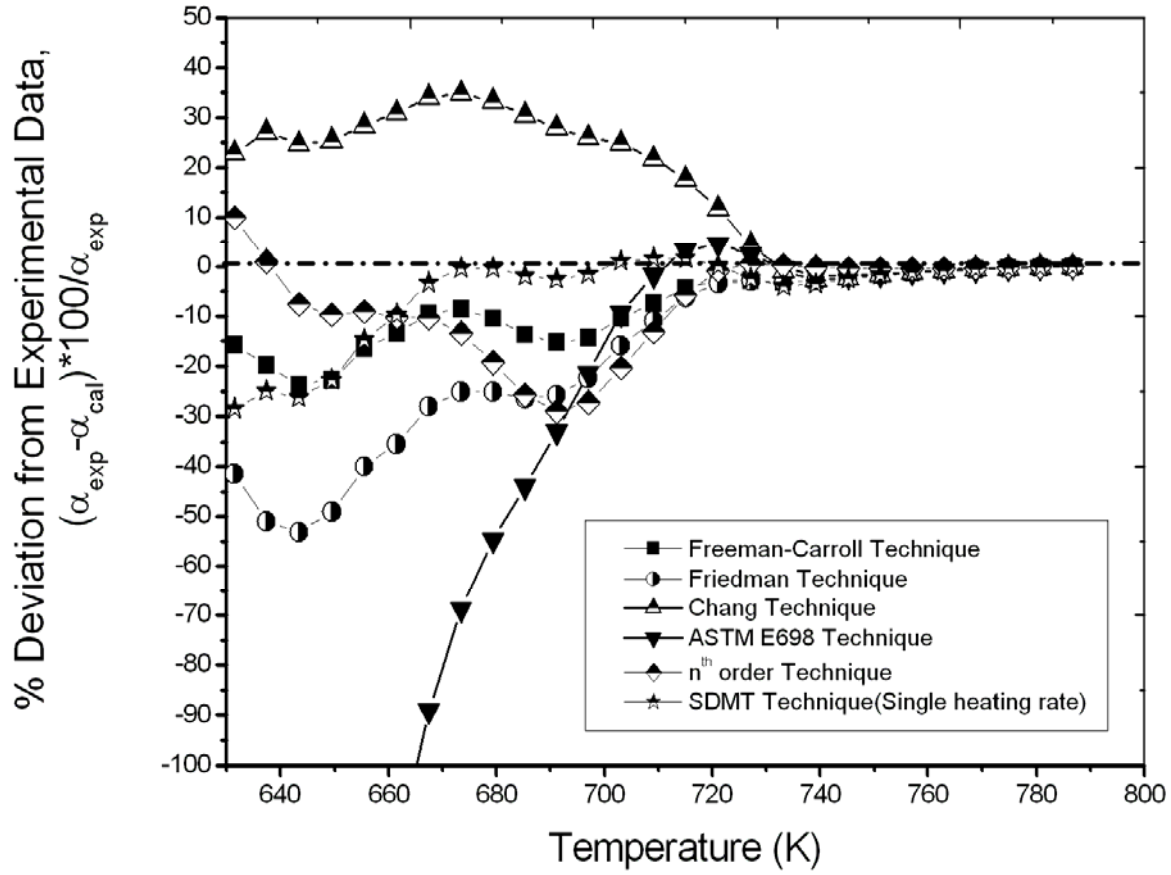

Figure 4.88. Percentage deviation of the simulation results for nonisothermal decomposition at 10Kmin^{-1} heating rate

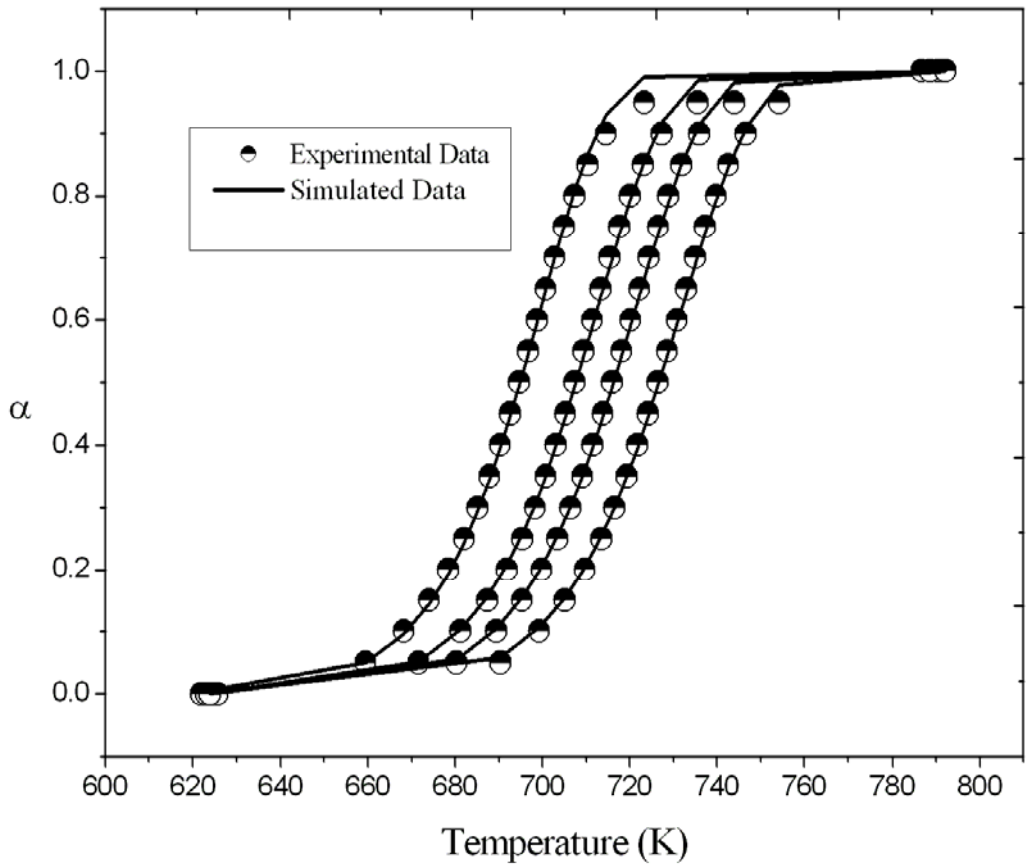

Figure 4.89. Simulations and the experimental data for nonisothermal decomposition (waste PET) using SDMT (multiple heating rates) for first order model

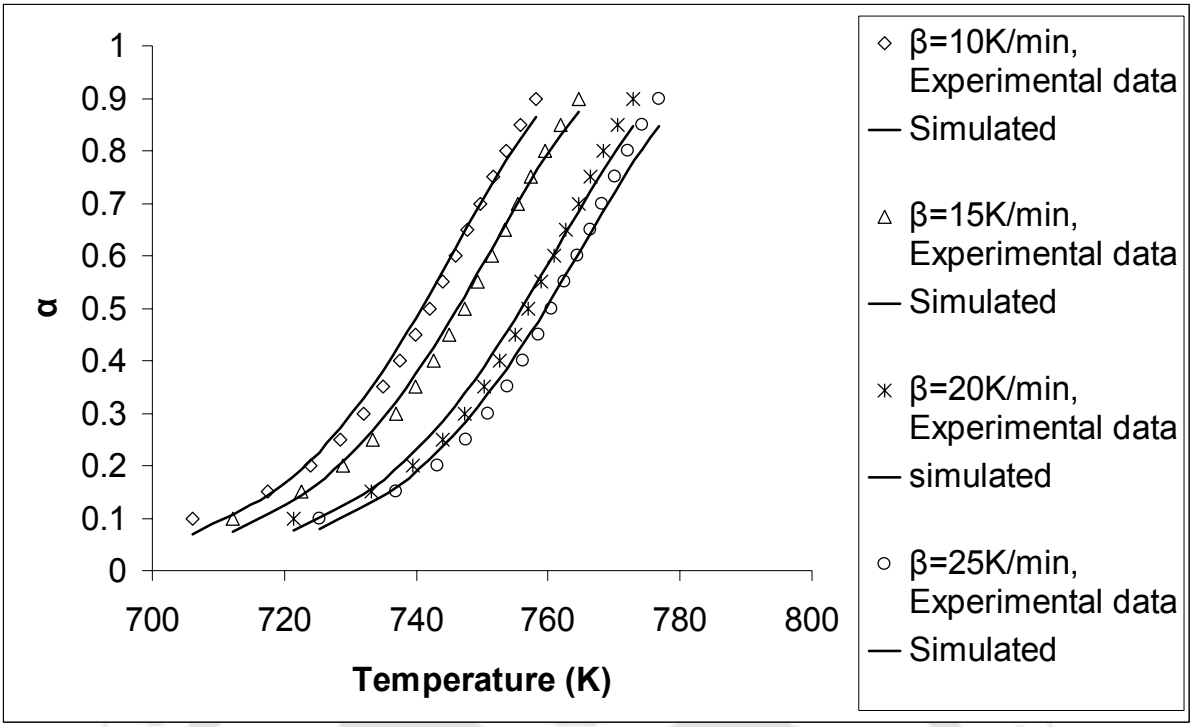

Figure 4.90. Simulations and the experimental data for nonisothermal decomposition (waste PE) for first order model (with standard deviation 0.02314, 0.03063, 0.002266 and 0.030359 respectively)

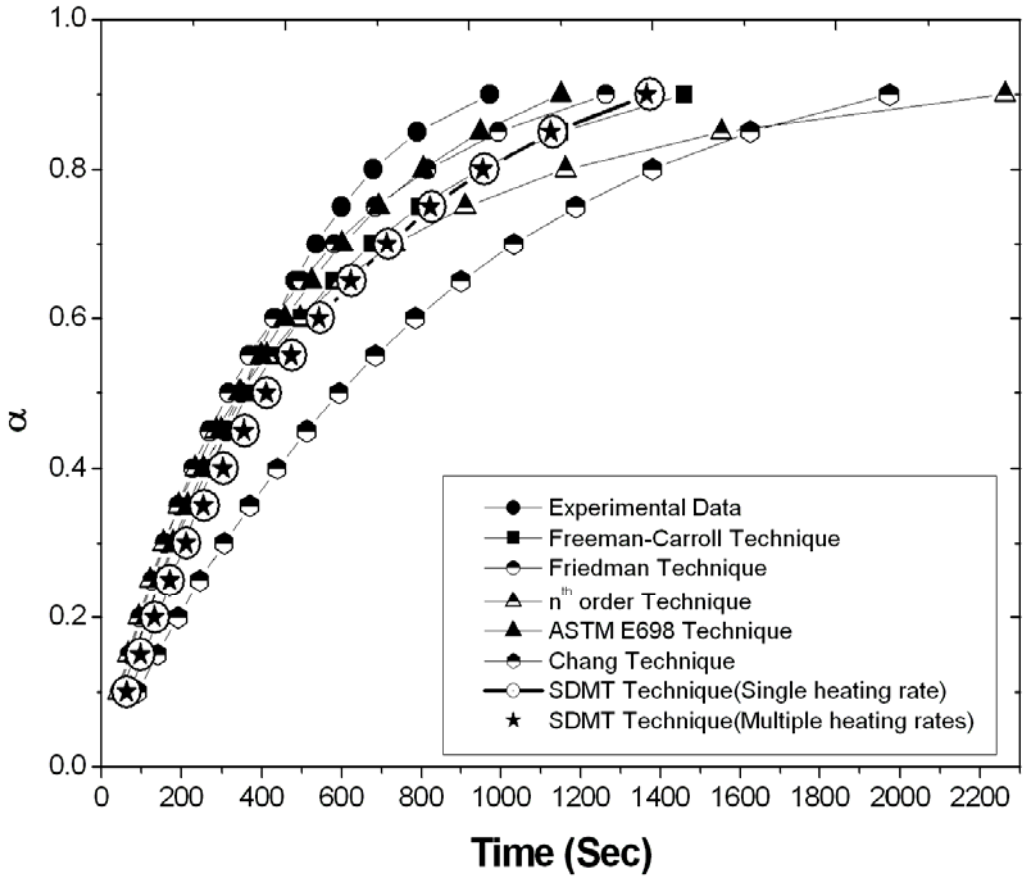

Figure 4.91. Isothermal (685K) prediction from various model fitting kinetics analysis techniques at a heating rate of 10K min^{-1}

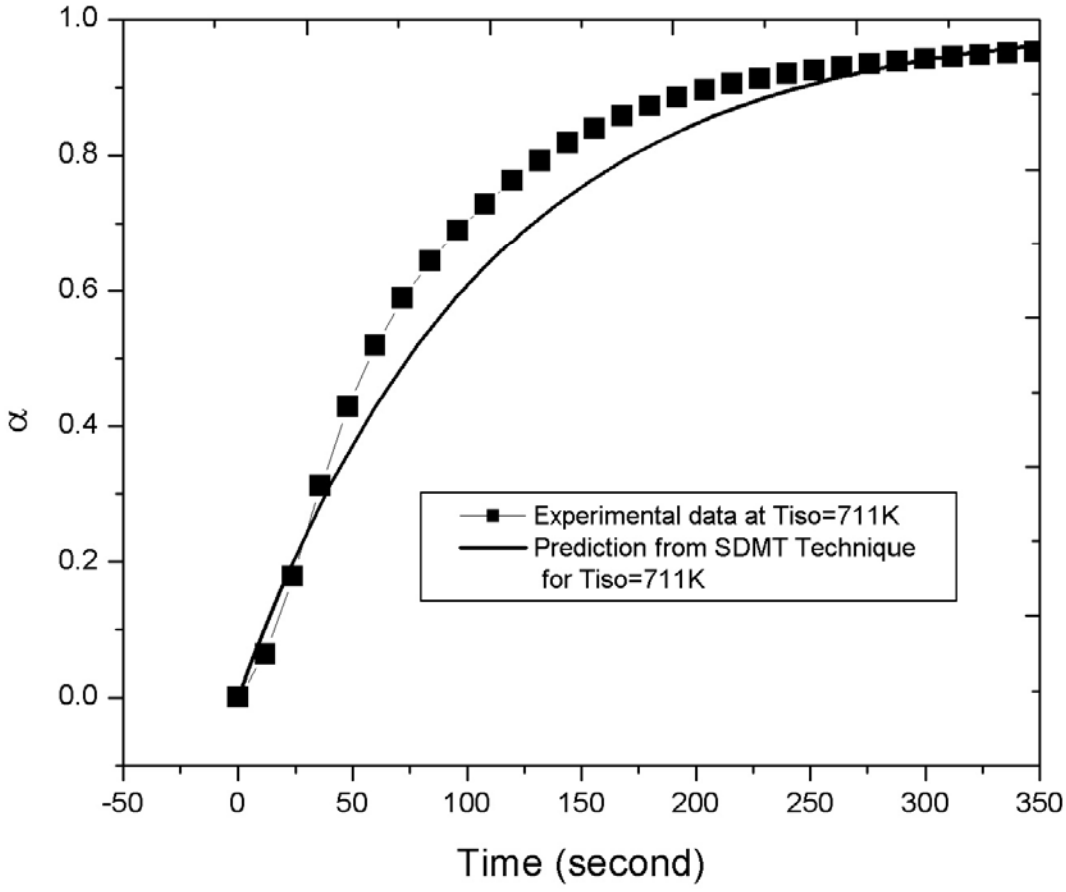

Figure 4.92. Isothermal (711K) prediction from SDMT (multiple heating rates)

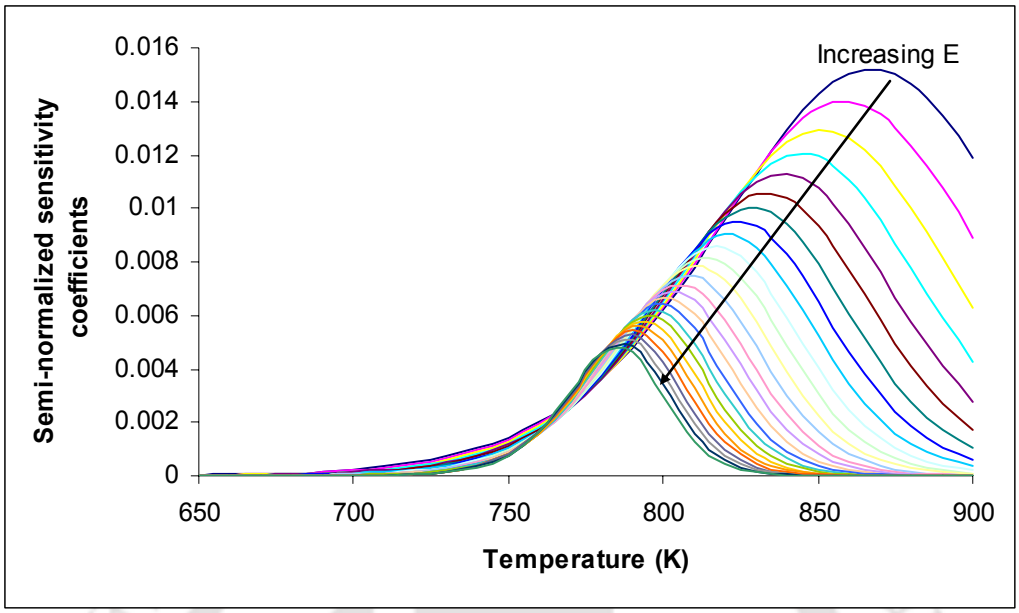

Figure 4.93. Dependency of first order sensitivity coefficient on temperature for $\tilde{K}_0$

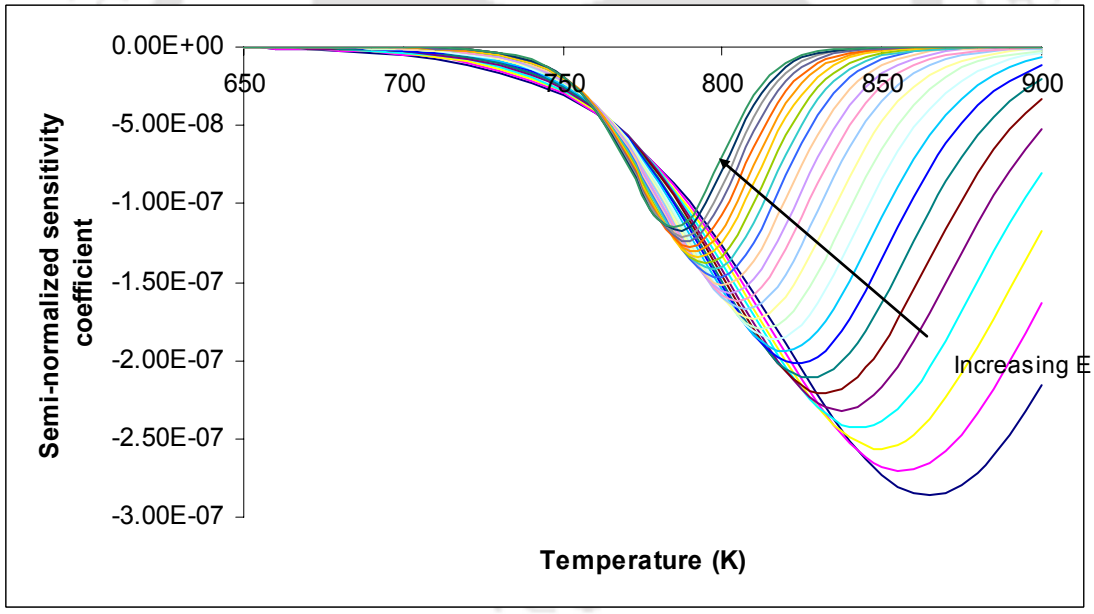

Figure 4.94. Dependency of first order sensitivity coefficient on temperature for E

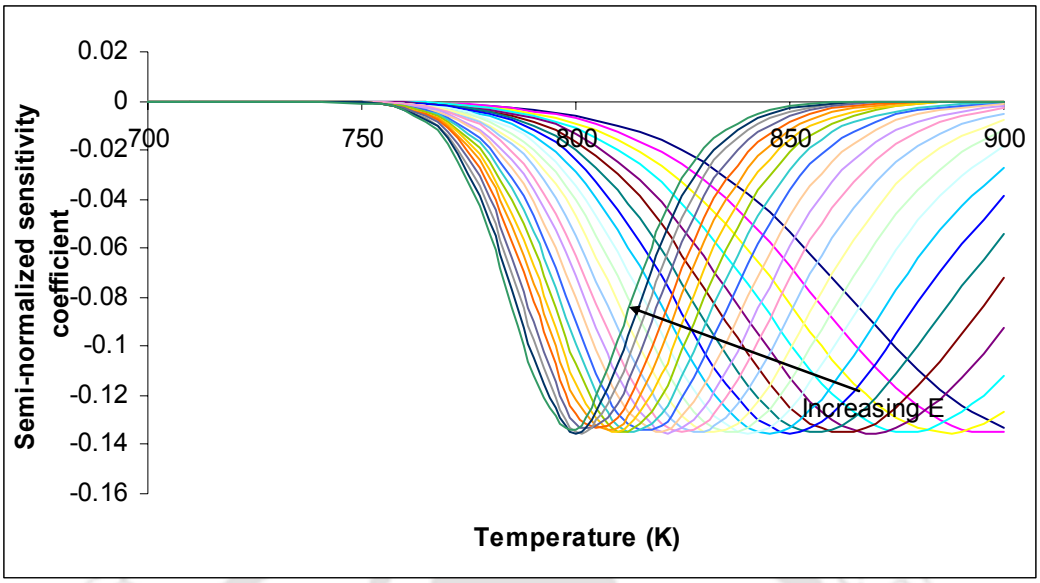

Figure 4.95. Dependency of first order sensitivity coefficient on temperature for n

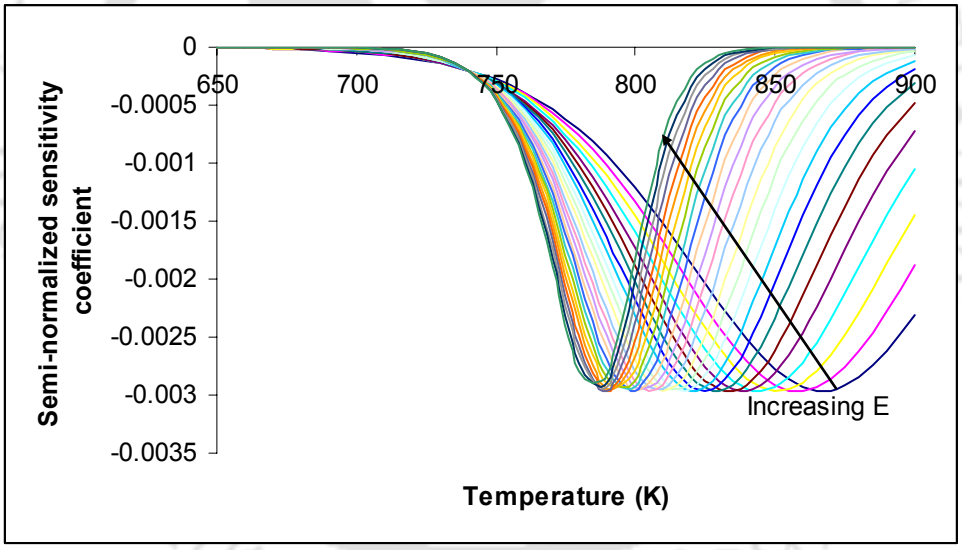

Figure 4.96. Dependency of first order sensitivity coefficient on temperature for β

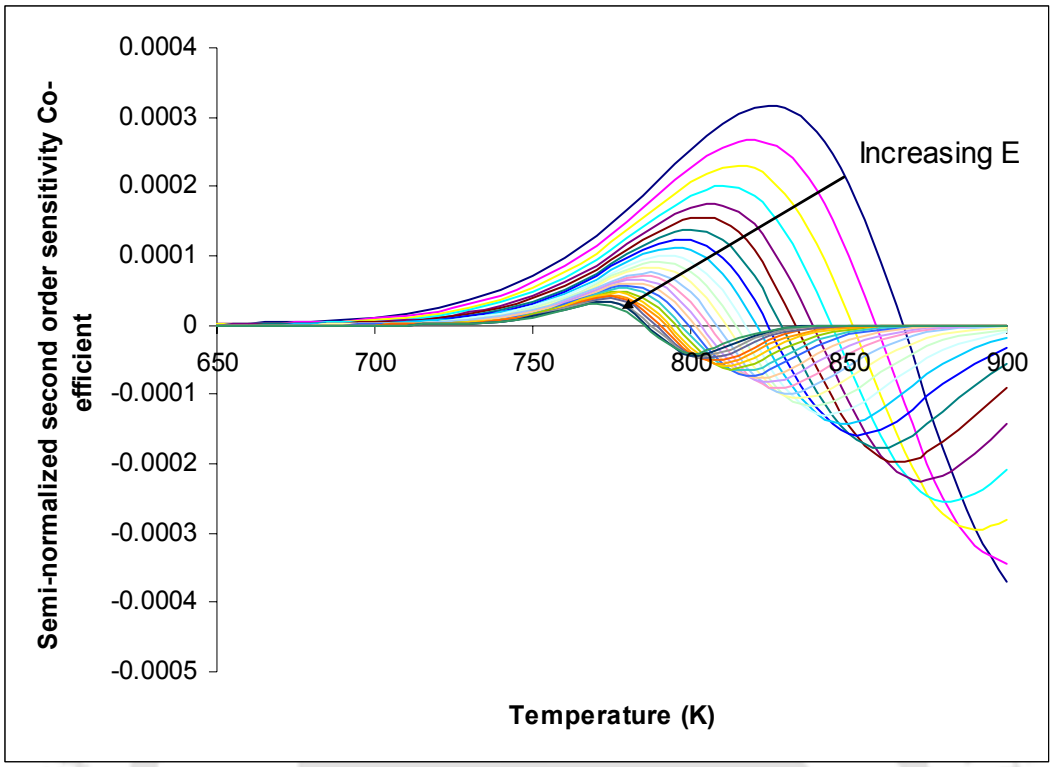

Figure 4.97. Dependency of second order sensitivity coefficient on temperature for $\tilde{K}_0$

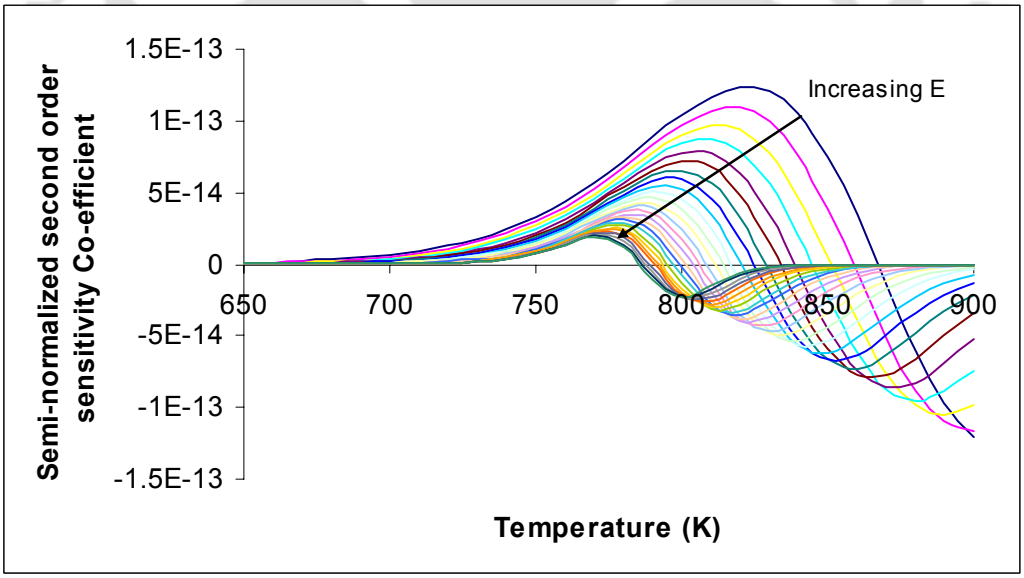

Figure 4.98. Dependency of second order sensitivity coefficient on temperature for E

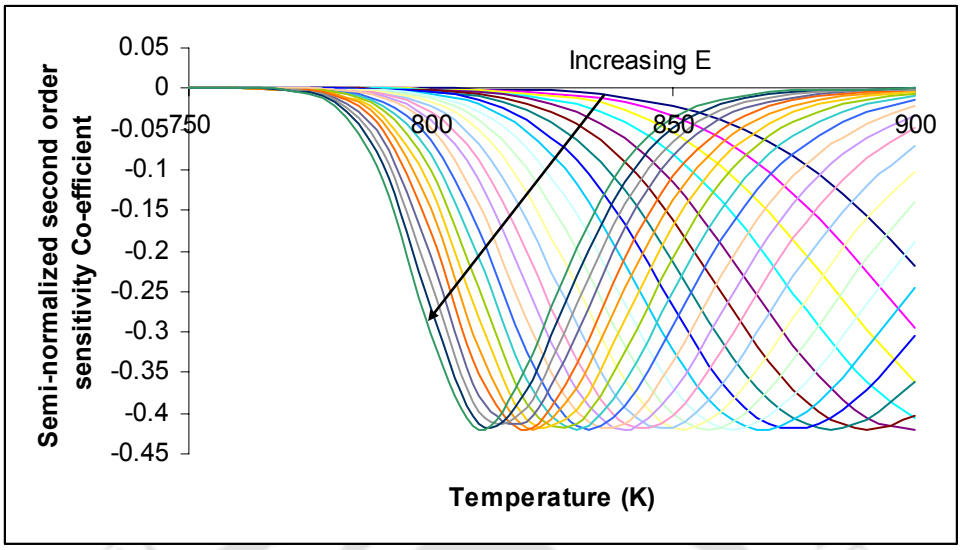

Figure 4.99. Dependency of second order sensitivity coefficient on temperature for n

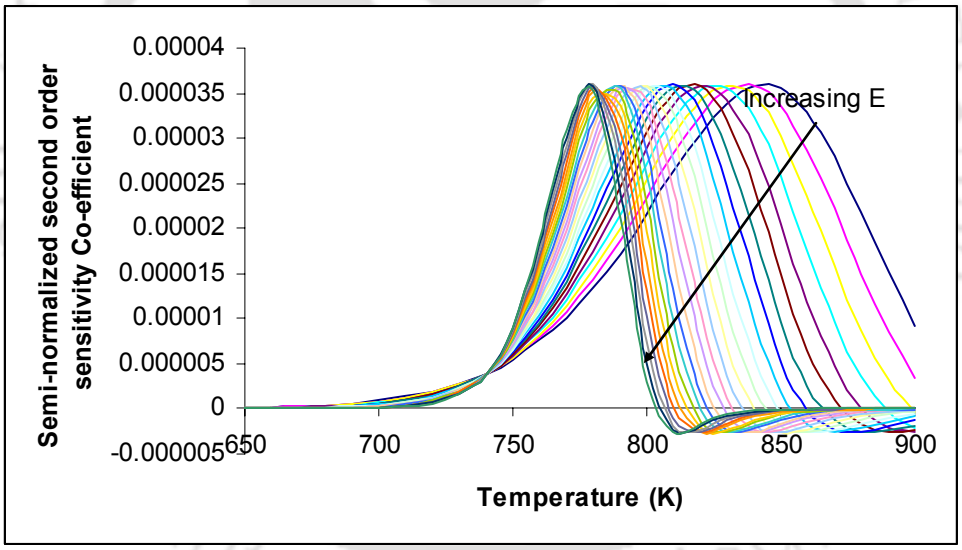

Figure 4.100. Dependency of second order sensitivity coefficient on temperature for β

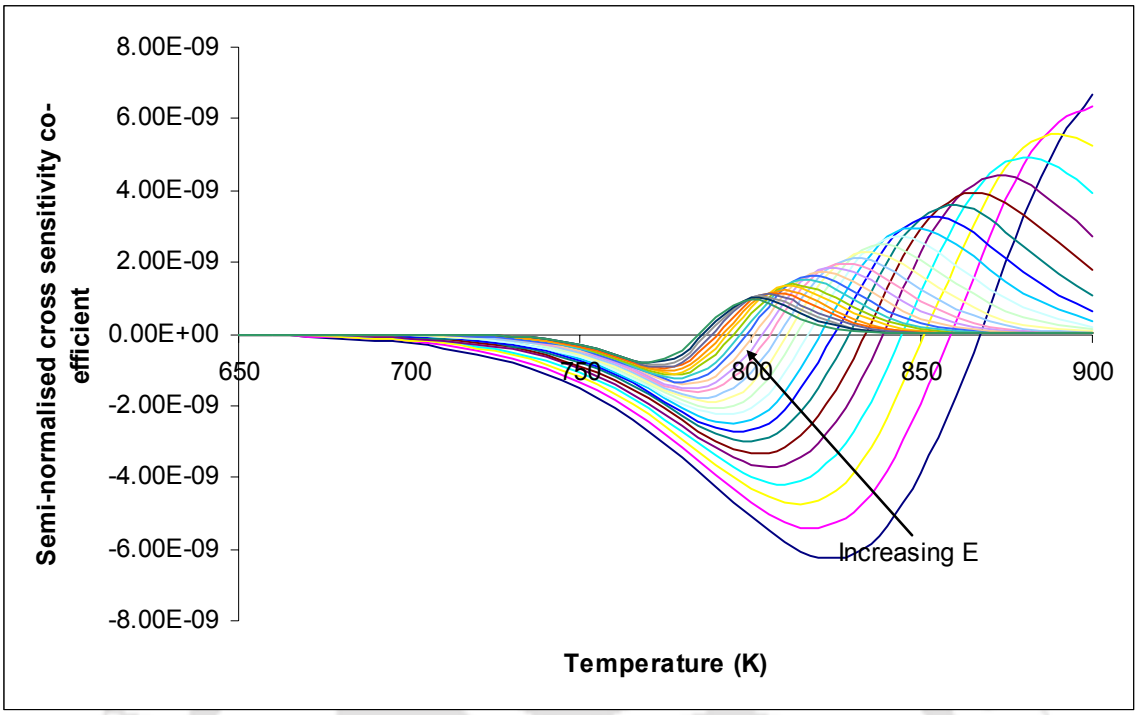

Figure 4.101. Dependency of cross second order sensitivity coefficient on temperature for $\tilde{K}_0$ E

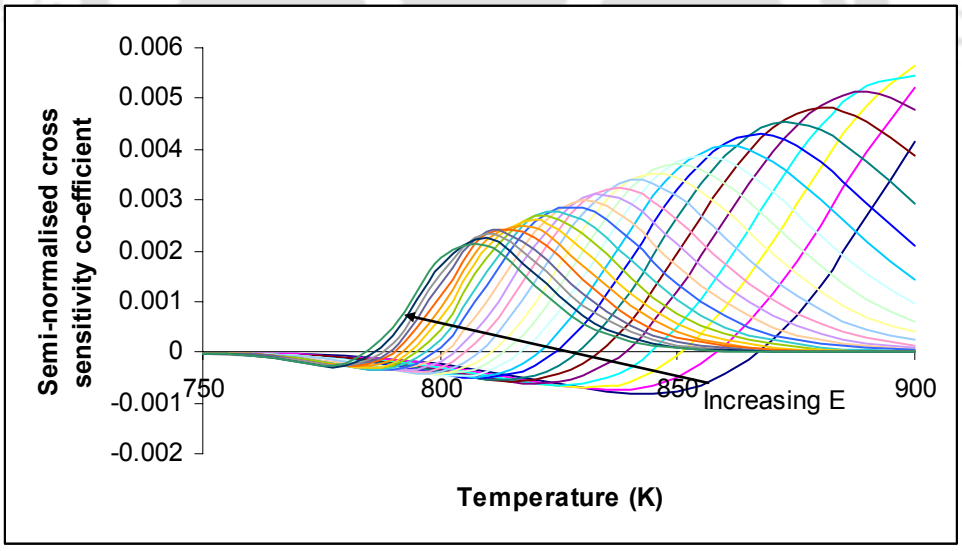

Figure 4.102. Dependency of cross second order sensitivity coefficient on temperature for $\tilde{K}_0$ n

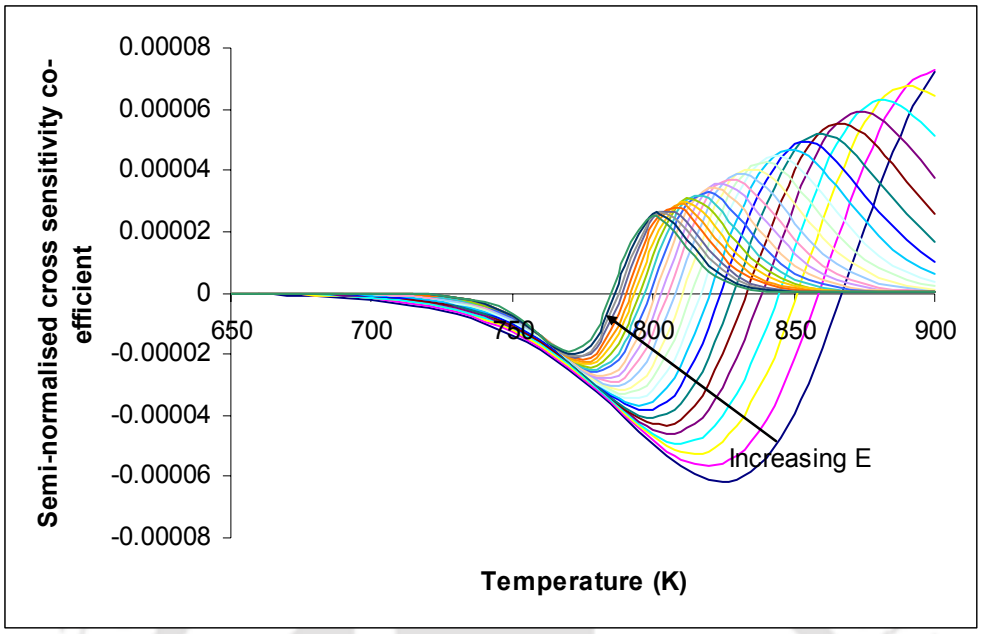

Figure 4.103. Dependency of cross second order sensitivity coefficient on temperature for $\tilde{K}_0 \beta$

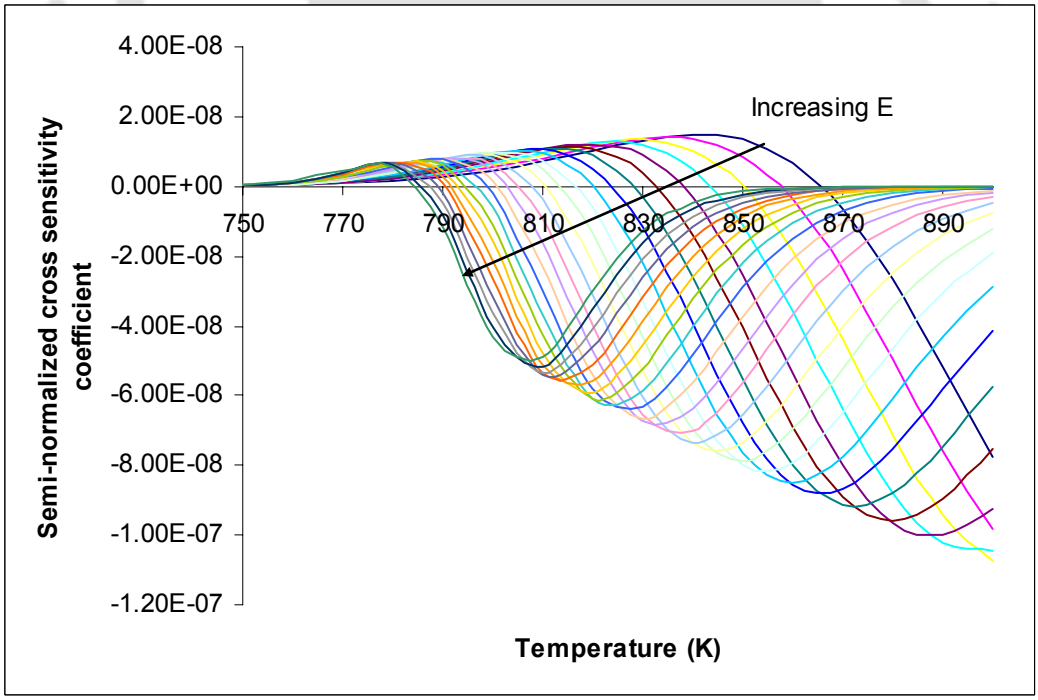

Figure 4.104. Dependency of cross second order sensitivity coefficient on temperature for En

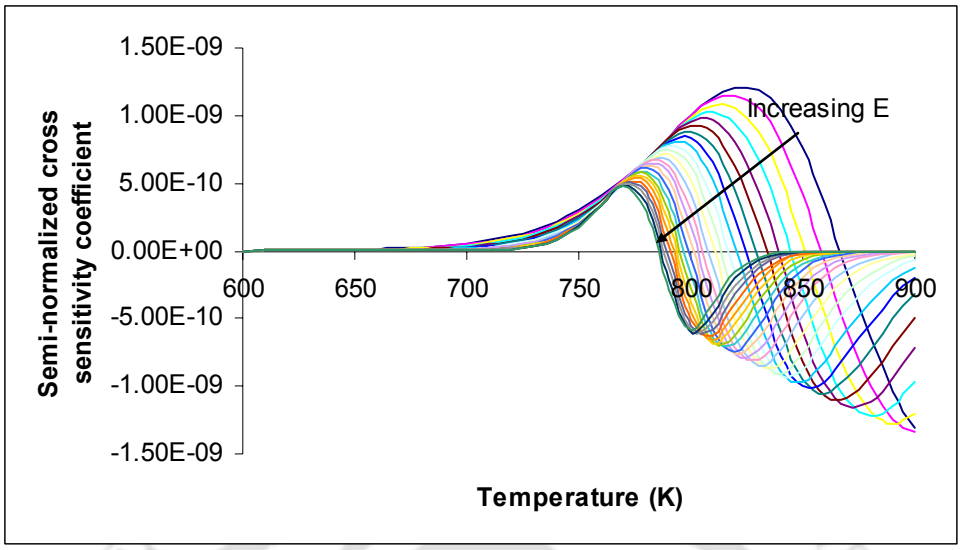

Figure 4.105. Dependency of cross second order sensitivity coefficient on temperature for Eβ

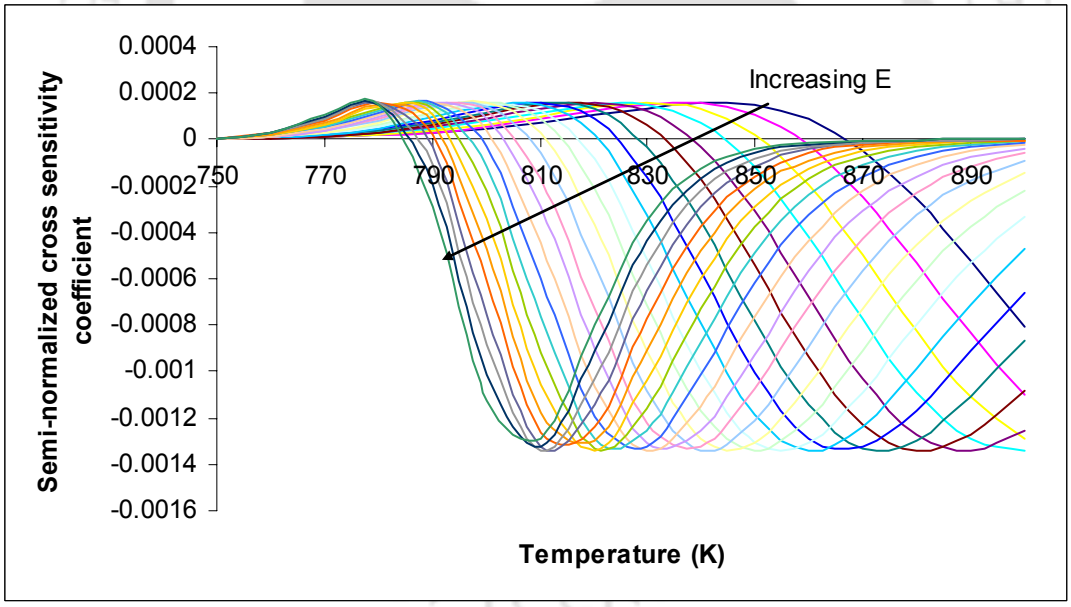

Figure 4.106. Dependency of cross second order sensitivity coefficient on temperature for nβ

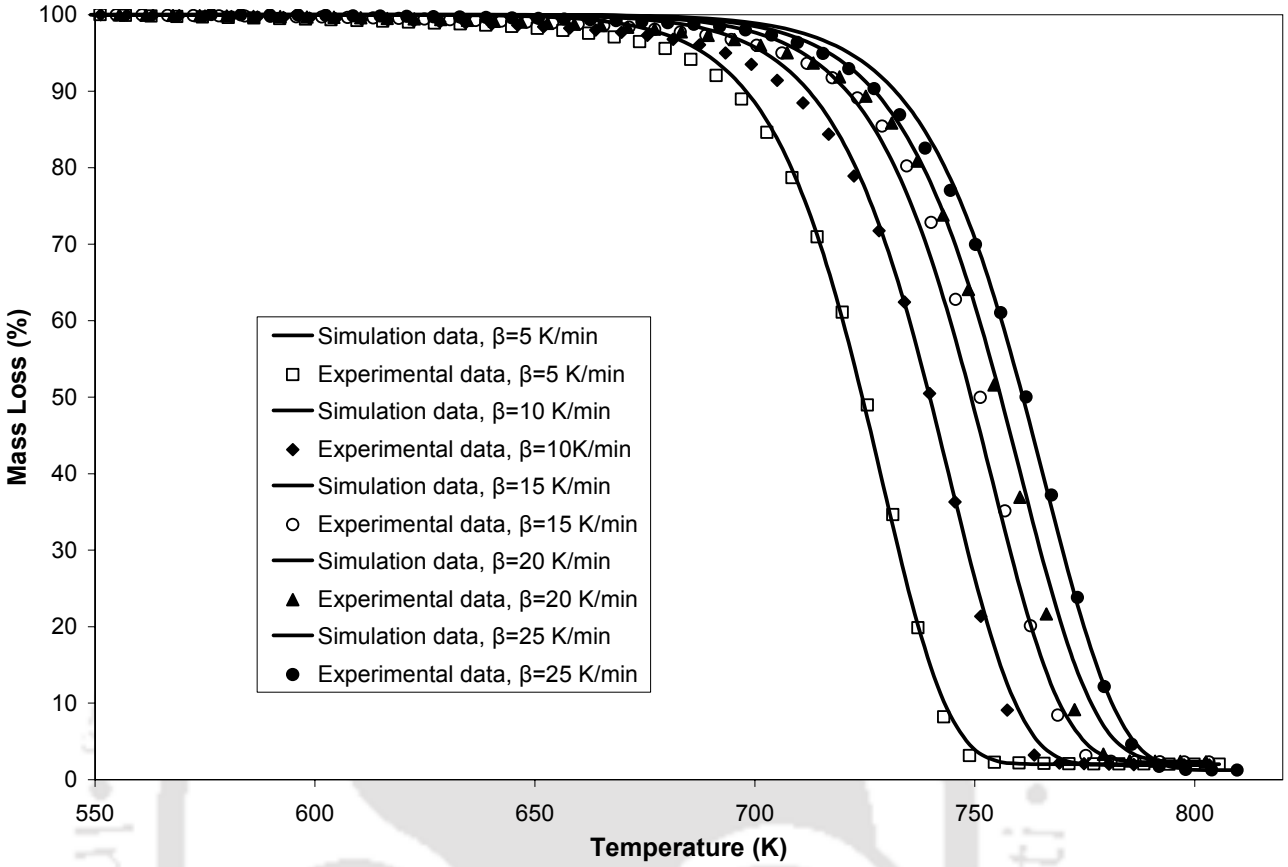

Figure 4.107. Comparison between simulated (using HGA predicted kinetics triplet) and experimental mass loss during non-isothermal pyrolysis of LDPE at five different heating rates for nucleation and growth (n=2/3) model (Experimental data and Simulated data)

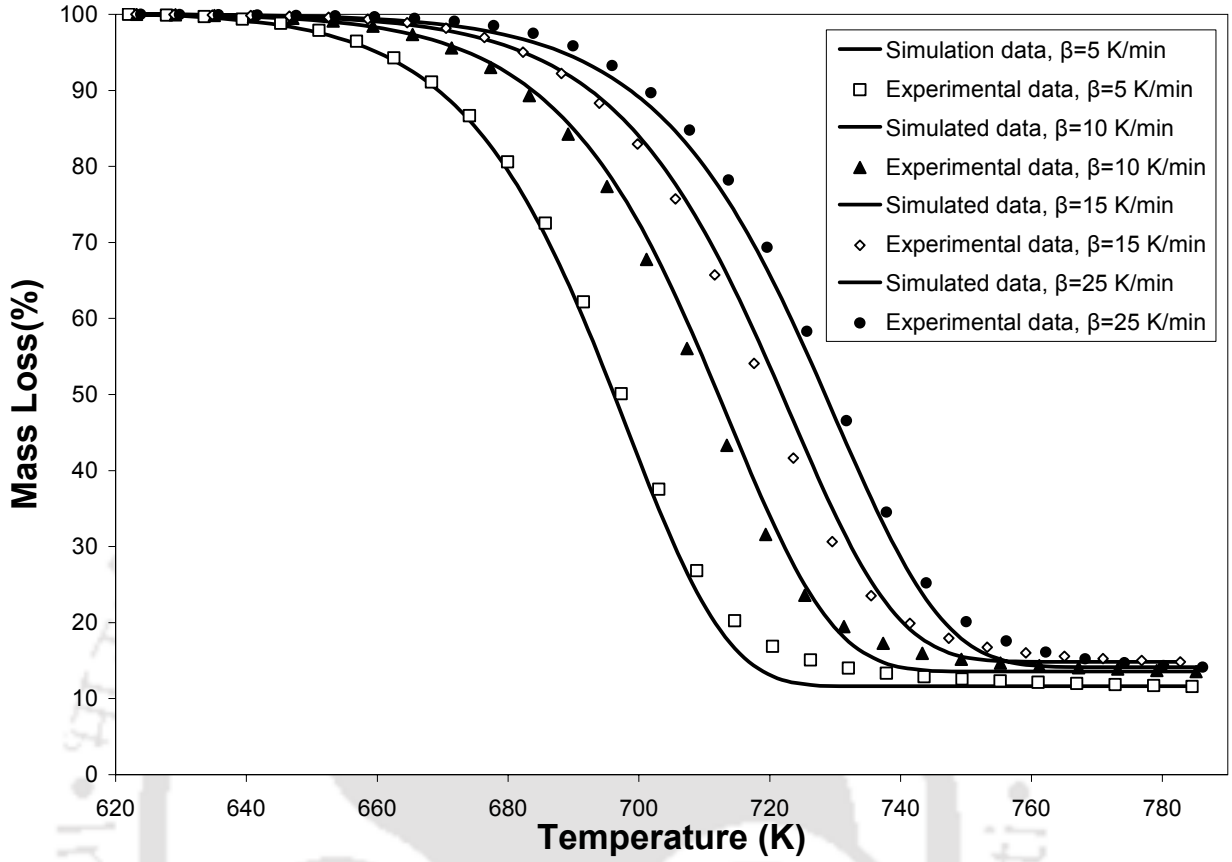

Figure 4.108. Comparison between simulated (using HGA predicted kinetics triplet) and experimental mass loss during non-isothermal pyrolysis of PET at four different heating rates for nucleation and growth (n=2/3) model (Experimental data and Simulated data)

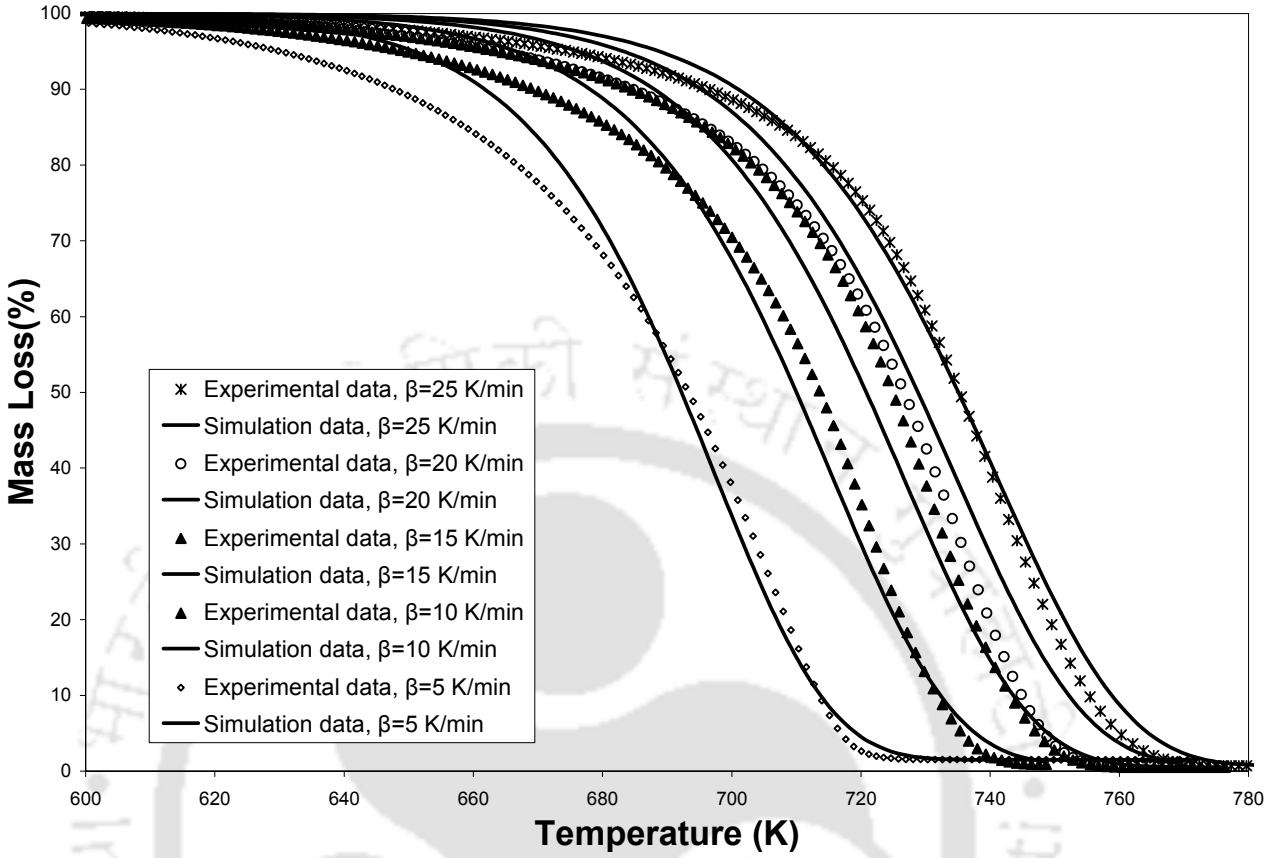

Figure 4.109. Comparison between simulated (using HGA predicted kinetics triplet) and experimental mass loss during non-isothermal pyrolysis of PP at five different heating rates for nucleation and growth (n=2/3) model (Experimental data and Simulated data)

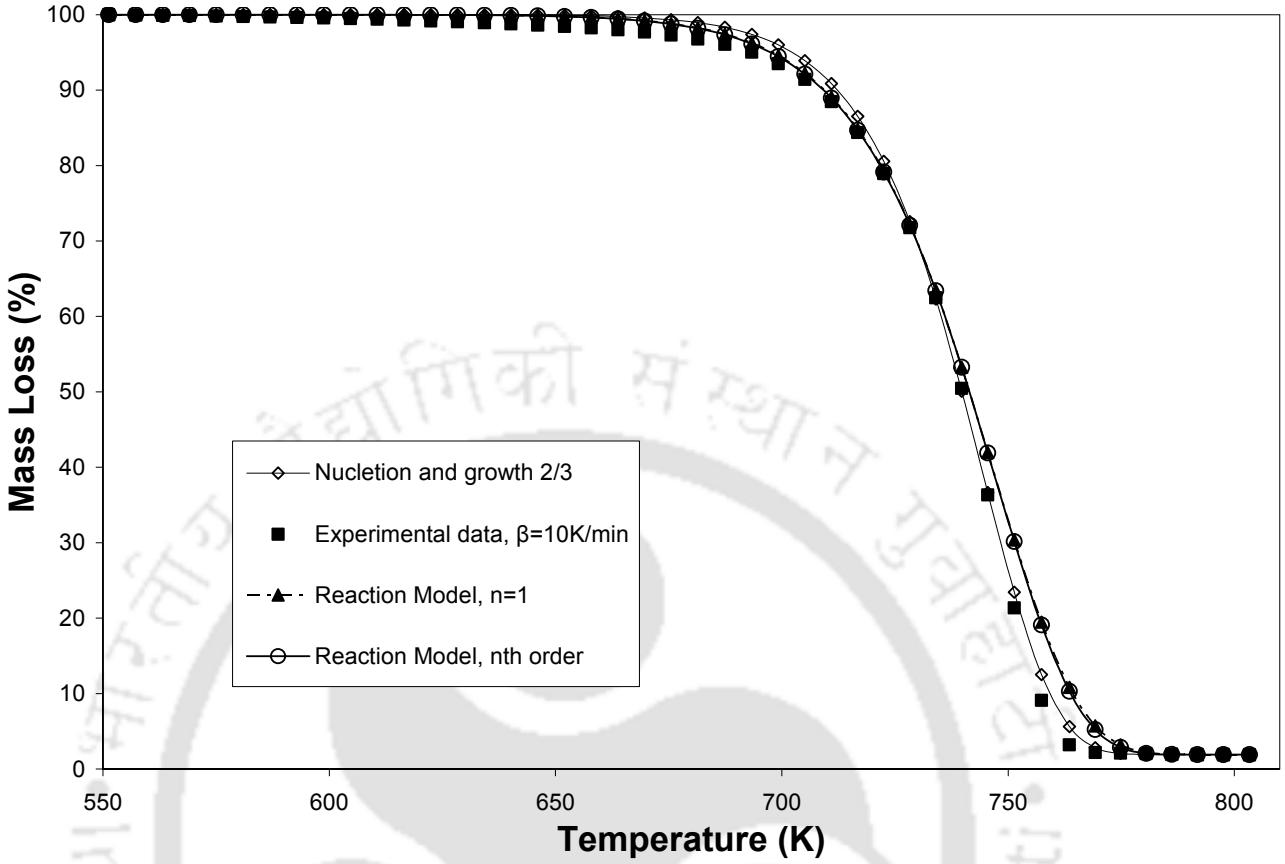

Figure 4.110. Comparison of (mass loss Vs temperature) curves of different models having very less AIC_c scores with experimental values for LDPE and at $10Kmin^{-1}$

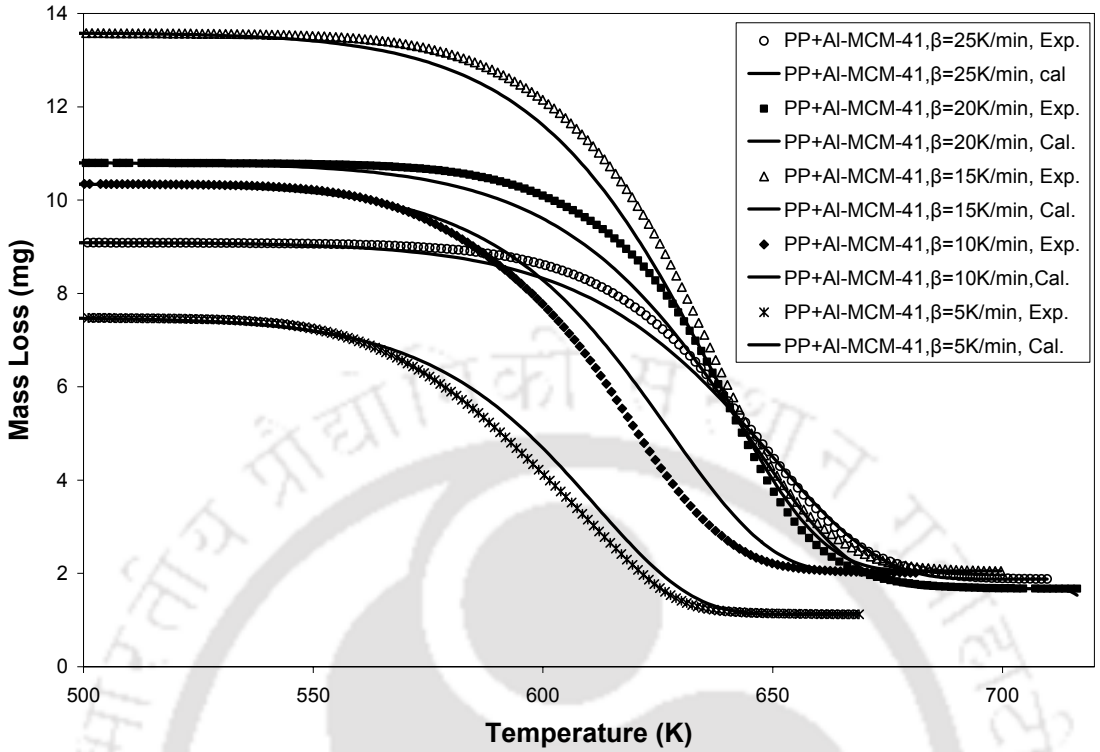

Figure 4.111. Comparison between simulated (using HGA predicted kinetics triplet) and experimental mass loss during catalytic decomposition of PP over Al-MCM-41 (sol-gel) catalyst at five different heating rates for n^{th} order reaction model (Exp, Experimental data and Cal, Calculated data)

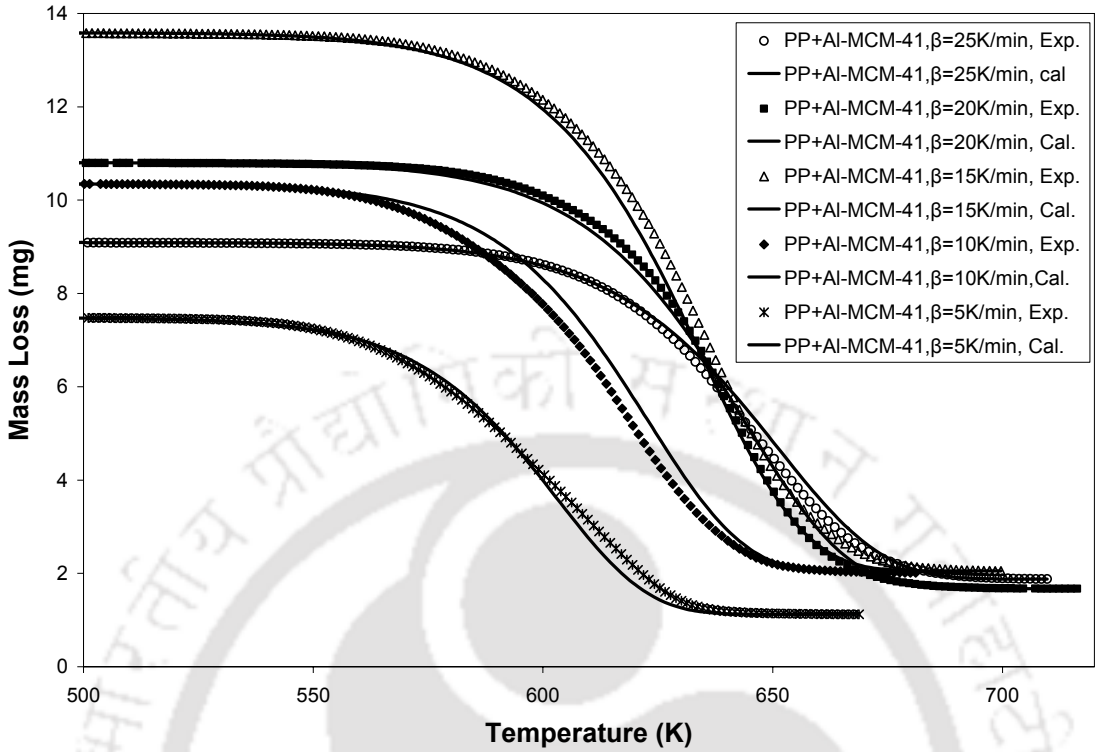

Figure 4.112. Comparison between simulated (using HGA predicted kinetics triplet) and experimental mass loss during catalytic decomposition of PP over Al-MCM-41 (sol-gel) catalyst at five different heating rates for Nucleation and Growth model (n=2/3) (Exp, Experimental data and Cal, Calculated data)

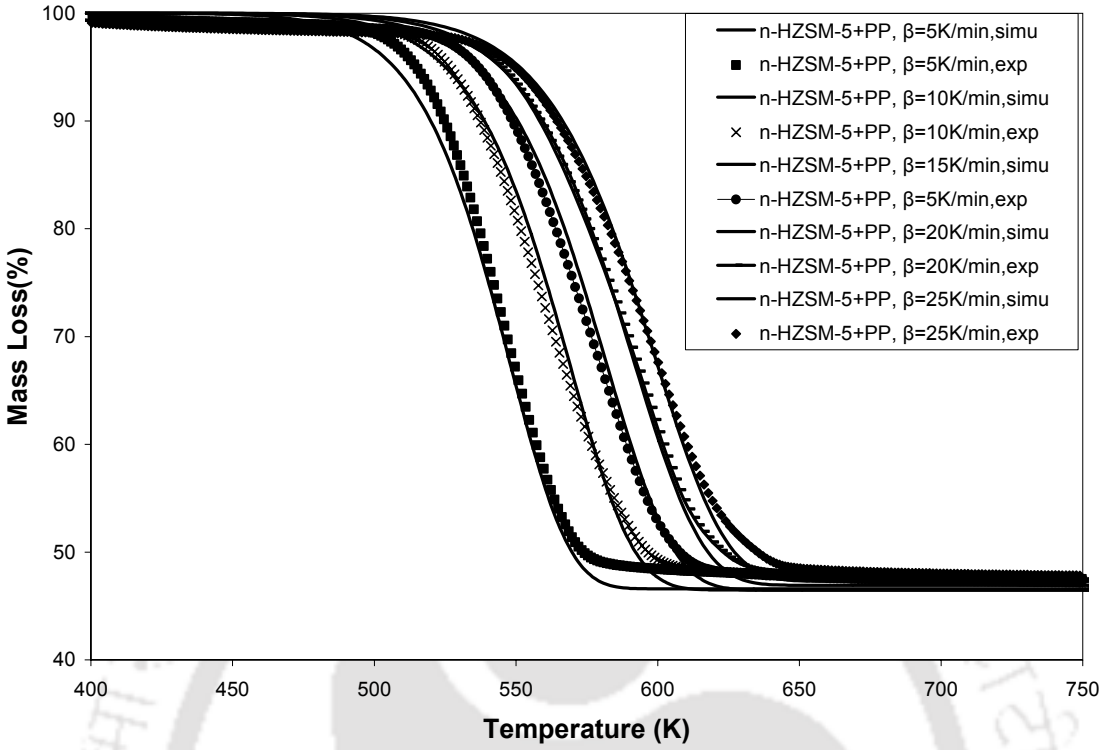

Figure 4.113. Comparison between simulated (using HGA predicted kinetics triplet) and experimental mass loss during catalytic decomposition of PP over n-HZSM-5 catalyst at five different heating rates for Nucleation and Growth model (n=2/3) (exp, experimental data and simu, simulated data)

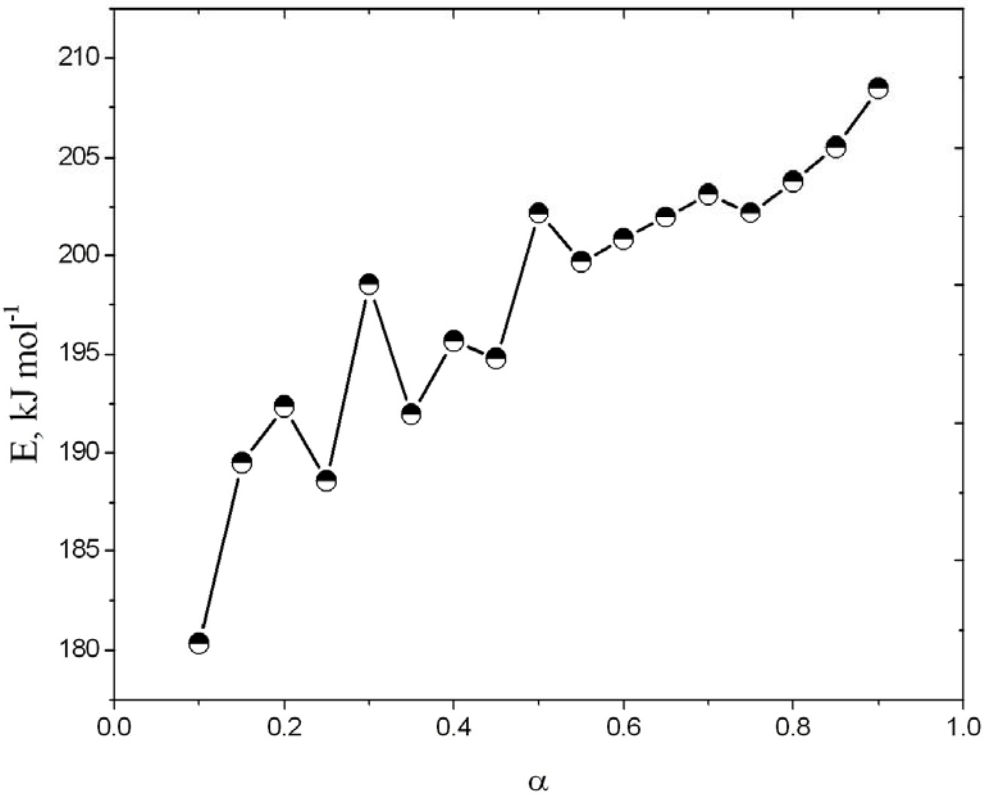

Figure 4.114. Dependency of activation energy on conversion of nonisothermal decomposition of waste PET samples using model free isoconversion technique and Agrawal and Sivasubramanian approximation [187] method to evaluate the temperature integral

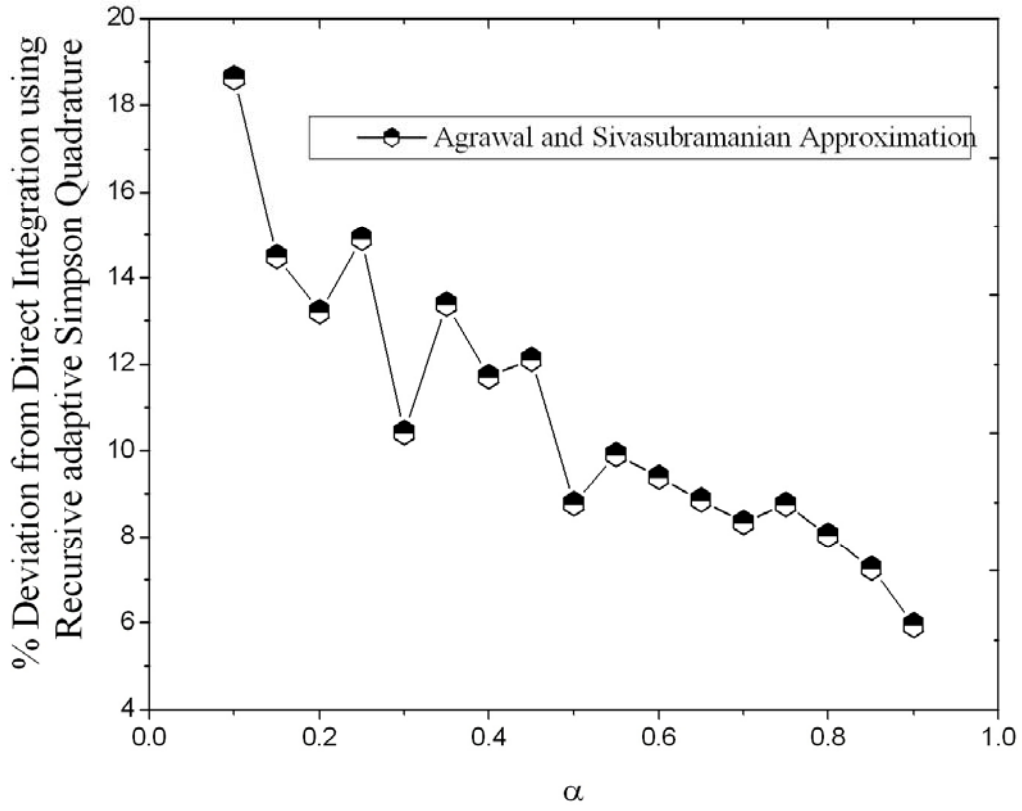

Figure 4.115. Comparison of direct integration method and approximation relations used in model free kinetics analysis

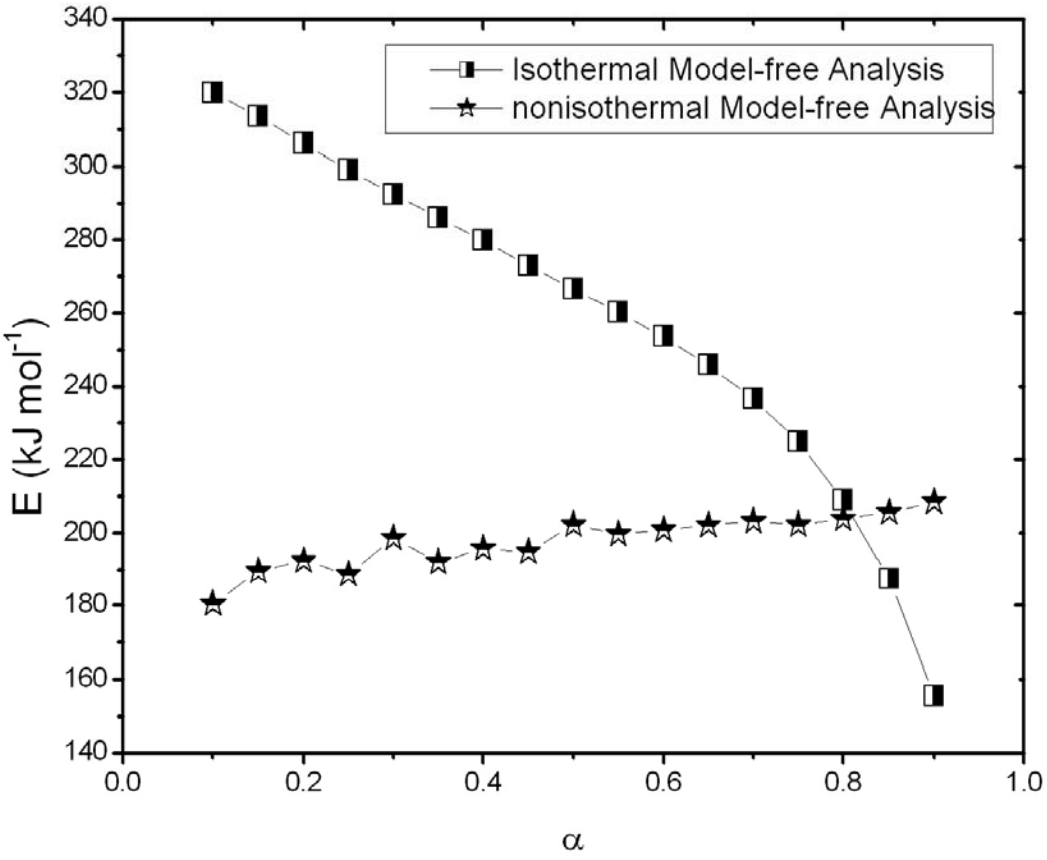

Figure 4.116. Dependency of activation energy on conversion using model free isoconversion technique for nonisothermal (Agrawal and Sivasubramanian approximation [187]) and isothermal decomposition of waste PET samples

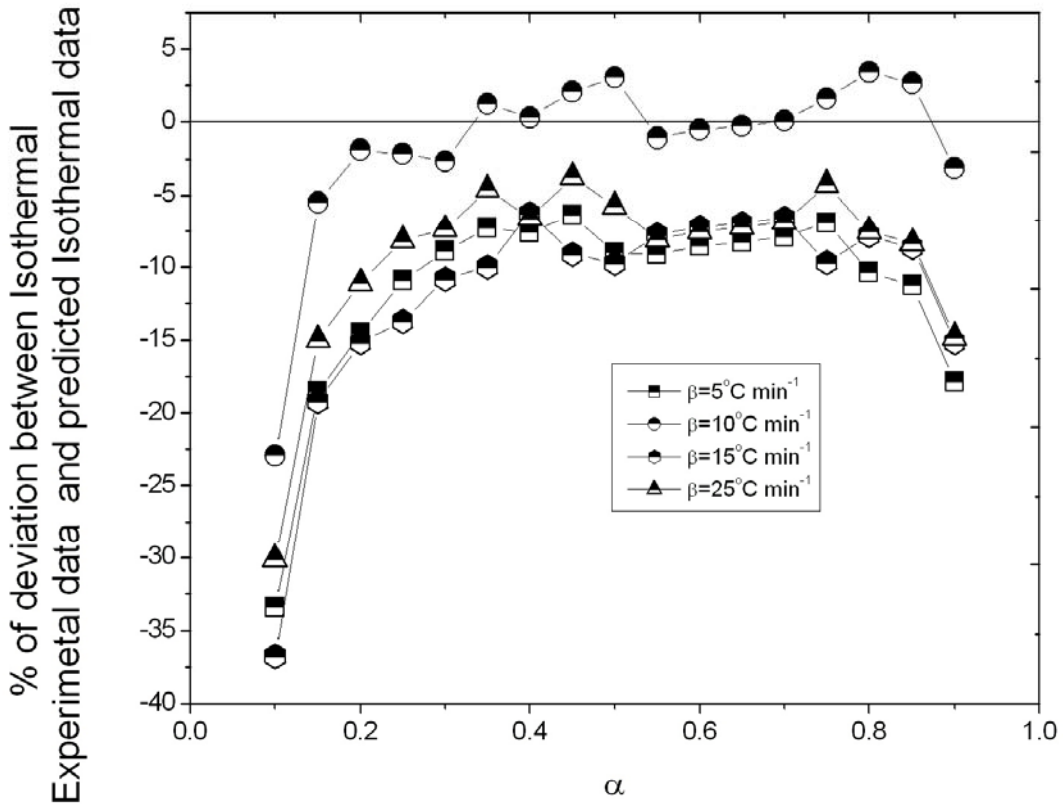

Figure 4.117. Percentage deviation from experimental data for isothermal (685K) prediction at different heating rates using Agrawal and Sivasubramanian approximation (The ARD values are 11.59, 1.51, 11.80 and 9.24 respectively for heating rates 5, 10, 15 and 25°C min^{-1})

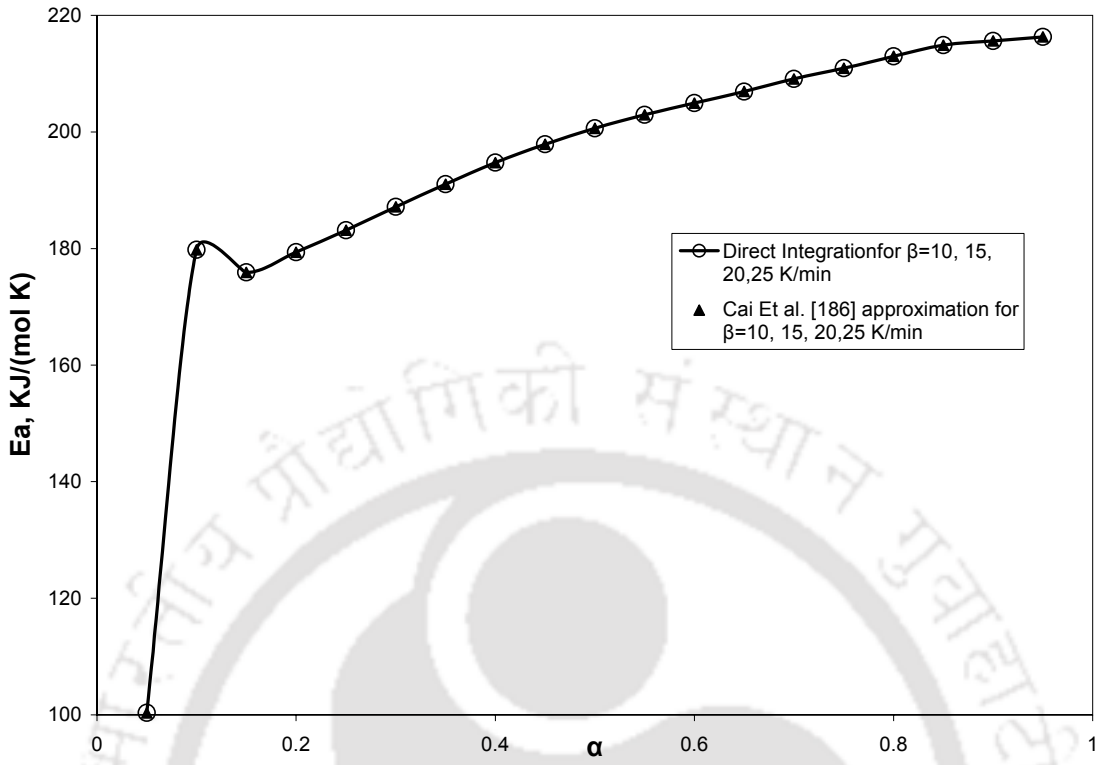

Figure 4.118. Dependency of activation energy on conversion of nonisothermal decomposition of waste PE sample using model free isoconversion technique using direct numerical integration and approximation of Cai et al. [186] to evaluate the temperature integral

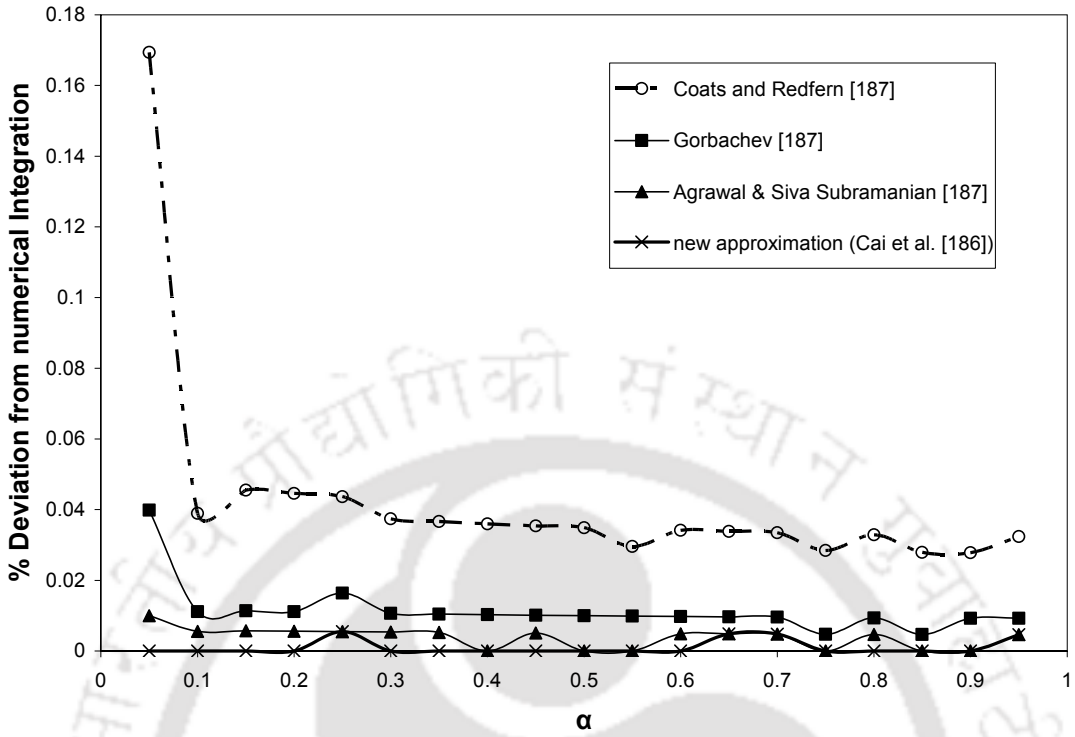

Figure 4.119. Percentage deviation from direct numerical integration (The %ARD values are 0.04225, 0.01145, 0.00377 and 0.00104 respectively for Coats and Redfern, Gorbachev, Agrawal &Subramanian and New approximation (Cai et al. [186]))

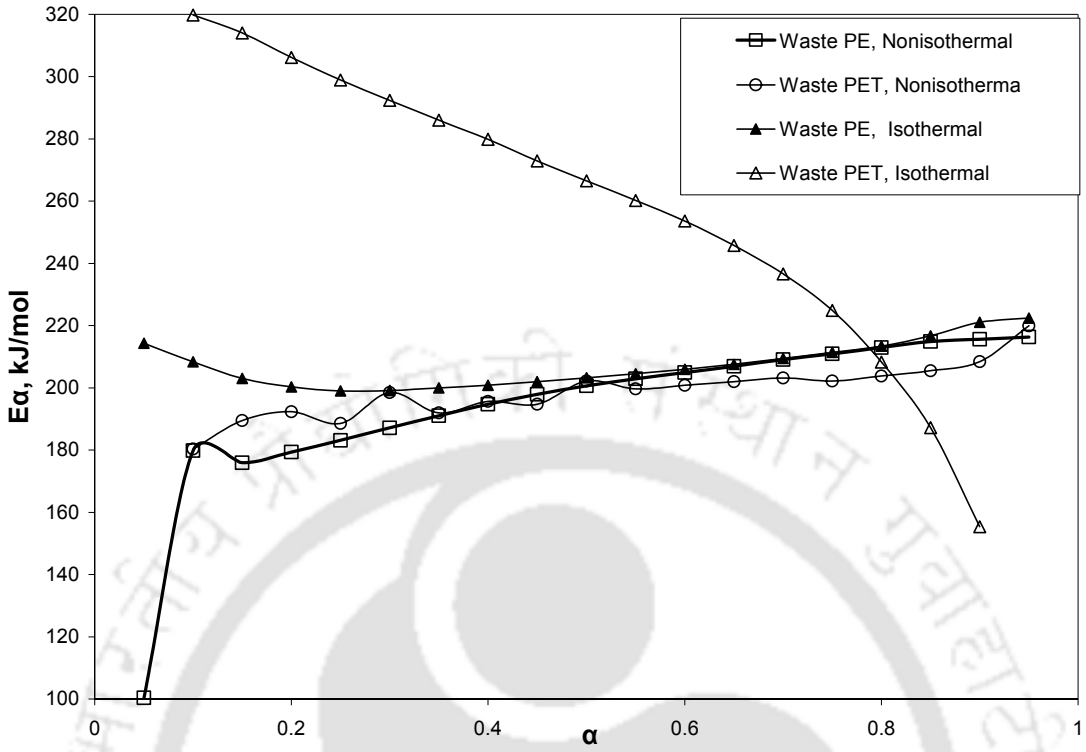

Figure 4.120. Comparison of the dependency of activation energy on conversion using model free isoconversion technique under nonisothermal (direct numerical integration) and isothermal for decomposition of waste PE and PET [174] samples

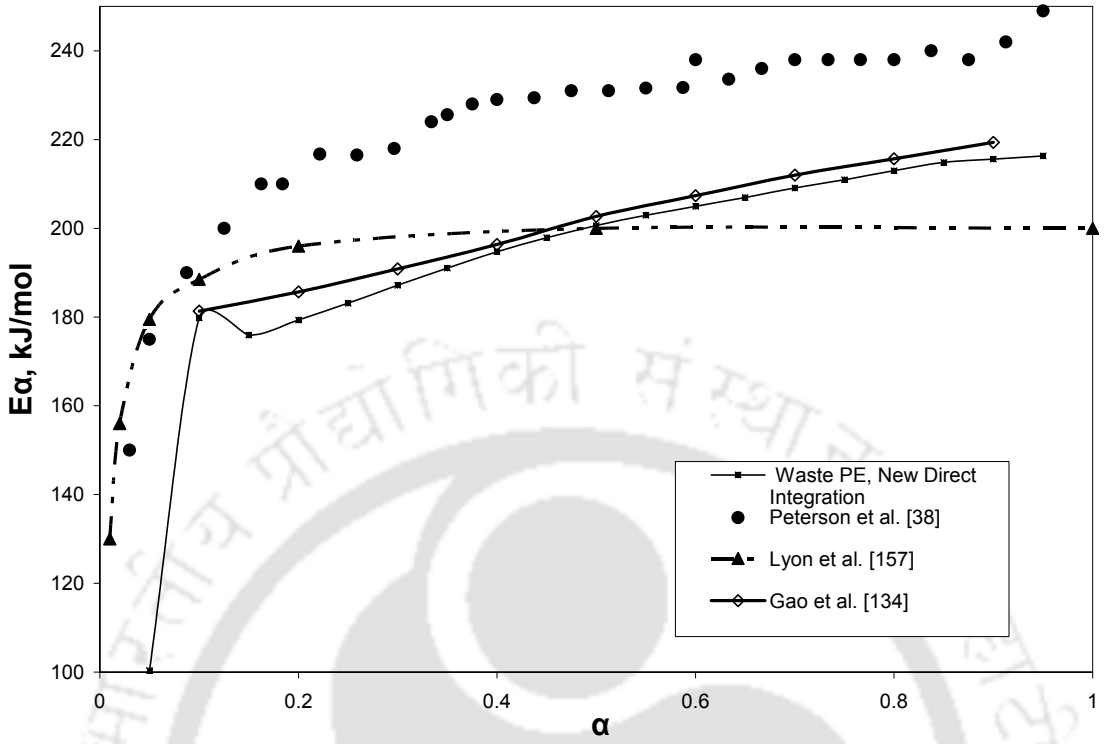

Figure 4.121. Comparison between present work and the literature reported data (Lyon [157], Peterson et al. [38], and Gao et al. [134]) for variation of E_α with α

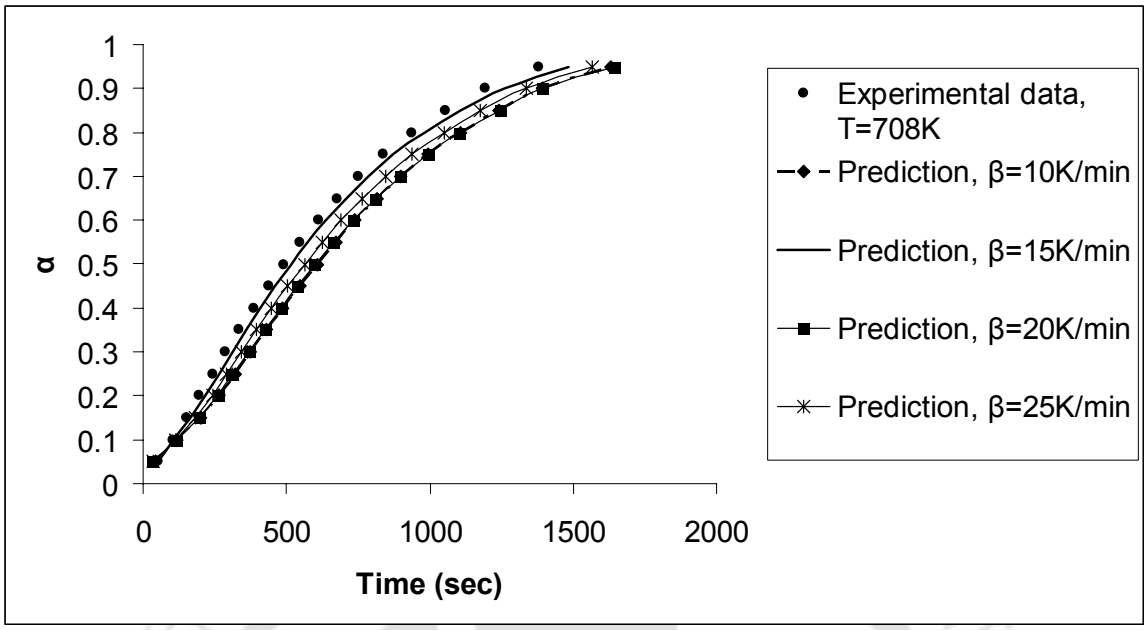

Figure 4.122. Prediction at different heating rates using direct integration for isothermal data (708K) (The %ARD values are 21.133, 5.4928, 18.674and 12.229respectively for heating rates 10, 15, 20 and 25°C min^{-1})

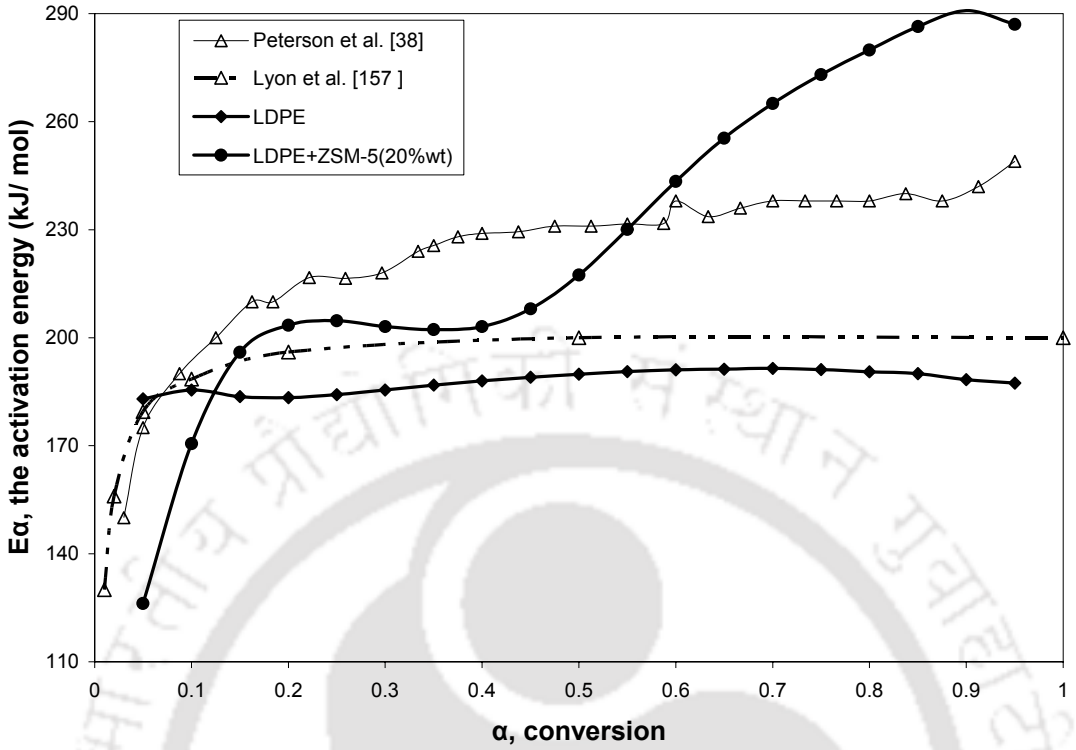

Figure 4.123. Dependency of activation energy on conversion of catalytic and noncatalytic nonisothermal decomposition of waste LDPE sample (present work and literature reported data)

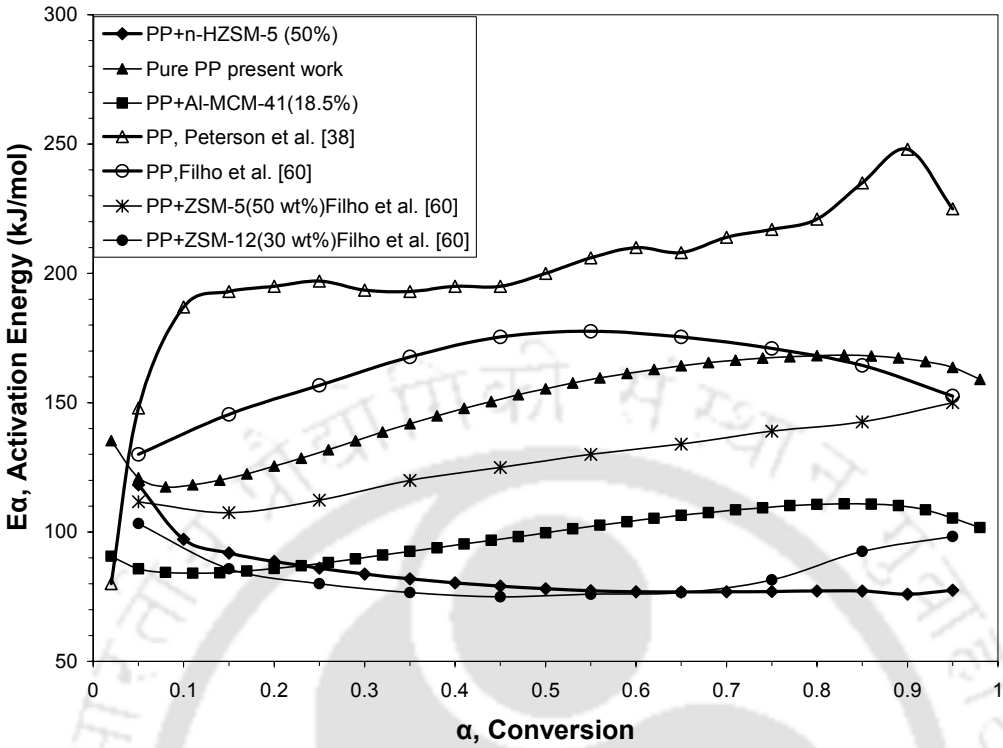

Figure 4.124. Dependency of activation energy on conversion of catalytic and noncatalytic nonisothermal decomposition of PP sample (present work and literature reported data)

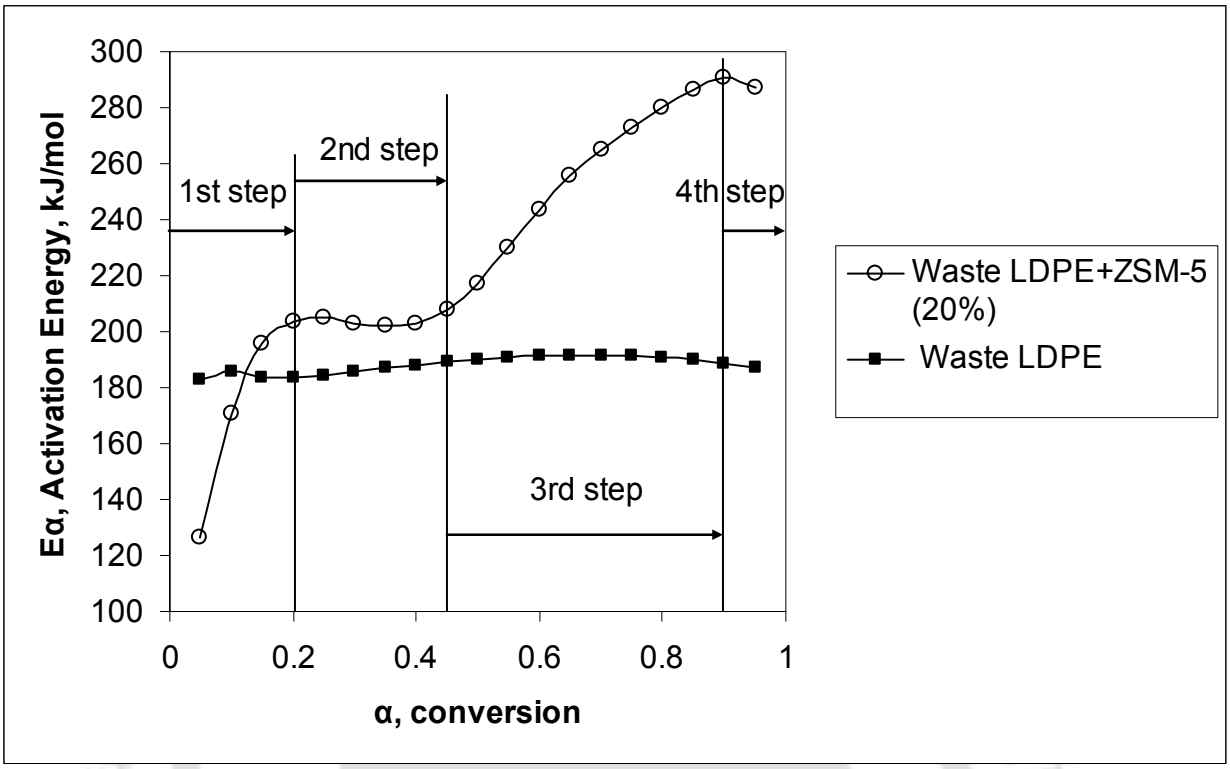

Figure 4.125. Dependency of activation energy on conversion of catalytic nonisothermal decomposition of waste LDPE sample

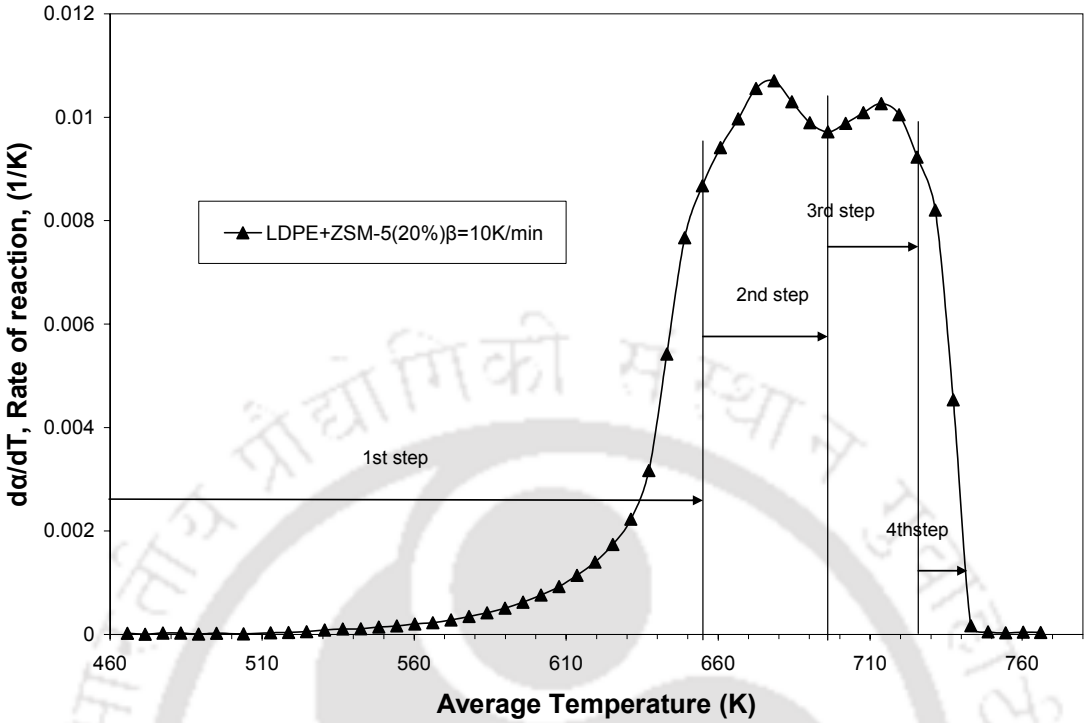

Figure 4.126. Variation of rate of decomposition (dα/dT) with temperature during catalytic nonisothermal pyrolysis of waste LDPE sample at 10K/min heating rate

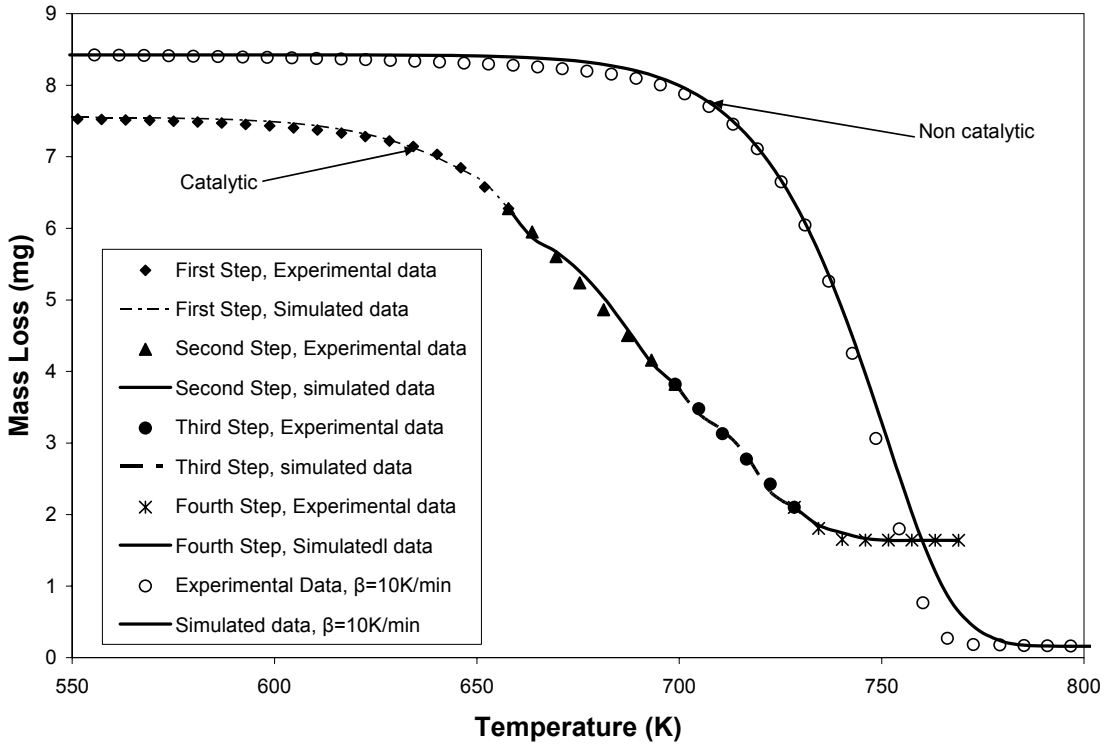

Figure 4.127. Comparison between simulated (using HGA predicted kinetics triplet) and experimental mass loss during noncatalytic and catalytic decomposition of waste LDPE at heating rate of 10 K min^{-1} (Standard Deviation: 0.031 and 0.009 for noncatalytic and catalytic decompositions respectively)

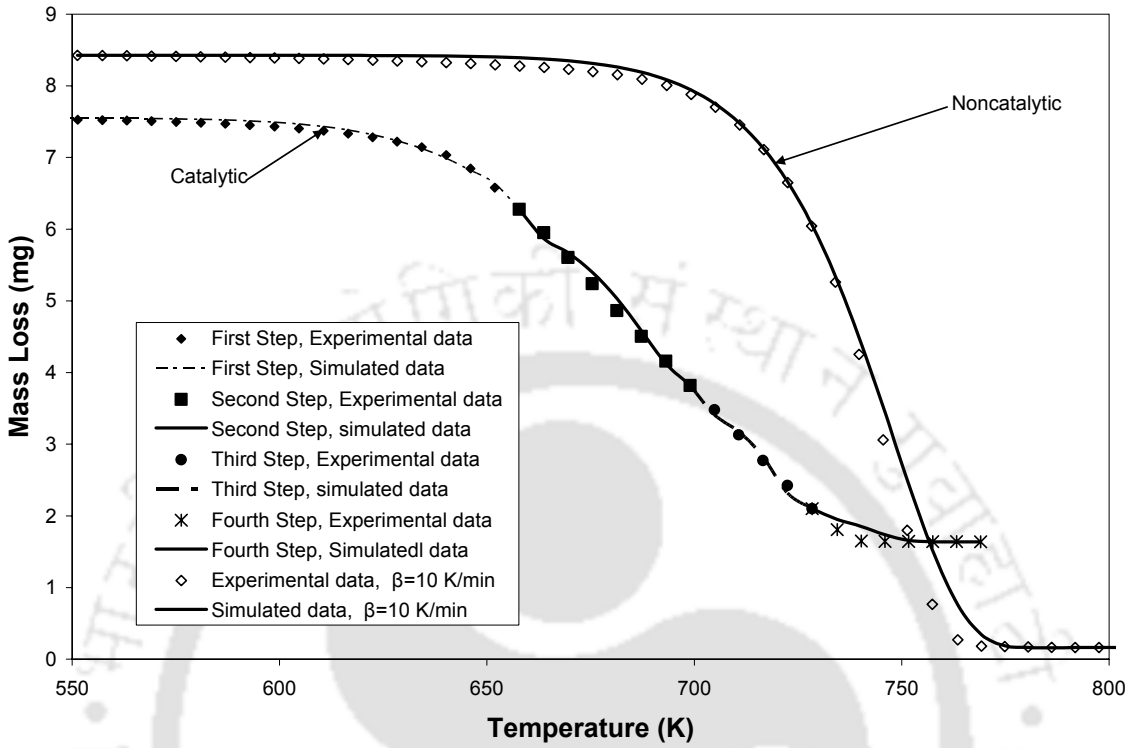

Figure 4.128. Comparison between simulated (using Model-free coupled with direct search method) and experimental mass loss during noncatalytic and catalytic decomposition of waste LDPE at heating rate of 10 K min^{-1} (Standard Deviation: 0.034 and 0.007 for noncatalytic and catalytic decompositions respectively)

5. Conclusion

This chapter reports the inferences drawn from the research work. Major inferences from the studies on thermal pyrolysis of plastics, catalytic pyrolysis of plastics, GC analysis, kinetics analysis of thermal and catalytic pyrolysis of plastics, sensitivity analysis of kinetics parameters, and hybrid genetics algorithm coupled or model-free coupled model-fitting techniques are presented below.

- Thermal (noncatalytic) decomposition behaviors under dynamic conditions of waste PET, virgin PET, waste PE, waste LDPE, and PP are similar, showing the constant pattern TG curves at different heating rates and a single peak in derivative thromogravimetric (DTG) curves. Higher heating rate finishes the decomposition phenomenon faster.
- The isothermal decomposition behaviour of the virgin PET varies significantly from that of waste PET samples. The residue left for waste PET sample is within 13-17 % and that for virgin PET sample is within 12-14%. In case of waste PE residue left around 15%.
- During catalytic decomposition, catalysts are selective to the plastics and significantly reduce decomposition temperature. Catalysts with stronger acidic character showed higher catalytic activity for decomposition of LDPE. Comparatively weaker acid properties of mesostructured catalysts are partly compensated by their comparatively larger pore dimensions and surface area, which provide an easier accessibility to their internal acid sites. Fresh FCC and the spent FCC catalysts remained almost inactive on LDPE. Catalytic decomposition shows single as well as multi-peaks in the DTG

curves for different plastics, indicating possible existence of multi-step reactions taking place in presence of catalysts.

- Catalytic effect in terms of reduction in T_m on waste LDPE follow the sequence ZSM-5>Al-41-P(15)>Al-41-P(30)>Al-41-P(60)>Al-41-P(100)>Fresh FCC>Spent FCC and on PP follow the sequence n-HZSM-5>Al-41-P(15)≈Al-41-P(30)>Al-41-P(60)>Fresh FCC>Al-41-P(100)>Spent FCC>ZSM-5.
- PP molecules are much larger than the pore size of zeolites. Therefore, catalytic decomposition of PP over ZSM-5 is more difficult as degraded chain segments cannot easily diffuse through the channels. The n-HZSM-5 catalyst sample with higher external surface area, pore size, and acidic nature accelerated the decomposition process of PP, as the diffusion hindrance reduces with increase in pore diameters of these catalysts sample. Similarly, mesoporous Al-41-P(30) and Al-41-P(15) catalysts with considerable amount of aluminium (acid site) showed very good effect on the catalytic decomposition of PP due to higher external surface area and pore size.
- Product analysis indicates that microporous ZSM-5 and high external surface area containing n-HZSM-5 produce high amount of light hydrocarbons whereas mesoporous Al-MCM-41 produce high amount of heavier hydrocarbons, which is also supported by the literature findings.
- The optimum catalysts percentage obtained for decomposition of waste LDPE over ZSM-5, PP over Al-MCM-41, and waste LDPE over n-HZSM-5 are around 20, 18.5 and 50 wt % respectively.
- Reusability study suggests that Al-MCM-41 is still very active even after its use for seven times.

- nth-order model, which is suggested first time in this work, shows better results compared to ASTM E698, Freeman-Carroll, Friedman, and Chang techniques. All the techniques are based on single heating rate TGA curve. Standard deviation minimization technique (SDMT) is developed and shown to be a promising model-fitting technique as it takes care of both single and multi heating rate TGA curves.
- According to the sensisitivity analysis, reaction order is found to be the most sensitive one and activation energy to be the least sensitive one. Thus, sensitivity analysis reduced the three-parameter optimization problem for polymer kinetics is to single parameter (E) optimization problem.
- Hybrid genetic algorithm is successfully employed to estimate the globally optimum kinetics triplet. Akaike's Information Criteria (AIC) is also applied to choose the appropriate reaction model. Results showed that Nucleation and Growth model with reaction order, n = 2/3 is the best suited one and it also predicted the experimental TGA data successfully. However, n^{th} order model also shows good AIC_c score and well predicted the experimental TGA data.
- Vyazovkin nonlinear model-free (isoconversional) analysis showed different trends for different cases in the variation of activation energy with conversion. This trend also helps getting first hand information on the possible reaction steps involved during pyrolysis e.g. model-free analysis indicates the possible existence of four different reaction mechanisms in the different steps during catalytic decomposition of LDPE over ZSM-5 catalyst.
- The nonlinear Vyazovkin model-free analysis approach also narrows down the range of guess values of activation energy for optimization using traditional model-fitting

methods. The estimated optimized kinetics triplet obtained by the model-free coupled with local optimization method (LOA) successfully predicted the experimental TGA data.

- Both GA coupled with LOA and model free method of analysis coupled with LOA gives almost same kinetics triplet values and predicts the experimental TGA data equally well. Since either of the two approaches can be effectively used for pyrolysis kinetics analysis, model free (isoconversional) method coupled with LOA should be the preferred one as this approach additionally helps to reveal the complexity of multiple reactions due to the dependencies of activation energy on the extent of conversion understand the different reaction steps taking place during pyrolysis from the variation of activation energy with conversion.
- In practice, while going for solid waste management, most of the waste materials happen to be a non-standard one, particularly in developing countries. Therefore, the present study reflects that it becomes mandatory to study the decomposition behaviour of the waste materials before design of an incinerator and/or pyrolysis unit and one should not use blindly the information available for standard samples.

Scope of Future Work

- Establishment of the detailed kinetic scheme about the real reaction mechanisms taking place during catalytic and non noncatalytic pyrolysis of waste polymers through the thorough analysis of products
- Identification of the valuable products from the above analysis
- Extension of the study covering wide spectrum of waste plastic materials
- Decomposition studies, product analysis and kinetics analysis of noncatalytic and catalytic pyrolysis of plastic mixtures to represent real life solid waste system.
- Development of suitable reactor for noncatalytic and catalytic pyrolysis of plastic mixtures

List of Publications

1. B. Saha, A.K. Ghoshal, Thermal degradation kinetics of poly (ethylene terephthalate) from waste soft drinks bottles, Chem. Eng. J. 111 (2005) 39.
2. B. Saha, A.K. Maiti, A.K. Ghoshal, Model-free Method for Isothermal and nonisothermal Decomposition Kinetics Analysis of PET Sample, Thermochimi. Acta. 444 (2006) 46.
3. B. Saha, A.K. Ghoshal, Model-Fitting Methods for Evaluation of Kinetics Triplet during Thermal Decomposition of PET Soft Drink Bottles, Ind. Eng. Chem. Res., 45 (2006) 7752.
4. B. Saha, A.K. Ghoshal, Model-Free Kinetics Analysis of waste PE, Thermochimica Acta, 451 (2006) 27.
5. B. Saha, A.K. Ghoshal, Model-free Kinetics Analysis of ZSM-5 Catalysed Pyrolysis of waste LDPE, Thermochimi. Acta. 453 (2007) 120.
6. B. Saha, A.K. Ghoshal, Model-free Kinetics Analysis of Decomposition of Polypropylene over Al-MCM-41, Thermochimica Acta**,** 2007, doi: 10.1016/j.tca.2007.05.016.
7. B. Saha, P. Karthik Reddy, A.K. Ghoshal, Hybrid Genetic Algorithm to Find the Best Model and the Globally Optimized Overall Kinetics Parameters for Thermal Decomposition of Plastics, Chem. Eng. J.**,** 2007, doi: 10.1016/j.cej.2007.05.024.
8. B. Saha, A.K. Ghoshal, Hybrid Genetic Algorithm and Model Free Coupled Direct Search Methods for Pyrolysis Kinetics of ZSM-5 Catalyzed Decomposition of Waste LDPE, Ind. Eng. Chem. Res.**,** 2007 doi: 10.1021/ie0615483.
9. B. Saha, P. Chowdhury, A.K. Ghoshal, Al-MCM-41 Catalyzed Decomposition of Polypropylene and Hybrid Genetic Algorithm for Kinetics Analysis**,** Appl. Catal. B**,** 2006 (under review).

National Conference:

1. B. Saha, A.K. Maiti, A.K. Ghoshal, Sensitivity Analysis of Pyrolysis Kinetics of Poly (ethylene terephthalate), Chemcon, 2005, IIT Delhi.

Literature cited

1. M.-W. Ho, P. Bunyard, P. Saunders, E. Bravo, R. Gala, Which Energy? Announcing ISIS 2006 Energy Report, http://lists.ifas.ufl.edu/cgi-bin/wa.exe?A2=ind0603&L=sanet-mg&P=13291(As see on dated: 06/03/07).
2. World Bank, Urban Development Sector Unit East Asia and Pacific Region, What a Waste: Solid Waste in Asia May 1999, (http://www.worldbank.org/html/fpd/urban/publicat/whatawaste.pdf)(As see on dated: 16/03/05).
3. http://www.indiatogether.org/2004/apr/env-rethink.htm (As see on dated: 25/09/05)
4. http://www.icpenviro.org/Statistics.asp (As see on dated: 25/09/05)
5. P. Narayan, Analysing Plastic Waste Management in India Case study of Polybags and PET bottles. Thesis for the fulfillment of the Master of Science in Environmental Management and Policy, Lund, Sweden, September 2001.
6. S. Gupta, K. Mohan, R. Prasad, S. Gupta, A. Kansal. Solid waste management in India: Options and opportunities. Resour Conserv Recycl. 24 (1998) 137-154.
7. S. Yedla, J. K. Parikh, Development of a purpose built landfill system for the control of methane emissions from municipal solid waste. Waste Manage. 22 (2002) 501.
8. http://www.indiatogether.org/upload/stats2.doc (As see on dated: 25/09/05)
9. http://www.indiatogether.org/2004/mar/hlt-pyrolysis.htm (As see on dated: 25/09/05)
10. 20th WEDC Conference: Colombo, Sri Lanka, 1994, Solid waste management in India, A.P.Jain, G.B.Pant (http://info.lboro.ac.uk/departments/cv/wedc/papers/jain.html) (As see on dated: 25/09/05)
11. http://www.thermaxindia.com/busarea/homepagewmd.htm(As see on dated: 08/012/04)
12. http://news.bbc.co.uk/2/hi/uk_news/4624700.stm (As see on dated: 15/04/07).

13. G. Finnveden, J Johansson, P Lind, A. Moberg, Life cycle assessment of energy from solid waste—part 1: general methodology and results, J. clean prod. 13 (2005) 213.

14. http://news.bbc.co.uk/2/hi/europe/4620041.stm (As see on dated: 15/04/07).

15. M. Abu-Quadis, H. A. Abu-Quadis, Energy content of municipal solid waste in Jordan and its potential utilization, Energy Convers. Manage. 41 (2000) 983.

16. A. G. Buckens, H. Huang, Catalytic plastics cracking for recovery of gasoline-range hydrocarbons from municipal plastic wastes, Resour Conserv Recycl. 23(1998) 163.

17. M. N. Islam, M. N. Islam, M. R. A. Beg, The fuel properties of pyrolysis liquid derived from urban solid wastes in Bangladesh, Bioresour. Technol. 92 (2004) 181.

18. M. Thomas, Novel and innovative pyrolysis and gasifiaction technologies for energy efficent and environmentally sound MSW disposal, Waste Manage. 24 (2004) 53.

19. K.V. Sharma, M. Mincarini, F. Fortuna, F. Cognini, G. Cornacchin, Disposal of waste tyres for energy recovery and safe environment—Review, Energy Convers. Manage. 39 (1998) 511.

20. J. B. Parra, C. O. Ania, A. Arenillas, F. Rubiera and J. J. Pis, High value carbon materials from PET recycling, Appl. Surf. Sci. 238 (2004)304.

21. J. B. Parra, C. O. Ania, A. Arenillas, F. Rubiera, J. M. Palacios, J. J. Pis, Textural development and hydrogen adsorption of carbon materials from PET waste, J. Alloys Compd. 379, (2004) 280.

22. T. Masuda, Y.Miwa, K. Hashimoto, Y. Ikeda**,** Recovery of oil from waste poly(ethylene terephthalate) without producing any sublimate materials, Polym. Degrad. Stab. 61 (1998) 217.

23. P.T. Williams, E.A. Williams, Fluidised bed pyrolysis of low density polyethylene to produce petrochemical feedstock, J. Anal. Appl. Pyrol. 51 (1999) 107.

24. B. J. Milne; A.L. Behie, F. Berruti, Recycling of waste plastics by ultrapyrolysis using an internally circulating fluidized bed reactor, J. Anal. Appl. Pyrol. 51 (1999) 157.
25. X. Dai, X. Yin, C. Wu, W. Zhang, Y. Chen, Pyrolysis of waste tires in a circulating fluidized-bed reactor, Energy 26 (2001) 385.
26. W. Kaminsky, M.Predel, A.Sadiki, Feedstock recycling of polymers by pyrolysis in a fluidised bed, Polym. Degrad. Stab. 85 (2004) 1045.
27. M. Predel, W. Kaminsky, Pyrolysis of mixed polyolefins in a fluidised-bed reactor and on a pyro-GC/MS to yield aliphatic waxes, Polym. Degrad. Stab. 70 (2000) 373.
28. N. Miskolczi, L.Bartha, G. Deak, B. Jover, Thermal degradation of municipal plastic waste for production of fuel-like hydrocarbons, Polym. Degrad. Stab. 86 (2004) 357.
29. M. E. Brown, M Maciejewski, S. Vyazovkin, R. Nomen, , J. Sempere, A. Burnham, J. Opfermann, R. Strey, H. L. Anderson, A. Kemmler, R. Keuleers, J. Janssens, H.O. Desseyn, C. R. Li, T. B. Tang, B. Roduit, J. Malek, T. Mitsuhashi, Computational aspects of kinetic analysis: Part A: The ICTAC kinetics project-data, methods and results ,Thermochim. Acta 355 (2000) 125.
30. H. J. Flammersheim, J. R. Opfermann, Formal kinetic evaluation of reactions with partial diffusion control ,Thermochim. Acta 337 (1999) 141.
31. J. R. Opfermann, E. Kaisersberger, H. J. Flammersheim, Model-free analysis of thermoanalytical data-advantages and limitations, Thermochim. Acta 391 (2002) 119.
32. S. Vyazovkin, V. Goriyachko, Potentialities of software for kinetic processing of thermoanalytical data by the isoconversion method, Thermochim. Acta 194 (1992) 221.
33. S. Vyazovkin, C. A. Wight, Model-free and model-fitting approaches to kinetic analysis of isothermal and nonisothermal data, Thermochim. Acta 340-341 (1999) 53.

34. S.Vyazovkin, Computational aspects of kinetic analysis. Part C. The ICTAC Kinetics Project — the light at the end of the tunnel?,Thermochim. Acta 355 (2000) 155.
35. S. Vyazovkin, D. Dollimore, Linear and Nonlinear Procedures in Isoconversional Computations of the Activation Energy of Nonisothermal Reactions in Solids J. Chem. Inf. Comp. Sci. 36 (1996) 42.
36. S. Vyazovkin, A unified approach to kinetic processing of nonisothermal data, Int. J. Chem. Kinet. 28 (1996) 95.
37. S. Vyazovkin, N. Sbirrazzuoli, Isoconversional Kinetic Analysis of Thermally Stimulated Processes in Polymers,Macromol. Rapid Commun. 27 (2006) 1515.
38. J. D. Peterson, S. Vyazovkin, C. A. Wight, Kinetics of the Thermal and Thermo-Oxidative Degradation of Polystyrene, Polyethylene and Poly(propylene), Macromol. Chem. Phys. 202 (2001) 775.
39. R. Smith, Chemical process design and integration, John Wiley & Sons Ltd. Pp-77-141 (ISBN: 0471-48680-9).
40. A. Umbetro, M. L. Maria, Defluidization phenomena during the pyrolysis of two plastic wastes, Chem. Eng. Sci. 55(2000) 2849.
41. M. L. Maria, A. Umbetro, Fluidized-bed pyrolysis of polyolefins wastes: Predictive defluidization model, AIChE J. 48 (2002) 1439.
42. M. L. Mastellone, F. Perugini, M. Ponte, U. Arena, Fluidized bed pyrolysis of a recycled polyethylene, Polym. Degrad. Stab., 76(2002) 479.
43. A. Karaduman, H. E. Simsek., B. Cicek., Y. A. Bilgesu, Flash pyrolysis of polystyrene wastes in a free-fall reactor under vacuum, J. Anal. Appl. Pyrol. 60 (2001) 179.
44. H. Bockhorn, A. Hornung, U. Hornung, P. Jakobstroer, M. Kraus, Dehydrochlorination of plastic mixtures, J. Anal. Appl. Pyrol. 49 (1999) 97.
45. H. Bockhorn, A. Hornung, U. Hornung, Environmental engineering: Stepwise pyrolysis of plastic waste, Chem. Eng. Sci. 54 (1999) 3043.
46. H. Bockhorn, A. Hornung, U. Hornung, Stepwise pyrolysis for raw material recovery from plastic waste, J. Anal. Appl. Pyrol. 46(1998) 1.

47. T. Bhaskar, M. Azharuddin, K. Murai, J. Kancko, K. Hemano, T. Kusaba, A. Muto,Y. Sakata, Comparison of thermal degradation products from real municipal waste plastic and model mixed plastics, J. Anal. Appl. Pyrol. 70(2003) 579.

48. T. Bhaskar, M. Tanabea, A. Mutoa, Y. Sakataa, C.-F. Liub, M.-D. Chenb, C. C. Chao, Analysis of chlorine distribution in the pyrolysis products of poly(vinylidene chloride) mixed with polyethylene, polypropylene or polystyrene, Polym. Degrad. Stab. 89 (2005) 38.

49. H. Bockhorn, A. Hornung, U. Hornung, Mechanisms and kinetics of thermal decomposition of plastics from isothermal and dynamic measurements, J. Anal. Appl. Pyrol. 50 (1999) 77.

50. V. Mamleev, S. Bourbigot, M. L. Bras, S. Duquesne, J. Šesták, Modeling of nonisothermal kinetics in thermogravimetry Phys, Chem.Chem. Phys. 2 (2000) 4708.

51. H. Bockhorn, A. Hornung, U. Hornung, D. Schawaller, Kinetic study on the thermal degradation of polypropylene and polyethylene, J. Anal. Appl. Pyrol. 48 (1999) 93.

52. B. J. Holland, J. N. Hay, The thermal degradation of PET and analogous polyesters measured by thermal analysis–Fourier transform infrared spectroscopy, Polymer 43 (2002) 1835.

53. L. Wang, C. Peng, Development of first-stage co-liquefaction of Chinese coal with waste plastics, Chem. Eng. Process. 43(2004) 145.

54. E. Ha´jekova´, M. Bajus,Recycling of low-density polyethylene and polypropylene via copyrolysis of polyalkene oil/waxes with naphtha: product distribution and coke formation, J. Anal. Appl. Pyrol. 74 (2005) 270.

55. V. I. Sharypov, N.G. Beregovtsova, B.N. Kuznetsov, V.L. Cebolla, S. Collura, G. Finqueneisel, T. Zimny and J.V. Weber, Influence of reaction parameters on brown coal–polyolefinic plastic co-pyrolysis behavior, J. Anal. Appl. Pyrol. 78 (2007) 257.

56 G. Karishma, G. Manos, Polymer degradation to fuels over microporous catalysts as a novel tertiary plastic recycling method, Polym. Degrad. Stab. 83 (2004) 267.

57. G. Karishma, G. Manos, Thermogravimetric study of polymer catalytic degradation over microporous materials, Polym. Degrad. Stab. 86 (2004), 225.
58. A. Marcilla, A. Go´mez, J.A. Reyes-Labarta, A. Giner, F. Herna´ndez, Kinetic study of polypropylene pyrolysis using ZSM-5 and an equilibrium fluid catalytic cracking catalyst, J. Anal. Appl. Pyrol. 68-69 (2003) 467.
59. A. Marcilla, M. Beltran, J.A. Conesa, Catalyst addition in polyethylene pyrolysis Thermogravimetric study, J. Anal. Appl. Pyrol. 58-59 (2001) 117.
60. J. G. A. P. Filho, E.C. Graciliano, A.O.S. Silva, M.J.B. Souza, A.S. Araujo, Thermo gravimetric kinetics of polypropylene degradation on ZSM-12 and ZSM-5 catalysts, Catal.Today, 107-108 (2005)507.
61. Q. Zhou, L. Zheng, Y.Z. Wang, G.M. Zhao, B. Wang, Catalytic degradation of low-density polyethylene and polypropylene using modified ZSM-5 zeolites, Polym. Degrad. Stab. 84 (2004) 493.
62. Q. Zhou, Y. Z. Wang, C. Tang, Y. H. Zhang, Modifications of ZSM-5 zeolites and their applications in catalytic degradation of LDPE, Polym. Degrad. Stab. 80(2003) 23.
63. J. Aguado, D. P. Serrano, G. S. Miguel, J. M. Escola, J. M. Rodrı´guez, Catalytic activity of zeolitic and mesostructured catalysts in the cracking of pure and waste polyolefins, J. Anal. Appl. Pyrol., 78 (2007) 153.
64. A. Durmus¸ A.; S. N. Koc, G. S. Pozan, A. Kasgoz, Thermal-catalytic degradation kinetics of polypropylene over BEA, ZSM-5 and MOR zeolites, Appl. Catal. B 61 (2005) 316.
65. C. Vasile, H. Pakdel, B. Mihai, P. Onu, H. Darie, S. Ciocâlteu, Thermal and catalytic decomposition of mixed plastics, J.Anal. Appl.Pyrol. 57 (2001) 287.
66. D.P.Serrano, J. Aguado, J. M. Escola, J. M. Rodrı´guez, G. S. Miguel, An investigation into the catalytic cracking of LDPE using Py-GC/MS, J. Anal. Appl. Pyrol. 74 (2005) 370.
67. A. Marcilla, M. I. Beltran, R. Navarro, TG/FT-IR analysis of HZSM5 and HUSY deactivation during the catalytic pyrolysis of polyethylene, J. Anal. Appl. Pyrol. 76 (2006) 222.

68. A. Marcilla, A. Go´mez-Siurana, D. Berenguer, Study of the influence of the characteristics of different acid solids in the catalytic pyrolysis of different polymers, Appl. Catal. A, 301 (2006) 222.

69. A. Marcilla, A. Go´mez-Siurana, F. Valde´s, Catalytic pyrolysis of LDPE over H-beta and HZSM-5 zeolites in dynamic conditions Study of the evolution of the process, J. Anal. Appl. Pyrol. 79 (2007) 433.

70. Y.-H. Lin, H.-Y. Yen, Fluidised bed pyrolysis of polypropylene over cracking catalysts for producing hydrocarbons, Polym. Degrad. Stab. 89 (2005)101.

71. R.A. Garcı´a, D.P. Serrano, D. Otero, Catalytic cracking of HDPE over hybrid zeolitic–mesoporous materials, J. Anal. Appl. Pyrol. 74 (2005) 379.

72. P. Onu, C. Vasile, S. Ciocilter, E. Iojoiu, H. Darie, Thermal and catalytic decomposition of polyetheylene and polypropylene, J. Anal. Appl. Pyrol., 49 (1999)145.

73. A. Marcilla,; M.I. Beltra´n, F.Herna´ndez, R. Navarro, HZSM5 and HUSY deactivation during the catalytic pyrolysis of polyethylene, Appl. Catal. A. 37 (2004) 278.

74. Y.-H. Lin, M.-H. Yang, Catalytic conversion of commingled polymer waste into chemicals and fuels over spent FCC commercial catalyst in a fluidised-bed reactor, Appl. Catal. B. 69 (2006)145.

75. N. S. Akpanudoh, K. Gobin, G. Manos,; Catalytic degradation of plastic waste to liquid fuel over commercial cracking catalysts effect of polymer to catalyst ratio/acidity content, J. Mol. Catal. A: Chem. 235 (2005) 67.

76. A. S. Araujo, J. V. J. Fernandes, G. J. T. Fernandes, Thermogravimetric kinetics of polyethylene degradation over silicoaluminophoshate, Thermochim. Acta. 392-393 (2002) 55.

77. G. J. T. Fernandes, J. V. J. Fernandes, A.S. Araujo, Catalytic degradation of polyethylene over SAPO-37 molecular sieve, Catal. Today 75 (2002) 233.

78. K. Takuma, Y. Uemichi, A. Ayame, Product distribution from catalytic degradation of polyethylene over H-gallosilicate, Appl. Catal. A. 192 (2000)273.

79. J. Aguado, D. P. Serrano, J. M. Escola, E. Garagorri, J. A. Fernández, Catalytic conversion of polyolefins into fuels over zeolite beta, Polym. Degrad. Stab. 69 (2000)11.

80. A. Marcilla, A. Gómez,; Á.N. García, M.M. Olaya, Kinetic study of the catalytic decomposition of different commercial polyethylenes over an MCM-41 catalyst, J. Anal. Appl. Pyrol. 64 (2002) 85.

81. A. Marcilla, A. Go´mez, J.A. Reyes-Labarta, A. Giner, F. Herna´ndez, Catalytic pyrolysis of polypropylene using MCM-41: kinetic model, Polym. Degrad. Stab. 80 (2003) 233.

82. J. Walendziewski, M. Steininger, Thermal and catalytic conversion of waste polyolefines, Catal. Today , 65 (2001) 323.

83. J. Walendziewski, Engine fuel derived from waste plastics by thermal treatment, Fuel, 81 (2002) 473.

84. G. D. L. Puente, C. Klocker, U. Sedran, Conversion of waste plastics into fuels: Recycling polyethylene in FCC, Appl. Catal. B, 36 (2002) 279.

85. A. Marcilla, R. Ruiz-Femenia, J. Herna´ndez, J.C. Garcı´a-Quesada, Thermal and catalytic pyrolysis of crosslinked polyethylene, J. Anal. Appl. Pyrol. 76 (2006) 254.

86 J. S. Kim, W. Y.Lee, S. B. Lee, S. B. Kim, M. J Choi, Degradation of polystyrene waste over base promoted Fe catalysts, Catal. Today**,** 87(2003) 59.

87. T. Masuda, H. Kuwahara, S. R. Mukai, K. Hashimoto, Production of high quality gasoline from waste polyethylene derived heavy oil over Ni-REY catalyst in steam atmosphere, Chem. Eng. Sci. 54 (1999) 2773.

88. T. Masudaa, T. Kushino, T. Matsuda, S. R. Mukaia, K. Hashimoto, S. Yoshida, Chemical recycling of mixture of waste plastics using a new reactor system with stirred heat medium particles in steam atmosphere, Chem. Eng. J. 82 (2001) 173.

89. H. Ohkita, R. Nishiyama, Y. Tochihara, T. Mizushima, N. Kakuta, Y. Morioka, A. Ueno, Y. Namiki, S. Tanifuji, H. Katoh, H. Sunazuka, R. Nakayama, T Kuroyanagi, Acid properties of silica-alumina catalysts and catalytic degradation of polyethylene, Ind. Eng. Chem. Res. 32 (1993) 3112.

90. G. Manos, A. Garforth, J. Dwyer, Catalytic Degradation of High-Density Polyethylene over Different Zeolitic Structures, Ind. Eng. Chem. Res. 39 (2000) 1198.

91. G. Manos, A. Garforth, J. Dwyer, Catalytic Degradation of High-Density Polyethylene on an Ultrastable-Y Zeolite. Nature of Initial Polymer Reactions, Pattern of Formation of Gas and Liquid Products, and Temperature Effects, Ind. Eng. Chem. Res. 39 (2000) 1203.

92. G. Manos, I. Y. Yusof, N. Papayannakos,N. H. Gangas, Catalytic Cracking of Polyethylene over Clay Catalysts. Comparison with an Ultrastable Y Zeolite, Ind. Eng. Chem. Res. 40 (2001) 2220.

93. J. Aguado, D. P. Serrano, J. L. Sotelo, R. Van Grieken, J. M. Escola, Influence of the Operating Variables on the Catalytic Conversion of a Polyolefin Mixture over HMCM-41 and Nanosized HZSM-5, Ind. Eng. Chem. Res. 40 (2001) 5696.

94. D. P. Serrano, J. Aguado, J. M. Escola**,** Catalytic Cracking of a Polyolefin Mixture over Different Acid Solid Catalysts, Ind. Eng. Chem. Res. 39 (2000) 1177.

95. Z. Zhang, T. Hirose, S. Nishio, Y. Morioka, N. Azuma, and A.Ueno, H. Ohkita, M. Okada, Chemical Recycling of Waste Polystyrene Acids and Bases into Styrene over Solid, Ind. Eng. Chem. Res. 34 (1995) 4514.

96. G. d. l. Puente, J. M. Arandes, U. A. Sedran, Recycled Plastics in FCC Feedstocks: Specific Contributions, Ind. Eng. Chem. Res. 36 (1997) 4530.

97. K. Takuma, Y. Uemichi, M. Sugioka, A. Ayame, Production of Aromatic Hydrocarbons by Catalytic Degradation of Polyolefins over H-Gallosilicate, Ind. Eng. Chem. Res. 40 (2001) 1076.

98. P Filomena, C. Paula, I.Gulyurtlu, I. Cabrita, Pyrolysis of plastic wastes: 2. Effect of catalyst on product yield, J. Anal. Appl. Pyrol. 51 (1999) 57.

99. A. Matsumoto, H. Chen, K. Tsutsumi, M. Gru¨n, K. Unger, Novel route in the synthesis of MCM-41 containing framework aluminum and its characterization, Micro. Meso. Mat. 32 (1999) 55.

100. M.M.L. Ribeiro Carrott, F.L. Conceic¸a˜o, J.M. Lopes, P.J.M. Carrott, C. Bernardes, J. Rocha, F. Ramoˆa Ribeiro, Comparative study of Al-MCM

materials prepared at room temperature with different aluminium sources and by some hydrothermal methods, Micro. Meso. Mat. 92 (2006) 270.

101. R. H. P. R. Poladi, C. C. Landry, Synthesis, Characterization, and Catalytic Properties of a Microporous/Mesoporous Material, MMM-1, J. solid state chem. 167 (2002) 363.

102. J. Aguado, D.P. Serrano, J.M. Escola, A sol–gel approach for the room temperature synthesis of Al-containing micelle-templated silica, J. solid state chem. 34 (2000) 43.

103. D.P. Serrano, J. Aguado, J.M. Escola, E. garagorri, J.M. Rodriguez, G. Palazzi, R. Orsi, Feedstock recycling of agriculture plastic film wastes by catalytic cracking, Appl. Catal. B. 49 (2004) 257.

104. N. Lingaiah.,.Md. A. Uddin, A. Muto.., T. Imai., Y. Sakata. , Removal of organic chlorine compounds by catalytic dehydrochlorination for the refinement of municipal waste plastic derived oil ,Fuel, 80 (2001) 1901.

105. Jale.Yanik,.Md. A. Uddin, Kazno. Ikenchi, Y.Sakata, The catalytic effect of Red Mud on the degradation of poly (vinyl chloride) containing polymer mixture into fuel oil , Polym. Degrad. Stab. 73(2001) 335.

106. Q. Zhou, C. Tang, Y.-Z. Wang, L. Zheng, Catalytic degradation and dechlorination of PVC-containing mixed plastics via Al–Mg composite oxide catalysts, Fuel 83 (2004) 1727.

107. M. Brebu, T.bhaskar, K. Murai, A. Muto, Y. Sakata, Md. A. Uddin, Removal of nitrogen, bromine, and chlorine from PP/PE/PS/PVC/ABS–Br pyrolysis liquid products using Fe- and Ca-based catalysts, Polym. Degrad. Stab. 87 (2005) 225.

108. F. Carrasco, The evaluation of kinetic parameters from thermogravimetric data: comparison between established methods and the general analytical equation, Thermochimi. Acta, 213 (1993) 115.

109. Y.-H. Lin, W.-H. Hwu, M.-D. Ger , T.-F. Yeh , J. Dwyer, A combined kinetic and mechanistic modelling of the catalytic degradation of polymers, J. Mol. Catal. A: Chem. 171 (2001) 143.

110. B. J. McCoy, G. Madras, Analytical solution for a population balance equation with aggregation and fragmentation, Chem. Eng. Sci. 58 (2003) 3049..

111. Y. Kodera, B. J. McCoy, Distribution Kinetics of Radical Mechanisms: Reversible Polymer Decomposition, AIChE J, 43 (1997) 3205.
112. W. J. Sterling, B. J. McCoy, Distribution Kinetics of Thermolytic Macromolecular Reactions, AIChE J, 47 (2001) 2289.
113. B. J. McCoy, M. Wang, Continuous Kinetics of Cracking of Reaction: Thermolysis and Pyrolysis, Chem. Eng.Sci. 51 (1996) 2903.
114. B. J. McCoy, Continuous-Mixture Fragmentation Kinetics: Particle size reduction and Molecular Cracking, Chem. Eng. Sci. 49 (1994) 3773.
115. W. J. Sterling, K. S. Walline, B. J. McCoy, Experimental study of polystyrene thermolysis to moderate conversion, Polym. Degrad. Stab. 73 (2001) 75.
116. G. Madras, B. J. McCoy , Effect of hydrogen donors on polymer degradation, Catal. Today 40 (1998) 321.
117. B. J. McCoy, Polymer thermogravimetric analysis: e!ects of chain-end and reversible random scission, Chem. Eng. Sci. 56 (2001) 1525..
118. G. Madras, J. M. Smith, B. J. McCoy, Thermal degradation of poly(cw-methylstyrene) in solution, Polym. Degrad. Stab. 52 (1996) 349.
119. K. Mehta, G. Madras, Dynamics of Molecular Weight Distributions for Polymer Scission, AIChE J, 47 (2001) 2289.
120. G. Sivalingam, G. Madras, Oxidative degradation of poly (vinyl acetate) and poly (ε-caprolactone) and their mixtures in solution, Chem. Eng. Sci. 59 (2004) 1577.
121. G. Sivalingam, P. De, R. Karthik, G. Madras, Thermal degradation kinetics of vinyl polyperoxide copolymers, Polym. Degrad. Stab. 84 (2004) 173.
122. G. Sivalingam, G. Madras, Thermal degradation kinetics of poly(ε-caprolactone), Polym. Degrad. Stab. 84 (2004) 173.
123. G. Sivalingam, R. Karthik, G. Madras, Thermal degradation kinetics of poly(ε-caprolactone), J. Anal. Appl. Pyrol. 70 (2003) 631.
124. S. Chattopadhyay, G. Madras, Degradation kinetics of poly(vinyl acetate) in the presence of aluminum chloride, Polym. Degrad. Stab. 73 (2001) 83.
125. T. M. Kruse, O. S. Woo, H.-W. Wong, S. S. Khan, L. J. Broadbelt, Mechanistic Modeling of Polymer Degradation: A Comprehensive Study of Polystyrene, Macromolecules 35 (2002) 7830.

126. T. M. Kruse, O. S. Woo, L. J. Broadbelt, Detailed mechanistic modeling of polymer degradation: application to polystyrene, Chem. Eng. Sci. 56 (2001) 971.
127. A. K. Burnham, Application of the sestak-Berggren equation to organic and inorganic materials of practical interest, J. Therm. Anal. Cal. 60 (2000) 895.
128. A. K. Burnham, R. K. Weese, Kinetics of thermal degradation of explosive binders Viton A, Estane, and Kel-F, Thermochimi. Acta. 42 (2005) 85.
129. I. Martin-Gullon, M. Esperanza,R. Font, Kinetic model for the pyrolysis and combustion of poly-(ethylene terephthalate) (PET), J. Anal. Appl. Pyrol. 58-59 (2001) 635.
130. I. Martin-Gullon, M. F.Gomez-Rico,A.Fullana; R.Font, Interrelation between the kinetic constant and the reaction order in pyrolysis, J. Anal. Appl. Pyrol. 68-69 (2003) 645.
131. V. Mamleev, S. Bourbigot, Modulated thermogravimetry in analysis of decomposition kinetics, Chem. Eng. Sci. 60 (2005) 747.
132. J. Lefebvrea, V. Mamleev, M. L. Brasa, S. Bourbigot, Kinetic analysis of pyrolysis of cross-linked polymers, Polym. Degrad. Stab. 88 (2005) 85.
133. X. Wang, X. Li, D. Yan, Thermal decomposition kinetics of poly(trimethylene terephthalate). Polym. Degrad. Stab. 69 (2000) 361.
134. Z. Gao, I. Amasaki, M. Nakada, A thermogravimetric study on thermal degradation of polyethylene, J. Anal. Appl. Pyrol., 67 (2003) 1.
135. T. Faravelli, G. Bozzano, M. Colombo, E. Ranzi, M. Dente, Kinetic modeling of the thermal degradation of polyethylene and polystyrene mixtures, J. Anal. Appl. Pyrol. 70 (2003) 761.
136. H. Bockhorn, S. Donner, M. Gernsbeck, A. Hornung, U. Hornung, Pyrolysis of polyamide 6 under catalytic conditions and its application to reutilization of carpets, J. Anal. Appl. Pyrol. 58–59 (2001) 79.
137. D.Y.C Leung, C.L. Wang, Kinetics study of scrap tyre pyrolysis and combustion, J. Anal. Appl. Pyrol. 45 (1998)153.
138. J. A.Conesa, J.A. Caballero, J.A. Reyes-Labarta, Artificial neural network for modelling thermal decomposition, J. Anal. Appl. Pyrol. 71 (2004) 343.

139. J.J. Baeza-Baeza, G. Ramis-Ramos, Analysis of the sensitivity to the systematic error in least-squares regression models, Analytica Chemica Acta. 515 (2004) 15.
140. M. Guay, D.D. McLean, Optimization and sensitivity analaysis for multiresponse paramerter estimation in systems of ordinary differential equations, Computers Chem. Eng. 12 (1994) 1271.
141. R.W. Atherton, R. B.Schaniker, E.R. Ducot On the Statistical Sensitivity Analysis of Models for Chemical Kintics, *AIChE J*. 21(1975) 441.
142. R.P. Dickinson, R.J. Gelinas, Sensitivity analysis of ordinary differential equation systems-a direct method, J. Comput. Phys. 21 (1976) 123.
143. J.T. Hwang, E.P. Dougherty, S. Rabitz, H. Rabitz, The green's function method of sensitivity analysis in chemical kinetics, J. Chem. Phys. 69 (1978) 5180.
144. A.M. Dunker, The decoupled direct method for calculating sensitivity coefficients in chemical kinetics, J. Chem. Phys. 81 (1984) 2385.
145. S. Li, L. Petzold, Software and algorithms for sensitivity analysis of large-scale differential algebraic systems, J. Comput. Appl. Math. 125 (2000) 131.
146. A. Hakami, M. T. Odman, G. A. Russell, Nonlinearity in atmospheric response: a direct sensitivity analysis approach, J. Geophys. Res. 109 (2004) D15303.
147. A. Sandu, N. D. Daescu, R. G. Carmichael, Direct and adjoint sensitivity analysis of chemical kinetics systems with KPP: Part I-theory and software tools, Atmos. Environ. 37 (2003) 5083.
148. R. G. Carmichael, A. Sandu, A. F. Potra, Sensitivity analysis for atmospheric chemistry models via automatic differentiation, Atmos. Environ. 31 (1997) 475.
149. D. Hwang, W.D. Byun, T.M. Odman, An automatic differentiation technique for sensitivity analysis of numerical advection schemes air quality models, Atmos. Environ. 31 (1997) 879.
150. L. Sherman, C.A. Taylor III, L. L. Green, A. P. Newman, W. G. Hou, M. V. Korivi, First- and second order aerodynamica sensitivity derivatives via automatic differentiation with incremental iterative methods, J. Comput. Phys. 129 (1996) 307.
151. D. E Zak, J Stelling, F.J. Doyle III, Sensitivity analysis of oscillatory (bio) chemical systems, Comput. Chem. Eng. 29 (2005) 663.

152. M Zanfir, A. Gavariilidis, An investigation of catalytic plate reactors by means of parametric sensitivity analysis, Chem. Eng. Sci. 57 (2002) 1653.
153. N. Sun, N. –Z. Sun, M. Elimelech, N.J. Ryan, Sensitivity analysis and parameters identifiability for colloid transport in geochemically heterogeneous porous media, Water Resour. Res. 37 (2001) 209.
154. B. A. Salah, S. Kliem, U. Rohde, F. D'Auria, A. Petruzzi, Uncertainty and sensitivity analyses of the Kozloduy pump trip test using coupled thermal-hydraulic 3D kinetics code, Nucl. Eng. Des. 236 (2006) 1240.
155. S. Vyazovkin, C.A. Wight, Kinetics of Thermal Decomposition of Cubic Ammonium Perchlorate, Chem. Mater. 11 (1999) 3386.
156. A Khawam, D R. Flangan, Role of isoconversional methods in varying activation energies of solid-state kinetics: I. isothermal kinetic studies, Thermochimi. Acta 429 (2005) 93.
157. R. E. Lyon, An integral method of nonisothermal kinetic analysis, Thermochim. Acta. 297 (1997) 117.
158. J. D. Peterson, S. Vyazovkin, C.A. Wight, Kinetic Study of Stabilizing Effect of Oxygen on Thermal Degradation of Poly(methyl methacrylate), J. Phys. Chem. B. 103 (1999) 8087.
159. X. Meng, Y. Huang, H. Yu, Z. Lv, Thermal degradation kinetics of polyimide containing 2,6-benzobisoxazole units, Polym. Degrad. Stab. 92 (2007) 962.
160. B. Janković, B. Adnadević, J. Jovanović, Application of model-fitting and model-free kinetics to the study of non-isothermal dehydration of equilibrium swollen poly (acrylic acid) hydrogel: Thermogravimetric analysis, Thermochimi. Acta. 452 (2007) 106.
161. C. Vasile, E. Costea, L. Odochian, The thermoxidative decomposition of low density polyethylene in non-isothermal conditions, Thermochimi. Acta 184 (1991) 305.
162. P.Carniti, A.Gervasini Thermogravimetric study of the kinetics of degradation of polypropylene with solid catalysts. Thermochim. Acta. 379 (2001) 51.
163. A. Marcilla, J.C. Garc´ıa-Quesada, R. Ruiz-Femenia, Additional considerations to the paper entitled: "Computational aspects of kinetic analysis. Part B: The ICTAC

Kinetics Project—the decomposition kinetics of calcium carbonate revisited, or some tips on survival in the kinetic minefield." Thermochimi. Acta 445 (2006) 92.

164. L. Elliotta, D.B. Inghama, A.G Kyneb, N.S. Merab, M. Pourkashanianc, C.W. Wilson, Genetic algorithms for optimisation of chemical kinetics reaction mechanisms. Prog. Energy Combust. Sci. 30 (2004) 297.

165. S. Katare, A. Bhan, J. M. Caruthers, W. N. Delgass, V. A. Venkatasubramanian hybrid genetic algorithm for efficient parameter estimation of large kinetic model, Comput. Chem. Eng. 28 (2004) 2569.

166. L. Balland, L. Estel, J.-M. Cosmao, N. Mouhab, A genetic algorithm with decimal coding for the estimation of kinetic and energetic parameters, Chemometr. Intell. Lab. Syst. 50 (2000) 121

167. G. Rein, C. Lautenberger, A. C. Fernandez-Pello, J. L. Torero, D. L. Urban, Application of genetic algorithms and thermogravimetry to determine the kinetics of polyurethane foam in smoldering combustion, Combust. Flame 146 (2006) 95.

168. S.D Harris, L. Elliott, D.B. Ingham, M. Pourkashanian, C.W. Wilson, The optimisation of reaction rate parameters for chemical kinetic modelling of combustion using genetic algorithms, Comput. Methods Appl. Mech. Engrg. 190 (2000) 1065.

169. L. Elliott, D. B. Ingham, A.G. Kyne, N. S. Merab, M. Pourkashanian, S. Whittake, Reaction mechanism reduction and optimisation for modelling aviation fuel oxidation using standard and hybrid genetic algorithms, Comput. Chem. Eng. 30 (2006) 889.

170. T.-Y. Park, G. F. Froment, A Hybrid Genetic Algorithm for the Estimation of Parameters in Detailed Kinetic Models, Computers Chem. Eng. 22 (1998) Suppl.. S103.

171. D. B. Hibbert, A hybrid genetic algorithm for the estimation of kinetic parameter, Chemometr. Intell. Lab. Syst. 19 (1993), 319.

172. P. K. Gudla, R. Ganguli, An automated hybrid genetic-conjugate gradient algorithm for multimodal optimization problems, Appl. Math. Comput. 167 (2005) 1457.

173. MATLAB® help, Version 7.0.0.19920 (R14), The Math Works, Inc.: Natick, MA (2004).

174. S. Vyazovkin, C.A. Wight, Estimation realistic confidence intervals for the activation energy determined from thermoanalytical measurements, Anal. Chem. 72 (2000) 3171.

175. B. Saha, A.K. Ghoshal, Thermal degradation kinetics of poly (ethylene terephthalate) from waste soft drinks bottles, Chem. Eng. J. 111 (2005) 39.

176. B. Saha, A.K. Maiti, A.K. Ghoshal, Model-free Method for Isothermal and nonisothermal Decomposition Kinetics Analysis of PET Sample, Thermochimi. Acta. 444 (2006) 46.

177. B. Saha, A.K. Ghoshal, Model-Fitting Methods for Evaluation of Kinetics Triplet during Thermal Decomposition of PET Soft Drink Bottles, Ind. Eng. Chem. Res., 45 (2006) 7752.

178. B. Saha, A.K. Ghoshal, Model-Free Kinetics Analysis of waste PE, Thermochimi. Acta., 451 (2006) 27.

179. B. Saha, A.K. Ghoshal, Model-free Kinetics Analysis of ZSM-5 Catalysed Pyrolysis of waste LDPE, Thermochimi. Acta. 453 (2007) 120.

180. B. Saha, A.K. Ghoshal, Model-free Kinetics Analysis of Decomposition of Polypropylene over Al-MCM-41, Thermochimi. Acta., 2007, doi: 10.1016/j.tca.2007.05.016.

181. B. Saha, P. Karthik Reddy, A.K. Ghoshal, Hybrid Genetic Algorithm to Find the Best Model and the Globally Optimized Overall Kinetics Parameters for Thermal Decomposition of Plastics, Chem. Eng. J., 2007, doi: 10.1016/j.cej.2007.05.024.

182. B. Saha, A.K. Ghoshal, Hybrid Genetic Algorithm and Model Free Coupled Direct Search Methods for Pyrolysis Kinetics of ZSM-5 Catalyzed Decomposition of Waste LDPE, Ind. Eng. Chem. Res., 2007: doi: 10.1021/ie0615483.

183. B. Saha, P. Chowdhury, A.K. Ghoshal, Al-MCM-41 Catalyzed Decomposition of Polypropylene and Hybrid Genetic Algorithm for Kinetics Analysis, Appl. Catal. B, 2006 (under review).

184. H. J.Motulsky, A. Christopoulos, Fitting Models to Biological Data Using Linear and Nonlinear Regression; Oxford University Press: New York, 2003; pp 143-148. (ISBN No. 0195171802).

185. METTLER TOLEDO STARe System Manual for Kinetic Analysis by TGA/DSC.

186. J. Cai, F.Yao, W. Yi, F. He, New temperature integral approximation for nonisothermal kinetics, AIChE J 52 (2006) 1554.

187. R.K. Agarwal, M.S. Sivasubramanian, Integral Approximation for nonisothermal kinetics, AIChE J 33 (1987) 1212.

188. Tamás Turányi, Sensitivity analysis of complex kinetic systems. Tools and applications, J. Math. Chem., 5 (1990) 203.

189. S.V. Vyazovkin, A.I. Lesnikovich, Practical application of isoconversional methods, Thermochimi. Acta. 203 (1992) 177.

190. http://webstore.ansi.org/ansidocstore/product.asp?sku=ASTM+E1131-03(As see on dated 05/04/ 2007).

191. http://www.chemistry.mcmaster.ca/~ayers/chem2PA3/labs/2PA37a.pdf (As see on dated 01/05/ 2007).

192. R. V. Grieken, J.M. Escola, J. Moreno, R. Rodrı´guez, Liquid phase oligomerization of 1-hexene over different mesoporous aluminosilicates (Al-MTS, Al-MCM-41 and Al-SBA-15) and micrometer/nanometer HZSM-5 zeolites ,Appl. Catal. A. 305 (2006) 176.

193. R. V. Grieken, J. L. Sotelo, J. M. Menéndez, J. A. Melero, Anomalous crystallization mechanism in the synthesis of nanocrystalline ZSM-5 Micro. Meso. Mat. 39 (2000) 135.

194. D.P. Serrano, J. Aguado, J. M. Escola, J.M. Rodrı´guez, Influence of nanocrystalline HZSM-5 external surface on the catalytic cracking of polyolefins, J. Anal. Appl. Pyrol. 74 (2005) 353.

195. Yang, R. Miranda, C. Roy, Using the DTG curve fitting method to determine the apparent kinetic parameters of thermal decomposition of polymers, Polym. Degrad. Stab. 73 (2001) 455.

196. B. J. Holland, J. N. Hay, The value and limitations of non-isothermal kinetics in the study of polymer degradation, Thermochimi. Acta. 388 (2002) 253.

197. R.W.J. Westerhout, R.H.P. Balk, R. Meijer, J.A.M. Kuipers, W.P.M. van Swaaij, Examination and evaluation of the use of screen heaters for the measurement of the high temperature pyrolysis kinetics of polyethene and polypropene, Ind. Eng. Chem. Res. 36 (1997) 3360.

198. R.W.J. Westerhout, J. Waanders, J.A.M. Kuipers, W.P.M. van Swaaij, Kinetics of the low-temperature pyrolysis of polyethene, polypropene, and polystyrene. Modeling, experimental determination, and comparison with literature models and data, Ind. Eng. Chem. Res. 36 (6) (1997) 1955.

199. M. Day, J.D. Cooney, M. MacKinnon, Degradation of contaminated plastics: a kinetic study, Polym. Degrad. Stab. 48 (3) (1995) 341.

200. C. Wu, C. Chang, J. Hor, S. Shih, L. Chen, F. Chang, On the thermal treatment of plastic mixtures of MSW: pyrolysis kinetics, Waste Manage. 13 (1993) 221.

201. J.A. Conesa, A. Marcilla, R. Font, J.A. Caballero, Thermogravimetric studies on the thermal decomposition of polyethylene, J. Anal. Appl. Pyrol. 36 (1996)1.

202. P.L. Beltrame, P. Carniti, G. Audisio, F. Bertini, Catalytic degradation of polymers. Part II: Degradation of polyethylene, Polym. Degrad. Stab. 26 (1989) 209.

203. J.R. Fried, Polymer Science and Technology, Prentice-Hall, India, 2000, pp. 291, 473.

Appendix I

Computation of sensitivity matrix

Variance or var (p_i): For a random variable pi with mean value $< p_i >$, ($p_i - < p_i >$) represents the deviation of the variable from its mean. Deviation can be either positive or negative. By definition:

$$\mathrm{var}(p_i) = \sigma^2(p_i) = \frac{\sum (p_i - < p_i >)^2}{N}, \text{ N=total number of data points and } \sigma^2(p_i) \text{ known as variance} \quad \text{(AI.1)}$$

Similarly, covariance of two variables pi and p_j is defined as

$$\mathrm{cov}(p_i, p_j) = \left\langle (p_i - < p_i >)(p_j - < p_j >) \right\rangle \quad \text{(AI.2)}$$

For a model out put variable, X which is a function of parameters pi and p_j, by Taylor series expansion

$$\langle X \rangle = X + \frac{1}{2}\sum_{i=1}^{n} \frac{\partial^2 X}{\partial p_i^2} \mathrm{var}(p_i) + \sum_i \sum_j \frac{\partial^2 X}{\partial p_i \partial p_j} \mathrm{cov}(p_i, p_j) \quad \text{(AI.3)}$$

Subscripts i and j are the coloum counter of parameters vector matrix.

The variance of X is represented as follows

$$\mathrm{var}(X) = \sum_i \left(\frac{\partial X}{\partial p_i}\right)^2 \mathrm{var}(p_i) + 2\sum_i \sum_j \left(\frac{\partial X}{\partial p_i}\right)\left(\frac{\partial X}{\partial p_j}\right) \mathrm{cov}(p_i, p_j) + \sum_i \left(\frac{\partial X}{\partial p_i}\right)\left(\frac{\partial^2 X}{\partial p_i^2}\right) \mu_3(p_i) \quad \text{(AI.4)}$$

Equation (AI.4) is simplified to Eq. (AI.5) after the following assumption:

For each parameter pi, either $\mu_3(p_i)$ or $\frac{\partial^2 X}{\partial p_i^2}$ is zero or small. So, the third term on the right hand side of Eq. (AI.4) can be neglected. Thus,

$$\mathrm{var}(X) = \sum_i \left(\frac{\partial X}{\partial p_i}\right)^2 \mathrm{var}(p_i) + 2\sum_i \sum_j \left(\frac{\partial X}{\partial p_i}\right)\left(\frac{\partial X}{\partial p_j}\right) \mathrm{cov}(p_i, p_j) \quad \text{(AI.5)}$$

If the parameters p_i are uncorrelated, then the second term can be neglected. The resulting equation for variance of X [Eq. (AI.6)] can be used to calculate the first order sensitivity coefficients.

$$\mathrm{var}(X) = \sum_i \left(\frac{\partial X}{\partial p_i} \right)^2 \mathrm{var}(p_i) \tag{AI.6}$$

The overall pyrolysis kinetics often described by a nonlinear stiff ordinary differential equation [Eq. (AI.7)].

$$\frac{d\alpha}{dT} = \left(\exp(\tilde{K}_0) \Big/ \beta \right) \exp\left(-E \Big/ RT \right) (1-\alpha)^n \tag{AI.7}$$

Defining the first order sensitivity co-efficient ($S^{\langle 1 \rangle}_{\alpha p_i}$) for parameter p_i (i.e. $\tilde{K}_0$, E, n and β), $S^{\langle 1 \rangle}_{\alpha p_i} = \left. \frac{\partial \alpha}{\partial p} \right|_{\alpha = T, p_i}$, Eq. (AI.7), can be rewritten as:

$$\frac{d\alpha}{dT} = f(\alpha, p) \equiv g \tag{AI.8}$$

Here, α changes with temperature but the parameters, p_i do not. In order to calculate the sensitivity matrix, we take the derivative of sensitivity co-efficient with respect to temperature. Thus,

$$\frac{dS^{\langle 1 \rangle}_{\alpha p_i}}{dT} = \frac{d}{dT}\left(\frac{\partial \alpha}{\partial p_i} \right) = \frac{\partial}{\partial p_i}\left(\frac{d\alpha}{dT} \right) = \frac{\partial}{\partial p_i} f(\alpha, p) \tag{AI.9}$$

Since α is function of p_i, the right hand expression is extended to give

$$\frac{\partial}{\partial p_i} f(\alpha, p) = \left. \frac{\partial g}{\partial p_i} \right|_{\alpha} + \left. \frac{\partial g}{\partial \alpha} \right|_{p_i} \frac{\partial \alpha}{\partial p_i} \tag{AI.10}$$

Therefore, $\frac{dS_{\alpha p_i}^{\langle 1\rangle}}{dT} = \frac{\partial g}{\partial p_i} + \frac{\partial g}{\partial \alpha} S_{\alpha p_i}^{\langle 1\rangle}$ (AI.11)

Thus, for four parameters (i.e. $\tilde{K}_0$, E, n and β) we have

$$\frac{dS_{\alpha \tilde{K}_0}^{\langle 1\rangle}}{dT} = \frac{\partial g}{\partial \tilde{K}_0} + \frac{\partial g}{\partial \alpha} S_{\alpha \tilde{K}_0}^{\langle 1\rangle} \quad \text{(AI.12)}$$

$$\frac{dS_{\alpha E}^{\langle 1\rangle}}{dT} = \frac{\partial g}{\partial E} + \frac{\partial g}{\partial \alpha} S_{\alpha E}^{\langle 1\rangle} \quad \text{(AI.13)}$$

$$\frac{dS_{\alpha n}^{\langle 1\rangle}}{dT} = \frac{\partial g}{\partial n} + \frac{\partial g}{\partial \alpha} S_{\alpha n}^{\langle 1\rangle} \quad \text{(AI.14)}$$

$$\frac{dS_{\alpha \beta}^{\langle 1\rangle}}{dT} = \frac{\partial g}{\partial \beta} + \frac{\partial g}{\partial \alpha} S_{\alpha \beta}^{\langle 1\rangle} \quad \text{(AI.15)}$$

Now, $\frac{\partial g}{\partial \tilde{K}_0} = \frac{\partial}{\partial \tilde{K}_0}\left(\left(\exp(\tilde{K}_0)/\beta\right)\exp\left(-E/RT\right)(1-\alpha)^n\right) = g$ (AI.16)

Similarly,

$$\frac{\partial g}{\partial E} = -\frac{g}{RT} \quad \text{(AI.17)}$$

$$\frac{\partial g}{\partial n} = g\ln(1-\alpha) \quad \text{(AI.18)}$$

$$\frac{\partial g}{\partial \beta} = -\frac{g}{\beta} \quad \text{(AI.19)}$$

$$\frac{\partial g}{\partial \alpha} = -\frac{gn}{(1-\alpha)} \quad \text{(AI.20)}$$

Therefore, the matrix form of equations for first order sensitivity co-efficient is

$$\frac{d}{dT}\begin{vmatrix} S^{\langle 1\rangle}_{\alpha\tilde{K}_0} \\ S^{\langle 1\rangle}_{\alpha E} \\ S^{\langle 1\rangle}_{\alpha n} \\ S^{\langle 1\rangle}_{\alpha\beta} \end{vmatrix} = \begin{vmatrix} g - \dfrac{gn}{(1-\alpha)} S^{\langle 1\rangle}_{\alpha\tilde{K}_0} \\ -\dfrac{g}{RT} - \dfrac{gn}{(1-\alpha)} S^{\langle 1\rangle}_{\alpha E} \\ g\ln(1-\alpha) - \dfrac{gn}{(1-\alpha)} S^{\langle 1\rangle}_{\alpha n} \\ -\dfrac{g}{\beta} - \dfrac{gn}{(1-\alpha)} S^{\langle 1\rangle}_{\alpha\beta} \end{vmatrix} \tag{AI.21}$$

Similarly, the matrix form of equations consisting of first order sensitivity coefficient for n = 1 is

$$\frac{d}{dT}\begin{vmatrix} S^{\langle 1\rangle}_{\alpha\tilde{K}_0} \\ S^{\langle 1\rangle}_{\alpha E} \\ S^{\langle 1\rangle}_{\alpha\beta} \end{vmatrix} = \begin{vmatrix} g - \dfrac{g}{(1-\alpha)} S^{\langle 1\rangle}_{\alpha\tilde{K}_0} \\ -\dfrac{g}{RT} - \dfrac{g}{(1-\alpha)} S^{\langle 1\rangle}_{\alpha E} \\ -\dfrac{g}{\beta} - \dfrac{g}{(1-\alpha)} S^{\langle 1\rangle}_{\alpha\beta} \end{vmatrix} \tag{AI.22}$$

Further differentiation of Eq.(AI.11) with respect to same parameter p_i gives second order sensitivity co-efficient $\left(S^{\langle 2\rangle}_{p_i}\right)$ matrix equation as follows:

$$\frac{d}{dT}\left(\frac{\partial^2\alpha}{\partial p_i^{\,2}}\right) = \left[\frac{\partial^2 g}{\partial\alpha^2}\left(\frac{\partial\alpha}{\partial p_i}\right) + \frac{\partial^2 g}{\partial\alpha\partial p_i}\right]\frac{\partial\alpha}{\partial p_i} + \left(\frac{\partial g}{\partial\alpha}\right)\frac{\partial^2\alpha}{\partial p_i^{\,2}} + \frac{\partial^2 g}{\partial p_i\partial\alpha}\left(\frac{\partial\alpha}{\partial p_i}\right) + \frac{\partial^2 g}{\partial p_i^{\,2}} \tag{AI.23}$$

$$\frac{d}{dT}\left(S^{\langle 2\rangle}_{p_i}\right) = \left[\frac{\partial^2 g}{\partial\alpha^2} S^{\langle 1\rangle}_{\alpha p_i} + \frac{\partial^2 g}{\partial\alpha\partial p_i}\right] S^{\langle 1\rangle}_{\alpha p_i} + \frac{\partial g}{\partial\alpha} S^{\langle 2\rangle}_{p_i} + \frac{\partial^2 g}{\partial p_i\partial\alpha} S^{\langle 1\rangle}_{\alpha p_i} + \frac{\partial^2 g}{\partial p_i^{\,2}} \tag{AI.24}$$

Thus, for four parameters (i.e. $\tilde{K}_0$, E, n and β) we have

$$\frac{d}{dT}\left(S^{\langle 2\rangle}_{\tilde{K}_0}\right) = \left[\frac{\partial^2 g}{\partial\alpha^2} S^{\langle 1\rangle}_{\alpha\tilde{K}_0} + \frac{\partial^2 g}{\partial\alpha\partial\tilde{K}_0}\right] S^{\langle 1\rangle}_{\alpha\tilde{K}_0} + \frac{\partial g}{\partial\alpha} S^{\langle 2\rangle}_{\tilde{K}_0} + \frac{\partial^2 g}{\partial\tilde{K}_0\partial\alpha} S^{\langle 1\rangle}_{\alpha\tilde{K}_0} + \frac{\partial^2 g}{\partial\tilde{K}_0^{\,2}} \tag{AI.25}$$

$$\frac{d}{dT}\left(S_E^{\langle 2\rangle}\right)=\left[\frac{\partial^2 g}{\partial\alpha^2}S_{\alpha E}^{\langle 1\rangle}+\frac{\partial^2 g}{\partial\alpha\partial E}\right]S_{\alpha E}^{\langle 1\rangle}+\frac{\partial g}{\partial\alpha}S_E^{\langle 2\rangle}+\frac{\partial^2 g}{\partial E\partial\alpha}S_{\alpha E}^{\langle 1\rangle}+\frac{\partial^2 g}{\partial E^2} \quad \text{(AI.26)}$$

$$\frac{d}{dT}\left(S_n^{\langle 2\rangle}\right)=\left[\frac{\partial^2 g}{\partial\alpha^2}S_{\alpha n}^{\langle 1\rangle}+\frac{\partial^2 g}{\partial\alpha\partial n}\right]S_{\alpha n}^{\langle 1\rangle}+\frac{\partial g}{\partial\alpha}S_n^{\langle 2\rangle}+\frac{\partial^2 g}{\partial n\partial\alpha}S_{\alpha n}^{\langle 1\rangle}+\frac{\partial^2 g}{\partial n^2} \quad \text{(AI.27)}$$

$$\frac{d}{dT}\left(S_\beta^{\langle 2\rangle}\right)=\left[\frac{\partial^2 g}{\partial\alpha^2}S_{\alpha\beta}^{\langle 1\rangle}+\frac{\partial^2 g}{\partial\alpha\partial\beta}\right]S_{\alpha\beta}^{\langle 1\rangle}+\frac{\partial g}{\partial\alpha}S_\beta^{\langle 2\rangle}+\frac{\partial^2 g}{\partial\beta\partial\alpha}S_{\alpha\beta}^{\langle 1\rangle}+\frac{\partial^2 g}{\partial\beta^2} \quad \text{(AI.28)}$$

Differentiation of Eq. (AI.11) with respect to other parameter p_j, where $i\neq j$ gives the second order cross sensitivity co-efficient $\left(S_{p_ip_j}^{\langle 2\rangle}\right)$ matrix equation as follows:

$$\frac{d}{dT}\left(\frac{\partial^2\alpha}{\partial p_i p_j}\right)_{\substack{i\neq j\\ i\prec j}}=\left[\frac{\partial^2 g}{\partial\alpha^2}\left(\frac{\partial\alpha}{\partial p_j}\right)+\frac{\partial^2 g}{\partial\alpha\partial p_j}\right]\frac{\partial\alpha}{\partial p_i}+\left(\frac{\partial g}{\partial\alpha}\right)\frac{\partial^2\alpha}{\partial p_i\partial p_j}+\frac{\partial^2 g}{\partial p_i\partial\alpha}\left(\frac{\partial\alpha}{\partial p_j}\right)+\frac{\partial^2 g}{\partial p_i\partial p_j} \quad \text{(AI.29)}$$

$$\frac{d}{dT}\left(S_{p_ip_j}^{\langle 2\rangle}\right)_{\substack{i\neq j\\ i\prec j}}=\left[\frac{\partial^2 g}{\partial\alpha^2}S_{\alpha p_j}^{\langle 1\rangle}+\frac{\partial^2 g}{\partial\alpha\partial p_j}\right]S_{\alpha p_i}^{\langle 1\rangle}+\frac{\partial g}{\partial\alpha}S_{p_ip_j}^{\langle 2\rangle}+\frac{\partial^2 g}{\partial p_i\partial\alpha}S_{\alpha p_j}^{\langle 1\rangle}+\frac{\partial^2 g}{\partial p_i\partial p_j} \quad \text{(AI.30)}$$

Thus, for four parameters (i.e. $\tilde{K}_0$, E, n and β) we have

$$\frac{d}{dT}\left(S_{\tilde{K}_0E}^{\langle 2\rangle}\right)=\left[\frac{\partial^2 g}{\partial\alpha^2}S_{\alpha E}^{\langle 1\rangle}+\frac{\partial^2 g}{\partial\alpha\partial E}\right]S_{\alpha\tilde{K}_0}^{\langle 1\rangle}+\frac{\partial g}{\partial\alpha}S_{\tilde{K}_0E}^{\langle 2\rangle}+\frac{\partial^2 g}{\partial\tilde{K}_0\partial\alpha}S_{\alpha E}^{\langle 1\rangle}+\frac{\partial^2 g}{\partial\tilde{K}_0\partial E} \quad \text{(AI.31)}$$

$$\frac{d}{dT}\left(S_{\tilde{K}_0n}^{\langle 2\rangle}\right)=\left[\frac{\partial^2 g}{\partial\alpha^2}S_{\alpha n}^{\langle 1\rangle}+\frac{\partial^2 g}{\partial\alpha\partial n}\right]S_{\alpha\tilde{K}_0}^{\langle 1\rangle}+\frac{\partial g}{\partial\alpha}S_{\tilde{K}_0n}^{\langle 2\rangle}+\frac{\partial^2 g}{\partial\tilde{K}_0\partial\alpha}S_{\alpha n}^{\langle 1\rangle}+\frac{\partial^2 g}{\partial\tilde{K}_0\partial n} \quad \text{(AI.32)}$$

$$\frac{d}{dT}\left(S_{\tilde{K}_0\beta}^{\langle 2\rangle}\right)=\left[\frac{\partial^2 g}{\partial\alpha^2}S_{\alpha\beta}^{\langle 1\rangle}+\frac{\partial^2 g}{\partial\alpha\partial\beta}\right]S_{\alpha\tilde{K}_0}^{\langle 1\rangle}+\frac{\partial g}{\partial\alpha}S_{\tilde{K}_0\beta}^{\langle 2\rangle}+\frac{\partial^2 g}{\partial\tilde{K}_0\partial\alpha}S_{\alpha\beta}^{\langle 1\rangle}+\frac{\partial^2 g}{\partial\tilde{K}_0\partial\beta} \quad \text{(AI.33)}$$

$$\frac{d}{dT}\left(S_{En}^{\langle 2\rangle}\right)=\left[\frac{\partial^2 g}{\partial\alpha^2}S_{\alpha n}^{\langle 1\rangle}+\frac{\partial^2 g}{\partial\alpha\partial n}\right]S_{\alpha E}^{\langle 1\rangle}+\frac{\partial g}{\partial\alpha}S_{En}^{\langle 2\rangle}+\frac{\partial^2 g}{\partial E\partial\alpha}S_{\alpha n}^{\langle 1\rangle}+\frac{\partial^2 g}{\partial E\partial n} \quad \text{(AI.34)}$$

$$\frac{d}{dT}\left(S_{E\beta}^{\langle 2\rangle}\right)=\left[\frac{\partial^2 g}{\partial\alpha^2}S_{\alpha\beta}^{\langle 1\rangle}+\frac{\partial^2 g}{\partial\alpha\partial\beta}\right]S_{\alpha E}^{\langle 1\rangle}+\frac{\partial g}{\partial\alpha}S_{E\beta}^{\langle 2\rangle}+\frac{\partial^2 g}{\partial E\partial\alpha}S_{\alpha\beta}^{\langle 1\rangle}+\frac{\partial^2 g}{\partial E\partial\beta} \quad \text{(AI.35)}$$

$$\frac{d}{dT}\left(S_{n\beta}^{\langle 2\rangle}\right)=\left[\frac{\partial^2 g}{\partial\alpha^2}S_{\alpha\beta}^{\langle 1\rangle}+\frac{\partial^2 g}{\partial\alpha\partial\beta}\right]S_{\alpha n}^{\langle 1\rangle}+\frac{\partial g}{\partial\alpha}S_{n\beta}^{\langle 2\rangle}+\frac{\partial^2 g}{\partial n\partial\alpha}S_{\alpha\beta}^{\langle 1\rangle}+\frac{\partial^2 g}{\partial n\partial\beta} \tag{AI.36}$$

Using Eq. (AI.17- AI.21), we get

$$\frac{\partial^2 g}{\partial\alpha^2}=\frac{n(n-1)g}{(1-\alpha)^2} \tag{AI.37}$$

$$\frac{\partial^2 g}{\partial\tilde{K}_0^{\,2}}=g \tag{AI.38}$$

$$\frac{\partial^2 g}{\partial E^2}=\frac{g}{\left(RT\right)^2} \tag{AI.39}$$

$$\frac{\partial^2 g}{\partial n^2}=g\left[\ln(1-\alpha)\right]^2 \tag{AI.40}$$

$$\frac{\partial^2 g}{\partial\beta^2}=\frac{2g}{\beta^2} \tag{AI.41}$$

$$\frac{\partial^2 g}{\partial\alpha\partial\tilde{K}_0}=\frac{\partial^2 g}{\partial\tilde{K}_0\partial\alpha}=-\frac{ng}{(1-\alpha)} \tag{AI.42}$$

$$\frac{\partial^2 g}{\partial\alpha\partial E}=\frac{\partial^2 g}{\partial E\partial\alpha}=\frac{ng}{RT(1-\alpha)} \tag{AI.43}$$

$$\frac{\partial^2 g}{\partial\alpha\partial n}=\frac{\partial^2 g}{\partial n\partial\alpha}=-\frac{ng\ln(1-\alpha)}{(1-\alpha)} \tag{AI.44}$$

$$\frac{\partial^2 g}{\partial\alpha\partial\beta}=\frac{\partial^2 g}{\partial\beta\partial\alpha}=\frac{ng}{\beta(1-\alpha)} \tag{AI.45}$$

$$\frac{\partial^2 g}{\partial\tilde{K}_0\partial E}=-\frac{g}{RT} \tag{AI.46}$$

$$\frac{\partial^2 g}{\partial\tilde{K}_0\partial n}=g\ln(1-\alpha) \tag{AI.47}$$

$$\frac{\partial^2 g}{\partial \tilde{K}_0 \partial \beta} = -\frac{g}{\beta} \tag{AI.48}$$

$$\frac{\partial^2 g}{\partial E \partial n} = -\frac{\ln(1-\alpha) g}{RT} \tag{AI.49}$$

$$\frac{\partial^2 g}{\partial E \partial \beta} = \frac{g}{RT\beta} \tag{AI.50}$$

$$\frac{\partial^2 g}{\partial n \partial \beta} = -\frac{\ln(1-\alpha) g}{\beta} \tag{AI.51}$$

So, the matrix forms of equations consisting of second order sensitivity coefficient and second order cross sensitivity coefficient is

$$\frac{d}{dT}\begin{vmatrix} S^{\langle 2\rangle}_{\tilde{K}_0} \\ S^{\langle 2\rangle}_{E} \\ S^{\langle 2\rangle}_{n} \\ S^{\langle 2\rangle}_{\beta} \\ S^{\langle 2\rangle}_{\tilde{K}_0 E} \\ S^{\langle 2\rangle}_{\tilde{K}_0 n} \\ S^{\langle 2\rangle}_{\tilde{K}_0 \beta} \\ S^{\langle 2\rangle}_{En} \\ S^{\langle 2\rangle}_{E\beta} \\ S^{\langle 2\rangle}_{n\beta} \end{vmatrix} = \begin{vmatrix} \left[\frac{n(n-1)g}{(1-\alpha)^2} S^{\langle 1\rangle}_{\alpha\tilde{K}_0} - \frac{ng}{(1-\alpha)}\right] S^{\langle 1\rangle}_{\alpha\tilde{K}_0} - \frac{ng}{(1-\alpha)} S^{\langle 2\rangle}_{\tilde{K}_0} - \frac{ng}{(1-\alpha)} S^{\langle 1\rangle}_{\alpha\tilde{K}_0} + g \\ \left[\frac{n(n-1)g}{(1-\alpha)^2} S^{\langle 1\rangle}_{\alpha E} + \frac{ng}{RT(1-\alpha)}\right] S^{\langle 1\rangle}_{\alpha E} - \frac{ng}{(1-\alpha)} S^{\langle 2\rangle}_{E} + \frac{ng}{RT(1-\alpha)} S^{\langle 1\rangle}_{\alpha E} + \frac{g}{(RT)^2} \\ \left[\frac{n(n-1)g}{(1-\alpha)^2} S^{\langle 1\rangle}_{\alpha n} - \frac{ng\ln(1-\alpha)}{(1-\alpha)}\right] S^{\langle 1\rangle}_{\alpha n} - \frac{ng}{(1-\alpha)} S^{\langle 2\rangle}_{n} - \frac{ng\ln(1-\alpha)}{(1-\alpha)} S^{\langle 1\rangle}_{\alpha n} + g\left[\ln(1-\alpha)\right]^2 \\ \left[\frac{n(n-1)g}{(1-\alpha)^2} S^{\langle 1\rangle}_{\alpha\beta} + \frac{ng}{\beta(1-\alpha)}\right] S^{\langle 1\rangle}_{\alpha\beta} - \frac{ng}{(1-\alpha)} S^{\langle 2\rangle}_{\beta} + \frac{ng}{\beta(1-\alpha)} S^{\langle 1\rangle}_{\alpha\beta} + \frac{2g}{\beta^2} \\ \left[\frac{n(n-1)g}{(1-\alpha)^2} S^{\langle 1\rangle}_{\alpha E} + \frac{ng}{RT(1-\alpha)}\right] S^{\langle 1\rangle}_{\alpha\tilde{K}_0} - \frac{ng}{(1-\alpha)} S^{\langle 2\rangle}_{\tilde{K}_0 E} - \frac{ng}{(1-\alpha)} S^{\langle 1\rangle}_{\alpha E} - \frac{g}{RT} \\ \left[\frac{n(n-1)g}{(1-\alpha)^2} S^{\langle 1\rangle}_{\alpha n} - \frac{ng\ln(1-\alpha)}{(1-\alpha)}\right] S^{\langle 1\rangle}_{\alpha\tilde{K}_0} - \frac{ng}{(1-\alpha)} S^{\langle 2\rangle}_{\tilde{K}_0 n} - \frac{ng}{(1-\alpha)} S^{\langle 1\rangle}_{\alpha n} + g\ln(1-\alpha) \\ \left[\frac{n(n-1)g}{(1-\alpha)^2} S^{\langle 1\rangle}_{\alpha\beta} + \frac{ng}{\beta(1-\alpha)}\right] S^{\langle 1\rangle}_{\alpha\tilde{K}_0} - \frac{ng}{(1-\alpha)} S^{\langle 2\rangle}_{\tilde{K}_0\beta} - \frac{ng}{(1-\alpha)} S^{\langle 1\rangle}_{\alpha\beta} - \frac{g}{\beta} \\ \left[\frac{n(n-1)g}{(1-\alpha)^2} S^{\langle 1\rangle}_{\alpha n} - \frac{ng\ln(1-\alpha)}{(1-\alpha)}\right] S^{\langle 1\rangle}_{\alpha E} - \frac{ng}{(1-\alpha)} S^{\langle 2\rangle}_{En} + \frac{ng}{RT(1-\alpha)} S^{\langle 1\rangle}_{\alpha n} - \frac{g\ln(1-\alpha)}{RT} \\ \left[\frac{n(n-1)g}{(1-\alpha)^2} S^{\langle 1\rangle}_{\alpha\beta} + \frac{ng}{\beta(1-\alpha)}\right] S^{\langle 1\rangle}_{\alpha E} - \frac{ng}{(1-\alpha)} S^{\langle 2\rangle}_{E\beta} + \frac{ng}{RT(1-\alpha)} S^{\langle 1\rangle}_{\alpha\beta} + \frac{g}{RT\beta} \\ \left[\frac{n(n-1)g}{(1-\alpha)^2} S^{\langle 1\rangle}_{\alpha\beta} + \frac{ng}{\beta(1-\alpha)}\right] S^{\langle 1\rangle}_{\alpha n} - \frac{ng}{(1-\alpha)} S^{\langle 2\rangle}_{n\beta} - \frac{ng\ln(1-\alpha)}{(1-\alpha)} S^{\langle 1\rangle}_{\alpha\beta} - \frac{g\ln(1-\alpha)}{\beta} \end{vmatrix} \tag{AI.52}$$

Similarly, the matrix form of equations consisting of second order sensitivity coefficient and second order cross sensitivity coefficient for n = 1 is

$$\frac{d}{dT}\begin{vmatrix} S^{\langle 2\rangle}_{\tilde{K}_0} \\ S^{\langle 2\rangle}_{E} \\ S^{\langle 2\rangle}_{\beta} \\ S^{\langle 2\rangle}_{\tilde{K}_0 E} \\ S^{\langle 2\rangle}_{\tilde{K}_0 \beta} \\ S^{\langle 2\rangle}_{E\beta} \end{vmatrix} = \begin{vmatrix} \left[-\frac{g}{(1-\alpha)}\right] S^{\langle 1\rangle}_{\alpha\tilde{K}_0} - \frac{g}{(1-\alpha)} S^{\langle 2\rangle}_{\tilde{K}_0} - \frac{g}{(1-\alpha)} S^{\langle 1\rangle}_{\alpha\tilde{K}_0} + g \\ \left[\frac{g}{RT(1-\alpha)}\right] S^{\langle 1\rangle}_{\alpha E} - \frac{g}{(1-\alpha)} S^{\langle 2\rangle}_{E} + \frac{g}{RT(1-\alpha)} S^{\langle 1\rangle}_{\alpha E} + \frac{g}{(RT)^2} \\ \left[\frac{g}{\beta(1-\alpha)}\right] S^{\langle 1\rangle}_{\alpha\beta} - \frac{g}{(1-\alpha)} S^{\langle 2\rangle}_{\beta} + \frac{g}{\beta(1-\alpha)} S^{\langle 1\rangle}_{\alpha\beta} + \frac{2g}{\beta^2} \\ \left[\frac{g}{RT(1-\alpha)}\right] S^{\langle 1\rangle}_{\alpha\tilde{K}_0} - \frac{g}{(1-\alpha)} S^{\langle 2\rangle}_{\tilde{K}_0 E} - \frac{g}{(1-\alpha)} S^{\langle 1\rangle}_{\alpha E} - \frac{g}{RT} \\ \left[\frac{g}{\beta(1-\alpha)}\right] S^{\langle 1\rangle}_{\alpha\tilde{K}_0} - \frac{g}{(1-\alpha)} S^{\langle 2\rangle}_{\tilde{K}_0\beta} - \frac{g}{(1-\alpha)} S^{\langle 1\rangle}_{\alpha\beta} - \frac{g}{\beta} \\ \left[\frac{g}{\beta(1-\alpha)}\right] S^{\langle 1\rangle}_{\alpha E} - \frac{ng}{(1-\alpha)} S^{\langle 2\rangle}_{E\beta} + \frac{g}{RT(1-\alpha)} S^{\langle 1\rangle}_{\alpha\beta} + \frac{g}{RT\beta} \end{vmatrix} \quad \text{(AI.53)}$$

Appendix - II

General features of genetic algorithm (GA) [173]

Parameters like population size, crossover probability, mutation probability, and the numbers of generations together form the parameters of the GA and determine the performance of the GA [165].

The initial population: Initial population is randomly constructed by generating solution vectors within the problem space. If any information about the objective function is available then the initial population should be constructed such that it covers the regions of interest in the solution vector space.

Evaluation of the initial population: Creation function specifies the function that creates the initial population. The default creation function 'Uniform' creates a random initial population with a uniform distribution.

Creating the Next Generation: At each step, the genetic algorithm uses the current population to create the children that make up the next generation. The algorithm selects a group of individuals in the current population, called parents, who contribute their genes, the entries of their vectors, to their children. The algorithm usually selects individuals that have better fitness values as parents. The genetic algorithm creates three types of children for the next generation:

Elite children are the individuals in the current generation with the best fitness values. These individuals automatically survive to the next generation.

Crossover children are created by combining the vectors of a pair of parents.

Mutation children are created by introducing random changes, or mutations, to a single parent.

Selection Options: The selection function chooses parents for the next generation based on their scaled values from the fitness scaling function. The selection function can be chosen from the following functions:

Stochastic uniform lays out a line in which each parent corresponds to a section of the line of length proportional to its expectation. The algorithm moves along the line in steps of equal size, one-step for each parent. At each step, the algorithm allocates a parent from the section it lands on. The first step is a uniform random number less than the step size.

Remainder assigns parents deterministically from the integer part of each individual's scaled value and then uses roulette selection on the remaining fractional part.

Uniform selects parents at random from a uniform distribution using the expectations and number of parents. This results in an undirected search. Uniform selection is not a useful search strategy, but can be use it to test the genetic algorithm.

Roulette simulates a roulette wheel with the area of each segment proportional to its expectation. The algorithm then uses a random number to select one of the sections with a probability equal to its area.

Tournament - The function selects each parent by choosing individuals at random, the number of which can be specify by Tournament Size, and then choosing the best individual out of that set to be a parent.

Reproduction Options: Reproduction options determine how the genetic algorithm creates children at each new generation. Elite count specifies the number of individuals that are guaranteed to survive to the next generation. Set Elite count to be a positive integer less than or equal to Population Size. Crossover fraction specifies the fraction of the next generation, other than elite individuals, that are produced by crossover. The

remaining individuals, other than elite individuals, in the next generation are produced by mutation. Set Crossover fraction to be a fraction between 0 and 1, either by entering the fraction in the text box or moving the slider. We have set elite count is 2 and crossover fraction is 0.8.

Mutation Options: Mutation functions make small random changes in the individuals in the population, which provide genetic diversity and enable the GA to search a broader space.

Uniform is a two-step process. First, the algorithm selects a fraction of the vector entries of an individual for mutation, where each entry has a probability of Mutation Rate of being mutated. In the second step, the algorithm replaces each selected entry by a random number selected uniformly from the range for that entry.

Gaussian adds a random number to each vector entry of an individual. This random number is taken from a Gaussian distribution centered on zero. The variance of this distribution can be controlled with two parameters. The Scale parameter determines the variance at the first generation. The Shrink parameter controls how variance shrinks as generations go by. If the Shrink parameter is 0, the variance is constant. If the Shrink parameter is 1, the variance shrinks to 0 linearly as the last generation is reached.

Crossover Options: Crossover combines two individuals, or parents, to form a new individual, or child, for the next generation.

Single point chooses a random integer n between 1 and Number of variables, and selects the vector entries numbered less than or equal to n from the first parent, selects genes numbered greater than n from the second parent, and concatenates these entries to form the child. For example,

p1 = [a b c d e f g h]

p2 = [1 2 3 4 5 6 7 8]

crossover point (at random) = 3

child = [a b c 4 5 6 7 8]

Two point selects two random integers m and n between 1 and Number of variables. The algorithm selects genes numbered less than or equal to m from the first parent, selects genes numbered from m+1 to n from the second parent, and selects genes numbered greater than n from the first parent. The algorithm then concatenates these genes to form a single gene. For example,

p1 = [a b c d e f g h]

p2 = [1 2 3 4 5 6 7 8]

crossover points (at random) = 3,6

child = [a b c 4 5 6 g h]

Scattered creates a random binary vector. It then selects the genes where the vector is a 1 from the first parent, and the genes where the vector is a 0 from the second parent, and combines the genes to form the child. For example,

p1 = [a b c d e f g h]

p2 = [1 2 3 4 5 6 7 8]

random crossover vector = [1 1 0 0 1 0 0 0]

child = [a b 3 4 e 6 7 8]

Intermediate creates children by a weighted average of the parents. Intermediate crossover is controlled by a single parameter Ratio:

child1 = parent1 + rand * Ratio * (parent2 - parent1)

If the Ratio is in the range [0,1] then the children produced are within the hypercube defined by the parents locations at opposite vertices.
If Ratio is in a larger range, say 1.1 then children can be generated outside the hypercube. Ratio can be a scalar or a vector of length Number of variables. If Ratio is a scalar, then all of the children will lie on the line between the parents. If Ratio is a vector then children can be any point within the hypercube.

Heuristic creates children that lie on the line containing the two parents, a small distance away from the parent with the better fitness value in the direction away from the parent with the worse fitness value.

Migration Options: Migration is the movement of individuals between subpopulations, which the algorithm creates if one set Population size to be a vector of length greater than 1. Every so often, the best individuals from one subpopulation replace the worst individuals in another subpopulation. One can control how migration occurs by the following three parameters. Direction - Migration can take place in one direction or two.

Forward: migration takes place toward the last subpopulation. That is the nth subpopulation migrates into the (n+1)'th subpopulation.

Both: the nth subpopulation migrates into both the (n-1)th and the (n+1)th subpopulation.

Migration wraps at the ends of the subpopulations. That is, the last subpopulation migrates into the first, and the first may migrate into the last. To prevent wrapping, specify a subpopulation of size zero.

Fraction controls how many individuals move between subpopulations. Fraction is the fraction of the smaller of the two subpopulations that moves. If individuals migrate from a subpopulation of 50 individuals into a population of 100 individuals and Fraction is 0.1,

5 individuals (0.1 * 50) migrate. Individuals that migrate from one subpopulation to another are copied. They are not removed from the source subpopulation. Interval controls how many generations pass between migrations.

Hybrid Function Options: The hybrid function uses the final point from the genetic algorithm as its initial point. The choices are

None

fminsearch

patternsearch

fminunc

Stopping Criteria Options: Stopping criteria determine what cause the algorithm to terminate.

Generations specifies the maximum number of iterations the genetic algorithm performs.

Time limit specifies the maximum time in seconds the genetic algorithm runs before stopping.

Fitness limit - If the best fitness value is less than or equal to the value of Fitness limit, the algorithm stops.

Stall generations - If there is no improvement in the best fitness value for the number of generations specified by Stall generations, the algorithm stops.

Stall time limit - If there is no improvement in the best fitness value for an interval of time in seconds specified by Stall time limit, the algorithm stops.